



HAL
open science

Characterization of two primary metabolism enzymes in *Arabidopsis thaliana*: phosphoglycerate mutase and phosphoglycolate phosphatase

Pauline Duminil

► To cite this version:

Pauline Duminil. Characterization of two primary metabolism enzymes in *Arabidopsis thaliana* : phosphoglycerate mutase and phosphoglycolate phosphatase. Biochemistry, Molecular Biology. Université Paris Saclay (COMUE), 2019. English. NNT : 2019SACLS591 . tel-03966873

HAL Id: tel-03966873

<https://theses.hal.science/tel-03966873>

Submitted on 1 Feb 2023

HAL is a multi-disciplinary open access archive for the deposit and dissemination of scientific research documents, whether they are published or not. The documents may come from teaching and research institutions in France or abroad, or from public or private research centers.

L'archive ouverte pluridisciplinaire **HAL**, est destinée au dépôt et à la diffusion de documents scientifiques de niveau recherche, publiés ou non, émanant des établissements d'enseignement et de recherche français ou étrangers, des laboratoires publics ou privés.

Characterization of two primary metabolism enzymes in *Arabidopsis thaliana*: phosphoglycerate mutase and phosphoglycolate phosphatase

Thèse de doctorat de l'Université Paris-Saclay préparée à l'Université
Paris-Sud, à l'Institut des Sciences des Plantes de Paris-Saclay

École doctorale n°567 : Sciences du végétal : du gène à
l'écosystème (SDV)
Spécialité Biologie

Thèse présentée et soutenue à Gif-sur-Yvette, le 18/12/2019, par

Pauline DUMINIL

Thèse de doctorat

Composition du Jury :

Anja KRIEGER-LISZKAY Directrice de recherche CNRS au CEA-Saclay, France Institut de biologie intégrative de la cellule	Présidente
Andreas WEBER Professeur à l'université de Düsseldorf, Allemagne Institut de la biochimie des plantes	Rapporteur
Jean ALRIC Chargé de recherche CNRS au CEA-Cadarache, France Institut de Biosciences et Biotechnologies d'Aix-Marseille	Rapporteur
Pierre CAROL Professeur à l'université Paris-Sorbonne, France Institut d'écologie et des sciences de l'environnement de Paris	Examineur
Pierre PETRIACQ Maitre de conférences à l'université de Bordeaux, France Biologie du fruit et Pathologie	Examineur
Nathalie GLAB-PERRET Chargée de recherche CNRS à l'université Paris-Saclay, France Institut des sciences des plantes de Paris-Saclay	Directrice de thèse

Remerciements

I would like first to thank the jury who agreed to read and assess my work. I can't wait to meet you at the (I hope) future defense !

Merci aux membres de mon comité de thèse Christian Meyer, Patrice Meimoun et Jean Colcombet pour vos conseils, votre écoute et votre investissement dans mon travail.

Ma Nat, ma mémé, ma danseuse, je ne sais même pas par où commencer tant il y a de choses à dire... Tu es une directrice de thèse hors norme, extrêmement généreuse, incroyablement dynamique et adorablement sensible. Je suis plus que chanceuse d'avoir croisé ton chemin, cela fait maintenant quelques années. J'ai énormément appris et grandi (au sens figuré bien sûr 😊) à tes côtés scientifiquement et humainement. Alors voilà, après quelques tablettes de chocolats, des litres de cafés, des heures de semis de graines, des milliers de ppm de CO₂, des kilomètres de courses à pieds, des larmes des rires que quelques achats de bijoux compulsifs plus tard il est temps de pour moi de te remercier du fond du cœur. Merci pour tout ce que tu m'as appris, pour tout tes conseils pour ta bienveillance et surtout ta patience. Merci de m'avoir accueillie à bras ouverts et de m'avoir gardée !

Merci aussi au reste de l'équipe, et quelle équipe haute en couleur ! Merci Michael HODGES de m'avoir accueillie dans m'équipe et ponctué ma thèse de ton humour anglais, merci à Bertrand pour tes conversations toujours endiablées et ton énergie à toute heure et à Mathieu pour ton calme à toute épreuve ! Merci à Caro de m'avoir faire découvrir (et aimé !) la RMN et Florence et les filles de la plateforme pour votre soutien et vos sourires. Merci à ma Sophy pour ton énergie débordante et ton réconfort à tout moment ! Merci à Céline pour tout ce que tu m'as appris, pour ton aide dans les manips, tes conseils avisés, ton soutien au jour le jour, et tes de tricots qui nous tiennent chaud ! Merci à toi Axel pour tous tes précieux conseils, et pour le dynamisme que tu apportes ou que tu ailles ! Mais surtout merci pour ta bonne humeur permanente et toutes ces bières partagées.

Merci à tous ceux que j'ai croisé sur mon chemin pendant cette thèse Linda et Emilie les meilleures coachs sportives qu'il soient, Emeline (always mon boulet préféré 😊), Julie et Julie, William, Miriam, Amanda, Jing fang, Tiffany, Camille.

Merci à la team Doc'en herbe pour toutes ces heures de réunions, ces PhD days et surtout ces EPSR inoubliables !

Merci à notre Jean VIDAL pour ton enthousiasme et ton œil neuf !

Merci Marie et petit Jean pour vos coups de main en manips !

Merci à tous eux qui ont partagé et partage encore cette galère qu'on appelle la thèse : ma petite Gouda, Quentin, et Anis, Marine, courage pour la suite, je crois en vous 😊 !

Merci à ma Cécilou adorée pour ton soutien sans faille et ton réconfort ou que tu sois dans le monde, tu es une personne en or.

Merci à mon chauve préféré, probablement une des plus belles rencontres de ces années. Merci de m'avoir accompagné pendant toutes ces années, merci d'être si attentionné et généreux (profite de ce moment de gentillesse, ça ne va pas durer) !

Merci aux médiateurs scientifiques de la cité des sciences. Merci à tous de m'avoir accueilli et chouchouté quand je voulais changer d'air. Merci de m'avoir fait découvrir votre monde, et j'espère que vous savez à quel point j'ai adoré travailler avec vous. Une petite dédicace spéciale à Val pour ta

bonne humeur et ton sourire, Marlène pour ton franc parlé et ta gentillesse, et bien sûr Graciela pour ta bienveillance et ton dévouement.

Merci à toi mon Vlad mon pépé d'avoir été là au quotidien (presque) jusqu'au bout que ce soit pour de longues conversations, des soirées endiablées ou des câlins de réconfort.

A huge tank you to my Sweet Yanpei. You are such a beautiful person I could never tell how happy and thankful I am to meet you. Thanks for all your hugs, your advices and your support.

Merci à tous ceux qui de près ou de loin, pour un coup de main, une manip, un déjeuner partagé, un sourire bienveillant, une discussion au coin d'un couloir ont participé à faire de cette thèse une expérience inoubliable.

Enfin merci à mon crew, mon gang, ma bande, mon roc depuis et pour toujours Julie, Camille Marie, Agathe, Baptiste, papa et maman pour votre soutien absolument sans faille.

Merci à ma famille et mes amies de plus ou moins longue date qui ont patiemment écoutés mes problèmes de plantes et de pipettes : Anysia, Maëlys, Laurine, Charlotte, Maëva, ma petite Garfield, Flo, Jess, ma DD, ma Manoush, Didier, Nelly et Iris ainsi que tous les autres !

Merci à la coloc' de m'avoir supportée pendant la rédaction !

Et bien sûr, et non tu n'y échapperas pas, merci à toi Maël. Merci pour tout ce soutien au jour le jour, tout le réconfort que tu m'apportes, de m'avoir remotivée après chaque manip ratée. Mais surtout de cette confiance que tu as en moi.

List of abbreviations

α -ABA	α -Amino-n-Butyric Acid	dNTP	Deoxyribonucleotide triphosphate
1,3-BPGA	1,3-biphosphoglycerate	DTT	Dithiothreitol
2-OG	2-oxoglutarate	dTTP	Deoxyribothymine triphosphate
2-PG	2-phosphoglycolate	E-4-P	Erythrose 4-phosphate
3-AT	3-amino-1,2,4-triazole	EDTA	Ethylene diamine tetraacetic acid
3D	3 dimensions	EGTA	Ethylene glycol tetraacetic acid
3-PGA	3-phosphoglycerate	Em	oxidation-reduction potential
3-PHP	3-phosphohydroxypyruvate	EMS	Ethyl methanesulfonate
3-PS	3-phosphoserine	ETR	Electron transfer rate
4Mn-1Ca	Metallic catalytic core of PSII	F6P	Fructose-6-phosphate
A	Alanine	FA	Formic acid
$A_{x\text{ nm}}$	Absorbance at x nm	FAD	Flavine adenine dinucleotide
ABA	Abscisic acid	FBPase	Fructose-1,6-bisphosphatase
ACN	Acetonitrile	Fd	Ferredoxine
AH-AT	Alanine-hydroxypyruvate aminotransferase	FMN	Flavin mononucleotide
Ald	Aldolase	FNR	Ferredoxin reductase at NADP
am	<i>ante meridiem</i>	Fru1,6P ₂	Fructose-1,6-biphosphate
AQ	Assimilatory quotient	FTR	Ferredoxin thioredoxin reductase
ATP	Adenosine triphosphate	G3P	Glyceraldehyde-3-phosphate
BASS	Bile acid sodium symporter	GAPDH	G3P dehydrogenase
BOU	A BOUT DE SOUFFLE	GCL	Glyoxylate carboligase
Ca	Calcium	GDC	Glycine Decarboxylase
CAM	Crassulacean acid metabolism	GDH	Protein H from the GDC
CAT	Catalase	GDP	Protein P of the GDC
cDNA	Complementary DNA	GDT	Protein T of the GDC
Chl	Chlorophyll	GOGAT	Glutamine: 2-OG aminotransferase
Co	Cobalt	GOX	Glycolate oxidase
CoA	Coenzyme A	GFP	Green Fluorescent Protein
Cyt b ₆ f	cytochrome b ₆ f	GGT	Glutamate:glyoxylate aminotransferase
D	Aspartic acid	GIDH	glycolate dehydrogenase
dATP	Deoxyriboadenine triphosphate	Glu 1-P	Glucose 1-phosphate
dCTP	Deoxyribocytosine triphosphate	Glu 6-P	Glucose 6-phosphate
dGTP	Deoxyriboguanosine triphosphate	Gln	Glutamine
DHAP	Dihydroxyacetone phosphate	Glu	Glutamate
DiT	Carrier of dicarboxylates	GLYK	Glycerate kinase
DMSO	Dimethyl sulfoxide	GRX	Glutharedoxin
DNA	Deoxyribonucleic acid	GS	Glutamate synthetase
		GTP	Guanosine triphosphate

HAD Haloacid dehalogenase
 HAOX Hydroxy-acid oxidase
 HC High CO₂
 His Histidine
 HP Hydroxypyruvate
 HPLC High performance liquid chromatography
 HPR Hydroxypyruvate reductase
 HRP Horseradish peroxidase
 IAA Iodoacetamide
 IDH Isocitrate dehydrogenase
 IPTG Isopropyl β-D-1-thiogalactopyranoside
 k_{cat} Catalytic constant
 KGDH α-ketoglutarate dehydrogenase
 K_i Inhibitor constant
 K_m Michaelis-Menten constant
 LC Liquid Chromatography
 LHCI and II Light harvesting complex I and II
 LiAc Lithium acetate
 LPD Protein L from the GDC
 MBP Maltose binding protein
 MDH Malate dehydrogenase
 ME Malic enzyme
 MES 2-(N-morpholino) ethanesulfonic acid
 Mg Magnesium
 Mn Manganese
 mRNA Ribonucleic acid messenger
 MS Malate synthase
 MS Mass spectrometry
 MW Molecular weight
 NaCl Sodium chloride
 NADH Nicotinamide adenosine dinucleotide
 NADPH NADH phosphate
 Ni Nickel
 NiR Nitrite reductase
 NMR Nuclear magnetic resonance
 NO Nitric oxide
 NPQ Non-photochemical quenching
 NR Nitrate reductase
 NTA Nitrilotriacetic acid
 OAA Oxaloacetate
 OD Optic density
 OEC Oxygen-evolving complex
 OEP Outer envelope proteins
 OG Oxoglutarate
 ORF Open reading phase
 OXO Oxalate oxidase
 P680 Primary donor of PSII
 P700 Primary donor of PSI
 pABA p-Aminobenzoate
 PAGE Polyacrylamide gel electrophoresis with
 PC Plastocyanin
 PCR Polymerase chain reaction
 PDH Pyruvate dehydrogenase
 PDK Pyruvate dehydrogenase kinase
 PEG Polyethylene glycol
 PEP Phosphoenolpyruvate
 PEPc Phosphoenolpyruvate carboxylase
 PFK Phosphofructokinase
 PGAP 3-phosphoglycerate phosphatase
 PGDH 3-phosphoglycerate dehydrogenase
 PGK Phosphoglycerate kinase
 PGLP Phosphoglycolate phosphatase
 pH potential of hydrogen
 Pheo Pheophytin
 PLGG Plastid glycolate / glycerate transporter
 PLP Pyridoxal 5-phosphate
pm post meridiem
 PPDK Pyruvate phosphate dikinase
 ppm Parts per million
 PQ/PQH₂: oxidized and reduced plastoquinone
 PRK Phosphoribulokinase
 Ps Photosystem subunit
 PSAT 3-phosphoserine aminotransferase
 PSI and II Photosystems I and II
 PSP 3-phosphoserine phosphatase
 PTM Post-translational modification

QA Quinone A	Zn Zinc
R5P Ribose-5-phosphate	Units
RBCL Large sub-unit of RuBisCO	% Percent
RBCS Small subunit of RuBisCO	μ Micro
RC Reaction centre	° C degree Celsius
RNA Ribonucleic acid	bp base pair
ROS Reactive oxygen species	Da Dalton
RPE Ribose phosphate epimerase	g gramme
Ru-5-P Ribulose 5-phosphate	g acceleration unit
RuBisCO RuBP carboxylase / oxygenase	h hour
RuBP Ribulose-1,5-bisphosphate	Hz Hertz
S Serine	k kilo
S-1,7-P ₂ Sedoheptulose-1,7-biphosphate	kb kilo base
S7P Sedoheptulose-7-phosphate	L Litre
SA Salicylic acid	M Mega
SAB Serum albumin bovine	M Molar
SBPase Sedoheptulose-1,7-biphosphatase	m meter
SDS Sodium dodecyl sulfate	m milli
SGAT Serine: glyoxylate aminotransferase	min Minute
SHMT Serine hydroxymethyl-amino-transferase	n nano
SMM S-methylmethionine	Pa Pascal
T Threonine	s second
TBST Tris buffered saline with tween 20	V Volt
TCA Tricarboxylic acid	v volume
T-DNA Transfer DNA	
TE Tris-EDTA Buffer	
TFA Trifluoroacetic acid	
THF Tetrahydrofolate	
TiO ₂ Titanium dioxide	
Tm Temperature of melting	
TRX Thioredoxin	
TPI Triose Phosphate isomerase	
TPT Triose Phosphate translocator	
TSR Tartronate semialdehyde reductase	
U Unit	
UTP/UDP Uridine tri/di-phosphate	
XIC Xcalia intermediation core	
Xyl-5-P Xylulose-5-phosphate	

Résumé

Les plantes sont des organismes sessiles. Elles doivent réagir rapidement et efficacement aux stress biotiques et abiotiques qu'elles subissent. Pour cela, elles utilisent plusieurs niveaux de régulation. L'un d'eux, rapide et réversible, consiste à ajouter des modifications post-traductionnelles (PTMs) sur ses enzymes. Il existe de nombreuses modifications post-traductionnelles dans le monde du vivant (méthylation, acétylation, glycosylation, myristoylation, ubiquitination...). Cependant, la PTM la plus répandue est la phosphorylation protéique, qui intervient dans diverses voies du métabolisme primaire. La glycolyse permet la production d'énergie (ATP) et de pouvoir réducteur à partir de glucose. La régulation de la phosphoglycérate mutase d'*Arabidopsis thaliana* (*AtiPGAM*) a été étudiée grâce à une analyse d'un site de phosphorylation dans le but d'élucider le mécanisme réactionnel de la protéine. Dans cette partie du projet, l'activité de la protéine sauvage d'abord été analysée grâce à la production et la purification de protéines recombinantes. L'importance de la phosphorylation et le mécanisme réactionnel de la protéine ont été étudiés grâce à une mutagenèse dirigée de certains acides aminés spécifiques.

La photorespiration est un processus essentiel pour les organismes photosynthétiques. Ce cycle est initié par l'activité oxygénase d'une des enzymes les plus importante pour les organismes photosynthétiques, la ribulose-1,5-biphosphate carboxylase / oxygénase (RuBisCO). Cette activité produit notamment une molécule de 2-phosphoglycolate (2-PG), toxique pour la plante. Le recyclage, coûteux, du 2-PG par le cycle photorespiratoire se déroule dans quatre compartiments (chloroplaste, peroxyosome, mitochondrie et cytosol). Ce complexe cycle métabolique est sensible aux stress biotiques et abiotiques que subit la plante. La RuBisCO joue également un rôle primordial dans la photosynthèse *via* son activité carboxylase, mettant en compétition photosynthèse et photorespiration, ce qui fait de ce dernier une cible de choix pour l'amélioration des plantes. Les 8 enzymes principales du cycle photorespiratoire ainsi que la plupart des enzymes associées ont été caractérisées, cependant la régulation de ce cycle reste méconnue. Sept des huit enzymes du cycle photorespiratoire sont phosphorylables. Cette thèse de doctorat porte également sur la régulation post-traductionnelle de la première enzyme du cycle, la phosphoglycolate phosphatase (*AtPGLP1*). L'importance de cette protéine est visible notamment à travers le sévère phénotype développemental du mutant homozygote perte de fonction. Ce mutant *pglp1* chez

Arabidopsis thaliana est létal à l'air ambiant (400 ppm de CO₂) et requiert une forte concentration en CO₂ (10 000 ppm) pour se développer et se reproduire. Diverses expériences de phosphoprotéomiques ont montré que AtPGLP1 était associée à quatre phosphosites, dans trois phosphopeptides. La méthode employée pour tester le rôle de chaque potentiel phosphosite a été de muter ces résidus en alanine, qui est un acide aminé non phosphorylable ou en aspartate qui est susceptible de mimer une phosphorylation constitutive. Ces formes mutées ont été utilisées pour déterminer leurs paramètres cinétiques *via* une approche *in vitro*. Deux de ces phosphosites, qui semblaient les plus prometteurs, ont été étudiés de manière plus approfondie *in planta*. Pour cela, les mutants *pglp1* homozygotes ont été transformés avec les différentes formes mutées du gène. L'activité de la protéine *in vivo* a également été étudiée chez la plante sauvage Col-0, après différents stress connus pour moduler le cycle photorespiratoire.

La phosphoglycolate phosphatase n'est pas uniquement présente chez les plantes mais également chez les mammifères chez qui cette protéine ne joue pas un rôle dans la photorespiration, mais dans la détoxification du 2-PG produit lors de la réparation des coupures ADN double brins. Il a été prouvé que dans ce contexte, l'activité PGLP pouvait être dépendante de l'environnement redox de la protéine. La régulation de AtPGLP1 par oxydo-réduction a donc également été étudié dans cette thèse.

La régulation post-traductionnelle des protéines est le moyen le plus rapide que possèdent les plantes pour réagir à leur environnement. Il existe dans le règne du vivant de nombreuses modifications post-traductionnelles qui peuvent être associées les unes aux autres, rendant l'étude de ces phénomènes complexes mais primordiaux analyser l'impact des stress biotiques et abiotiques sur le développement de la plante.

Contents

INTRODUCTION.....	3
I) Photosynthesis and primary metabolism in plants	4
1) <i>Photosynthesis</i>	4
a) The light side	4
b) The dark side: the Calvin-Benson cycle	7
c) C ₄ and CAM photosynthesis	8
2) <i>RuBisCO (EC 4.1.1.39) and 3-PGA</i>	10
II) Glycolysis.....	12
1) <i>Global description of glycolysis</i>	12
2) <i>Can metabolites move between the cytosol and plastids?</i>	14
3) <i>How are plant glycolytic proteins regulated?</i>	16
III) The photorespiratory cycle	18
1) <i>What is photorespiration?</i>	18
2) <i>What are the core photorespiratory enzymes?</i>	21
a) The core photorespiratory enzymes	21
b) Photorespiratory transporters.....	28
c) Other photorespiratory-related proteins, implied in recycling side products of the pathway.....	31
3) <i>How do photorespiratory mutants behave?</i>	33
4) <i>Is it possible to improve plant yield by targeting photorespiration?</i>	35
5) <i>How does the 2C-cycle interact with primary metabolism?</i>	38
a) Photorespiration and photosynthesis	38
b) Photorespiration and nitrogen assimilation	40
c) Photorespiration and the TCA cycle.....	41
d) Photorespiration and 1C metabolism.....	42
6) <i>How does photorespiration react under stress?</i>	43
a) Biotic stresses and photorespiration.....	44
b) Abiotic stresses and photorespiration.....	44
7) <i>Is photorespiration regulated by phosphorylation?</i>	47
a) Post translational modifications (PTMs).....	47
b) Photorespiration and protein phosphorylation	48
c) Photorespiration and redox regulation	48
IV) Two different proteins, two different pathways; one reaction mechanism?.....	49
1) <i>Phosphoglycolate phosphatase (EC 3.1.3.19): a HAD family protein forming a transitory phosphoenzyme</i>	49
a) In C ₃ plants	49
b) In C ₄ plants	51
c) In other organisms.....	52
d) Description of the HAD protein superfamily.....	53
e) PGLP1 regulation	56
2) <i>Cytosolic iPGAM: phosphoregulation or a transitory catalytic phosphoenzyme?</i>	56
V) My PhD objectives and strategies	59
RESULTS.....	62
CHAPTER I.....	63

I)	Characterization of phosphoglycerate mutase catalytic mechanism in <i>Arabidopsis thaliana</i>	65
II)	Additional results.....	86
	CHAPTER II.....	90
	CHAPTER III	126
I)	AtPGLP1 activity in plants	128
	1) <i>Introduction</i>	128
	2) <i>Results</i>	128
II)	Functional complementation of a homozygous <i>pglp1</i> mutant	131
	1) <i>Introduction</i>	131
	2) <i>Results</i>	132
	GENERAL DISCUSSION AND PERSPECTIVES.....	136
I)	Reminder of the scientific background	137
	1) <i>Investigation of the AtiPGAM reaction mechanism, a glycolytic enzyme</i>	137
	2) <i>Analyses of post-translational regulations of AtPGLP1, a photorespiratory enzyme</i>	138
II)	Catalytic mechanism of the phosphoglycerate mutase	139
III)	Phosphoglycolate phosphatase activity and regulation in <i>A. thaliana</i>	141
	1) <i>AtPGLP1 activity</i>	141
	2) <i>AtPGLP1 phosphoregulation</i>	142
	3) <i>AtPGLP1 and HAD proteins family</i>	145
	4) <i>AtPGLP1 and regulation by oxidation-reduction</i>	146
IV)	Photorespiration and plant yield improvement	148
	MATERIALS AND METHODS.....	151
I)	Materials	152
	1) <i>Plant material</i>	152
	2) <i>Growth conditions</i>	152
	3) <i>Plasmids</i>	152
	4) <i>Bacterial strains</i>	156
	5) <i>Yeast Strain</i>	157
	6) <i>Culture Media</i>	157
II)	Methods	158
	1) <i>Molecular biology</i>	158
	2) <i>Cloning experiments</i>	163
	3) <i>Complementation of the Arabidopsis thaliana homozygous <i>pglp1</i> mutant</i>	168
	4) <i>Biochemistry methods</i>	170
	5) <i>Phosphopeptide measurements by PAPPISO</i>	176
	6) <i>Yeast methods</i>	180
	REFERENCES.....	182

INTRODUCTION

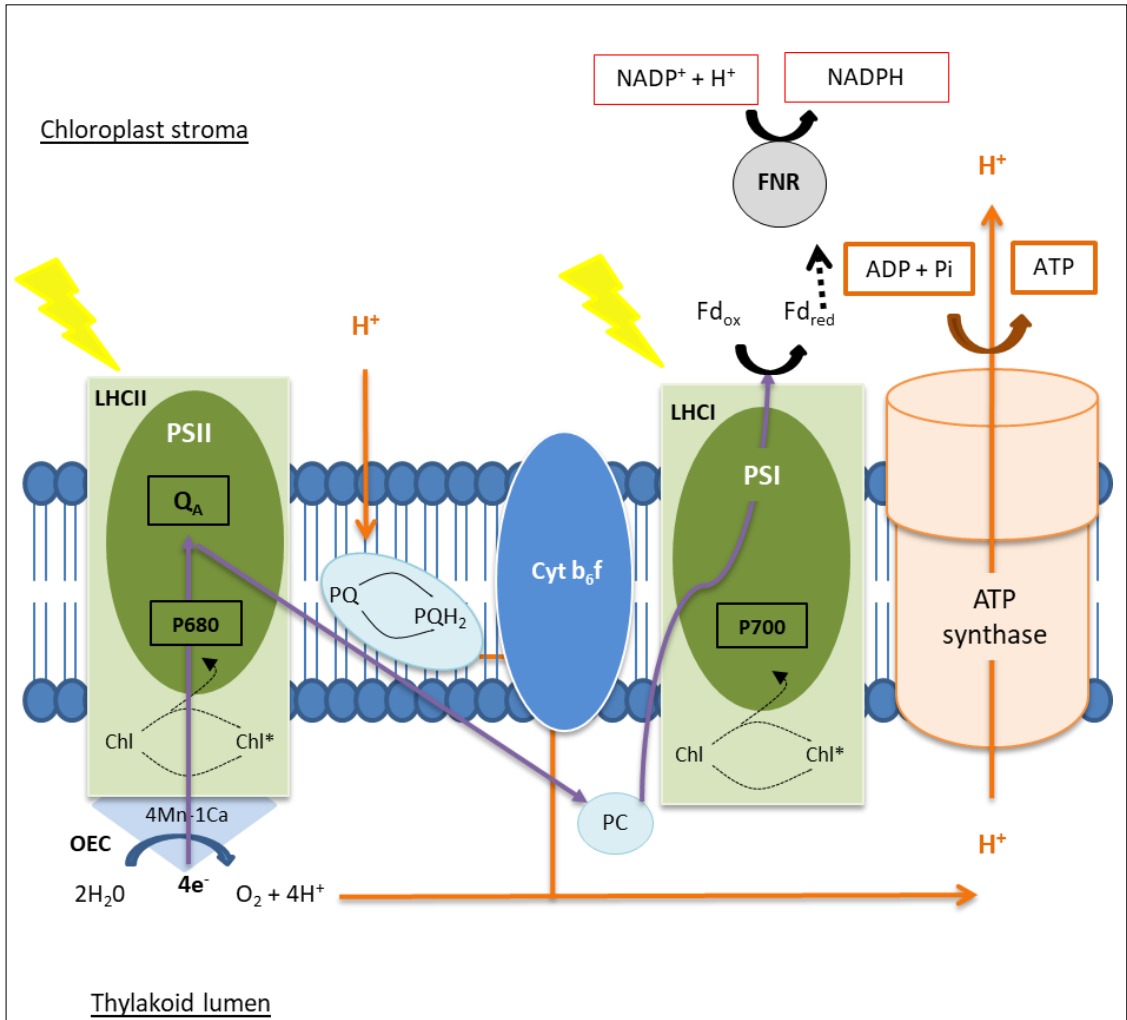


Figure 1: A simplified diagram of the photosynthetic electron transfer chain and proton gradient formation in the chloroplast

LHCI and LHCII: light harvesting complex I and II; PSI and PSII: photosystem I and II; OEC: oxygen-evolving complex; Chl: chlorophyll; P680 and P700: special chlorophyll a pairs associated with PSI and PSII; Q_A : quinone A; PQ/PQH₂: oxidized and reduced plastoquinone; 4Mn-1Ca: metallic catalytic core of PSII; Cyt b_6/f : cytochrome b_6/f complex; PC: plastocyanin; Fd: ferredoxin; FNR: ferredoxin-NADP⁺ reductase; purple lines: electron flux; orange lines: proton flux.

I) Photosynthesis and primary metabolism in plants

1) Photosynthesis

Photosynthesis consists of the conversion of light energy into chemical energy (and oxygen) needed to (re)generate the ribulose 1,5 biphosphate (RuBP) used to assimilate atmospheric CO₂ *via* the Ribulose-1,5-Biphosphate Carboxylase/Oxygenase (RuBisCO) to form organic 3C molecules used to make other C-based molecules such as sugars, amino and ribonucleic acids, proteins, lipids etc. This can happen in plants, algae, some protists and bacteria. Photosynthesis occurs in chloroplasts and it can be divided into two processes called the light and dark reactions.

The chloroplasts are organelles with two outer membranes enclosing an aqueous space (the stroma), where a third membrane structure can be found known as the thylakoid. The light reactions of photosynthesis take place in the thylakoid membrane and involve electron and proton transfers to produce energy and reducing power as ATP and NADPH, while the dark reactions occur in the stroma with the fixation of CO₂ to produce 3C acid-phosphates (3PGA) that serve as building blocks for the biosynthesis of organic molecules such as starch and sugar but also for the regeneration of RuBP, using the ATP and NADPH produced by the light reactions

a) The light side



The light-driven electron transfer reactions depend on multiple protein-complexes that work successively to convert light energy into chemical energy. The Z-scheme is a representation of the electron transfer chain and the oxidation-reduction potential (E_m) of the different components. It thus describes how electrons move from the redox couple water-oxygen *via* a chain of oxidation-reduction reactions to NADP⁺/NADPH. It should be noted that two of the steps associated with photosystems II and I use light energy to generate low redox potential components. Electrons are then transferred from a low (more negative) redox potential component to those with a higher (more positive) potential.

The simplified scheme (Figure 1) represents the main steps of photosynthetic electron transfer and ATP production. The electron transfer chain is of several protein-complexes; photosystems I and II (PSI and PSII) and their light-harvesting complexes (LHC I and LHC II), the oxygen-evolving complex (OEC) which is associated with PSII, the cytochrome-b6f complex (cyt-b6f). It is also associated with

the ATP-synthase. In PS II, the special chlorophyll P680 undergoes a light energy-induced charge separation, and the generated electrons are transferred to a quinone acceptor while the OEC complex reduces P680⁺. Two electrons are transferred to a mobile lipophilic plastoquinone PQ molecule that carries the electrons to another membrane protein, the cytochrome b₆f (cyt b₆f) complex that reduces plastocyanin. A light-dependent reaction also takes place at photosystem I (PSI), that allows the oxidation of reduced plastocyanin in the lumen and the reduction of ferredoxin (Fd) attached to PSI at the stromal side of the thylakoid membrane. The reduced Fd *via* the Fd-NADP oxidoreductase (FNR) then produces NADPH from NADP. It can be seen that certain steps release protons into the lumen, that results in a build-up of protons in the lumen compared to the stroma. This proton gradient is used by the ATP synthase in the thylakoid membrane to produce ATP from ADP and inorganic phosphate. (Govindjee et al., 2017).

The global organization of the two photosystems is rather comparable. They are made of a core complex containing the reaction center (RC) where the photochemical reactions occur and numerous peripheral light harvesting complexes (LHC) containing chlorophylls and other pigments.

The PSII core complex is composed of four large membrane subunits, Psb A (D1), Psb B (CP47), Psb C (CP43) and Psb D (D2). In this organization, D1 and D2 make up the dimeric PSII RC involved in charge separation and electron transfer to PQ, while CP43 and CP47 act as internal antenna, collecting and transporting light energy from the LHC-II antenna to the RC special pair Chl_a called P680. In this same PSII core complex, there are 12 low molecular mass membrane subunits surrounding the RC, forming what is called the “belt like structure”. These subunits are primordial both for dimerization and stabilization of the core complex and its association with the peripheral antenna complexes. The light harvesting complexes of PSII (LHC-II) are very abundant in thylakoid membranes and they are found as heterotrimers constituted by three proteins: Lhcb1, Lhcb2 and Lhcb3 (Jackowski et al., 2001). These proteins contain three transmembrane regions and their C-terminal is luminal. Through the binding and orientation of chlorophyll pigments within the proteins, light energy can be transferred by excitation energy transfer from LHC-II to P680 of the PSII RC dimer. P680 was so named because of its absorption peak at 680 nm which is in the red part of the light spectrum. Once P680 is excited to P680*, a charge separation is produced leading to a reduced pheophytin (Pheo⁻) in the PSII RC and an oxidized P680⁺ species that will be reduced during the water splitting process. The electron transferred to Pheo (a Chl molecule lacking Mg), will be transferred within the PSII RC *via* a bound quinone (Q_A) to a plastoquinone (PQ) bound to the Q_B pocket. The transformation of water into oxygen requires four electrons and four protons from two molecules of water, and this involves the oxygen-evolving complex (OEC). It is attached to the luminal side of PSII and contains a metallic catalytic core (called the 4Mn-1Ca cluster). Manganese is a transition metal that can exist in five different oxidation states and therefore it accumulates positive charges delivered by each light driven

turn-over of P680. After four turnovers, oxygen is produced from water and the manganese cluster returns to its initial state, while protons released into the lumen are used to produce ATP via the ATP synthase. Since PQ reduction to plastoquinol requires two electrons, two molecules of plastoquinol are produced per oxygen released.

If the global structure of PSI is quite similar to that of PSII with a RC surrounded by LHC to capture and to transfer light energy, several elements differ. The reaction center of PSI is composed of two large subunits called Psa A and Psa B that form a heterodimer containing twenty-two transmembrane helices. The PSI complex also contains a large non-protein content with about one third of its mass consisting of pigments and cofactors such as chlorophylls, carotenoids, phyloquinones and Fe_4S_4 clusters, that are important for its function. Psa A and B harbor most of these cofactors (from P700 to the first Fe_4S_4 cluster) but many other subunits coordinate the proper functioning of this complex, including cofactor binding and the docking of electron donors and acceptors located at both sides of the thylakoid membrane. One of these subunits, PsaG plays a role in the binding of LHCI. In PSI, LHC is composed of four proteins (Lhca1-4) assembled in two heterodimers arranged as Lhca1-Lhca4 and Lhca2-Lhca3 (Pan et al., 2019). Overall, PSI is a light driven plastocyanin-Fd oxidoreductase, and its role is to catalyze the electron transfer from the thylakoid lumen copper-containing plastocyanin to Fd at the stromal side of the thylakoid. Again, this requires light energy and the involvement of special Chls. The PSI special chlorophylls are known as P700 because of their absorption peak at 700 nm. As in PSII, the excited P700 transfers an electron to a primary acceptor called A_0 (a special Chla) this leads to a series of electron transfer reactions involving A_1 (phylloquinon), F_x , F_A and F_B (three Fe-S center proteins) before Fd is reduced. Once Fd is reduced it can be used as a reductant for several chloroplastic enzymes including the Fd-thioredoxin reductase and the Fd-glutamate synthase (Fd-GOGAT). However, it is mainly used to produce NADPH required to regenerate RuBP *via* the Calvin cycle as part of the “dark side” of photosynthesis. NADPH reduction requires FNR, a flavin-adenine dinucleotide (FAD)-containing protein that can be found as both soluble and thylakoid membrane-bound forms (Mulo, 2011). This cofactor can accept two electrons and so two Fd molecules are needed to produce one molecule of NADPH. This constitutes the last step of the photosynthetic electron transfer chain (Tikhonov and Subczynski, 2019).

During the light-driven photosynthetic steps, a proton gradient is generated across the thylakoid membrane between the thylakoid lumen and the chloroplast stroma. This is used by an ATP synthase to produce ATP, a primordial source of energy for the plant. ATP synthase is a macromolecular structure that transforms an electrochemical transmembrane gradient into the chemical energy of a covalent bond. ATP synthases from mitochondria and chloroplasts share the same global structure and function, with a F_1 head, a F_0 motor and a stalk that connects them. The F_1 head of the chloroplast ATP synthase (cF_1) is composed of three dimers of two subunits called α and β . These

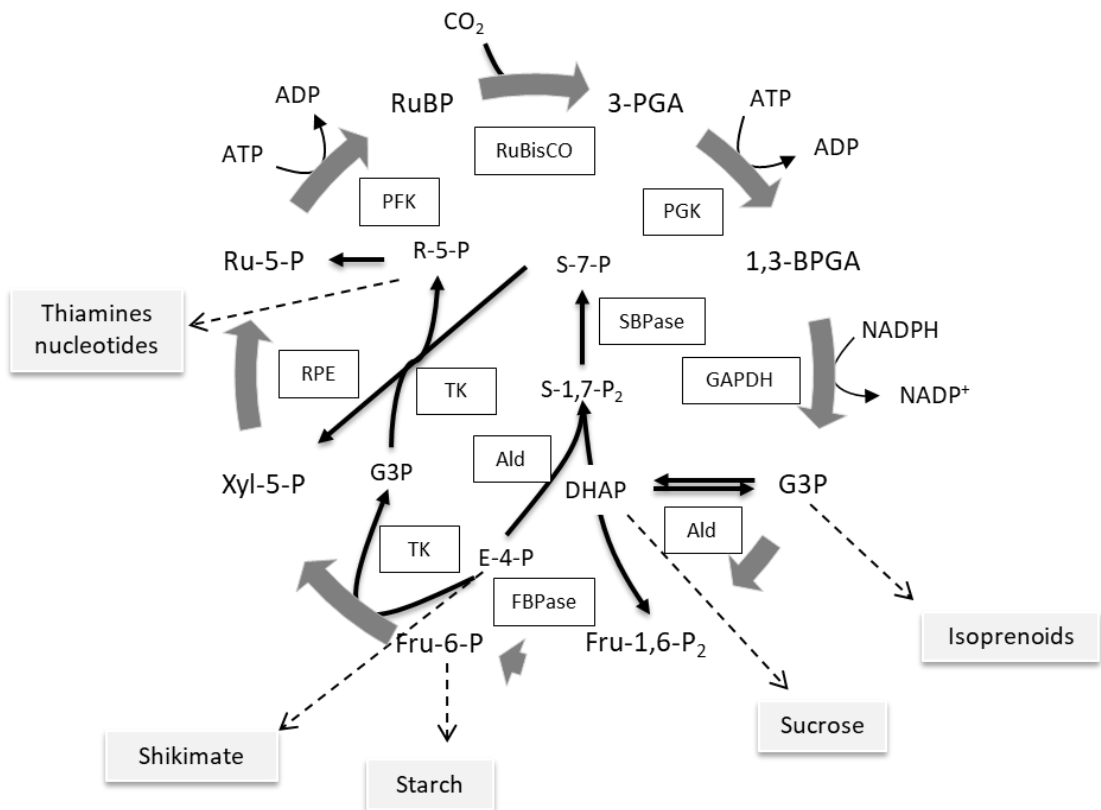


Figure 2: Overview of the Calvin-Benson cycle

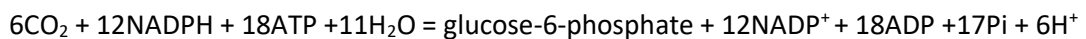
3-PGA: 3-phosphoglycerate; **1,3-BPGA:** 1,3-bisphosphoglycerate; **G3P:** glyceraldehyde 3-phosphate; **Fru-1,6-P₂:** fructose 1,6-bisphosphate; **Fru-6-P:** Fructose 6-phosphate; **DHAP:** dihydroxyacetone phosphate; **S-1,7-P₂:** sedoheptulose 1,7-bisphosphate; **S-7-P:** sedoheptulose 7-phosphate; **E-4-P:** erythrose 4-phosphate; **Xyl-5-P:** xylulose 5-phosphate; **Ru-5-P:** ribulose 5-phosphate; **RuBP:** ribulose 1,5-bisphosphate

RuBisCO: Ribulose 1,5-bisphosphate Carboxylase Oxygenase; **PGK:** phosphoglycerate kinase; **GAPDH:** glyceraldehyde 3-phosphate dehydrogenase; **Ald:** aldolase; **FBPase:** fructose 1,6-bisphosphatase; **SBPase:** sedoheptulose 1,7-bisphosphatase; **TK:** transketolase; **RPE:** ribose phosphate epimerase; **PRK:** phosphoribulose kinase; **ATP:** adenosine triphosphate; **ADP:** adenosine diphosphate; **NADPH/NADP⁺:** nicotinamide adenine dinucleotide phosphate reduced/oxidized.

three α β pairs contain the nucleotide binding domains, and they can have different conformations (open, loose and tight). The F_0 part is a multi-protein complex inserted in the thylakoid membrane linked to another multiprotein complex, the c-ring (Saroussi et al., 2012); these two structures are linked by a central peripheral stalk. This structure can have three rotational steps and after one complete rotation it will produce three ATP molecules (Junge and Nelson, 2015; Kohzuma et al., 2017).

b) The dark side: the Calvin-Benson cycle

The following chemical equation shows the assimilation of 6CO_2 molecules to produce glucose-6-phosphate:



Atmospheric inorganic CO_2 can be assimilated into organic carbohydrate molecules *via* the Calvin-Benson cycle (CB cycle), that consumes ATP and NADPH produced during the light reactions of photosynthesis.

The CB cycle can be described by three major steps (Figure 2):

- In the first step, CO_2 is combined with a RuBP, thanks to the famous Ribulose 1,5-bisphosphate carboxylase (RuBisCO described p10). As indicated by its name, this enzyme possesses two activities, but the interesting one here is the carboxylase activity while the other one will be addressed later.

This reaction forms a very instable six carbon intermediate that immediately splits into two molecules of 3-PGA.

- In a second step, 3-PGA is reduced to a triose phosphate. The molecule is first phosphorylated by the phosphoglycerate kinase (PGK) using a molecule of ATP (leaving behind an ADP and a P_i) to produce one molecule of 1,3-bisphosphoglycerate (1,3-BPGA), that is reduced by the glyceraldehyde 3-phosphate dehydrogenase (GAPDH), using NADPH (releasing NADP^+ and H^+), to form a 3C sugar called glyceraldehyde 3-phosphate (G3P). It is important to note that for every three molecules of CO_2 fixed to RuBP molecules, six G3P molecules are produced while six ATP and six NADPH molecules are consumed. However, only one of these six G3P molecules leaves the cycle, because the others are required to regenerate RuBP via the Calvin-Benson pathway that includes several ATP consuming steps. The G3P that leaves the cycle will be used by a range of metabolic pathways to make simple sugars and complex carbohydrates like starch, and eventually other organic molecules like amino and organic acids, lipids etc.

The third step consists in the regeneration of three RuBP molecules from the remaining five G3P molecules. Indeed, the major function of the CB cycle is to allow the regeneration of RuBP to ensure the assimilation of CO₂. This regeneration begins with the isomerization of two molecules of G3P into dihydroxyacetone phosphate (DHAP), catalyzed by triose phosphate isomerase (TPI). The aldolase enzyme then combines DHAP and G3P to produce a 6C sugar, the fructose 1,6-bisphosphate (Fru1,6P₂) which is dephosphorylated by fructose 1,6-bisphosphatase (FBPase) to produce fructose 6-phosphate and a P_i. The next generated molecule is a 4C called erythrose 4-phosphate, it is produced by transketolase that removes and transfers two carbons from fructose 6-phosphate to another G3P molecule to generate a 5C sugar called xylulose 5-phosphate (xyl-5-P). Meanwhile, the erythrose 4-phosphate formed is combined with a DHAP (resulting from the isomerization of a G3P) to produce a 7C sugar, sedoheptulose 1,7-bisphosphate (S-1,7-P₂) *via* an aldolase. This 7C molecule is then dephosphorylated by sedoheptulose 1,7-bisphosphatase (SBPase), to make sedoheptulose phosphate (S-7-P) while releasing another P_i. Again, the transketolase removes two carbons from sedoheptulose phosphate to generate ribose 5-phosphate and transfers the 2C onto a G3P to make a second xyl-5-P. At this point three 5C sugars are available for the phosphopentose isomerase to produce three molecules of ribulose 5-phosphate (Ru-5-P) that are then phosphorylated using three molecules of ATP to finally produce three RuBP molecules.

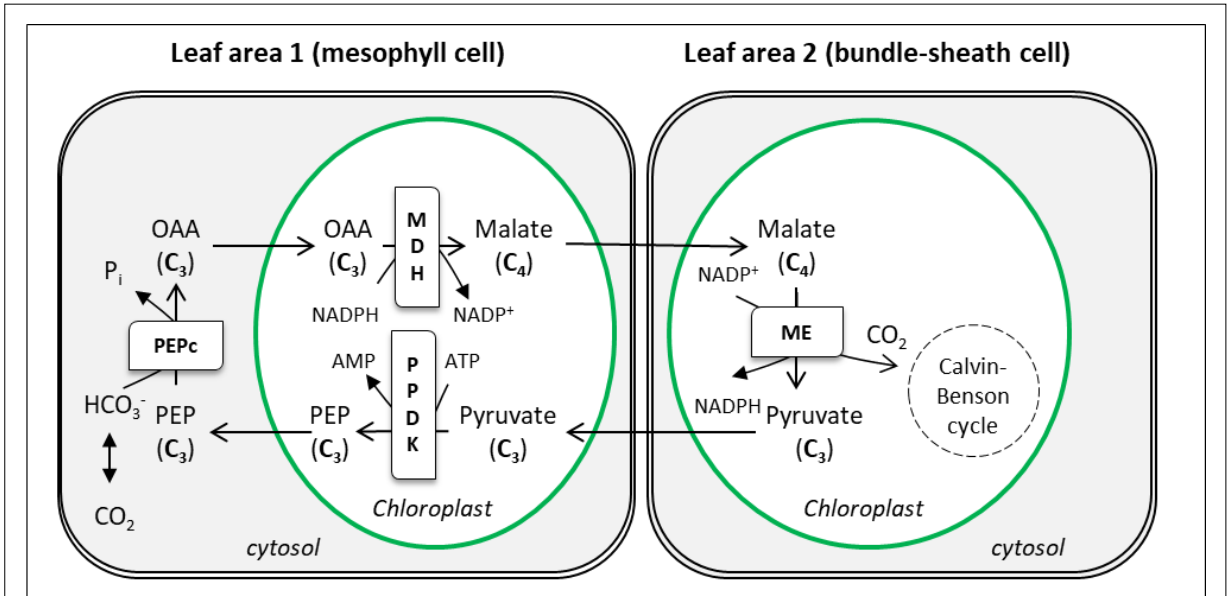
Many Calvin cycle enzymes are redox regulated by thioredoxins (TRX) and this helps to coordinate the dark reactions with the light reactions of photosynthesis. In the light, the electron transfer chain can reduce chloroplastic TRXs *via* the Fd/FTR (Fd-Trx reductase) system. In plants, there are five chloroplastic TRX forms called TRX f, m, x, y, and z that can regulate different target proteins *via* the reduction of disulfide bonds. Many Calvin cycle enzymes such as PRK, FBPase, SBPase, GAPDH and RuBisCO activase are activated in the light mainly by TRXf (Lemaire et al., 2007). Light-driven changes in stromal Mg²⁺/H⁺ concentrations can also have an influence on CB enzyme activities (Portis, 1981). Since the product of this cycle is a 3C sugar, plants in which this primary CO₂ assimilatory process occurs are called C₃ plants. A large panel of crop plants has this kind of photosynthesis like rice, wheat and potato but also our plant model *Arabidopsis thaliana*. However, some plants use different primary photosynthetic metabolic pathways like C₄ and CAM plants.

c) C₄ and CAM photosynthesis

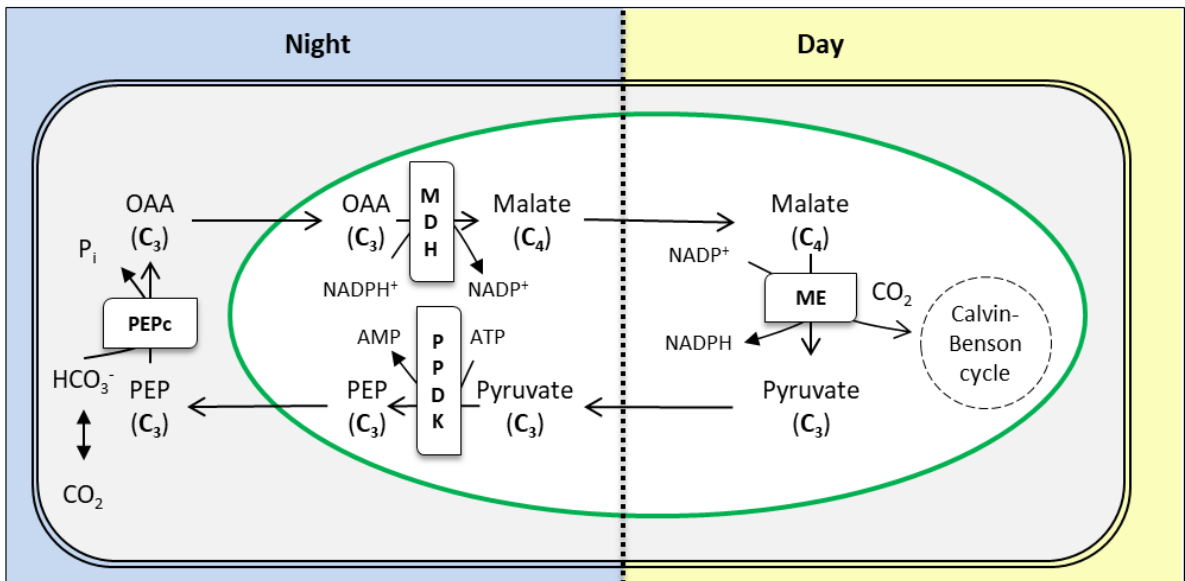
C₄ plants are so called because the first organic molecule produced *via* CO₂ assimilation is a 4C oxaloacetate molecule and not 3-PGA as in C₃ plants. Historically, C₄ plants have been classified under two major subtypes according to the decarboxylating enzyme of the 4C-acid: NAD-dependent malic enzyme (NAD-ME), NADP-dependent malic enzyme (NADP-ME) or PEP carboxykinase C₄

photosynthesis. In C_4 plants, the light-dependent reactions and the CB cycle are physically separated (Figure 3). Light-dependent reactions occur in the mesophyll cells (large tissues in the middle of leaves) and the CB cycle occurs in specialized bundle-sheath cells that surround the vascular tissues and are surrounded by mesophyll cells, ensuring an easy communication between these two cell types. Primary CO_2 assimilation is carried out by the phosphoenolpyruvate carboxylase (PEPc) in the mesophyll cells and this produces oxaloacetate (a 4C organic acid) that is converted to malate (by malate dehydrogenase) in the NADP-ME subtype (while aspartate is produced in the NAD-ME type). I will continue to describe only the NADP-ME form of C_4 -photosynthesis. Malate is exported to the bundle-sheath cells where it is decarboxylated to release a molecule of CO_2 that is reassimilated by RuBisCO and the resulting 3-PGA either enters the CB cycle or it is used to make carbohydrates and other organic molecules as in C_3 plants. However, C_4 photosynthesis is more energy dependent. When a molecule of CO_2 is produced from malate, a molecule of pyruvate is formed, and it must return to the mesophyll cells to continue the C_4 -process. To obtain the 3C molecule needed to fix another CO_2 , pyruvate is transformed to phosphoenolpyruvate *via* pyruvate orthophosphate dikinase which requires a molecule of ATP. However, C_4 photosynthesis has the advantage of maintaining a high concentration of CO_2 around the RuBisCO, and this minimizes a wasteful metabolic process called photorespiration. The C_4 pathway is used in about 3% of vascular plants, like sorghum, sugarcane, and maize, and it is common in hot climate areas. The photosynthetic rate of C_4 plants is much better than that of C_3 plants for the same amount of light and their water-use is more efficient since they can maintain their stomata less open and still undertake efficient photosynthesis. It has been determined that the evolution of C_4 photosynthesis occurred independently more than 60 times through 19 angiosperm families (Brautigam and Gowik, 2016).

Some plants adapted to dry environments, such as cacti and pineapples, have developed another way of carrying out photosynthesis called crassulacean acid metabolism (CAM), and named after a family of plants, the Crassulaceae, in which scientists first discovered this pathway. Instead of a compartmentation in space of the photosynthetic steps like the C_4 plants, compartmentation occurs in time, however both pathways are similar (Figure 3). During the night, stomata of CAM plants remain open and CO_2 enters the cells where it is fixed by PEPc as in C_4 plants. This produces oxaloacetate which is converted to malate by a NAD-dependent malate dehydrogenase. Malate is stored in vacuoles until daylight when CAM plants close their stomata and malate is transported out of the vacuole, and decarboxylated to generate CO_2 that is fixed by RuBisCO.



C₄: spatially separated



CAM: temporally separated

Figure 3: Other photosynthetic pathways: C₄ and CAM

PEPc: phosphoenolpyruvate carboxylase; MDH: malate dehydrogenase; ME: malic enzyme; PDK: pyruvate phosphate dikinase; PEP: phosphoenolpyruvate; OAA: oxaloacetate; AMP: adenosine monophosphate; ATP: adenosine triphosphate; NADPH/NADP⁺: nicotinamide adenine dinucleotide phosphate reduced/oxidized.

2) RuBisCO (EC 4.1.1.39) and 3-PGA

Ribulose 1,5-bisphosphate carboxylase oxygenase is a bifunctional enzyme as indicated from its name. For its carboxylase activity, RubisCO uses RuBP and CO₂ as substrates to produce two molecules of 3-PGA that is the starting point to build all organic molecules in a plant. For its oxygenase activity, RuBisCO also uses RuBP as a substrate but binds O₂ instead of CO₂. This reaction produces one molecule of 3-PGA that can still feed the CB cycle, and one molecule of 2-phosphoglycolate (2-PG) that initiates the 2C-cycle (or photorespiratory cycle). The partitioning between these two activities depends on the CO₂/O₂ balance around the RuBisCO (Servaites and Ogren, 1977).

RuBisCO is a high importance enzyme and it is the most abundant in C₃ plants, it contains up to 30 % of the total leaf N content. It is a divalent cation dependent enzyme (mostly known as Mg²⁺ dependent but also Mn²⁺) localized in the chloroplast, composed of two types of subunits, usually called the large chain (RBCL; about 55kDa) encoded by a chloroplast gene and the small chain (RBCS; about 15k Da) encoded by several nuclear genes. There are three forms of RuBisCO in the kingdom of life: the form I is made of 8 RBCS and 8 RBCL and thus it is a hexa-decamer, while the form II is made of one or more iso-dimers composed of a subunit sharing about 30 % identity with RBCL from form I, and finally the form III is also composed of one to five iso-dimers of subunits homologous to those found in form II. A fourth form, form IV of RuBisCO, is called the RuBisCO-like protein and although it is structurally related to RuBisCO it is involved in sulfur metabolism. The predominant form is the form I that can be found in terrestrial and marine plants, eukaryotic algae, and some bacteria, while the form II is found in other bacteria and dinoflagellates and the form III is found in archaea (Tabita et al., 2007; Tabita et al., 2008). In *Arabidopsis thaliana*, four nuclear genes encode the small subunits (*RBCS1A*, At1g67090; *RBCS1B*, At5g38430; *RBCS2B*, At5g38420; *RBCS3B*, At5g38410), and only one chloroplastic gene encodes the large subunit (*RBCL*, AtCG00490) (Krebbers et al., 1988; Sato et al., 1999). For a functional RuBisCO, chaperones are needed to fold and assemble the different subunits (Vitlin Gruber and Feiz, 2018). The enzyme is then activated by carbamylation (addition of CO₂) of a specific lysine in the active site and the binding of a divalent cation (Mg²⁺ or Mn²⁺) (Miziorko and Sealy, 1980; McCurry et al., 1981; Pierce and Reddy, 1986). The use of Mg²⁺ or Mn²⁺ by the RuBisCO is still debated (Bloom and Lancaster, 2018a) because while the fixation site is the same, it has been suggested that this could change the RuBisCO activity and especially the oxygenase/carboxylase activities of the enzyme. However, all RuBisCO structures described in the RCBS databank contain only Mg²⁺. Once RuBisCO is activated by carbamylation and cation fixation, the active site becomes “open”, forming a ternary complex, and the activated lysine can act as a base

for the transfer of a proton from RuBP. The enzyme containing its substrate, RuBP, constitutes an enol-RuBP, leading to the formation of an instable 2-carboxy-3-ketoarabinitol-1,5-bisphosphate or 2-peroxy-3-ketoarabinitol-1,5-bisphosphate, by respectively fixing CO₂ or O₂ (Cleland et al., 1998; Bloom and Lancaster, 2018a). The carboxylase activity of the RuBisCO produces two molecules of 3-PGA while its oxygenase activity releases a molecule of 3-PGA and a molecule of 2-PG. RuBisCO can be inhibited by several molecules, like sugar phosphates that obstruct the active site by binding to the carbamylated or decarbamylated form of the enzyme but they can be removed by RuBisCO activase (Parry et al., 2008). This last enzyme is a member of the AAA⁺ super family, a large family of NTPases that typically form hexameric ring complexes involved in remodelling of macromolecules (Iyer et al., 2004). Its role is to remove inhibitors from the active site with the consumption of ATP, allowing the RuBisCO to perform a new catalysis (Spreitzer and Salvucci, 2002). It is redox activated in the light *via* TRXf which is reduced by the photosynthetic electron transfer chain. Moreover this enzyme is dependent on the ATP/ADP ratio for its ATPase activity (Portis Jr et al., 2007). RuBisCO is a notoriously inefficient enzyme due to its low catalytic rate, but this appears to be compensated for by very high amounts of the enzyme in chloroplasts. It has become a target to improve C₃-plant photosynthesis, with an aim to express either a more efficient RuBisCO or a RuBisCO with an improved carboxylase/oxygenase activity balance even though it has been proposed that RuBisCO is probably already optimized (Tcherkez et al., 2006; Evans, 2013).

Both carboxylase and oxygenase activities of RuBisCO produce 3-PGA, a key metabolite in plants. It enters the Calvin-Benson cycle during the dark side of photosynthesis where it is transformed into DHAP and G3P, both triose-phosphates involved in the regeneration of RuBP *via* the Calvin-Benson cycle. In the chloroplast, 3-PGA is also a molecule involved in starch biosynthesis, making a carbon stock during day that can be used in the absence of light. Triose-phosphates and 3-PGA are also exported outside of the chloroplast by a triose phosphate transporter (TPT) in exchange for inorganic phosphate. Here they can enter gluconeogenesis and make sugars including sucrose that can be exported to other organs (Facchinelli and Weber, 2011). In the cytosol, 3-PGA is also involved in glycolysis that leads to the production of pyruvate which is converted to acetyl-CoA to feed the TCA cycle (in mitochondria) and lipid biosynthesis.

Since my PhD project focuses on the regulation of two primary metabolism proteins, phosphoglycerate mutase (PGAM) involved in glycolysis and phosphoglycolate phosphatase (PGLP) in photorespiration, both pathways will be described below, starting with glycolysis.

II) Glycolysis

Glycolysis is a ubiquitous process that occurs in living cells, tissues and organs. It is a catabolic pathway producing energy and reductant as ATP and NADH and it produces building blocks for other metabolic pathways. The reverse pathway, called gluconeogenesis, generates hexoses from low weight molecules. Glycolysis can produce pyruvate which fuels the TCA cycle and respiration in mitochondria which are both very important for autotrophic organisms. In glycolysis, for each molecule of glucose, 2 ATP molecules are utilized, while 4 ATP, 2 NADH, and 2 pyruvate molecules are produced. The enzymes of the glycolytic pathway were first characterized mainly in yeast and muscle cells and it was called the Embden-Meyerhof-Parnas pathway in honour of the major contributors to the discovery. Between 1900 and 1950, the glycolytic pathway was also studied in plants. In 1948, P Stumpf (Stumpf, 1948) purified and characterized the first plant glycolytic enzyme, an aldolase. After which, cytosolic enzymes of glycolysis were discovered and studied in higher plants. By comparing these enzymes with some chloroplastic enzymes, it became clear over the years that a nearly complete set of glycolytic isoenzymes was present in plastids strongly suggesting that the glycolysis pathway might partly occur in chloroplasts or non-photosynthetic plastids. However, it has been shown that the kinetic and regulatory properties of the plastid enzymes differ compared to the cytosolic ones. This is probably the result of the evolution, the major role of this pathway in plant development and its function to produce energy and reductant. Some glycolytic enzymes in the cytosol are not in the “conventional pathway”, like the pyrophosphate-dependent phosphofructokinase, the non-phosphorylating and non-reversible glyceraldehyde 3-phosphate dehydrogenase, a phosphoenolpyruvate phosphatase and some enzymes that allow the production of pyruvate while avoiding the pyruvate kinase step. Glycolysis in plants is surely a primordial pathway but the plant has evolved and adopted some specific tricks (bypasses, special enzymes) to gain flexibility and pursue its role under stress conditions (Plaxton, 1996; Givan, 1999).

1) Global description of glycolysis

The function of glycolysis is to oxidize hexoses to provide ATP, reducing power and pyruvate while also producing precursors for anabolism. Glycolysis can be divided in two parts: the first produces two molecules of G3P from one molecule of glucose while consuming two molecules of ATP. During the second part, transformation of glyceraldehyde 3-phosphate to pyruvate produces 4 molecules of ATP (Figure4).

Glucose is first transformed into glucose 6-phosphate (Glu-6-P) *via* hexokinase that need Mg^{2+} to be activated, thus consuming ATP. Glu-6-P is then isomerized by phosphoglucose isomerase to produce

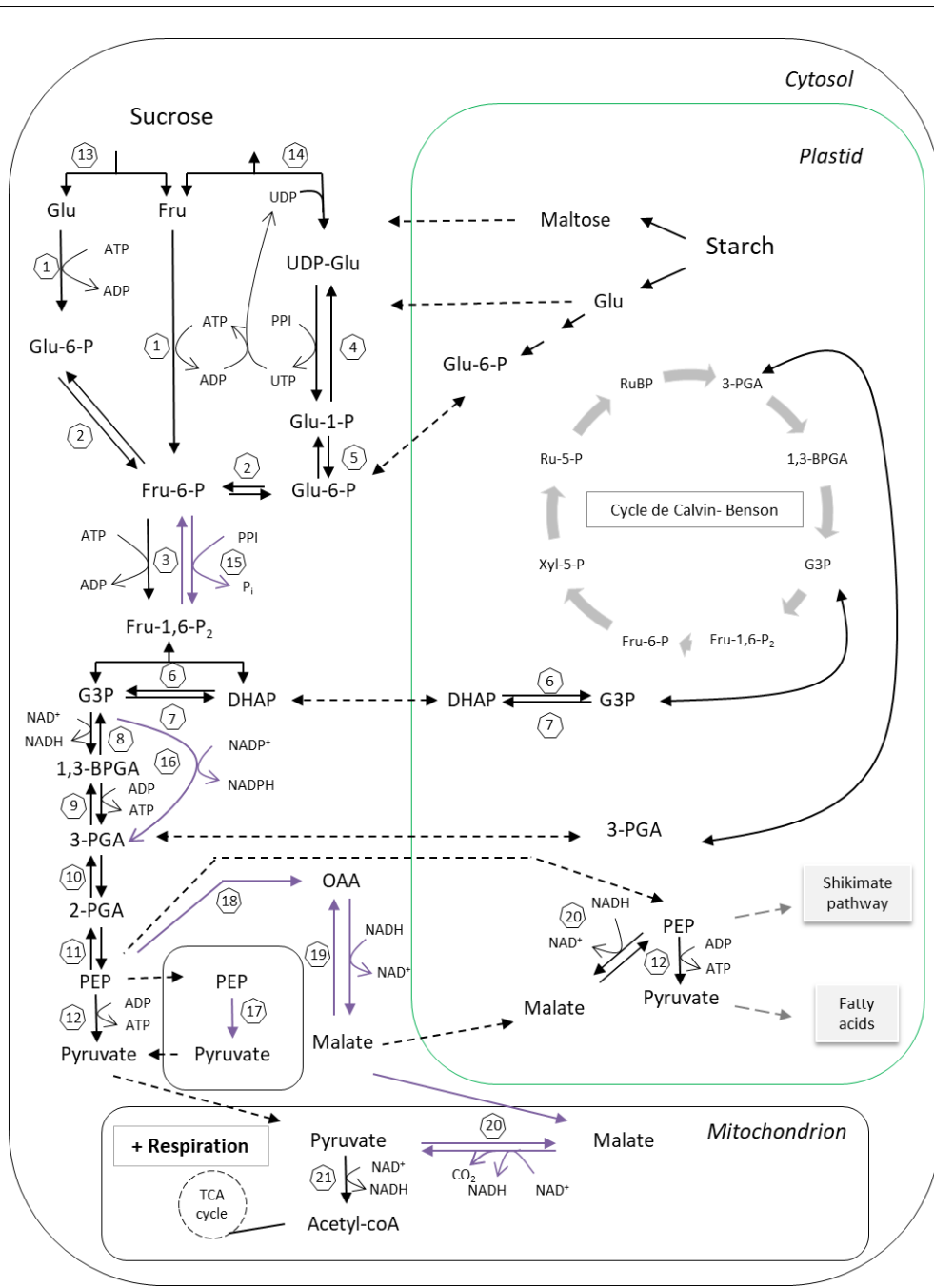


Figure 4: Overview of glycolysis in plants

Glu: glucose; Fru: Fructose; P: phosphate; Pi: orthophosphate; PPI: pyrophosphate; Glu-1-P: glucose 1-phosphate; Glu-6-P: glucose 6-phosphate; Fru-6-P: fructose 6-phosphate; Fru-1,6-P₂: fructose 1,6-biphosphate; DHAP: dihydroxyacteon phosphate; G3P: glyceraldehyd 3-phosphate; 3-PGA: 3-phosphoglycerate; 1,3-BPGA: 1,3-biphosphoglycerate; PEP: phosphoenolpyruvate; OAA: oxaloacetate; NADH/NAD⁺: nicotinamide adenine dinucleotide reduced/oxidized; NADPH/NADP⁺: nicotinamide adenine dinucleotide phosphate reduced/oxidized; UTP/UDP: Uridine tri/di-phosphate; 1:hexokinase; 2: phosphoglucose isomerase; 3: ATP-dependent phosphofruktokinase; 4: UDP-glucose phosphorylase; 5: phosphoglucomutase; 6: aldolase; 7: triose phosphate isomerase; 8: NAD-dependent glyceraldehyd 3-phosphate dehydrogenase; 9: 3-phosphoglycerate kinase; 10: phosphoglycerate mutase; 11: enolase; 12: pyruvate kinase; 13: invertase; 14: sucrose synthase; 15: pyrophosphate-dependent phosphofruktokinase; 16: NADP-dependent glyceraldehyd 3-phosphate dehydrogenase; 17: phosphoenolpyruvate phosphatase; 18: phosphoenolpyruvate carboxylase; 19: malate dehydrogenase; 20: malic enzyme; 21: pyruvate dehydrogenase.

fructose 6-phosphate (Fru-6-P) which is phosphorylated by the ATP-dependent phosphofructokinase (PFK) generating a molecule of fructose 1,6-bisphosphate (Fru-1,6-P₂), and consuming a molecule of ATP. Hydrolysis of Fru-1,6-P₂ by aldolase produces two 3C molecules, DHAP and G3P. DHAP is converted to G3P by triose phosphate isomerase. G3P is then oxidized to 1,3-diphosphoglycerate (1,3-DPGA) by NAD-dependent glyceraldehyde 3-phosphate dehydrogenase (NAD-GAPDH) thus producing NADH. The next step is the first energy producing step, it transforms 1,3-BPGA into 3-phosphoglycerate (3-PGA) and makes an ATP. This 3-PGA is transformed into 2-phosphoglycerate (2-PGA) by phosphoglycerate mutase and an enolase then catalyses the conversion of 2-PGA to phosphoenolpyruvate (PEP). The second ATP-producing step is catalysed by pyruvate kinase which forms pyruvate from PEP. At the end of glycolysis, one molecule of glucose gives two molecules of pyruvate and one NADH while there has been a net production of two molecules of ATP. It is also important to note that substrates for glycolysis can have origins other than cytosolic sucrose, for instance glucose can come from starch breakdown that produces maltose and glucose. Some metabolites are mutual with the pentose phosphate pathway and move between plastids and the cytosol (Ruan, 2014).

The key source of glucose in the cytosol is sucrose coming from hydrolysis of sucrose by an invertase thus producing glucose and fructose. The fructose formed is then phosphorylated by hexokinase to make fructose 6-phosphate, the same enzyme that phosphorylates glucose. On the other hand, sucrose synthase can produce UDP-glucose that is then converted to glucose 1-phosphate (Glu-1-P) while producing a molecule of uridine triphosphate (UTP) that is recycled to produce UDP-glucose. The Glu-1P is isomerized by UDP-glucose pyrophosphorylase to form Glu-6P to pursue glycolysis. Moreover, the “regular” described glycolysis is not a single straight-ahead pathway and some “bypasses” are possible for the conversion of some molecules. For example, the conversion of Fru-6-P to Fru-1,6-P₂ can be catalysed by a pyrophosphate-dependent phosphofructokinase (PFP), using pyrophosphate as a phosphoryl donor in a reversible reaction which is dependent of fructose 2,6-bisphosphate (Carnal and Black, 1979). Most of this activity occurs under low-phosphate conditions that are not optimal for a full ATP-dependent phosphofructokinase activity (Sabularse and Anderson, 1981; Wu et al., 1983; Hajirezai et al., 1993). Another possible bypass is the non-reversible conversion of G3P to 3-PGA by a NADP-specific 3-phosphate dehydrogenase enzyme (NADP-GAPDH) with no requirement for neither orthophosphate nor ADP (Iglesias and Losada, 1988; Scagliarini et al., 1990). Finally, an important bypass concerns the conversion of PEP to pyruvate in the cytosol that does not involve pyruvate kinase which is the only enzyme that can transform PEP to pyruvate in the plastid, however there are several other pathways in the cytosol. First, PEP can exit glycolysis and undergo a carboxylation to produce OAA in a reaction mediated by PEPc. The OAA is reduced to malate by a malate dehydrogenase where it can enter directly into the mitochondria to be converted

to pyruvate by NAD-specific malic enzyme. Radiocarbon-labelling showed that this pathway was activated mostly by phosphate deficiencies even if it contributed to pyruvate formation in normal conditions but at a low rate (Bryce and ap Rees, 1985; Duff et al., 1989; Edwards et al., 1998). A vacuolar phosphatase that prefers PEP to any other phosphorylated substrate also represents another possible bypass to produce pyruvate. Again, the highest activity of this phosphatase was found in conditions of low phosphate. This suggests the existence of movements of both PEP and pyruvate across the vacuole membrane (Duff et al., 1989; Plaxton, 1996).

Moreover, in plastids, glucose for glycolysis can come from starch that can produce glucose and maltose respectively from maltodextrin (a linear glucan) by a disproportionation enzyme (DPE1) or β -amylase (Lu and Sharkey 2006; Stitt and Zeeman 2012). Besides its enzymatic activity, hexokinase is a glucose sensor involved in sugar-sensing and the regulation of gene expression (Smeekens et al., 2010). However, some steps of glycolysis cannot be completed in the chloroplast but the presence of many transporters allow the required molecules to be imported (Weber and Linka, 2011).

Surprisingly, a study of the mitochondrial enzymes revealed that a set of glycolytic enzymes were present in low abundance on the outer mitochondrial membrane, this was proved by protease. This was confirmed by enzymatic assays using mitochondrial fractions and ^{13}C -labelling experiments. The hypothesis of the authors was the presence of this set of glycolytic enzymes associated with mitochondria allowed a direct production of pyruvate around the mitochondria to feed the TCA cycle (Giegé et al., 2003)

2) Can metabolites move between the cytosol and plastids?

Having established the existence of two glycolysis pathways (partial or entire) a remaining question concerns the exchange of metabolites between the subcellular compartments. It is known for many years now that triose phosphates, and 3-PGA can be exported from the chloroplast to the cytosol (Weber and Linka, 2011). Since plastids do not have a complete set of glycolytic enzymes, these movements between cytosol and plastids are therefore very important to complete the pathway. Some aspects of transport processes differ between photosynthetic and non-photosynthetic cells. Most of the transport occurring between plastids and cytosol are counter exchanges due to chloroplasts arising from an endosymbiotic event and the need to maintain host and endosymbiont mutual benefits. The inner membrane of plastids contains many kinds of transporters. In general, plastid translocators are highly hydrophobic proteins with at least eight α -helical transmembrane domains linked by short hydrophilic spacers. Some glycolytic intermediates need to circulate from one compartment to another. The corresponding transporters are described

below, although it should be noted that there are many other transporters in the inner chloroplast membrane.

The triose phosphate/phosphate translocator (TPT) exchanges triose phosphates (DHAP, G3P) and 3-PGA against orthophosphates is an important transporter since these metabolites are shared between the Calvin cycle in the chloroplast and glycolysis in the cytosol (Heldt et al., 1991). Moreover, triose phosphates can move from the chloroplast to the cytosol and be transformed into 3-PGA thus producing NADH. The 3-PGA can be re-introduced into the chloroplast to be re-assimilated *via* the CB cycle (Flügge and Heldt, 1984).

The Gluc-6-P/phosphate translocator is found mainly in non-photosynthetic tissues. Indeed, sucrose is transported in the phloem to non-photosynthetic cells where Gluc-6-P synthesized in the cytosol can enter the plastid *via* this translocator to allow either starch biosynthesis or feeding of the pentose phosphate cycle to generate reducing power required for the synthesis of many molecules like fatty acids, for example (Tetlow et al., 1996; Kammerer et al., 1998; Bowsher et al., 2007b). In heterotrophic tissues the plastidic glucose transporter moves the glucose produced from the starch degradation from the plastid to the cytosol (Weber et al., 2000).

Maltose is the major product of starch degradation at night. The high level of maltose accumulated in an *A. thaliana* mutant allowed the identification of the plastid maltose transporter called MEX (Niittyla et al., 2004).

The PEP/phosphate translocator imports PEP from the cytosol in exchange for Pi. PEP is a key metabolite in several pathways including fatty acid biosynthesis due to pyruvate and acetyl-CoA production, and PEP is a precursor along with erythrose 4-P in the shikimate pathway which is important for aromatic amino acid and secondary metabolite biosynthesis (Fischer et al., 1997; Herrmann and Weaver, 1999).

Further information about plastid inner membrane transporters can be found in the following reviews (Linka and Weber, 2010; Weber and Linka, 2011).

The movement of metabolites through the plastid outer membrane is possible through outer envelope proteins (OEP) that were first discovered in *Pisum sativum*. There are several OEPs that have their own specificities and affinities. For example *Arabidopsis thaliana* has three isoforms of OEP16 which are specific for amino acids and amines, OEP21 is specialized in the movement of phosphorylated carbohydrates such as triose phosphates, hexose phosphates and inorganic phosphate while OEP24 is not very selective and it can move amino acids, ATP, Pi and even dicarboxylates. Finally, the recently characterized OEP37 was found to be highly expressed in germinating seedlings and at embryogenesis stages implying a role in storage-type plastids. Even if its expression and conformation has been deciphered, little is known about its selectivity but its

presence in storage organs suggests that OEP37 probably transports fatty acids and amino acids (Goetze et al., 2006; Duy et al., 2007).

3) How are plant glycolytic proteins regulated?

Since glycolysis is a primordial metabolic pathway and a vital source of energy and pyruvate, it is a highly regulated pathway and this depends on the environment, the development stage, the tissue and the subcellular localization of the proteins. Indeed, it is now admitted that glycolytic pathways are not isolated and can interact with one another, although the different isoenzymes are not regulated the same way. For example, a study of PFK from castor bean revealed that the plastid PFK was activated by orthophosphate while the cytosolic protein was insensitive. Moreover the plastid protein was more inhibited by PEP when compared to the corresponding cytosolic enzyme and it was inactivated by ATP while cytosolic PFK was inactivated by 3-PGA (Garland and Dennis, 1980).

Broadly speaking, glycolytic enzymes can be regulated at many levels:

As seen for many metabolic pathways, glycolysis can be regulated by the variation in substrate/cofactor levels. Some assays with privation of either adenylates or Pi induced a decrease of adenylate-dependent enzyme activities, like PFK, 3-phosphoglycerate kinase and pyruvate kinase, or the Pi-dependent proteins efficiency such as NAD-glyceraldehyde 3-phosphate dehydrogenase. As previously mentioned, Pi starvation tended to increase cytosolic bypass pathways.

Furthermore, the pH in plant organelles often changes according to environmental conditions, soil nutrients and between day and night, it can affect glycolytic enzymes. During the daylight, pH increases in the stroma of plastids and inhibits leaf PFK (Copeland and Turner, 1987). When pH increases in the cytosol, PEPc has a greater activity and is less sensitive to inhibitors. This has been observed in several plant species and tissues (soybean nodules, maize leaves, banana fruits and cotyledons of *R.communis*). It has also been shown that the light-alkalinisation and dark-acidification of the cytosol are correlated with the light activation and dark inactivation of PEPc in C_4 plants (Rajagopalan et al., 1993).

Metabolic effectors represent another level of glycolysis regulation. There is a ubiquitous effect of PEP, Fru-2,6-P₂, Pi, and TCA cycle intermediates on glycolytic enzymes. PFK from plastids and the cytosol were both inhibited by PEP while PEP also allosterically inhibited cytosolic aldolase. Fru-2,6-P₂ activated PFK but had no impact on PFK. Moreover, TCA cycle intermediates like citrate, 2-oxoglutarate, succinate, and malate are feedback inhibitors of many plant PK and PEPc enzymes. When these intermediates are consumed *via* anabolism, glycolytic flux can increase again (Podestá and Plaxton, 1994). Finally, some amino acids like glutamate and aspartate have been reported to

have a negative impact on some PEPc and cytosolic PKs like in the green algae *S.minutum* and soybean root nodules (Schuller et al., 1990b; Schuller et al., 1990a).

It has also been shown that oligomer dissociation is often linked to a decrease of enzyme activity. This is an important regulatory mechanism for cytosolic PK, PFK and PEPc (Traut, 1994).

An important way to achieve protein regulation is *via* post-translational enzyme modifications. This is highlighted by the redox regulation of sugar metabolism. Starch metabolism has been shown to be highly regulated by oxidation-reduction and that this could be a part of its day/night regulation (Skryhan et al., 2018). Moreover, in the context of glycolysis, there is consistent evidence that some enzymes are regulated by disulphide-dithiol interconversion like PFK (Funato et al., 2013). Thiol reduction is shown to increase PFP efficiency in tomato fruit and wheat endosperm as well as in potato tuber (Podestá and Plaxton, 1994). Several recent works have focused on the regulation of NAD-GAPDH by oxidation-reduction. NAD-GAPDH undergoes several redox-related post-translational modifications like S-glutathionylation and S-nitrosylation. Site-directed mutagenesis of cysteines showed that these residues were important for substrate binding, activity, and sub-cellular localization. This protein has been suggested to be a cell redox sensor (Vescovi et al., 2013; Zaffagnini et al., 2013b; Zaffagnini et al., 2013a; Schneider et al., 2018). It has been demonstrated *in vitro* using a recombinant protein and *in vivo* that Fru 1,6-biphosphate aldolase is S-glutathionylated (van der Linde et al., 2011). Finally, it was established that TPI can be inhibited by S-glutathionylation and that this modification can be reverted by glutaredoxin (GRXC1 and GRXC2 in *A. thaliana*) (Dumont et al., 2016).

However, the most common post-translational modification is protein phosphorylation. Many plant glycolytic enzymes have been shown to be regulated by this mechanism including PEP carboxykinase, and sucrose phosphate synthase, while the best characterized is PEPc (see Boex-Fontvieille et al., 2013). Indeed, even if this last enzyme is not a glycolytic enzyme strictly speaking, it is associated with this pathway *via* its anaplerotic function (Walker and Leegood, 1995; Chollet et al., 1996; Huber and Huber, 1996). Among potential phosphosites, it has been proved that cytosolic pyruvate kinase can be phosphorylated, and this triggers its proteasome addressing (Tang et al., 2003).

Finally, since the next paragraph is going to deal with photorespiration and 2-PG detoxification, it seems important to mention that it has been shown for a long time that PFK and triose phosphate isomerase can be inhibited by 2-PG (Anderson, 1971; Kelly and Latzko, 1976).

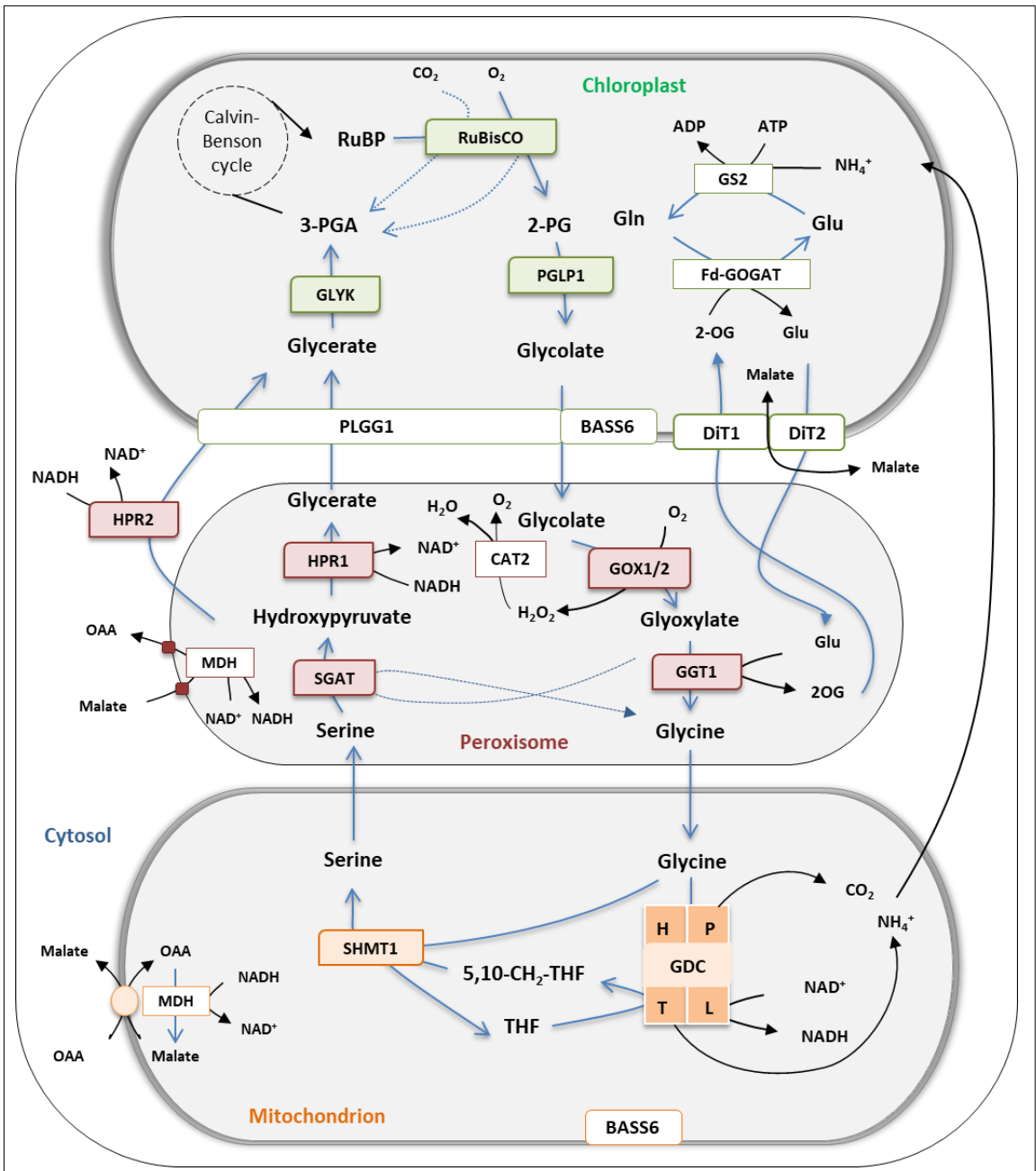


Figure 5: Overview of the photorespiratory cycle and some related pathways

2-PG: 2-phosphoglycolate; 3-PGA: 3-phosphoglycerate; RuBP, ribulose-1,5-bisphosphate; 2OG: 2-oxoglutarate; Gln: Glutamine; Glu: Glutamate; NADH/NAD⁺: nicotinamide adenine dinucleotide reduced/oxidized; RuBisCO, RuBP carboxylase/oxygenase; PGLP1: 2-phosphoglycolate phosphatase 1; PLGG1: plastidial glycolate/glycerate transporter; BASS6: bile acid sodium symporter 6; GOX1/2: glycolate oxidase 1 and 2; GGT : glutamate:glyoxylate aminotransferase 1; GDC: glycine decarboxylase complex (composed of the P, T, L, H proteins); SHMT1: serine hydroxymethyl transferase 1; BOU: A BOUT DE SOUFFLE; SGAT: serine:glyoxylate aminotransferase 1; HPR1/2: hydroxyypyruvate reductase 1/2; GLYK1: glycerate kinase 1; CAT2: catalase 2; DiT: Chloroplatic decarboxylate transporters: DiT1, plastidial 2OG/malate transporter 1 and DiT2, plastidial glutamate-malate transporter 2; Fd-GOGAT: ferredoxin-dependent glutamate synthase; GS2: plastidial glutamine synthetase; OAA: oxaloacetate; THF: tetrahydrofolate.

III) The photorespiratory cycle

1) What is photorespiration?

The photorespiratory cycle (or 2C-cycle) is a major metabolic pathway initiated by the oxygenase activity of RuBisCO that can be defined as a process of O₂ uptake and CO₂ release occurring in the light (Figure 5). It is a complex pathway taking place in four different cell compartments: chloroplasts, mitochondria, cytosol and peroxisomes. In C₃-plants, the proportion of oxygen fixation by RuBisCO is about 25 % against 75 % for CO₂ but this depends on environmental conditions. RuBisCO oxygenase activity leads to the production of two molecules. One is 3-PGA, a useful molecule that can feed the Calvin-Benson cycle, the other is 2-PG which is a toxic molecule that can inhibit several primary metabolism enzymes; TPI and SBPase of the CB cycle, and the glycolytic enzyme PFK (Anderson, 1971; Kelly and Latzko, 1976; Flügel et al., 2017). The aim of the 2C-cycle is therefore to recycle this toxic compound to form another useful 3-PGA molecule, thus it has detoxification and C-recovery roles. The recycling of two 2-PG molecules leads to the release of one CO₂ and a molecule of NH₄⁺ in mitochondria, therefore C and N can be lost unless they are reassimilated. Moreover, since the fixation site for CO₂ and O₂ on RuBisCO is the same (Tcherkez et al., 2006), there is competition between carboxylase and oxygenase activities and thus between photosynthesis and photorespiration that reduces plant photosynthetic potential. Since, photorespiration was considered an energetically wasteful process, the photorespiratory cycle became a target to improve plant productivity and to create high-yield crops (Betti et al., 2016). The photorespiratory cycle requires eight core enzymes for the recycling of 2-PG produced by RuBisCO, several transporters and some auxiliary enzymes that contribute and interact with the cycle (Foyer et al., 2009; Bauwe et al., 2010; Hodges et al., 2013; Hodges et al., 2016). The discovery and the study of photorespiratory mutants, not only for genes coding for the core enzymes but also those associated with interacting pathways, showed impaired development and metabolism in ambient air that highlighted the major role of this pathway for plant productivity. Indeed, the 2C-cycle is interacting with many other metabolic pathways like amino acid metabolism, 1C metabolism, redox homeostasis, nitrogen metabolism, TCA cycle and respiration. Such interactions appear to be important for plant stress responses. For example, photorespiratory H₂O₂ production in peroxisomes has been shown to have an impact on plant-pathogen responses (Rojas and Mysore, 2012). Moreover, the 2C-cycle is a sink for ATP and NADPH consumption that is required to maintain photosynthetic electron transfer and limit the eventual production of reactive oxygen species (ROS) under certain conditions like high light. The oxygenase activity of RuBisCO is also involved in the

regulation of abiotic stresses *via* ROS production and stomatal aperture, for example (Wingler et al., 2000; Hodges et al., 2016). Finally, photorespiration is tightly coupled to nitrogen metabolism *via* the re-assimilation of photorespiratory ammonium by the GS-GOGAT cycle and the important need of Glu for photorespiratory amino-transferase activity (Coschigano et al., 1998; Linka and Weber, 2005).

The appearance and evolution of the photorespiratory cycle have been debated since a very long time. However new insights into the understanding of this pathway and the phylogeny of photorespiratory proteins has led to a new hypothesis, notably an earlier appearance and evolution of the 2C-cycle dating back to cyanobacteria. Indeed, the first considerations on photorespiratory evolution ignored the fact that there were times when RuBisCo had to deal with high O₂ levels even when under water, thus leading to the appearance of CO₂ concentration mechanisms (CCMs) in algae, before plants colonized the land (Becker, 2013). It is now believed that photorespiration co-evolved in cyanobacteria because of the presence of 2-PG produced due to local O₂ enrichment (Lalonde and Konhauser, 2015). To test the hypothesis of an early photorespiratory cycle in cyanobacteria two approaches were pursued: first, the phylogenetic study of photorespiratory enzymes in prokaryotes and eukaryotes, and second the dating of CCMs using fossils and isotope signatures (Hagemann et al., 2016). It was found that photorespiratory enzymes have a dual origin from cyanobacteria and α -proteobacteria, which is against the cyanobacteria to land plants evolutionary theory. However, an explanation could come from the endosymbiotic α -proteobacterium and cyanobacterium ancestors that gave rise to plant mitochondria and chloroplasts. During these events, endosymbiotic gene transfer(s) and segregation(s) occurred that led to the loss of some gene copies from cyanobacteria because of a functional redundancy with those already established in the proteobacteria. However, a cyanobacterial contribution can be detected from the presence of a cyanobacterial derived L protein of the GDC complex in the mitochondria of land plants. The deciphering of the origin of photorespiratory enzymes predated the evolution of oxygenic photosynthesis and thus glycolate metabolism required for the removal of toxic 2-PG (Kern et al., 2011; Kern et al., 2013). Although the case of GOX seems more complex and is still debated only the phosphoglycolate phosphatase evolution is different since it originated from Archaea. The phylogeny study of the photorespiratory enzymes brought the first evidence suggesting a coevolution of photosynthesis and the 2C-cycle 2700 million years ago. Moreover, an early appearance and evolution of CCMs in cyanobacteria could be another hint for an early photorespiratory cycle before the colonization of land plants. Indeed, geological elements suggest that the CCMs appeared in cyanobacteria before 400 Mya (when a high increase of atmospheric O₂ appeared) (Eisenhut et al., 2008). Another clue for the early evolution of CCMs in cyanobacteria, comes from their division into two sub-groups of α - and β -cyanobacteria according to the CMM type (α - or β - carboxysome). The β -carboxysome is specific of cyanobacteria and the main divergence of

the β -cyanobacteria occurred around 2200 Mya ago before the “Great Oxygenation Event”, suggesting that at least this type of CMM evolved before the separation (Blank and Sánchez-Baracaldo, 2010; Schirromeister et al., 2013). These considerations led to the conclusion of the coevolution of photosynthesis, photorespiration and CCMs from cyanobacteria to algae and land plants (Hagemann et al., 2016).

A genetic approach using *Arabidopsis* was primordial to identify photorespiratory genes and to show the importance of the C₂-pathway in air-grown plants. In the late seventies, while working in the Ogren laboratory, Chris Somerville devised an EMS-mutagenesis approach and a high (1 %) -to-low (0.03-0.035 %) CO₂ growth phenotype screen which led to the discovery of several *Arabidopsis* photorespiratory mutants. Since the 1 % CO₂ environment led to a very low photorespiratory activity, seeds mutated in the 2-cycle pathway were able to develop normally (Somerville, 2001). Plants that showed either growth delay or chlorosis were eliminated from the screen and the remaining plants were shifted to a “low CO₂” environment. Plants that developed chlorosis in these conditions were identified as potential photorespiratory mutants and they were shifted back to 1 % of CO₂ to observe if they recovered (Somerville, 2001). The first photorespiratory mutant published had a mutation in the *phosphoglycolate phosphatase (PGLP1)* gene and was named *CS119* (Somerville and Ogren, 1979). Then, *sat*, *stm* and *glyD* were characterized as mutants of peroxisomal serine-glyoxylate aminotransferase, mitochondrial serine hydroxymethyl transferase and the gene coding for the P-protein of the mitochondrial glycine decarboxylase complex. These mutants were described as “photorespiratory mutants” by Somerville’s team, defined by chlorosis and growth arrest that could be rescued at high CO₂ concentrations. Moreover *CS119*, *sat*, *stm* and *glyD* showed an important decrease of net photosynthetic CO₂ assimilation rate at 50 % O₂ that disappeared at 2 % O₂ (Somerville and Ogren, 1980c; Somerville and Ogren, 1980a; Somerville and Ogren, 1981; Somerville and Ogren, 1982). Some mutants were not identified during this screen because of an absence of phenotype that was partly due to genetic redundancy for example, in *A. thaliana* there are five GOX-related genes although only two of them are involved in photorespiration (Reumann et al., 2007; Deller et al., 2016a). This redundancy can also be seen *via* bypasses such as HPR1/HPR2/HPR3 (Timm et al., 2008; Timm et al., 2011a). The collection of “Somerville” mutants was the first evidence showing the 2C-cycle to be primordial in a C₃ model plant. Since then, an extensive catalogue of photorespiratory mutants has been generated, including crop species such as barley, pea, tobacco, potato and rice (Wallsgrave et al., 1986; Murray et al., 1987; Blackwell et al., 1988; Schjoerring et al., 2006; Xu et al., 2009), leaving no doubt that this cycle is crucial for C₃-plants. If it is understandable that this cycle is necessary for C₃ plants, this appears to be also the case for C₄ plants even though RuBisCO oxygenase activity in C₄ plants is lower compared to that of C₃ plants because of their CO₂ concentration mechanism that promotes their RuBisCO carboxylase activity. For example the CO₂

Table1: Overview of Arabidopsis photorespiratory genes and publications corresponding to mutant characterization

Enzyme	Gene name	Location	References to Arabidopsis thaliana mutants
2-PG production			
RuBisCO	RBCS1A	At1g67090	Currently not identified/no publications
	RBCS1B	At5g38430	
	RBCS2B	At5g38420	
	RBCS3B	At5g38410	
	RBCL	AtCG00490	
2-PG recycling			
Phosphoglycolate phosphatase	PGLP1	At5g36700	Sommerville and Ogren, 1979 ; Schwarte et Bauwe, 2007
Glycolate oxidase	GOX1	At3g14420	Rojas et al., 2012 ; Deller et al., 2016
	GOX2	At3g14415	
Glutamate:glyoxylate aminotransferase	GGT1	At1g23310	Igarashi et al., 2003 ; Deller et al., 2015b
Glycine decarboxylase complex	GDP1	At2g26080	Engel et al., 2007
	GDP2	At4g33010	Engel et al., 2007
	GDT	At1g11860	Timm et al., 2018
	LPD2	At3g17240	Currently unidentified/no publications
	LPD1	At1g48030	
	GDH1	At2g35370	
	GDH2	At2g35120	
GDH3	At1g32470		
Serine hydroxymethyl transferase	SHMT1	At4g37930	Somerville and Ogren, 1981; Voll et al., 2006
	SHMT2	At5g26780	Engel et al., 2011
Serine:glyoxylate aminotransferase	SGAT1	At2g13360	Somerville and Ogren, 1980
Hydroxypyruvate reductase	HPR1	At1g68010	Timm et al., 2008 Timm et al., 2011
	HPR2	At1g79870	
	HPR3	At1g12550	
Glycerate kinase	GLYK1	At1g80380	Boldt et al., 2005
Ammonia re-assimilation			
Plastidial 2OG/malate transporter	DiT1	At5g12860	Taniguchi et al., 2002
Plastidial glutamate-malate transporter	DiT2.1	At5g64290	Renné et al., 2003
Fd-Glutamate synthase	Fd-GOGAT1	At5g04140	Coshigano et al., 1998
Plastidial glutamine synthetase	GS2	At5g35630	Currently unidentified/no publications
H ₂ O ₂ detoxification			
Catalase	CAT2	At4g35090	Queval et al., 2007
Core photorespiration transporters			
Plastidial glycolate/glycerate transporter	PLGG1	At1g32080	Pick et al., 2013
Plastidial glycolate transporter	BASS6	At4g22840	South et al., 2017

compensation point in C₄ plants like sorghum was 4 to 5 times lower than in sunflower (Laisk and Edwards, 2000). Furthermore, an antisense inhibition of photorespiratory GOX (*ZmGO1*) in *Zea mays* resulted in an air sensitive plant that could not develop (Zelitch et al., 2009). Taken together, the growth phenotypes of all photorespiratory mutants highlight the necessity of recycling toxic 2-PG to feed the CB cycle.

As mentioned above, the 2C-cycle is initiated by the oxygenase activity of RuBisCO (that occurs in all organisms containing a form I RuBisCO), producing one molecule of 3-PGA and one molecule of 2-PG that needs to be recycled. It is thus dephosphorylated by PGLP1 in the chloroplast, to produce glycolate that is exported to the cytosol from chloroplasts by two transporters PGGL1 and BASS6 (Pick et al., 2013; South et al., 2017). Glycolate then enters peroxisomes (by an unknown mechanism) where it is transformed to glyoxylate by GOX and this enzymatic step also releases H₂O₂. The glyoxylate produced is converted to glycine by glutamate:glyoxylate aminotransferase (GGT1) to form glycine. This step also converts glutamate to 2-oxoglutarate. Glycine moves from peroxisomes to mitochondria where it is converted into serine with the release CO₂ and NH₄⁺ and the reduction of NAD to NADH *via* two enzymes, the glycine decarboxylase complex (GDC) and serine hydroxymethyl transferase (SHMT). Serine thus generated is moved to peroxisomes where it is de-aminated to produce hydroxypyruvate *via* another aminotransferase called serine:glyoxylate aminotransferase (SGAT1), while also generating a glycine molecule from glyoxylate. Hydroxypyruvate is then reduced to glycerate by hydroxypyruvate reductase (HPR) that uses NADH as a cofactor. Since peroxisomes only contain a NAD carrier called PXN (van Roermund et al., 2016) and NADH cannot diffuse across the peroxisomal membrane it is produced enzymatically in the peroxisome by malate dehydrogenase (pMDH) (Cousins et al., 2008). The cycle ends where it started, in the chloroplast, where glycerate 3-kinase (GLYK) produces a molecule of 3-PGA from a molecule of glycerate. Therefore, to make one 3-PGA molecule requires two 2-PG molecules and therefore the photorespiratory cycle only recovers 3 of the 4 carbons that enter the pathway since a CO₂ molecule is also produced.

2) What are the core photorespiratory enzymes?

a) The core photorespiratory enzymes

The 2C-cycle is composed of eight core enzymes: Phosphoglycerate phosphatase (PGLP1); glycolate oxidase (GOX1 and GOX2 in Arabidopsis), glutamate:glyoxylate aminotransferase (GGT1), a glycine decarboxylase complex (GDC), serine hydroxymethyl transferases (SHMT1), serine:glyoxylate aminotransferase (SGAT1), hydroxypyruvate reductases (HPR1) and glycerate kinase (GLYK1) (Figure 5). The genes encoding these proteins were mostly identified by the photorespiratory phenotypes of

their respective mutants (chlorosis, retarded growth, lethality) in ambient air, their recovery in high CO₂ and perturbations in photosynthesis, metabolism and growth after their transfer from high CO₂ to ambient air (reviewed by Timm et al., 2013). All genes and related mutants are summarized in Table1.

Everything starts in the chloroplast...

Phosphoglycolate phosphatase (EC 3.1.3.18 ; PGLP):

Phosphoglycolate phosphatase 1 (PGLP1) is the first core enzyme of the photorespiratory cycle (if we do not consider the RuBisCO) and therefore it catalyses the first step of 2-PG detoxification and carbon recycling by dephosphorylating 2-PG to produce glycolate. Since my PhD work has been focused on this enzyme, it will be described later in more detail.

Continues in the peroxisome...

Glycolate oxidase (EC 1.1.3.15 ; GOX):

Glycolate oxidases belong to the (L)-2-hydroxy-acid oxidase flavin-dependent family (Esser et al., 2014) and they have evolved from bacterial lactate oxidase. In *Arabidopsis thaliana*, there are five GOX related genes: *At3g14420*, *At3g14415*, *At4g18360*, *At3g14130* and *At3g14150* encoding respectively GOX1, GOX2, GOX3, HAOX1 and HAOX2. GOX3 is mainly expressed in roots and senescent leaves, and it has a higher affinity for lactate compared to GOX1 and GOX2 and therefore it could play a role in lactate metabolism (Engqvist et al., 2015; Maurino and Engqvist, 2015). HAOX1 and HAOX2 are expressed in seeds and show fatty acid oxidase activities (Esser et al., 2014). Only GOX1 and GOX2 are considered to be redundant photorespiratory enzymes according to their tissue-specific expression, mainly in the leaves. Moreover, while single *gox1* and *gox2* mutants did not display a photorespiratory phenotype, an RNAi line targeting both genes did (Dellero et al., 2016b). In the photorespiratory cycle, the role of GOX is to transform glycolate into glyoxylate through an oxidation reaction that produces H₂O₂ and uses O₂ as a co-substrate and flavin mononucleotide (FMN) as a cofactor. No GOX mutant was identified as a photorespiratory mutant in the first screen of *Arabidopsis* by Somerville (Somerville and Ogren, 1982; Blackwell et al., 1988). Indeed, the single *gox1* and *gox2* mutants showed a residual GOX activity of 35 % and 65 % that allowed them to grow normally in air. Since a double mutant would be almost impossible to obtain as the two genes (*At3g14420* and *At3g14415*) are genetically linked, an *Arabidopsis* miRNA line (*amiRgox1/2*) was produced that only contained 5 % leaf GOX activity (Dellero et al., 2016b). *amiRgox1/2* plants showed a Class II (see definition in section III.3) photorespiratory phenotype that was rescued in

0.3 % CO₂. When these plants were transferred from high CO₂ to normal air, the amount of glycolate in the leaves increased more than 700-fold and there was a 50% decrease of net CO₂ assimilation rate and altered amino acid contents. These elements showed that GOX1 and GOX2 had a redundant role in photorespiration. However, by crossing the *gox2* mutant with the *cat2-2* mutant, mutated in the gene encoding peroxisomal catalase 2, the photorespiratory phenotype was not as important as the *cat2-2/gox1* mutant. This result together with the residual GOX activity in the single *gox* mutants strongly suggested that GOX1 was the predominant isoform (Kerchev et al., 2016). Finally, GOX activity *via* the formation of H₂O₂ plays a role in plant defence reactions as seen in *A. thaliana*, rice, tomato and tobacco (Rojas et al., 2012; Chern et al., 2013; Gilbert and Wolpert, 2013; Ahammed et al., 2018).

Glutamate:glyoxylate aminotransferase (EC 2.6.1.4 ; GGT):

Glutamate:glyoxylate aminotransferase is a peroxisomal enzyme that can transfer an amine group from glutamate to glyoxylate to form glycine and 2-OG. In *A. thaliana*, two loci encode glutamate:glyoxylate aminotransferases: *AtGGT1* (*At1g23310*) and *AtGGT2* (*At1g70580*) (Igarashi et al., 2003; Liepman and Olsen, 2003). This step of the cycle is linked to the GS/GOGAT cycle in the chloroplast that requires 2-OG and produces glutamate. Two plastidial transporters are involved in this exchange, DiT1 and DiT2 (described below). The *GGT1* gene was 50-fold more expressed than *GGT2* in *Arabidopsis* rosette leaves and the *ggt1* knock-out mutant, with only a residual 5 % activity, exhibited a weak class II photorespiratory phenotype (see section III.3) since it could survive in normal air (Igarashi et al., 2003; Deller et al., 2015). The phenotype of *ggt1* was rescued in high CO₂, low light intensity, or with 3 % glucose in the growth medium (Igarashi et al., 2003). *GGT1* is also expressed in roots and flowers albeit at very low levels thus suggesting that its activity could also be required in other pathways. As seen with other photorespiratory mutants, air-grown *ggt1* was not only impaired in its photosynthetic activity but also in its RuBisCO content when compared to the wild type. These phenotypes were found also after a transfer from high CO₂ to normal air. It was proposed that the photorespiratory mutation caused a decrease of photosynthetic carbon assimilation that reduced nitrogen assimilation and RuBisCO content to maintain C:N balance (Deller et al., 2015a).

Then move to the mitochondrion...

Photorespiratory glycine decarboxylase and serine hydroxymethyl-transferase reactions occur in mitochondria and together they produce one molecule of CO₂, NH₄⁺, NADH and tetrahydrofolate (THF) when making one molecule of serine from two molecules of glycine.

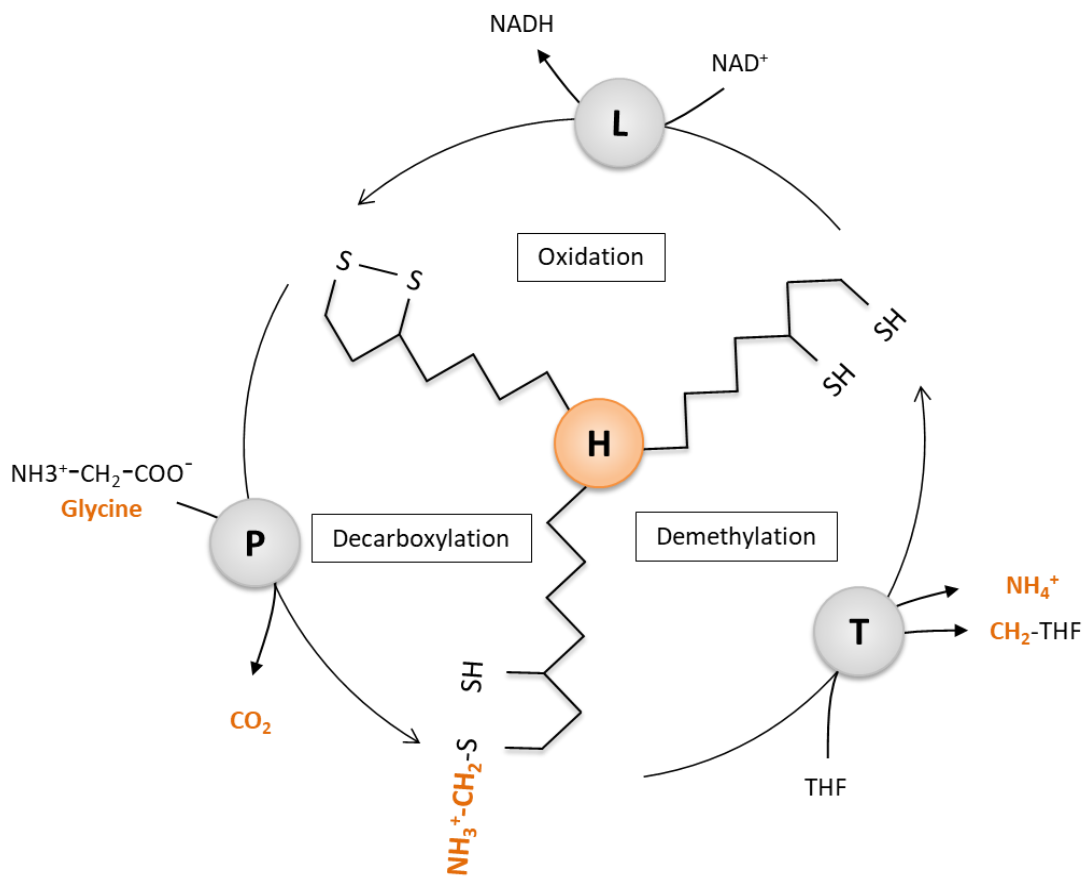


Figure 6: Diagram of the GDC system showing the different steps of the overall reaction and the role of each protein in the complex (inspired from Douce et al 2001)

NADPH/NADP: Nicotinamide adenine dinucleotide phosphate; THF: Tetrahydrofolate

Glycine decarboxylase complex (GDC)

The glycine decarboxylase complex (Figure 6) is a multienzyme complex involving four proteins that produce serine from two molecules of glycine. The P-protein (glycine decarboxylase; GDP; EC 1.4.4.2) is a pyridoxal-5-phosphate-containing homodimer (200 kDa) and it is the glycine decarboxylase per se that catalyses the decarboxylation of glycine and the release of photorespiratory CO₂ (Hasse et al., 2010). The H-protein (hydrogen carrier protein; GDH; 14 kDa) is a small protein that links the other proteins of the complex, being more a cofactor than an enzyme. The H-protein conveys the remaining amino-methylene group of glycine from the P-protein to the T-protein. The T-protein (aminomethyltransferase; GDT; EC 2.1.2.10) transfers the amino-methylene to a tetrahydrofolate (THF) to generate 5,10-methylene-THF (CH₂-THF), along with the production of NH₄⁺. Finally, the L-protein (LDP; EC 1.8.1.4, 45 kDa) is a homodimeric dihydrolipoamide dehydrogenase that re-oxidizes the fully reduced lipoamide arm of the H-protein. Here electrons are first transferred to an FAD cofactor, which is re-oxidized by NAD⁺ thus resulting in the formation of NADH (Bauwe and Kolukisaoglu, 2003a). In the *A. thaliana* genome, there are two P-protein genes (*At2g26080* and *At4g33010*), two L-protein genes (*At1g48030* and *At3g17240*), three H-protein genes (*At1g32470*, *At2g35120* and *At2g35370*) and a single T-protein encoding gene (*At1g11860*). The GDC step ensures links with other pathways since the release of NH₄⁺ can participate to N-metabolism, it involves glycine and serine and therefore amino acid metabolism while the intervention of THF makes a strong link with 1C metabolism (Douce et al., 2001; Bauwe and Kolukisaoglu, 2003b).

Single *gdp1* and *gpd2* mutants have no visible phenotype in normal air, thus suggesting a potential functional redundancy. However, at 4 °C under high light, there is a significant increase of glycine in leaves. On the other hand, the mutation of both P-protein encoding genes is lethal even in high CO₂, probably because of their importance in other essential pathways for plant development like 1C metabolism (Engel et al., 2007). Moreover, it was recently revealed that the knock-out mutant for the gene encoding the T-protein is lethal whatever the conditions (high CO₂, 2 % sucrose) (Timm et al., 2018) while 5 % of T-protein activity was enough to obtain 30 % activity of GDC and allow plant growth in normal air with only a slight phenotype (lower photosynthesis, higher amount of glycine, and a growth phenotype). Since *GDT* over-expressors did not promote a better plant development or photorespiratory rate, it is reasonable to think that this protein is not limiting for the GDC reaction (Timm et al., 2018). It is interesting to note that unlike the T-protein, the overexpression of either the H-protein or the L-protein led to a more efficient photorespiratory cycle, better photosynthesis and plant biomass (Timm et al., 2012a; Timm et al., 2015a; López-Calcagno et al., 2019)

Serine hydroxymethyl-transferase (EC 2.1.2.1 ; SHMT):

Serine hydroxymethyl-transferase catalyses the transfer of a hydroxymethyl group from 5,10-methylene-THF to a molecule of glycine to form serine. This step releases a molecule of THF that can be reused by the GDC complex. In *A. thaliana*, there are seven genes encoding serine hydroxymethyl-transferases (*AtSHMT1-7*) but only two proteins are targeted to mitochondria (SHMT1 57 kDa encoded by *At4g37930*, and SHMT2 59 kDa encoded by *At5g26780*). Mitochondrial SHMT appears to be very important since experiments using *Pisum sativum* showed that the hydroxymethyl-transferase activity was 10-fold higher in mitochondria when compared to other cell compartments (Neuburger et al., 1996). SHMT has been shown to be highly related to 1C metabolism in many organisms, not only plants but also bacteria and even humans (Renwick, 1998; Douce et al., 2001; Simic et al., 2002), but it also has a key role in the production of serine (Ros et al., 2014). The role of SHMT in the photorespiratory cycle was first demonstrated by Somerville and Ogren in 1980 with the *stm* mutant. Since then, the SHMT gene associated with *stm* was identified and the mutant was renamed *shm1-1* (Voll et al., 2006). The SHMT isoenzyme in leaf mesophyll cell mitochondria has been shown to be SHMT1 (Voll et al., 2006; Engel et al., 2011). The *shm1-1* mutant displays a moderate class II photorespiratory phenotype (see section III.3). In this mutant there was a 50 % decrease of leaf hydroxymethyl-transferase activity and almost a total absence of activity in mesophyll cell mitochondria. Serine levels were significantly lower than in WT leaves while the glycine level was 100-fold higher after a 5-day transfer from high CO₂ to normal air together with a decrease of CO₂ uptake (Somerville and Ogren, 1981; Engel et al., 2011). It turns out that *SHMT2* is more expressed in roots and shoot apical meristems and it is restricted to the vascular tissues of leaves. SHMT2 cannot complement the *shm1-1* photorespiratory phenotype (Voll et al., 2006; Engel et al., 2011). The *shmt2-1* mutant showed no visible phenotype in normal air, but the double mutant *shmt1-2×shmt2-2* has been defined as a class I photorespiratory mutant (see section II.3) since it was lethal even when grown in high CO₂. However, when grown *in vitro* in low light/0.9 % CO₂ with the addition of sucrose to the growth medium, plants eventually produced infertile seeds (Engel et al., 2011).

Let's go back to the peroxisome...

Serine:glyoxylate aminotransferase (EC 2.6.1.45 ; SGAT):

Serine produced in mitochondria is transferred to peroxisomes where it is de-aminated by serine:glyoxylate aminotransferase to form hydroxypyruvate and an amino group that is transferred to glyoxylate to produce glycine. Indeed, this reaction is important for the stoichiometry of the photorespiratory cycle because two glycine molecules are needed to produce serine in mitochondria.

In *A. thaliana*, a single gene (*SGAT1*, *At2g13360*) encodes this enzyme and a knock-out mutant was identified in the initial screen of Somerville (*sat* mutant) because of its photorespiratory phenotype. When compared to WT plants, leaves of *sat* assimilated 3-fold less CO₂, serine and glycine over-accumulated, while starch and sucrose contents were found to be lower (Somerville and Ogren, 1980b). Studies of recombinant SGAT protein revealed three distinct aminotransferase activities with alanine:glyoxylate, serine:glyoxylate and serine:pyruvate but the serine:glyoxylate activity was 5-fold higher than the others (Liepman and Olsen, 2001). Later it was shown that the most efficient substrate as an amino-donor was asparagine (Zhang et al., 2013). Surprisingly, in the *Arabidopsis* SGAT over-expressor, photosynthetic CO₂ uptake was much lower than in the WT and leaf area and number were reduced (25 % and 20-25 %, respectively). Moreover, in this mutant there was a decrease of asparagine and serine levels that was rescued in 1 % CO₂. This suggested that asparagine might be imported into the peroxisome to increase photorespiration. Finally, the decrease of photorespiratory serine led to an increase of the phosphoserine pathway during the night. This study gave new evidence supporting the importance of amino acids and especially serine content in the regulation of photorespiratory fluxes (Modde et al., 2017).

Hydroxypyruvate reductase (EC 1.1.1.29 ; HPR):

Hydroxypyruvate reductase is a NAD(P)H-dependent enzyme that catalyses the reduction of hydroxypyruvate to glycerate. There are three different genes encoding HPR reductases in *Arabidopsis thaliana* (*HPR1*, *At1g68010*; *HPR2*, *At1g79870*; *HPR3*, *At1g12550*). The peroxisomal enzyme is HPR1 (42 kDa) while HPR2 (34 kDa) is cytosolic and HPR3 (35 kDa) is plastidial (Timm et al., 2011a). *In vitro* measurements using either recombinant protein or leaf soluble extracts showed HPR1 to be the major NADH-dependent HPR although it can also use glyoxylate as a substrate and NADPH as cofactor. On the other hand, HPR2 is probably a NADPH-dependent reductase that showed little preference between hydroxypyruvate and glyoxylate. Finally, HPR3 activity was higher with glyoxylate than with hydroxypyruvate and its favourite cofactor was NADPH (Timm et al., 2008; Timm et al., 2011b). Studies of *hpr* mutants have allowed for a better understanding of the involvement of each enzyme in the photorespiratory cycle. First, *hpr1-1* knock-out mutants have a slight growth delay that can be rescued by a CO₂ concentration of around 0.15-0.2 %. This mutant was sensitive to photoperiod and light intensity as well as sucrose implementation and it showed a moderate class III photorespiratory phenotype probably due to functional redundancy. Isotope assays showed a 103-fold increase of hydroxypyruvate in *hpr1-1* compared to only a 3-fold increase in the *hpr2-1* mutant. The *hpr2-1* and *hpr3-1* mutants showed no visible phenotype in normal air and only slight metabolic changes in photorespiratory intermediates like glycerate, glycine and hydroxypyruvate. Furthermore, the double *hpr2-1*×*hpr3-1* mutant had no developmental phenotype.

All of these elements demonstrated that HPR1 was the major core enzyme of the photorespiratory cycle but hydroxypyruvate to glycerate conversion could be flexible (Timm et al., 2011b; Timm and Bauwe, 2013a). Concerning the other double mutants, contrary to the *hpr1-1* single mutant, the *hpr1-1×hpr2-1* double mutant had a stronger growth delay even if it was not lethal in normal air while *hpr1-1×hpr3-1* had a similar phenotype to the *hpr1-1* single mutant meaning that the involvement of the two different HPR-bypass reactions were not equal: chloroplastic HPR3 < cytosolic HPR2. Finally, the triple *hpr1-1×hpr2-1×hpr3-1* mutant showed a further impaired development, even though photochemical efficiency and CO₂ assimilation were similar to those of the *hpr1-1×hpr2-1* double mutant suggesting a secondary role for HPR3 in the 2C-cycle (Timm et al., 2011b). The LaPr 88/29 mutant of barley (*Hordeum vulgare* L.) lacking HPR1 has been shown to have residual 5 % NADH-dependent and 19 % NADPH dependent HPR activities, suggesting the presence of at least one other minor HPR protein (Murray et al., 1989). This minor protein was purified and characterized and named HPR2 (Kleczkowski et al., 1990). Finally, in rice, it was also shown that there was a peroxisomal OsHPR1 and a cytosolic OsHPR2 and only the double mutant showed a typical photorespiratory phenotype (Ye et al., 2014).

The cycle ends where it started, in the chloroplast...

Glycerate kinase (EC 2.7.1.31 ; GLYK):

Glycerate kinase is the final core enzyme of the photorespiratory cycle. It is a 39 kDa enzyme located in chloroplasts where it catalyses the phosphorylation of glycerate to produce 3-PGA thus connecting the 2C-cycle to the CB cycle. In *A. thaliana*, a single gene encodes glycerate kinase (*GLYK1*, *At1g80380*) and a mutant was not found initially in Somerville's screen because of its lethality at an early stage of plant development. The gene was identified using a partial protein sequence of glycerate kinase purified from *Arabidopsis* leaves (Boldt et al., 2005a). The *glyk1-1* and *glyk1-2* allelic mutants cannot grow in normal air but show a normal development in high CO₂ conditions. No glycerate kinase activity could be measured in these mutants and there was a 100-fold accumulation of glycerate in normal air-grown plants compared to high CO₂ thus confirming that *GLYK1* was the only gene encoding a photorespiratory glycerate kinase. It was first believed that *GLYK1* was only targeted to the chloroplast however a recent study has found that *GLYK1* mRNA displays a phytochrome-regulated alternative splicing. The longer mRNA produced the chloroplastic glycerate kinase during light-time while the shorter mRNA led to a cytosolic enzyme during darkness. Therefore, *GLYK1* has a light dependent subcellular localization. In the same study, using transgenic lines of *A. thaliana*, it was shown that when the chloroplastic protein was absent, the cytosolic form

could partially rescue the *glyk* lethal phenotype thus suggesting the existence of an eventual cytosolic bypass (Ushijima et al., 2017).

b) Photorespiratory transporters

All core photorespiratory enzymes have been identified, but this pathway is dispersed over four subcellular compartments: cytosol, chloroplast, mitochondrion and peroxisome. Theoretically, the photorespiratory cycle requires at least nine transporters since the core enzymes require cofactors and precursors that need to be imported and these events require at least five transporters. Moreover, the 2C-cycle is not an isolated metabolic pathway, it is intertwined with other major pathways like the re-assimilation of the NH_4^+ by the GS/GOGAT cycle, for example (these interactions are detailed in paragraph III.5.) and these photorespiratory-linked pathways depend on at least eleven transporters. Therefore, there is an estimated total of 25 transport events (Eisenhut et al., 2013a). Surprisingly, only five membrane transporters have been identified: DiT (chloroplastic dicarboxylate transporters, that include DiT1 and DiT2.1) (Taniguchi et al., 2002; Renné et al., 2003), PLGG1 (plastidial glycolate-glycerate transporter) (Pick et al., 2013), BASS6 (bile acid sodium symporter 6, which is a chloroplastic glycolate transporter) (South et al., 2017) and BOU (A BOUT DE SOUFFLE) (Lawand et al., 2002; Eisenhut et al., 2013b).

DiT transporters

Chloroplastic decarboxylate transporters were the first photorespiratory-related transporters identified and they are addressed to the inner chloroplast membrane. In *A. thaliana*, three genes encode DiT transporters: *At5g12860* (*AtpOTM1*) encodes DiT1, a 59 kDa protein, *At5g64290* (*AtDCT1*) encodes a 60 kDa protein DiT2-1 and finally *At5g64280* (*AtDCT2*) encodes a 58 kDa protein, DiT2-2. A mutant of one of these genes, *dct*, had been identified in a screen by Somerville and Ogren (1983) and it was shown to be a *dit2-1* mutant since it was complemented by the spinach ortholog *DiT2*. The Arabidopsis *dit2-1* knockout mutant has a class II photorespiratory, while the *dit2-2* mutant has no phenotype in normal conditions and therefore DiT2-2 is assumed either to be not involved in photorespiration, or there is a high redundancy (Taniguchi et al., 2002; Renné et al., 2003). The *omt1* mutant containing a T-DNA in the *DiT1* gene can grow in ambient air without any photorespiratory phenotype like a class IV mutant (Taniguchi et al., 2002). However, the antisense mutant for the same gene in tobacco displayed a growth delay, chlorosis, and a lower CO_2 assimilation rate combined with increased amounts of glyoxylate and ammonia in leaves, corresponding to a typical photorespiratory phenotype rescued in high CO_2 (Schneidereit et al., 2006). The use of reconstituted liposomes containing DiT-1 and DiT2-1 highlighted the fact that DiT1 could import 2-OG in exchange for malate, while DiT2-1 imported glutamate in exchange for malate (Taniguchi et al., 2002; Renné et

al., 2003). These chloroplastic transporters appear to have overlapping substrate specificities thus explaining the lack of a phenotype in the *Arabidopsis omt* mutant, but the role of DiT1 and DiT2-1 in the 2C-cycle is primordial because they are involved in the re-assimilation of ammonium generated by this pathway via the GS2/GOGAT cycle (described later in paragraph III.5).

Plastidial glycolate-glycerate transporter (PLGG1)

The plastidial glycolate-glycerate transporter is encoded by a single gene in *A. thaliana*, *PLGG1* (At1g32080), and as indicated by its name it can export glycolate from the chloroplast in exchange for glycerate. This transporter (54 kDa) was localized in the inner membrane of the chloroplast (Pick et al., 2013). While forward genetics allowed the identification of only one photorespiratory-related transporter (DiT2), PLGG1 was identified by a co-expression approach followed by a deep analysis using reverse genetics. The co-expression analysis assumed that genes involved in the same pathway showed similar expression patterns. PLGG1 was found to be co-expressed with 11 other 2C-cycle genes. PLGG1 was predicted to have 12 membrane-spanning helices, representing thus the best candidate as a transporter involved in this pathway (Pick et al., 2013). The T-DNA knockout mutant *plgg1-1* had a slightly retarded growth and leaf chlorosis. This phenotype was rescued by a high CO₂ environment, and corresponded to a class II photorespiratory phenotype. The role of PLGG1 was tested *in vitro* by measuring the amount of glycerate imported using reconstituted liposomes containing recombinant PLGG1 protein and labelled ¹⁴C-glycerate. Furthermore, ¹⁸O₂-label glycerate labelling of chloroplasts isolated from WT and *plgg1* leaves confirmed PLGG1 activity. Finally, the metabolite content of mutant leaves was measured following a transfer from high CO₂ to normal air, thus providing an *in vivo* demonstration of the role of PLGG1 as a glycolate/glycerate transporter of the photorespiratory pathway (Pick et al., 2013).

Bile acid sodium symporter 6 (BASS6)

The bile acid sodium symporter 6 (*BASS6*) is encoded by a single gene *At4g22840* in *A. thaliana*. Pick et al., (2013) first deciphered the role of PLGG1 as a photorespiratory transporter, however it has been demonstrated since, that the T-DNA *plgg1* mutant had the same CO₂ compensation point as WT plants, under low light conditions, suggesting another pathway for glycolate to exit the chloroplast (Walker et al., 2016). The identification of BASS6 was achieved by screening T-DNA insertion mutants for genes encoding proteins of the chloroplast inner membrane. The screen was to identify mutants impaired in PSII efficiency, displaying a reduction of F_v/F_m chlorophyll fluorescence (South et al., 2017). Bile acid sodium symporters are a family of proteins first identified in mammalian liver (Alrefai and Gill, 2007) but it is now known that BASS family transporters are present in many organisms like fungi, animals, and plants (mono- and di-

cotyledons), with a wide variety of substrates such as pyruvate, steroids, and xenobiotics (Furumoto et al., 2011; da Silva et al., 2013). The role of this transporter in *A. thaliana* was deciphered using the T-DNA insertion mutant *bass6-1*, displaying a photorespiratory phenotype rescued in high CO₂; slower growth in ambient air compared to the WT, accumulation or lack of photorespiratory intermediates (increased glycine and glycolate levels, lower amount of serine) and a lower photosynthetic rate. It showed a typical class III phenotype due to the functional redundancy of BASS6 and PLGG1. Moreover, the double mutant *bass6×plgg1* showed a further impairment of development and photosynthesis rate, while glycolate accumulated more than in the single mutants. These results support the idea that BASS6 and PLGG1 both export glycolate from the chloroplast but only PLGG1 can import glycerate (South et al., 2017).

A BOUT DE SOUFFLE (BOU)

As for PLGG1, *A BOUT DE SOUFFLE* was also identified as a potential photorespiratory gene using the co-expression analysis. Arabidopsis contains a single gene (*At5g46800*) and it was found to be co-expressed with 14 other photorespiratory genes. BOU is a 28 kDa protein that belongs to the mitochondrial carrier family and it has six transmembrane spanning domains. The T-DNA insertion mutant displayed a photorespiratory phenotype with fully repressed growth and chlorotic leaves that could be compensated by 0.3 % CO₂. The *bou-2* mutant also had a higher CO₂ compensation point and altered photorespiratory intermediate levels (increased glycine and 2-OG and decreased serine and glutamate) after a shift from high to low CO₂. The change in serine and glycine ratio was indeed due to a strongly reduced GDC activity due to P-protein degradation, measured after the transfer. Finally, *bou-2*, as with the previously characterized *bou-1* mutant (Lawand et al., 2002), stopped growing at the two cotyledon stage, a phenotype linked to a defective shoot apical meristem and the arrest of cell division in *bou-2* that was also found in the *shmt1* mutant (Eisenhut et al., 2013b). Until now, the exact substrate of BOU is still not yet clear but it is obvious that this transporter is essential for a balanced 2C-cycle and a well-organized and functional shoot apical meristem (Eisenhut et al., 2013b). Furthermore, the recent study focusing on the BOU transporter knock-down mutant *bou-2* showed that serine produced during photorespiration was the main precursor of cysteine biosynthesis, and therefore sulphate metabolism was impaired in this mutant. The modified GDC activity in *bou-2* disturbed sulphur-rich metabolites, but also led to a disrupted carbon and nitrogen metabolisms (Samuilov et al., 2018)

c) Other photorespiratory-related proteins, implied in recycling side products of the pathway

As mentioned before, the 2C-cycle is not an isolated pathway, but it is connected to several other metabolic pathways through metabolites produced during photorespiration. Indeed, from the H_2O_2 released by GOX activity in peroxisomes to the CO_2 and NH_4^+ produced in mitochondria by the GDC activity, several metabolites need to be either re-assimilated or detoxified. These processes participate actively to proper plant development, since mutants of these “photorespiratory-related genes” often display growth phenotypes in ambient air.

Catalase (EC 1.11.1.6 ; CAT)

Catalase is a 57 kDa peroxisomal protein allowing the transformation of $2\text{H}_2\text{O}_2$ to give O_2 and $2\text{H}_2\text{O}$. In *A. thaliana* there are three genes encoding catalases (*CAT1*, At1g20630; *CAT2*, At4g35090; *CAT3*, At1g20620). Although transcripts from each *CAT* gene can be found in *Arabidopsis* rosettes, *CAT2* and *CAT3* are more expressed in leaves while *CAT1* is more expressed in reproductive tissues like pollen and seeds. *CAT2* is mainly expressed in photosynthetic tissues but also in roots and seeds while *CAT3* is more expressed in vascular tissues (Frugoli et al., 1996; McClung, 1997). A mutant screen of barley first revealed the importance of catalase activity in C_3 plants and its involvement in the 2C-cycle. A catalase mutant with only 10 % of the WT activity displayed leaf bleaching and redox disturbances, but this was eradicated when grown at 0.2 % CO_2 (Kendall et al., 1983). In contrast, no photorespiratory catalase *Arabidopsis* mutant was identified in Somerville’s screen but the analysis of catalase RNAi lines showed smaller plants that were more sensitive to high light while this could be prevented by high CO_2 (Vandenabeele et al., 2004). Soon after, *Arabidopsis cat2* T-DNA mutants were identified that had a 10-15 % residual catalase activity in leaves and showed a typical class III photorespiratory phenotype with growth delay in ambient air, together with an accumulation of oxidized glutathione and a disruption in redox homeostasis, these phenotypes being rescued in high CO_2 (Queval et al., 2007). Since catalase activity in the mutant *cat1* leaves was the same as in Col-0 leaves, and the *cat3* mutant still showed 80% of Col-0 catalase activity, *CAT3* must have been responsible for the residual activity in *cat2* mutants. The *cat2cat3* double mutant was not smaller than the *cat2* single mutant. Since *cat1* and *cat3* single mutants did not exhibit neither a rosette size phenotype nor leaf glutathione level changes, this showed that *CAT2* in *A. thaliana* played the major role in the removal of photorespiratory-produced H_2O_2 and the maintenance of oxidation-reduction homeostasis in photosynthetic tissues (Queval et al., 2007; Mhamdi et al., 2010). Interestingly, while *cat2* displayed no leaf lesions in short day conditions, in long days the mutant developed necrotic lesions, together with redox changes and oxidized glutathione accumulation. At the same time, this mutant showed salicylic acid accumulation, while pathogen response genes and the camalexin

synthesis pathway were induced, thus improving the plant's resistance to pathogens (Chaouch and Noctor, 2010). Furthermore, during the transfer from high CO₂ to normal air, biotic and abiotic stress genes were induced (Queval et al., 2007). These studies support the notion that photorespiratory H₂O₂ is an important signal in biotic and abiotic stresses in *A. thaliana*.

The GS/FdGOGAT cycle

As mentioned above, photorespiratory GDC activity releases an equimolar amount of CO₂ and NH₄⁺. This latter molecule can be re-assimilated in the chloroplast by the action of two enzymes: chloroplastic glutamine synthetase (GS2) and Fd-dependent glutamine:oxoglutarate aminotransferase (Fd-GOGAT) that make up the GS/GOGAT cycle. The result of this coupled reaction is the production of glutamate from the assimilation of ammonium, a process that requires glutamine, ATP, 2-oxoglutarate and reduced Fd from photosynthetic electron transfer.

Glutamine synthetase (EC 6.3.1.2 ; GS)

The role of GS is to produce glutamine by the condensation of ammonium and glutamate, a process that consumes an ATP molecule. In *A. thaliana* there are 6 GS genes (*GS1-1*, *At5g37600*; *GS1-2*, *At1g66200*; *GS1-3*, *At3g17820*; *GS1-4*, *At5g16570*; *GS1-5*, *At1g48470*; and *GS2*, *At5g35630*). Interestingly, *GS2* is 10 times more expressed in *A. thaliana* rosette leaves than *GS1*; and its expression increases together with N concentrations. While *GS1* isoforms are cytosolic proteins (39-40 kDa), *GS2* is a 47 kDa chloroplastic protein (Moison et al., 2018). *GS2* is thus defined as the GS enzyme involved in the assimilation of NH₃ in the chloroplast (Lothier et al., 2010). Until now, there is no characterized mutant for the *GS2* gene of *A. thaliana*. Nevertheless, some mutants in orthologous genes can be found in other plants like *Lotus japonicus* (*Ljpr1-3*) and barley (*RPr83/32*). The barley *GS2* mutant showed a photorespiratory phenotype since it could not grow in normal air and required 0.8 % CO₂ to restore normal development. Furthermore after a transfer from high CO₂ to ambient air, this mutant accumulated ammonium (40 times more than the control) as early as 30 min after the transfer, while the assimilation of CO₂ was strongly impaired (Kendall et al., 1986; Wallsgrave et al., 1987). Similar results were found in *Lotus japonicus* with a 50-fold accumulation of ammonium in a *GS2* mutant that displayed only 30 % of normal leaf GS activity. After transfer from high CO₂ (7000 ppm) to ambient air, this mutant started to show chlorosis and necrosis after 48-72 h (Orea et al., 2002). These data demonstrated that *GS2* was the photorespiratory-related GS. A recent study with *A. thaliana* T-DNA mutants in *GS1* genes showed that *GS1-1*, *GS1-2*, *GS1-3*, and *GS1-4* had mostly redundant roles in the cytosol for primary N-assimilation, the regulation of seed production, germination, and pollen viability, and for an optimal vegetative growth. It was also mentioned that

GS1-1 played an important role in *Arabidopsis* tolerance to abiotic stresses and ROS homeostasis (Ji et al., 2019).

Fd-dependent glutamine:oxoglutarate aminotransferase (Fd-GOGAT, EC 1.4.7.1)

Glutamine:oxoglutarate aminotransferase (GOGAT) catalyses the transfer of an amide group from a glutamine to a 2-OG to produce two molecules of glutamate. There are two different forms of GOGAT depending on the reductant used: Ferredoxin (Fd-GOGAT; EC 1.4.7.1) and NADH (NADH-GOGAT; EC 1.4.1.14). It has been shown that a unique gene encodes NADH-GOGAT in *A. thaliana* (*GLT1*, At5g53460) and that this gene was more expressed in roots and vascular tissues. The corresponding mutant *glt1-T* displayed no photorespiratory phenotype but showed, on the contrary, a growth delay in high CO₂. This enzyme is believed to play a role in ammonium assimilation in non-green tissues (Coschigano et al., 1998; Lancien et al., 2002). Fd-GOGAT uses glutamine produced by GS2 as an amino-donor and they are both essential for the re-assimilation of NH₃ released during the 2C-cycle. In *Arabidopsis*, there are two genes encoding Fd-GOGAT (*Fd-GOGAT1*, At5g04140; *Fd-GOGAT2*, At2g41220). Both corresponding proteins are addressed to the chloroplast. In leaves, the most abundant enzyme is Fd-GOGAT1, and *Fd-GOGAT1* mutants with only 5 % of WT leaf activity had a class II photorespiratory phenotype and normal growth in 1 % CO₂. Mutants *CS30*, *CS103* and *CS113* that were found in the screen performed by Somerville and Ogren in 1980, had a 3-fold lower CO₂ assimilation rate when compared to WT plants and decreased glutamate levels besides an accumulation of ammonium and glutamine (Somerville and Ogren, 1980a). The mutation site was identified by cartography to be in *Fd-GOGAT1*. Additionally, *Fd-GOGAT2* mRNA was shown to preferentially accumulate in roots, suggesting that Fd-GOGAT1 was the main enzyme involved in leaf glutamate production and photorespiratory NH₄⁺ re-assimilation (Coschigano et al., 1998). It was proposed that both Fd-GOGAT1 and GS2 could be addressed also to mitochondria implying that re-assimilation of photorespiratory NH₃ could also happen in this compartment (Taira et al., 2004; Jamai et al., 2009). However, a point mutation line in *Fd-GOGAT1* (*glu1-201*) exhibited a photorespiratory phenotype like that of *shmt1-1* while neither Fd-GOGAT nor GS2 have been found in mitochondrial proteome analyses perhaps suggesting a low amount of these proteins in this compartment. The most plausible hypothesis was the regulation of SHMT activity by the presence of these proteins in mitochondria (Taira et al., 2004; Jamai et al., 2009).

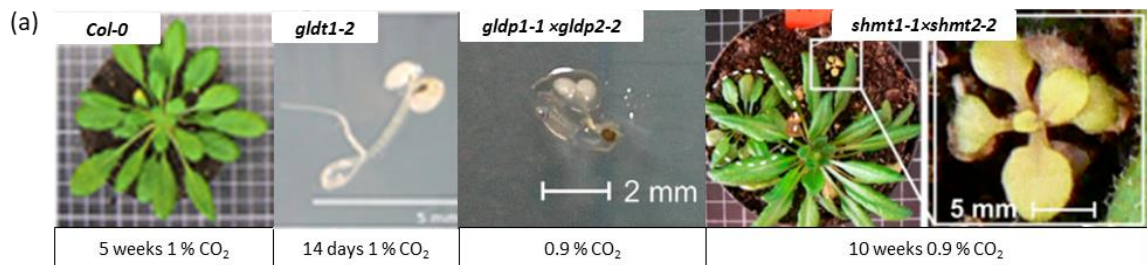
3) How do photorespiratory mutants behave?

Since the original screen performed by Somerville and co-workers who elaborated a strategy to identify and to characterize photorespiratory mutants (reviewed in Somerville, 2001), several other

mutants have been identified in *A. thaliana*. These not only include core enzymes but also some transporters and 2C-cycle related proteins involved for example in the re-assimilation of NH_3 and redox homeostasis. Studies of these mutants have helped to understand the key role of the 2C-cycle in plants, and how it impacts other metabolic pathways. This cycle was long considered as wasteful process however the phenotype of photorespiratory mutants led to the conclusion that it was not only an essential pathway in air-grown plants but also a potential target for crop plant improvement. Somerville and his colleagues worked on EMS-treated seeds and they tried to identify plants that displayed a growth phenotype in ambient air (growth delay, chlorosis and even lethality) that was absent in a high CO_2 environment. They described these features as a “photorespiratory phenotype”. The development of new analytical technics including access to *Arabidopsis* T-DNA insertion libraries led to the identification of yet undiscovered photorespiratory mutants which allowed a more specific and detailed classification of photorespiratory phenotypes. Indeed, there was not a unique photorespiratory phenotype but a range of phenotypes that relied on several criteria: physiological alterations, if the alterations could be rescued by a high CO_2 atmosphere, the presence of compensatory mechanisms, and the possible role of the enzyme in other metabolism pathways. Accordingly, four classes of photorespiratory mutants were described (Timm and Bauwe, 2013b) and they are summarized below.

Class I: Mutants show a lethal phenotype in normal air (Figure 7). Even a high CO_2 environment cannot rescue this phenotype, probably because its results from the inactivation of a gene encoding a protein required for other metabolic pathways. This class concerns two double mutants, *shmt1*×*shmt2* and *gldp1*×*gldp2*, and the recently identified GDC-T knockout mutant (*gldt1-2*), that is lethal even in 1 % of CO_2 . Indeed, this class includes proteins that are very important for amino acid biosynthesis, and 1C metabolism (Engel et al., 2007; Engel et al., 2011; Timm et al., 2018). The *gldp1*×*gldp2* double mutant and the *gldt1-2* mutant are respectively devoid of the P-protein and the T-protein of the mitochondrial GDC complex (Engel et al., 2007; Timm et al., 2018). The double mutant *shmt1*×*shmt2* can only grow in very specific conditions: *in vitro* with 1 % sucrose and 0.9 % of CO_2 (Engel et al., 2011). Therefore, class I is not strictly a “photorespiratory phenotype” as described by Somerville in 2001, because the phenotype is not fully rescued by high CO_2 .

Class II: These mutants have a similar phenotype to class I mutants since they are lethal in normal air and show chlorosis and developmental delays when transferred from high CO_2 to ambient air (Figure 8). However, the phenotype was rescued by high concentrations of CO_2 (Timm and Bauwe, 2013b). These mutants exhibit a high substrate accumulation and an important reduction of photosynthetic net CO_2 assimilation rate after a transfer from high CO_2 to ambient air. Even within the Class II, the

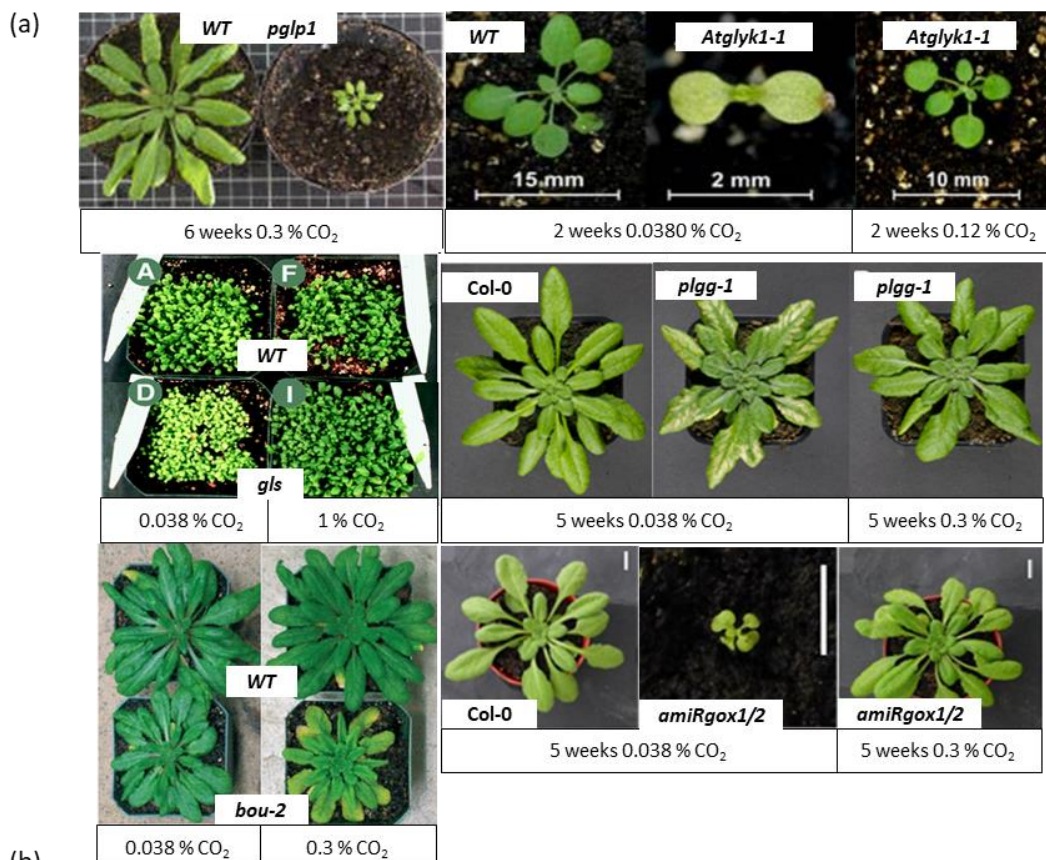


(b)

Enzyme	Mutant	Class	[CO ₂] recovery	Reference of mutants in <i>Arabidopsis thaliana</i>
GDC-P	<i>gldp1</i> × <i>gldp2</i>	Class I	no	Engel et al., 2007
GDC-T	<i>gldt1-2</i>	Class I	no	Timm et al., 2018
SHMT1 and SHMT2	<i>shm1-2</i> × <i>shm2-2</i>	Class I	no	Engel et al., 2011

Figure 7: Class I mutants

(a) Some examples of the Class I growth phenotype in *Arabidopsis* mutants. (b) List of Class I mutants and corresponding papers.

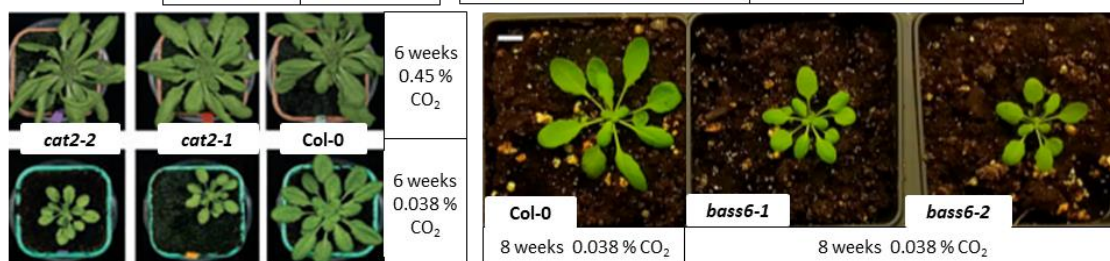
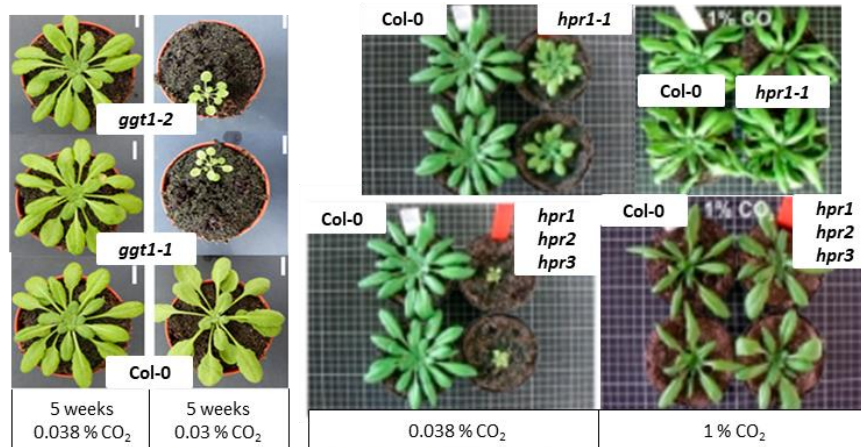


Enzyme	Mutant	Class	[CO ₂] recovery	Reference of mutants in <i>Arabidopsis thaliana</i>
PGLP1	<i>pglp1</i>	Class II	2%	Scharwtze et Bauwe, 2007
SHMT1	<i>shml-1</i>	Class II	0.3%	Somerville and Ogren, 1981
SGAT1	<i>sgatl</i>	Class II	1%	Somerville et Ogren, 1980a
GLYK1	<i>glyki</i>	Class II	0.15-0.2%	Boldt et al., 2005
GOX1 and GOX2	<i>amiRgox1/2</i>	Class II	0.3%	Dellero et al., 2016a
DIT2-1	<i>dctl</i>	Class II	1%	Renné et al., 2003
Fd-GOGAT1	<i>gls</i>	Class II	1%	Somerville and Ogren, 1980b
BOU	<i>bou-2</i>	Class II	0.3%	Eisenhut et al., 2013b
PLGG1	<i>plgg1</i>	Class II	0.3%	Pick et al., 2013

Figure 8: Class II mutants

(a) Some examples of the Class II growth phenotype in Arabidopsis mutants. (b) List of the Class II mutants and the corresponding papers.

(a)

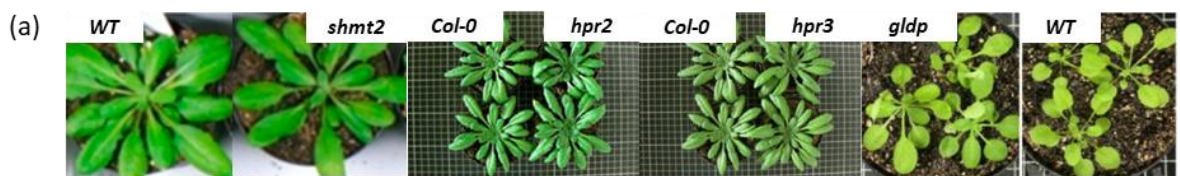


(b)

Enzyme	Mutant	Class	[CO ₂] recovery	Reference of mutants in <i>Arabidopsis thaliana</i>
GGT1	<i>ggt1</i>	Class III	0.3 %	Igarashi et al., 2003 Dellero et al., 2015a
HPR1	<i>hpr1</i>	Class III	0.15-0.2%	Timm et al., 2011
HPR1 and HPR2	<i>hpr1xhpr2</i>	Class III	0.3-0.4%	Timm et al., 2011
HPR1 and HPR2 and HPR3	<i>hpr1xhpr2xhpr3</i>	Class III	0.3-0.4%	Timm et al., 2011
CAT2	<i>cat2</i>	Class III	0.3-0.4%	Queval et al., 2007
BASS6	<i>bass6</i>	Class III	0.3%	South et al., 2017

Figure 9: Class III mutants

(a) Some examples of the Class III growth phenotype in Arabidopsis mutants. (b) List of the Class III mutants and the corresponding papers.



0.038% CO₂

(b)

Enzyme	Mutant	Class	[CO ₂] recovery	Reference of mutants in <i>Arabidopsis thaliana</i>
GOX	<i>gox1</i>	Class IV	0.038%	Rojas et al., 2012 Dellero et al., 2016a
GOX	<i>gox2</i>	Class IV	0.038%	Rojas et al., 2012 Dellero et al., 2016a
GOX	<i>gox3</i>	Class IV	0.038%	Rojas et al., 2012
GDC-P	<i>gldpl</i>	Class IV	0.038%	Engel et al., 2007
GDC-P	<i>gldp2</i>	Class IV	0.038%	Engel et al., 2007
HPR2	<i>hpr2</i>	Class IV	0.038%	Timm et al., 2011
HPR3	<i>hpr3</i>	Class IV	0.038%	Timm et al., 2011
SHMT2	<i>shm2</i>	Class IV	0.038%	Engel et al., 2011
DiT1	<i>omtl</i>	Class IV	0.038%	Taniguchi et al., 2002

Figure 10: Class IV mutants

(a) Some examples of the Class IV growth phenotype in *Arabidopsis* mutants. (b) List of the Class IV mutants and the corresponding papers.

severity of the phenotype in air varies and the concentration of CO₂ needed for recovery depends on the mutated gene. For example, *pglp1* did not recover a WT phenotype until 2 % CO₂ (Schwarte and Bauwe, 2007). On the another hand, some mutants were very similar to WT plants in 1 % of CO₂, like mutants in the following genes: *SGAT1* (*sagt1*; Somerville and Ogren, 1980b), *Fd-GOGAT* (*gls*; Coschigano et al., 1998), and *DiT2.1* (*dct1*; (Renné et al., 2003)). The RNAi mutant for photorespiratory *GOXs* (*amiRgox1/2*; Delloero et al., 2016) and the *SHMT1* (*shm1*; Somerville and Ogren, 1981) have a strong developmental phenotype in ambient air but they were rescued by 0.3 % of CO₂ while the *GLYK1* knockout mutant *glyk1* only needed a concentration of 0.15-0.2 % CO₂ to recover a WT phenotype (Boldt et al., 2005a). Finally, the mutated genes encoding the two recently described transporters, chloroplastic *PLGG1* (*plgg1*; Pick et al., 2013), and mitochondrial *BOU* (*bou-2*; Eisenhut et al., 2013b) were also considered as Class II mutants.

Class III: These photorespiratory mutants have a growth delay in ambient air but they survive because of other enzymes carry out the mutated step (Figure 9). However, several changes in metabolite content and photosynthesis rate remain. These plants are completely rescued by a 0.15 %-0.3 % CO₂ atmosphere. This class includes the following mutants: the core enzyme genes, *GGT1* (*ggat1*; Igarashi et al., 2003 and Delloero et al., 2015)), *HPR1* (*hpr1*; Timm et al., 2011a) and also the double and triple *HPR* lines (*hpr1xhpr2*, and *hpr1xhpr2xhpr3*; (Timm et al., 2011b)) and some 2C-cycle related genes like *CAT2* (*cat2*; Queval et al., 2007) and *BASS6* (*bass6*; South et al., 2017).

Class IV: Mutant plants of this class have no visible photorespiratory phenotype such as growth delay or chlorosis even if there are some physiological changes in metabolite contents and photosynthetic rates (Figure10). This could be due to several reasons, for instance either other enzymes compensate the missing protein or the role of the genes in photorespiration is indirect. Some core photorespiratory genes are associated with functional redundancy in *A. thaliana* like *GOX* (*gox1* and *gox2*; Delloero et al., 2016), *HPR* (*hpr2* and *hpr3*; (Timm et al., 2008, 2011)) *SHMT* (*shm2*; (Engel et al., 2011), *GLDP* (*gldp1* and *gldp2*; (Engel et al., 2007), and a gene encoding a transporter associated with photorespiration like *DiT1* (*omt1*; (Taniguchi et al., 2002). When these mutants accumulated other mutations (double or triple mutants) the classification changed.

4) Is it possible to improve plant yield by targeting photorespiration?

The phenotypic severity of most photorespiratory mutants proved the importance of recycling 2-PG, but this process had an energetic cost and it competed with photosynthetic CO₂ assimilation and

therefore it became a target for plant improvement. During recent years, there has been an effort to test the possibility of creating alternative pathways in the chloroplast, using synthetic biology, to efficiently recycle photorespiratory glycolate and thus alleviate the potential inhibitory action of 2-PG on photosynthesis, while preventing ammonium loss and relocating CO₂ release to the chloroplast where RuBisCO is found. Since the first report in 2007 by Kebeish and co-workers (Kebeish et al., 2007), several photorespiratory bypass strategies have been used to improve photosynthetic CO₂ assimilation and plant biomass (Figure 11). The initial bypass was based on the bacterial glycerate pathway where glyoxylate was converted to glycerate by two enzymes: glyoxylate carboligase (GCL) and tartronate semialdehyde reductase (TSR). The conversion of glycolate to glyoxylate in the chloroplast was achieved by expressing a bacterial glycolate dehydrogenase (GIDH). This enzyme had the advantage of not producing H₂O₂ that was seen to be toxic when glycolate oxidase was used without the additional expression of catalase in the chloroplast (see Fahnenstich et al., 2008). The bacterial glycerate pathway was expressed in *A. thaliana* chloroplasts and the transgenic lines produced bigger rosettes and more biomass while increasing photosynthetic assimilation rates (Kebeish et al., 2007). A similar strategy was used to increase biomass and seed yield by 50 % in *Camelina sativa* (Dalal et al., 2015). The bacterial GIDH alone was introduced also into *Solanum tuberosum* but expressed using a single construct to produce a polyprotein to avoid the observed instability when transgenic plants were generated using the three individual GIDH genes to produce the D, E and F subunits of GDH (Nölke et al., 2014). The GIDH potato lines exhibited an enhanced carbon assimilation rate at 0.04 % CO₂ (but not when measured at 0.2 % CO₂) and a 2-3-fold increase in tuber yield even if the complete glycerate pathway had not been introduced. Therefore, it appeared that the conversion of glycolate to glyoxylate in the chloroplast could be enough to enhance photosynthesis and yield. Indeed, this was observed also for *Arabidopsis* (Kebeish et al., 2007) and *Camelina sativa* (Dalal et al., 2015). Another successful photorespiratory bypass was achieved by expressing GOX, catalase and malate synthase (MS) in chloroplasts (Maier et al., 2012). Here, glyoxylate produced by the added GOX was metabolized by malate synthase to produce malate that could be oxidized to produce acetyl-CoA by the action of endogenous malic enzyme and pyruvate dehydrogenase. Such a bypass had the potential to completely oxidize glycolate to CO₂. The negative effect of GOX-produced H₂O₂ in the chloroplasts was again removed by introducing catalase into the plastids. *Arabidopsis* plants expressing this glycolate oxidation pathway exhibited a 38 % increase in leaf dry weight and an increase in net CO₂ fixation rates on a chlorophyll and dry weight basis but not on a leaf area basis. More recently, another chloroplastic photorespiratory bypass (named the GOC bypass) has been expressed in rice to increase photosynthetic efficiency (Shen et al., 2019). It consisted of three rice enzymes; GOX, oxalate oxidase (OXO) and catalase expressed in chloroplasts and designed to lead to the complete oxidation of glycolate to CO₂. It was found that

such efforts to improve photosynthesis and productivity appeared to depend on environmental conditions. Improved photosynthetic efficiency, biomass and yield were found in both greenhouse and field experiments although there were differences according to seeding season and the bypass appeared to be more advantageous under high light. To improve flux through alternative chloroplastic photorespiratory bypasses, glycolate export out of the chloroplast was manipulated by down-regulating *PLGG1* (Pick et al., 2013; South et al., 2019). In this work, previously successful bypasses were tested in tobacco and the best results were obtained with a variant of the glycolate oxidation pathway where bacterial GDH was replaced by *Chlamydomonas reinhardtii* GDH, which is encoded by a single gene unlike the *E. coli* enzyme. Again, this pathway had the potential to oxidize glycolate to CO₂ in the chloroplast thus increasing the CO₂ concentration around the RuBisCO. Field-grown tobacco expressing this version of an alternative photorespiratory pathway exhibited more than a 25 % increase in total vegetative biomass (without *PLGG1* inhibition) and a 40% increase (with inhibited *PLGG1*) while the impact on net CO₂ assimilation was quite low (5-8 %) and they accumulated more glyoxylate (7-fold) compared to control, non-transformed tobacco plants. However, no significant increase in seed yield was observed (South et al., 2019).

Overexpression of individual photorespiratory genes also led to increases in both biomass and light saturating net CO₂ assimilation rates. This was observed with mitochondrial *SHMT1* in rice where overexpressing lines had an improved photosynthetic efficiency and increased grain yield (Wu et al., 2015). The overexpression of individual GDC subunits also gave rise to increases in both photosynthesis and biomass. This was first observed in Arabidopsis by overexpressing either the H-protein (Timm et al., 2012) or the L-protein (Timm et al., 2015) of the GDC complex. When the H-protein was overexpressed in tobacco, improved biomass was observed when plants were grown in greenhouses and this was improved even further in field trials (although with seasonal variations). However, this was seen only when H-protein expression was under the control of a leaf-specific promoter while constitutively overexpressed H-protein brought about a detrimental effect on growth (López-Calcagno et al., 2019). Furthermore, the positive effect on photosynthesis only became significant at high light intensities in the field and even more so in the greenhouse. Interestingly, the additional overexpression of the H-protein in Arabidopsis lines overexpressing the CB cycle protein SBPase and FBPA (fructose biphosphate aldolase) (shown to improve photosynthesis rate and growth) led to further improvements in seed weight per plant (under high light growth conditions) and leaf area with no further increase in saturated CO₂ assimilation capacity compared to SBPase-FBPA lines alone (Simkin et al., 2017).

5) How does the 2C-cycle interact with primary metabolism?

As already mentioned, the photorespiratory cycle is not an isolated and closed pathway, but it is highly interconnected to primary metabolism. It first goes hand in hand with photosynthesis by sharing RuBisCO, and because CO₂ released during the cycle can be reassimilated. It is also linked to the CB cycle and carbohydrate metabolism since it produces 3-PGA that can be used either to regenerate RuBP or to produce sugar phosphates that will be used to make complex carbohydrates like starch and sugars. Some photorespiratory intermediates have been reported to inhibit CB cycle enzymes including RuBisCO (Anderson, 1971; Kelly and Latzko, 1976; Chastain and Ogren, 1985; Flügel et al., 2017). Furthermore, it has been shown that a decreased photorespiratory cycle flux (in mutants) led to a reduced photosynthetic CO₂ assimilation rate and impacted photosynthetic electron transfer (reviewed by Timm et al., 2016). While the 2C-cycle is feeding the CB cycle with 3-PGA, this molecule can also be a source for serine biosynthesis (Ros et al., 2014). Moreover, in mitochondria, the dehydrogenases of the Krebs cycle can compete with GDC to use NAD while photorespiratory NADH can be used to make ATP via respiration. Finally, photorespiration interacts with 1C metabolism, nitrogen metabolism, and amino acid biosynthesis (mainly glycine and serine).

a) Photorespiration and photosynthesis

Photorespiration and photosynthesis are obviously tightly associated since they are both using the same enzyme, RuBisCO. This means photorespiration and photosynthesis are in competition with each other since O₂ and CO₂ use the same catalytic site. In C₃ plants, the ratio between oxygenation and carboxylation is about one to three/four at the current atmosphere of 0.04 % CO₂/20.95 % O₂ (Busch, 2013). Since photorespiration recycles two molecules of 2-PG into one molecule of 3-PGA, 25 % of carbon is lost as CO₂ while the remaining 75 % can be used to feed the CB cycle. Mutants displaying a strong photorespiratory phenotype in air, exhibited a reduced photosynthetic CO₂ fixation rate compared to WT plants while the CO₂ compensation point was increased (reviewed by (Timm et al., 2016)). This could reflect an impact on either RuBisCO activation state or RuBisCO activity or RuBP regeneration via the Calvin-Benson cycle (Timm et al., 2016). For example, in rice antisense *GOX* lines, RuBisCO was less active because of a decrease in the amount of RuBisCO activase (Bykova et al., 2005; Xu et al., 2009). The rate of the CB cycle has a direct impact on photosynthesis because of RuBP regeneration, and it is known that some metabolites produced during photorespiration can inhibit some enzymes of this cycle. For example it had been shown that 2-PG could inhibit the *in vitro* activity of TPI purified from leaf extracts of *P. sativum* (Anderson, 1971), and this was recently confirmed in *A. thaliana* along with a new finding that this metabolite

could also inhibit SBPase (Flügel et al., 2017). Both enzymes are involved in the CB cycle and consequently a *pglp1* knockout mutant showed impaired RuBP regeneration and a perturbed carbohydrate metabolism such as starch content (Somerville and Ogren, 1979; Schwarte and Bauwe, 2007; Timm et al., 2012b; Flügel et al., 2017). 2-PG was also involved in the inhibition of spinach PFK, a glycolytic enzyme rather important for plastid starch synthesis and cytosolic sugar synthesis and glycolysis from glucose (Kelly and Latzko, 1976). Glyoxylate (produced by GOX) has been shown to reduce *in vitro* RuBisCO activity measured either with purified protein or chloroplast extracts in spinach and *A. thaliana*. It has also been demonstrated that this same molecule inhibited RuBisCO light activation, (Chastain and Ogren, 1985; Campbell and Ogren, 1990; Häusler et al., 1996). Finally, glycerate inhibited SBPase and fructose 1,6-bisphosphatase in spinach chloroplasts, thus interacting with the Calvin-Benson cycle and RuBP regeneration (Schimkat et al., 1990). When *Solanum tuberosum* was mutated in gene encoding the P-protein of the GDC complex, there was a decrease of RuBP (Bykova et al., 2005). However, Arabidopsis overexpressing either the H- or L-proteins of the GDC complex exhibited an increase of photosynthetic CO₂ assimilation probably due to the decrease of glyoxylate content and a change in glycine/serine ratio that was proposed to correspond to a regulatory signal for photorespiration rate (Timm et al., 2013; Timm et al., 2015b). Finally, either transcriptional or translational regulations could be involved that are linked to photorespiratory metabolite levels such as serine or the serine/glycine ratio, for example (Timm et al., 2013).

Another relationship between photorespiration and photosynthesis is the involvement of the C₂-cycle in protecting PSII against photoinhibition. Several photorespiratory mutants (*Fd-GOGAT*, *SHMT1*, *DIT2*, *GLYK GGAT*, *GOX*) showed a higher level of non-photochemical chlorophyll fluorescence quenching (NPQ) compared to the WT after illumination in air (Takahashi et al., 2007; Timm et al., 2012b; Dellero et al., 2015b; Dellero et al., 2016a). NPQ is a parameter that allows the evaluation of the dissipation of excess absorbed light energy as heat. It increases when there is an imbalance between produced and consumed photochemical energy (like ATP and NADPH). Furthermore, F_v/F_m , representing the maximal photochemical efficiency of PSII, also decreased less in several of the above-mentioned photorespiratory mutants compared to WT leaves (Takahashi et al., 2007). It was therefore suggested that photorespiration helped avoid photo-inhibitory damage to PS II brought about by singlet oxygen ¹O₂ produced by the interaction between oxygen and a triplet-excited P680 (Kozaki and Takeba, 1996). This photoinhibition is due to damaged D1 protein (encoded by a chloroplastic gene *pcbA*) that has to be replaced and thus can lead to a reduced active PSII content (Takahashi and Murata, 2005; Takahashi et al., 2007). It was proposed that this reduction of D1 protein in the photorespiratory mutants was due to an inhibition of D1 biosynthesis rather than an increase of degradation (Takahashi et al., 2007). A recent study has provided evidence that glycolate can also participate to PSII functioning by competing with HCO₃⁻ at the non-heme iron of PSII thus

altering the primary quinone acceptor redox potential (Q_A/Q_A^-). The author's proposed that this could be a regulatory mechanism to protect PSII from photooxidative stress under conditions that lowered chloroplastic CO_2 concentrations such as stresses where stomata become closed (Messant et al., 2018).

b) Photorespiration and nitrogen assimilation

Nitrogen is important for plant growth and it can effect leaf expansion, root architecture, flowering time and seed germination (Andrews et al., 2013), however in natural soils it is often a limiting factor. The major form of nitrogen taken up and used by plants can vary according to species and it can depend on the type of soil. In the case of *A. thaliana*, inorganic nitrogen enters the root mainly as nitrate (NO_3^-) via several specific transporters (reviewed by (Xu et al., 2012; Krapp et al., 2014). In the case of NO_3^- , it can either be assimilated directly in the roots or transported via the xylem to the shoots to either be stored in the vacuole or assimilated (Xu et al., 2012). In both organs, NO_3^- is first reduced to nitrite (NO_2^-) by a nitrate reductase (NR) then the NO_2^- is reduced to ammonium (NH_4^+) by nitrite reductase (NiR) (Lillo, 2008; Heidari et al., 2011). NR is a cytosolic enzyme that uses NADH as reductant while NiR is plastidial and uses reduced Fd (Vaughn and Campbell, 1988; Sakakibara et al., 2012). Ammonium is then incorporated into a molecule of glutamate by a GS to produce a molecule of glutamine in an ATP-dependent manner. A GOGAT then uses glutamine and 2-OG as substrates to generate two molecules of glutamate in a reaction that requires either reduced Fd or NADH. In non-photosynthetic cells, NADH-GOGAT is predominant while Fd-GOGAT is the main enzymes in leaves (Bowsher et al., 2007a).

A major source of ammonium is from photorespiration, since the GDC complex produces ten times more ammonium than nitrate reduction (Singh et al., 1986). This released ammonium is largely reassimilated by the GS2/Fd-GOGAT as mentioned previously thus producing glutamate that can be used by photorespiratory GGAT1 (Somerville and Ogren, 1980c; Coschigano et al., 1998). Indeed, in the *ggt1* mutant, there was a decrease of C-assimilation because of a lower amount of RuBisCO and this was proposed to be linked to the maintenance of C:N balance (Dellero et al., 2015b). Bloom and coworkers have carried out a lot of work on plant N assimilation under low photorespiratory conditions, namely elevated CO_2 . They focused their studies on the distinction between NO_3^- and NH_4^+ assimilation in such conditions. They used an assimilatory quotient (AQ) corresponding to net CO_2 consumption to O_2 evolution in leaves and they concluded that for wheat and *A. thaliana*, this AQ was greater with NH_4^+ nutrition compared to NO_3^- in high CO_2 , thus implying a better NH_4^+ assimilation and a lowering of NO_3^- assimilation under high CO_2 (Bloom et al., 2002a; Bloom et al., 2012; Bloom, 2015a; Bloom, 2015b; Rubio-Asensio and Bloom, 2016; Bloom and Lancaster, 2018a).

Their logic was that at elevated CO_2 , reductant was diverted to CO_2 assimilation and less was available for nitrate assimilation and that the ΔQA was proportional to nitrate use. It was demonstrated that nitrate assimilation was lower in high CO_2 (0.07 %) compared to ambient air in wheat and *A. thaliana* (Bloom et al., 2002b; Rachmilevitch et al., 2004). It was assumed that in ambient air, the photorespiratory cycle stimulated malate export to the chloroplast to provide NADH for the transformation of nitrate in nitrite by NR, and that this process was less important in high CO_2 . It was also proposed that nitrite import into the chloroplasts was also reduced as well as root nitrate uptake (Bloom, 2015c). However, a recent study has questioned these findings because developmental measurements were not consistent from one paper to another and because of the QA method to infer NO_3^- assimilation (Andrews et al., 2019). Furthermore, the concentrations of the different forms of nitrogen used by Bloom and co-workers were questioned since they were very low compared to levels usually applied during wheat nutritional studies (Bungard et al., 1999; Andrews et al., 2005; Andrews et al., 2013). Andrews and co-workers studied the dry weight of plants grown under different N nutrition as well as the N content of shoots, roots and the whole plant, at both high and low CO_2 , and they found no differences between NH_4^+ and NO_3^- conditions (Andrews et al., 2019).

c) Photorespiration and the TCA cycle

Photorespiratory 3-PGA allows the production of complex carbohydrates, particularly sucrose and starch, and also glycolysis intermediates like G3P and DHAP that lead to pyruvate, an important molecule for carbon entry into the TCA cycle *via* the production of acetyl-coA (Ruan, 2014). This latter step is catalysed by pyruvate dehydrogenase (PDH) that, like the photorespiratory GDC complex, releases both CO_2 and NADH. The produced acetyl-coA enters the TCA cycle by the action of citrate synthase to produce citrate, a 6-C molecule, from oxaloacetate a 4-C molecule. During the TCA (or Krebs) cycle, this 6-C molecule loses two C-molecules as CO_2 *via* two dehydrogenase enzymes (isocitrate dehydrogenase (IDH) and α -ketoglutarate dehydrogenase (KGDH)) that each produce a molecule of NADH. The 4-C molecule succinyl-coA undergoes additional reactions producing ATP (or GTP in some cells) and reducing FAD to FADH_2 successively forming succinate (*via* succinyl-coA synthetase) and fumarate (*via* succinate dehydrogenase = respiratory complex II). Succinate is converted to malate by fumarase and then a final dehydrogenase reaction carried out by malate dehydrogenase (MDH) converts malate to oxaloacetate thus making another NADH molecule. During one turn of the Krebs cycle, 2 CO_2 , 3 NADH, 1 FADH_2 and one ATP are produced. The electron carriers, NADH and FADH_2 , participate in the mitochondrial respiratory process by feeding the electron transport chain to drive ATP synthesis *via* the ATP synthase. The high potential electron carrier (NADH) enters at the first respiratory complex (Complex I, NADH dehydrogenase) while FADH_2

(a)



(b)

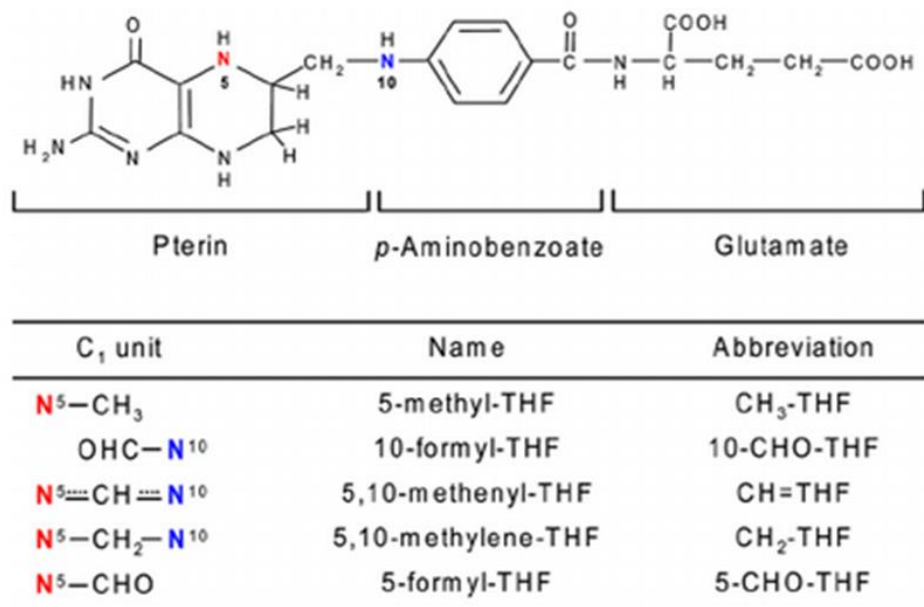


Figure 12: 1C metabolism and photorespiration

(a) Three-week-old Arabidopsis WT plants and double mutants of 10-formyl THF deformylase. (b) Structure of tetrahydrofolates and derivative molecules; 1C groups at different oxidation levels are attached to the pterin.

enters at the level of the second complex, the succinate dehydrogenase. Two other complexes, III and IV, complete the respiratory chain and lead to the reduction of O_2 to H_2O . The 2-OG produced during the TCA cycle could participate to chloroplastic glutamate production and re-assimilation of NH_4^+ released by the GDC complex. ^{13}C labelling appeared to confirm this hypothesis because it showed that under low CO_2 conditions, implying high 2C-cycle rates, the inhibition in the light of the TCA cycle was lowered, probably because of the need for NH_2 transfers to recover photorespiratory intermediates (mostly 2-OG for ammonium re-assimilation) (Tcherkez et al., 2008).

Despite this, several contradictory results are available. It has been shown for example that the accumulation of NH_4^+ produced by GDC can have a negative feedback on TCA cycle dehydrogenase activities such as PDH. Indeed, the PDH kinase (PDK) was found more active in pea accumulating NH_4^+ and as phosphorylated PDH is less active in *A. thaliana*, it was proposed that NH_4^+ accumulation inhibited PDH activity (Schuller and Randall, 1989; Thelen et al., 2000). It was also demonstrated that a higher NADH/NAD⁺ ratio could impact TCA cycle enzymes, mostly the dehydrogenases in maize and pea. A modification of this ratio was mainly observed in mitochondria during high photorespiratory rates (Thelen et al., 1998; Igamberdiev and Gardeström, 2003). Potato antisense GDC complex plants confirmed this relationship between TCA cycle and photorespiration, since the lack of GDC complex led to an increased activity of Krebs cycle enzymes (Bykova et al., 2005).

In summary, it can be seen that there is an undeniable link between photorespiration and the TCA cycle. Some finely regulated interactions appear to occur that depend on photorespiratory rate and GDC activity and that are both linked to NH_4^+ levels and the need to re-assimilate this toxic metabolite that requires 2-OG.

d) Photorespiration and 1C metabolism

1C metabolism is essential as it provides precursors for proteins (*via* methionine, glycine and serine), nucleic acids (*via* thymidylate), vitamin synthesis, and formylmethionyl-transfer RNA (Figure 12). 1C molecules are particularly important in tissues that produce lignin, alkaloids and betaines, and methylated molecules (Hanson and Roje, 2001; Collakova et al., 2008). C1 metabolism in plants is not very well-known but it can be split into four categories: folate-mediated reactions, folate-independent reactions, the activated methyl cycle and the related S-methylmethionine (SMM) cycle. The most pertinent in the context of photorespiration is the folate-mediated reactions. The mechanism of 1C molecule integration into the 2C-cycle has been confirmed by ^{13}C -formaldehyde labelling experiments using leaf discs and followed by ^{13}C -NMR analysis. It was thus confirmed that the photorespiratory intermediate THF can be transformed into 5,10-methylene tetrahydrofolate (5,10- CH_2 -THF), thus becoming a universal donor of methyl groups (Song et al., 2013). THF is composed of pterin, p-aminobenzoate (pABA) and glutamate moieties. The pterin ring of THF exists

in two forms, dihydro or tetrahydro, but only the tetrahydro form has a cofactor activity (Hanson and Gregory, 2011). For a long time, it was known that in plants, 1C units existed in different levels of oxidation (formyl, methylene, methyl) to form different forms of THF (5-methyl-THF or 10-formyl-THF or 5,10-methenyl-THF or 5,10-methylene-THF or 5-formyl-THF) depending on the attached pterin ring (Cossins and Chen, 1997). Even if the synthesis of THF and derivative molecules occur in mitochondria, it has been shown that these molecules can be found in other cell compartments like chloroplasts and the cytosol (Jardine et al., 2017). The interaction between 1C metabolism and photorespiration takes place in mitochondria during the glycine to serine conversion step. The T-protein of the GDC complex uses THF as a cofactor to incorporate a methyl group from glycine. SHMT1 then uses the 5,10-CH₂-THF molecule as a cofactor to transfer a methyl group onto glycine to produce serine. THF is thus available to be reused by the GDC complex. The importance of the C1 metabolism pathway has been discussed previously in studies of double mutants *shmt1-1xshmt2-2* and *gldp1-1xgldp2-2* and the single mutant for the T-protein of the GDC complex that are not viable even at very high concentrations of CO₂ (Engel et al., 2007; Engel et al., 2011; Timm et al., 2018). A mutant in 10-formyl THF deformylase (10-FDF) confirmed the importance of 1C metabolism in photorespiration. In *A. thaliana* this protein is encoded by two genes *At4g17360* and *At5g47435* and the double knockout mutant was lethal in ambient air, but it could be rescued in high CO₂. This typical photorespiratory phenotype thus confirmed the importance of these 1C derived molecules in the 2C-cycle (Collakova et al., 2008).

6) How does photorespiration react under stress?

As plants are sessile, they are obliged to face and adapt to all biotic and abiotic stresses to which they are confronted. Indeed, in the field, plants must adapt to a vast range of stresses including drought, temperature, salinity and even high light intensities, and they are also surrounded by many microorganisms, insects, mammals, all of which can be deleterious for plant production. Often, plants must face the effects of cumulative stresses. Photorespiration not only plays a key role in plant metabolism, but it also appears to be important in plant responses to environmental stresses. A combination of studies using different techniques (gas exchange and chlorophyll fluorescence, metabolomic analyses, ¹⁵N labelling proteomics etc) have often reported that impaired photorespiration can make the plant more susceptible to environmental stresses (see Hodges et al., 2016). Involvement of photorespiration against photoinhibition has already been discussed. Many stresses lead to stomatal closure, thus altering CO₂/O₂ balance in favour of photorespiration and limiting photosynthetic CO₂ fixation. The removal of 2-PG in stressed cells therefore becomes more

important for the plant and therefore it is predictable that photorespiratory mutants are more sensitive to environmental stresses.

a) Biotic stresses and photorespiration

A rapid response to a lot of stresses is ROS production that was for a long time considered deleterious due to cell damage and eventually cell death. However, ROS production has been shown to constitute an efficient molecular signal. For example, the production of H₂O₂ in peroxisomes is considered to be part of a plant-pathogen signalling mechanism (Mhamdi and Noctor, 2016; Noctor and Mhamdi, 2017; Williams et al., 2018). Some studies have highlighted a role for photorespiratory GOX in this H₂O₂ production, considering this to be a key component of plant resistance against several pathogens. For example, in *Nicotiana benthamiana*, GOX mutants were less resistant to *Pseudomonas syringae* (Rojas et al., 2012), in tobacco, GOX participated to resistance against Victoria blight, being necessary for victorin-induced cell death (Gilbert and Wolpert, 2013), while the silencing of *GLO1* in rice resulted in enhanced resistance against *Xanthomonas oryzae* because of an increased defence activation (Chern et al., 2013). GOX is not the only photorespiratory enzyme to participate in pathogen resistance. HPR, in soybean, GDC proteins and SGAT1 in tobacco were also shown to be involved (Hodges et al., 2016). A weak *shmt1* allele mutant was used to show that the perturbation of photorespiration in this mutant led to ROS accumulation, thus making the plant more susceptible to pathogen attack compared to WT (Moreno et al., 2005). Finally, a recent study in tomato demonstrated the involvement of three photorespiratory proteins (GOX2, SGAT1 and SHMT1) in resistance against *Pseudomonas syringae*. Indeed, an increase of the expression of the genes encoding these three proteins was reported after inoculation with the pathogen. Moreover, silenced lines were more sensitive to *P. syringae* compared to the WT, while their transient overexpression in tobacco led to a more resistant plant. Again, it was proposed that GOX produced H₂O₂ had a role in this resistance, *via* the salicylic acid signalling pathway (Ahammed et al., 2018).

b) Abiotic stresses and photorespiration

The photosynthetic electron transport chain is a major source of ROS, especially under limiting CO₂ that often occurs in stress conditions because of stomatal closure. Under such conditions, photorespiration would be expected to increase and help limit ROS accumulation by either directly or indirectly consuming both ATP and reducing power. Therefore, photorespiration is believed to be an important process for minimizing redox imbalance under stresses even if it is a source of H₂O₂ itself.

Drought and salinity

Drought stress is a very detrimental factor for the plant and this problem will become more important in the future. This stress leads to the closure of stomata and therefore to a change in the leaf mesophyll CO_2/O_2 ratio. Drought has been shown to increase photorespiration from 23 % to 40 % and photorespiratory mutants are more sensitive thus confirming the need to maintain this pathway in abiotic stress conditions (Haupt-Herting and Fock, 2002). Since photosynthetic CO_2 assimilation decreases during this stress, photorespiration could be important for photoprotection by energy dissipation. For example, an *Arabidopsis hpr1* mutant showed increased sensitivity to drought even though this mutant does not display a strong visible phenotype in normal conditions. In fact, this study underlined the fact that many peroxisomal proteins are involved in abiotic stress responses (Li and Hu, 2015). Another study in *Arabidopsis* revealed a role for SHMT1 in drought and salt stress responses (Liu et al., 2019). Barley mutated in genes encoding some proteins of the GDC complex showed the participation of photorespiration during a drought stress *via* an increase of HPR and the accumulation of glycine. Moreover, the *sgat* mutant displayed an accumulation of photorespiratory intermediates, implying an increase of the cycle during water deprivation (Wingler et al., 1999). Even in C_4 plants, a metabolite analysis in maize demonstrated the importance of the 2C-cycle in drought stress. A 2-3 fold accumulation of leaf glycine was measured and correlated with photorespiratory rate (Obata et al., 2015). The accumulation of glycine in stressed plants represents a precursor for glutathione biosynthesis, an antioxidant that protects cells from stress-induced ROS (Noctor and Foyer, 2000). Therefore, photorespiration can first generate a stress signal *via* H_2O_2 production (responsible for 70 % of H_2O_2 production under drought stress) and additionally produce glycine for glutathione production (Scheibe and Beck, 2011).

Salt stress also limits plant growth in the field, showing many similarities with drought stress. It is linked with a high ROS production in both C_3 and C_4 plants and it also disrupts photosynthesis and increases photorespiration (Miller et al., 2010). Indeed, a salt stress is characterized by an osmotic perturbation that leads to a water deficit. Salt stress experiments in tomato led to an up regulation of peroxisomal antioxidant due to a high H_2O_2 production probably *via* GOX. Photorespiration was thus suggested to play a protective role against high salinity under high light conditions (Mittova et al., 2003). In order to confirm this link, a salt treatment was applied to *Pancratium maritimum* where an increase of the glycine/serine ratio and glyoxylate was observed, thus suggesting an increase in photorespiration. Such conclusions were supported by an up-regulation of *GCD-H*, *SGAT*, and *GS2* transcripts under salt stress conditions (Voss et al., 2013). *Arabidopsis* SHMT1 was shown to play a role in salt stress, since the corresponding mutant had a more severe growth phenotype when treated with 50 mM NaCl and ROS accumulated (Moreno et al., 2005). A more recent study conducted with an *shmt1* mutant confirmed its higher sensitivity to a

100 mM NaCl stress compared to WT plants with the induction of cell death adding to a strong developmental phenotype (Zhou et al., 2012). Finally, a very recent study highlighted the need for SHMT1 activity under salt-stress and during ABA-induced stomatal movements in *A. thaliana* (Liu et al., 2019).

High temperature

During the last 150 years there has been an increase of temperature of about 0.8 °C, and during the current 21st century, average world temperature is predicted to increase between 1.7 °C and 3.9 °C in the worst scenario (Intergovernmental Panel on Climate Change, 2014). An increase in temperature will increase photorespiration, since CO₂ solubility decreases in water more than O₂ solubility thereby promoting RuBisCO oxygenation over carboxylation and thus limiting photosynthetic CO₂ assimilation (Foyer et al., 2009). Furthermore, to avoid excess evapotranspiration during drought periods, stomata close thereby further reducing photosynthesis and increasing photorespiration. Recently, many studies have applied a combination of drought and temperature stresses because both are predicted to increase in the future due to climate change. The metabolomic profiling of plants under a combination of drought and high temperature showed a significant increase in glycine and serine levels reflecting a change in photorespiratory rates (Obata et al., 2015). The effect of drought, heat and their combination can vary from one species to another. However most of the time there is a strong decrease in photosynthetic rate and PSII efficiency and the accumulation of ROS as seen in *Nicotiana tabacum*, wheat, *Populus yunnanensis*, and *Lotus japonicus* (for a review see Zandalinas et al., 2018). However, plant stomatal status in this stress combination is very challenging because stomata close during a drought stress to reduce water loss, while during heat stress, leaf temperature increases, and stomata tend to stay open to reduce leaf temperature. Another study on cucumber seedlings showed that under high temperature, there was a decrease of both RuBisCO carboxylase and activase activities that correlated with mRNA abundance (Sun et al., 2017). Another stress combination was studied in rice GOX overexpressing lines. The results suggested that GOX could have a role in response to the combination of high light and high temperature stresses that involved both H₂O₂ and SA signalling (Cui et al., 2016).

High light

Under ambient CO₂ conditions, high light intensities can increase the light dependent reactions of photosynthesis and thus stimulate photosynthetic electron transport thus leading to ROS over production. The photorespiratory pathway is considered a sink for excessive light energy by consuming ATP and reductant, and this is important to avoid photoinhibition of PSII, especially under the conditions that lead to stomatal closure (Kozaki and Takeba, 1996; Wingler et al., 2000). This link

Table 2: Overview of core photorespiratory enzyme phospho-peptides, indexed with the related protein, gene, phosphate position and origin

Enzyme	Gene	Phosphopeptide	Position	Biological material	Publication/ database
phosphoglycolate phosphatase	<i>PGLP1 At5g36700</i>	LIEGVPE(pT)LDMLR	96-108/362	Cauline leaf, 2 months old	Aryal et al. (2012)
		TLLVLSGV(pT)SISMLESPEPK	322-341/362	Cauline leaf, 2 months old	Aryal et al. (2012)
		ISDFL(pS)PK	351-358/362	Rosette, 22 days old	Reiland et al. (2009b)
		(pT)LLVLSGVTSISMLESPEK IQPDFYTSK	322-341/362	Cell culture (N starvation)	PhosPhAt
glycolate oxidase	<i>GOX1 At3g14420</i>	MEI(pT)NVTEYDAIAK	1-14/367	Leaves (O ₂ depletion)	PhosPhAt
		AIAL(pT)VDTPLR	151-161/367	Rosette	Choudhary et al. (2015)
		AIALTVD(pT)PRL	151-161/367	Rosette (ionizing irradiation using a Co ⁶⁰ treatment)	Roitinger et al. (2015)
				Seedling (ABA and dehydration treatment)	Umezawa et al. (2013)
				Rosette	Choudhary et al. (2015)
	NHITTEWD(pT)PR	347-357/367	Rosette	Choudhary et al. (2015)	
	<i>GOX2 At3g14415</i>	MEI(pT)NVTEYDAIAK	1-14/367	Leaves (O ₂ depletion)	PhosPhAt
				Rosette (ionizing irradiation using a Co ⁶⁰ treatment)	Roitinger et al. (2015)
				Seedling (ABA and dehydration treatment)	Umezawa et al. (2013)
				Rosette	Choudhary et al. (2015)
NHITTEWD(pT)PR				347-357/367	Rosette
TL(pS)WK	210-214/367	Seedling (ABA and dehydration treatment)	Umezawa et al. (2013)		
aminotransferases	<i>SGAT At2g13360</i>	AL(pS)LPTGLGIVCASPK	202-217/401	Cauline leaf, 2 months old	Aryal et al. (2012)
		ALSLPTGLGIVCA(pS)PK	202-217/401	Rosette, 22 days old	Reiland et al. (2009b)
		NNEDYR(pS)PAIPALTK	30-45/401	Rosette (ionizing irradiation using a Co ⁶⁰ treatment)	Roitinger et al. (2015)
	<i>GGAT1 At1g23310</i>	ALD(pY)DTLNENVK	5-16/481	Flowering plants	Yang et al. (2013)
				Cell culture (N starvation)	PhosPhAt
				Rosette (ionizing irradiation using a Co ⁶⁰ treatment)	Roitinger et al. (2015)
glycine decarboxylase complex	<i>GDH1 At2g35370</i>	EY(pT)KFLEEDAAH	153-165/165	Cauline leaf, 2 months old	Aryal et al. (2012)
		VKP(pS)SPAELESIMGPK	137-152/165	Cauline leaf, 2 months old	Aryal et al. (2012)
				Seedling (ABA and dehydration treatment)	Umezawa et al. (2013)
				Seedling (ABA treatment)	Wang et al. (2013)
		VKPS (pS) PAELESIMGPK	137-152/165	Seedling (ABA and dehydration treatment)	Umezawa et al. (2013)
				Rosette	Choudhary et al. (2015)
	Seedling (ABA treatment)			Wang et al. (2013)	
	<i>GDH2 At2g35120</i>	GF(s)s)VVLKDLK-	23-33/156	Seedling Isoxaben-treated	PhosPhAt
	<i>GDH3 At1g32470</i>	EY(pT)KFLEEDAAH	154-166/166	Cauline leaf, 2 months old	Aryal et al. (2012)
		(s)HLLPAF(s)I(s)R	32-42/166	Rosette, 25 days old	Reiland et al. (2009b)
		VKP(pS)SPAELEALMGPK	138-153/166	Seedling (ABA treatment)	Wang et al., (2013)
		VKPS(pS)PAEALMGPK	138-153/166	Seedling (ABA and dehydration treatment)	Umezawa et al. (2013)
				Seedling (ABA treatment)	Wang et al. (2013)
	<i>GPD1 At4G33010</i>	R(pY)IHKLQSK	556-564/1037	Seed, 7 days after flowering	Meyer et al. (2012)
ADGFDLKVVT(pS) DLK		257-270/1037	Cell culture (N starvation/Nitrate resupply)	PhosPhAt	
			Cell culture (N starvation/KCl supply)	PhosPhAt	
S(pS)KFWPTTGR		1001-1010/1037	Rosette (ionizing irradiation using a Co ⁶⁰ treatment)	Roitinger et al. (2015)	

Table 2 (continued): Overview of core photorespiratory enzyme phospho-peptides, indexed with the related protein, gene, phosphate position and origin

Enzyme	Gene	Phosphopeptide	Position	Biological material	Publication/ database		
glycine decarboxylase complex	<i>LPD1 At1g48030</i>	TPFT(pS)GLDLEK 315-325/507	315-325/507	Cell culture	Sugiyama et al. (2008).		
				Cell culture	Nakagami et al. (2010b)		
				Leaves one month in dark (Fig22 treatment)	Rayapuram et al. (2017)		
				Rosette (ionizing irradiation using a Co ⁶⁰ treatment)	Roitinger et al. (2015)		
				Seedling (ABA treatment)	Wang et al. (2013)		
				Seedling (ABA and dehydration treatment)	Umezawa et al. (2013)		
	<i>GDT1 At1g11860</i>	(pS)LPGITIDEK	190-199/507	Seedling (Phosphate starvation/Resupply)	PhosPhAt		
				Rosette (ionizing irradiation using a Co ⁶⁰ treatment)	Roitinger et al. (2015)		
				Seedling (PEG treatment)	Bhaskara et al., (2017)		
		GKPYEG(s)(t)K	387-396/408	Cell culture (N starvation/KCl supply)	PhosPhAt		
				Rosette (ionizing irradiation using a Co ⁶⁰ treatment)	Roitinger et al. (2015)		
				V(pT)DEHI(pY)LVVNA GCRDK	138-154/408	Seedling (Isoxaben-treated)	PhosPhAt
				(pS)HSEVHDESGN(K*)	337-348/408	Rosette (ionizing irradiation using a Co ⁶⁰ treatment)	Roitinger et al. (2015)
				SH (pS)EVHDESGN(K*)	337-348/408		
				LTGLGARD(pS)LR	259-270/408		
VGFFS(pS)GPPAR	296-336/408						
GGDV(pS)WHIHDER	170-181/408						
serine hydroxymethyl transferase	<i>SHMT1 At4g37930</i>	N(pT)VPGDV SAMVPG GIR	415-430/517	Cauline leaf, 2 months old	Aryal et al. (2012)		
		(pS)LPSEAVDEKER	31-42/517	Rosette, 22 days old	Reiland et al. (2009b)		
		(pS)LPSEAVDEK	31-40/517				
		LS(pS)SID(K*)PIR	10-19/517	Rosette (ionizing irradiation using a Co ⁶⁰ treatment)	Roitinger et al. (2015)		
		LS(pS)SID(K*)	10-16/517				
		LSS(pS)ID(K*)PIR	10-19/517				
		RLSS(pS)ID(K*)	9-16/517				
		SEAQG(pT)(K*)L(K*)	468-473/517				
		LS(pS)SIDKPIRPLIR	10-23/517	Rosette	Choudhary et al. (2015)		
		SRV(pT)WPK	43-49/517	Seedling (sucrose starvation)	Wu et al. (2013)		
	ST(pS)(C*)YMSSLPSE AVDEK	25-42/517	Seedling (ABA and dehydration treatment)	Umezawa et al. (2013)			
	STS(C*)(pY)(oxM)SSL PSEAVD EK	25-42/517	Rosette	Choudhary et al. (2015)			
	<i>SHMT2 At5g26780</i>	N(pT)VPGDV SAMVPG GIR	415-430/517	Seedling (PEG treatment)	Bhaskara et al. (2017)		
Cauline leaf, 2 months old				Aryal et al. (2012)			
hydroxypyruvate reductase	<i>HPR1 At1g68010</i>	EGMA(pT)LAALNVLG R	331-343/387	Cauline leaf, 2 months old	Aryal et al. (2012)		
		RAS(pS)MEEVLR	226-235/387	Seedling (ABA and dehydration treatment)	Umezawa et al. (2013)		
		AS(pS)MEEVLR	227-235/387	Rosette (ionizing irradiation using a Co ⁶⁰ treatment)	Roitinger et al. (2015)		
	<i>HPR2 At1g79870</i>	SVLLETHR(N)(pS)IR	36-47/313	Rosette (ionizing irradiation using a Co ⁶⁰ treatment)	Roitinger et al. (2015)		
	<i>HPR3 At1g12550</i>	VSGKR(VG)IVGLG(pS)IG (pS)FV AK	150-169/323	Seedling (Isoxaben-treated)	PhosPhAt		

between photoinhibition and photorespiration *via* photorespiratory mutants has been discussed earlier. It is known that glycine metabolism enzymes are induced by high light in *A. thaliana*, wheat and pea (Rios et al., 1991; Rogers et al., 1991; Lee et al., 2010) and this is believed to be linked to glutathione synthesis, an important component and maintain redox homeostasis under stress. Another study in rice highlighted the importance of serine/glycine metabolism in excess light conditions, showing that under high light a significant increase of GDC-P and -T subunits and SHMT1 was observed while the plants displayed a 50 % reduction of GDC-L suggesting a role of GDC stoichiometry during high light treatment (Huang et al., 2013).

7) Is photorespiration regulated by phosphorylation?

a) Post translational modifications (PTMs)

Plants are submitted to a range of environmental changes and therefore they must rapidly respond to these stimuli to survive and to continue their growth and development. This can involve mechanisms that can alter protein activities by post-translational modifications (PTMs). Indeed, a recent study investigating the short-term responses of WT and photorespiratory mutants to a shift from high CO₂ to low CO₂ in *A. thaliana* indicated that few genes showed a significant altered expression and therefore proposed a post translational regulation of the 2C-cycle (Eisenhut et al., 2017). In a well-known database (The UniProt Consortium, 2016) of Eukaryotic proteins, there are 461 types of modified amino acids registered, thus highlighting the importance of PTMs. For example, in *A. thaliana*, over 1000 proteins were annotated with at least two different modifications. Therefore, a crosstalk of diverse PTMs on the same protein is possible. There are numerous possible modifications like methylation, acetylation, glycosylation, myristoylation, ubiquitination, sumoylation, carbamylation, nitrosylation and, of course, phosphorylation which is probably the most prevalent PTM occurring in prokaryotes and eukaryotes. These PTMs can modify protein properties like stability, activity, sub-cellular localization, and various types of interactions. It has been estimated that in Eukaryotes, 1/3 to 2/3 of proteins can be phosphorylated, but in *A. thaliana*, the dataset is far from complete, thus it is difficult to estimate the number of phosphorylated proteins (Vlastaridis et al., 2017). Protein phosphorylation leads to the addition of a phosphoryl group to an amino acid in a protein. Mechanistically, it corresponds to a phosphoester bond formation and can therefore occur on serine, threonine, tyrosine and histidine residues. The most common phosphorylated amino acid in plants is serine while tyrosine phosphorylation is rather rare. This modification is catalysed by an enzyme called a protein kinase and it can be reversed *via* the action of protein phosphatases.

It is now possible to carry out a large-scale analysis of phosphorylated proteins of a specific extract at a chosen time point. This approach is called phosphoproteomics and it provides a more global view of the phosphorylated status of proteins. It can be used to compare mutants and WT plants, different environmental conditions or different tissues/organs. Global studies of *A. thaliana* proteins have allowed the detection of many phospho-peptides, but with this amount of data, the role of each phospho-peptide needs to be deciphered. There are several databases collecting a maximum of information concerning phospho-peptides, related studies and conditions including PhosPhAt 4.0 (Heazlewood et al., 2008; Durek et al., 2010) (<http://phosphat.uni-hohenheim.de>) that is specialized in phospho-peptides detected in *A. thaliana*, P3DB specialized in crop plants (Gao et al., 2009) (<http://www.p3db.org/>) and a PhosphoProtein Database for the plant legume model *Medicago trunculata* (Schulze et al., 2015) (<http://phospho.medicago.wisc.edu>).

b) Photorespiration and protein phosphorylation

Different phosphoproteomes and phospho-peptide databases available for *A. thaliana* revealed that all but one (GLYK) of the eight-core enzyme of the 2C-cycle displayed at least one phospho-peptide. Moreover, some of the photorespiratory related enzymes involved in NH_4^+ re-assimilation or H_2O_2 detoxification, were also associated with phospho-peptides like CAT2, DiT.1, and GS2 (PhosPhAt 4.0), suggesting that one level of regulation of photorespiration could involve protein phosphorylation. The core proteins and their corresponding phospho-sites are summarized in Table 2. Interestingly, more than one phospho-peptide has been found for each core photorespiratory enzyme, but rarely all in the same study. Some phospho-sites of photorespiratory enzymes have been characterized, for example, the phosphomimetic form of serine 31 mutated to aspartate in SHMT1 (S31D) modified enzyme stability in *A. thaliana* during a salt stress (Liu et al., 2019) and the phosphomimetic form of HRP1 at threonine 335, altered its cofactor specificity (unpublished data from the team).

c) Photorespiration and redox regulation

From this introduction, it is evident that photorespiration and redox homeostasis are linked through the production and consumption of NADH/NADPH/reduced Fd and the production and detoxification of H_2O_2 in the peroxisome by GOX1/2 and CAT2, respectively. In this context, a recent review focused on oxidative post-translational regulation of cysteines as a major target because of their capacity to form disulphide bonds, and some reversible modifications like glutathionylation, nitrosylation, and sulfhydrylation to mention just a few (Keech et al., 2017). By analysing a range of proteomes, it was proposed that most photorespiratory enzymes could be redox regulated but

experimental data confirming redox regulation of photorespiration were scarce (Keech et al., 2017). In *P. sativum*, GOX activity was shown to be reduced by S-nitrosylation and in the same study, GDC, GOX, HPR, SGAT, and CAT2 were also identified as being S-nitrosylated (Ortega-Galisteo et al., 2012). In *A. thaliana*, the protein P and H of the GDC complex as well as CAT3 and SHMT were found nitrosylated after 1 h in the presence of a protein secreted by *Erwinia amylovora*. This post-translational modification of the P, H and L proteins was shown to decrease GDC activities (Palmieri et al., 2010). Furthermore, both sub-units of RuBisCO can be S-nitrosylated in leaves after a 20 min incubation in an NO enriched air in *A. thaliana* and *K. pinnata* (Lindermayr et al., 2005; Abat et al., 2008). Almost all mitochondrial photorespiratory proteins (H, P and T protein of the GDC complex and SHMT) were found to interact with TRX (Balmer et al., 2004; Marchand et al., 2004). Recent studies have shown glycine to serine conversion by the GDC complex to be affected by TRXs. In a first study, an *A. thaliana* thioredoxin o1 (*trxo1*) mutant showed an increase of glycerate after transfer from high CO₂ to normal air together with a decrease of serine and 3-PGA. Moreover, the photorespiratory phenotype (decrease of NADH/NAD⁺ and NADPH/NADP⁺ ratios, growth delay and reduced PSII efficiency) of the double mutant *gldt1* (mutated in the T protein of the GDC complex) and *trxo1* named *T×GT* was exacerbated compared to the single *gldt1* mutant. Finally, reduced TRXo1 lowered the *in vitro* recombinant GDC-L activity suggesting a role for this TRX in 2C-cycle regulation (Reinholdt et al., 2019). A second study focused on the role of a cytosolic/mitochondrial TRXh2 by characterizing a T-DNA mutant that also exhibited a modified NADH/NAD⁺ ratio as well as altered glycine, glycolate, glyoxylate and serine contents. Furthermore, there was also a decrease of GDC and SHMT1 protein amounts. TRXh2, in the same way as TRXo1, inhibited GDC-L activity thus suggesting a role in photorespiratory regulation (Fonseca-Pereira et al., 2019).

IV) Two different proteins, two different pathways; one reaction mechanism?

1) Phosphoglycolate phosphatase (EC 3.1.3.19): a HAD family protein forming a transitory phosphoenzyme

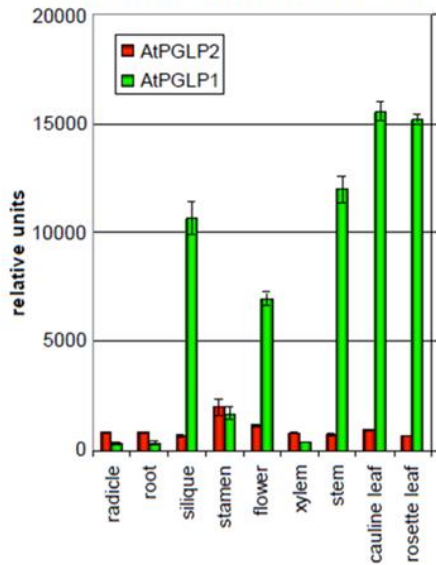
a) In C₃ plants

As indicated by its name, phosphoglycolate phosphatase (PGLP) dephosphorylates 2-PG to form glycolate. It was first reported in 1961 (Richardson and Tolbert, 1961), described as a protein of the

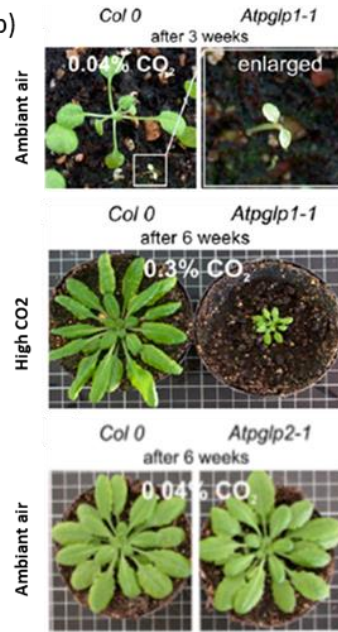
glycolate pathway and largely studied in C₃ photosynthetic organisms including higher plants, green algae, and cyanobacteria, with enzyme purification and the determination of various kinetic parameters. All studies demonstrated that this enzyme in plants was highly specific for 2-PG, that it always required Mg²⁺ or another divalent cation and that its activity was often more important in the presence of a chloride anion (Cl⁻). In plants, PGLP was reported to have an estimated MM of between 20-32 kDa depending on the species, and that it acted as a homodimer although it has been suggested that it could form a homo-tetramer (Hess and Tolbert, 1967; Christeller and Tolbert, 1978a; Christeller and Tolbert, 1978b; Christeller and Tolbert, 1978c; Husic and Tolbert, 1984; Husic and Tolbert, 1985; Seal and Rose, 1987; Norman and Colman, 1991a).

PGLP was identified as a photorespiratory enzyme during the EMS screen of Somerville and Ogren in 1979 (Somerville and Ogren, 1979) after the characterisation of the *CS119* mutant which showed a very strong Class II photorespiratory phenotype since it could not grow in ambient air and it displayed a growth delay even in 1 % CO₂, requiring a 2 % CO₂ atmosphere to rescue the phenotype. This drastic phenotype was also reported in barley (Blackwell et al., 1988). In this study, mutagenesis was achieved with azide while the same global approach as Somerville and Ogren was used to identify photorespiratory mutants from over 60 air sensitive M₂ plants thus leading to the identification of the RPr84/90 mutant of PGLP. Initially in 0.8 % of CO₂, this mutant exhibited similar growth to the WT but after 24 h in ambient air, like the *A. thaliana* mutant, RPr84/90 started to become pale, its leaves bleached and eventually the plant died. It only had 10 % PGLP activity and its photosynthetic CO₂ assimilation rate was only 35-50 % of the WT. The AraCyc database specializing in *A. thaliana* reported 13 putative PGLP-encoding genes but only seven were predicted to encode chloroplastic proteins (*At1g56500*, *At3g10970*, *At3g48420*, *At4g25840*, *At4g39970*, *At5g36700*, and *At5g36790*). Based on sequence homology with the PGP from *Chlamydomonas reinhardtii* (Mamedov et al., 2001), two candidates were studied further to identify the photorespiratory PGLP : *PGLP1*, *At5g36700*; *PGLP2*, *At5g47760* (Schwarte and Bauwe, 2007). To do so, knockout mutants of these two genes were characterized (Figure 13). It was thus demonstrated that the homozygous *Atpglp1-1* mutant (SALK_130837) like *CS119* was not able to grow normally in ambient air, while a better growth was recorded at 0.3 % CO₂ and even better in 0.9 % even if the photorespiratory phenotype did not completely disappear. Indeed, this mutant had a 97 % reduction of leaf PGLP activity. On the other hand, the homozygous mutant *Atpglp2-1* (SALK_147334) displayed no developmental phenotype. Moreover, their gene expression in GENEVESTIGATOR (Zimmermann et al., 2004) showed that *AtPGLP1* was 20-fold more expressed in leaves while *AtPGLP2* was more prevalent in non-photosynthetic organs. This study definitely showed that *AtPGLP1* was the photorespiratory enzyme in *A. thaliana* and the strong *pglp1* phenotype suggested that this was the only gene encoding a photorespiratory PGLP1 (Schwarte and Bauwe, 2007). This mutant was further used to

(a) Expression patterns for PGLP1 and PGLP2 in Arabidopsis (Genevestigator data)



(b)



(c)

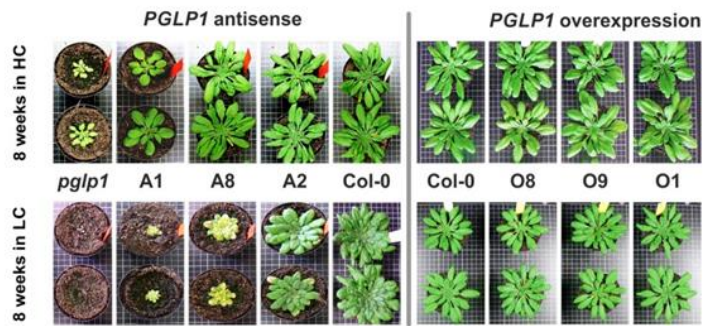


Figure 13: Characterization of photorespiratory *PGLP1* in *Arabidopsis thaliana*

(a) Relative expression of *PGLP1* and *PGLP2* in different organs described in Timm *et al.*, 2007; (b) Photorespiratory phenotype of the homozygous *pglp1* mutant described in Timm *et al.*, 2007; (c) *PGLP1* antisense and over-expresser described in Flügel *et al.*, 2017.

decipher the impact of an impaired PGLP1 on primary metabolism following a transfer from high CO₂ (HC, 1 %) to ambient air (LC). After a few days in LC, there were clear alterations of the leaves (growth retardation, chlorosis), PSII became impaired, net CO₂ assimilation declined and the CO₂ compensation point was modified. Moreover, there was a decrease of starch accumulation leading to a 5-fold reduction of night-time maltose, the major disaccharide produced by starch degradation and export to cytosol during the night. In terms of metabolite contents, the comparison between WT and *pglp1* showed an accumulation of photorespiratory intermediates, an obvious change in TCA metabolites and amino acid contents, however these impairments were mostly already visible in HC since the CO₂ concentration did not completely rescue the phenotype (Timm et al., 2012b). The importance of 2-PG removal in the chloroplast was studied using a range of *PGLP1* antisense lines with different amounts of PGLP activity together with several over-expressing *PGLP1* lines (Flügel et al., 2017). It was believed that 2-PG accumulation had a negative effect on CB cycle functioning because of C and P sequestration led to a reduction of cycle efficiency (Wingler et al., 1999), and because 2-PG inhibited chloroplastic enzymes including TPI (Calvin-Benson cycle) and PFK (starch metabolism) (Anderson, 1971; Kelly and Latzko, 1976). The different antisense lines (A1, A8 and A2) showed respectively 9 %, 18 % and 68 % of transcripts levels while the over-expressers (O8, O1 and O9) had respectively 140 %, 180 %, and 203 % of transcript levels leading to a PGLP activity range from 9 % (in A1) to 144 % (in O1). In HC there were no differences between the antisense lines but after transfer to LC the phenotype (decrease of photosynthetic rate and carbon assimilation, lower stomatal conductance) was correlated with the amount of AtPGLP1 activity and showed that even a small decrease of AtPGLP1 activity could affect *Arabidopsis* rosettes. This study concluded that 2-PG inhibited TPI (confirmed in the paper) and PFK, while it also inhibited SBPase activity and modified starch accumulation without changing the amount of sucrose. The existence of a potential feedback between photorespiratory rate and CB cycle to reach a balance between RuBP regeneration and starch production was proposed, and that 2-PG could be a sensor of photorespiratory to photosynthetic carbon flux involved in the regulation of stomatal conductance, photosynthetic CO₂ and photorespiratory O₂ fixation, and starch synthesis in response to changes in the environment (Haimovich-Dayana et al., 2015; Flügel et al., 2017).

b) In C₄ plants

The importance of the photorespiratory cycle in C₄ plants had been shown through the study of a maize GOX mutant (*go1*) that showed GOX to be necessary for plant growth in air (Zelitch et al., 2009). Concerning PGLP, it has also been studied in maize and shown to be present and important in this C₄ plant. The protein was purified from bundle-sheath strands and its kinetic parameters were measured thus showing a number of similar C₃-plant characteristics like its isoelectric point, divalent

cation requirement with a high affinity for Mg^{2+} and its high specificity for 2-PG (Hardy and Baldy, 1986; Baldy et al., 1989). A recent work focused on the need for 2-PG metabolism in C_4 plants but using *Flaveria bidentis* as a model. The phenotypes of eight transgenic RNAi lines with different PGLP expression levels were generated and characterised. As for C_3 plants, after transfer from high to low CO_2 conditions, leaves bleached, and some necrotic lesions appeared in one of the transgenic lines while other lines adapted to the ambient air condition. A clear photorespiratory phenotype was only visible in plants containing less than 5 % of normal PGLP activity in *Flaveria bidentis* compared to 20 % of PGLP activity in *A. thaliana*. This could reflect PGLP distribution between mesophyll and bundle sheath cells in C_4 plants. So, even in C_4 plants, efficient photosynthesis requires the elimination of 2-PG since the transgenic lines showed a decreased photosynthetic carbon assimilation and impaired amino acid metabolisms (Levey et al., 2019).

c) In other organisms

PGLP proteins are not just enzymes of photosynthetic organisms, they can be found in animals, human, yeast, and bacteria. Many PGLP proteins have been characterized in several organisms (Thaller et al., 1998). In human, this enzyme is active in all cells but mainly studied in red blood cells because 2-PG formed by the action of a pyruvate kinase was shown to activate the hydrolysis of 2,3-biphosphoglycerate and thus modified the oxygen affinity of haemoglobin. Interestingly some reports demonstrated that PGLP from plants and human red blood cells had some similarities like the need for a divalent cation and a monovalent anion (Rose et al., 1986). In autotrophic organisms, the role of PGLP as a component of plant photorespiration has already been discussed, but not in other organisms. Indeed, double strand DNA breaks produced by ionizing radiation leads to the formation of 3' terminal phosphoglycolate that can inhibit the DNA repair process and thus it needs to be eliminated. In mammals, this phenomenon has been well described in mice since the replacement of murine PGP with an inactive enzyme led to an embryo-lethal phenotype in ambient oxygen concentrations. Indeed, the absence of PGP caused a dramatic increase of 2-PG coming from ROS-induced double strand DNA breaks, that inhibited TPI and consequently cell proliferation (Segerer et al., 2016). The same role was shown for PGLP from *Thermoplasma acidophilum* and the protein was crystallized to decipher its structure (Kim et al., 2004). The equivalent protein in the Gram⁻ bacteria *Escherichia coli* is encoded by *NagD*, but a mutant displayed no phenotype suggesting functional redundancy. However, this protein can metabolise 2-PG produced during double strand breaks of DNA, and it showed the same affinity for Mg^{2+} and Cl^- but in contrast with the enzyme of other organisms it acted as a monomer (Lyngstadaas et al., 1999; Teresa Pellicer et al., 2003). Yeast contains a PGLP, called Pho13, and the *Pho13* mutant showed modified fermentation specificity and

a downregulation of the TCA cycle. On the other hand, the recently identified Pho15 has been shown to be involved in redox homeostasis. These proteins can also detoxify other toxic metabolites like L-2-P-lactate, produced from lactate, or 4-p-erythronate which can inhibit glycolytic enzymes (Kim et al., 2015; Xu et al., 2016; Krocová et al., 2019). The importance of PGLP can be seen from an evolutionary point of view. Indeed, some species like the pathogenic organism *Haemophilus influenzae* which evolved to maintain a very small genome still possesses a gene encoding a PGLP (Parsons et al., 2002). The genome of *Methanococcus jannaschii* no longer contains a PGLP gene but it evolved without oxygen and it has a very different RuBisCO (Bult et al., 1996). Such elements lead to the conclusion that most organisms have a PGLP that always catalyses the same reaction, the dephosphorylation of toxic 2-PG but it can be involved in different pathways. Therefore, from prokaryotes to eukaryotes, this enzyme is important to maintain cell viability.

d) Description of the HAD protein superfamily

The haloacid dehalogenase (HAD superfamily) was named after the prokaryotic enzyme 2-haloacid dehalogenase (Koonin and Tatusov, 1994) and constitutes a superfamily of hydrolases. It was the first study that tried to describe a new family of enzymes among all living kingdoms, and at that time the most obvious link between these enzymes was the covalent formation of a transitory ester (Verschuere et al., 1993). Identification of the HAD family began with bioinformatics analyses. Different methods of sequence comparisons were used (BLASTP, NRDB and BLASTN), and a tool that searches for special motifs (Motif search tool; MoST) using well described CAP program (consistent alignment parser) (Tatusov et al., 1994). This sequence comparison was followed by a secondary structure analysis using a protein structure prediction programme called PHD (Rost, 1996). In this way, PGLP was identified as being a member of this family. The protein structure of this family of enzymes was defined by at least three conserved and primordial motifs. It had been previously shown that HAD proteins formed a reactional intermediate and that a particular conserved aspartate played an important role, this aspartate being part of one of the HAD family-defining motifs (Seal and Rose, 1987; Schneider et al., 1991). Over the years, many HAD proteins have been characterized and it constitutes a very large family of enzymes that are found in all three super-kingdoms of life, with about 80 000 members that regroup a large range of biological functions. To date, more than 40 X-ray crystal structures have been determined and many sequences that allow a classification within this family. One classification was made according to the reaction catalysed by the enzyme: phosphatase, dehalogenase, phosphoramidases, sugar phosphomutases or phosphoglucomutase ATPases, and phosphonate. But among all groups, there is a predominance of phosphatases that are very different from protein phosphatases (tyrosine and serine-threonine phosphatases). In

contrast, most of these phosphatases target small metabolites and only in some rare cases proteins (Allen and Dunaway-Mariano, 2004; Burroughs et al., 2006a; Huang et al., 2015; Allen and Dunaway-Mariano, 2016). The number of HAD members in each species can vary from 10 to 20 in bacteria to around 100 in humans. It has been estimated for example that in *E.coli* 40 % of phosphatases are from the HAD family (Keseler et al., 2005). Little is known about this family in *A. thaliana* but according to databases there are around 115 genes encoding HAD superfamily proteins. These HAD proteins broadly share few sequence similarities, but they can be easily found by conserved motif sequence identities and predicted structural similarities. HAD enzymes are made up of a core subunit and a cap subunit.

The core is composed of a three layered $\alpha\beta$ -sandwich in which α and β repeated units form a parallel central sheet of five strands (from S1 to S5) that show the typical Rossmannoid topology class of α/β folding. A Rossmannoid topology refers to a structure initially described by Michael Rossmann (Rao and Rossmann, 1973) to describe the conformation of a range of proteins that bind nucleotides as cofactors. This fold is composed of alternative β -strands linked to each other by hydrogen bounds and thus forming a β -sheet and α -helices surround the sheets thus forming a three-layer sandwich of alternated $\alpha\beta$ structures. All derivatives of Rossmannoid structures are based on this description even if they can be applied to proteins other than nucleotide-binding proteins. The HAD Rossmannoid structure has two specific structural motifs:

- First, just after the S1, there are about six residues composing a single helical turn that has been called the “squiggle”.
- Then, downstream from this squiggle, a β -hairpin turn constitutes another highly conserved structure called the “flap”.

These very specific structures have a primordial role in HAD protein catalysis.

Although Koonin and Tatusov (Koonin and Tatusov, 1994) mentioned and briefly described three conserved motifs among the protein family, Burroughs et al., (2006) disclosed four conserved motifs :

- A DxD motif at the end of the S1 strand, where these two aspartates play a major catalytic role. The first one having nucleophile properties that allow the formation of the transitory aspartyl (Seal and Rose, 1987). The second one (+2) protonates the leaving substrate and deprotonates the first aspartate. This motif is true for the phosphatases and phosphoglucomutases (Lahiri et al., 2002), however, for P-type ATPases the +2 amino acid is a threonine, for phosphonates it is an alanine and for dehalogenases, a tyrosine can be found (Burroughs et al., 2006a). These two amino acids are also involved in Mg^{2+} coordination.
- At the end of the S2 strand, there are two conserved amino acids: a threonine and a serine.

- The third motif focuses on a highly conserved lysine at the N-terminus of the helix located upstream from the S4 strand. Sometimes, this lysine is inside the helix, but only in some rare cases. It is thus the less conserved motif but participates in the formation of the intermediate during hydrolysis.
- The fourth motif is a terminal acidic group of residues that have one of three signatures: DD, GDxxxD or GDxxxxD. This last motif is also involved in coordination with the divalent cation.

The core structure of HAD enzymes is highly conserved apart from the link with the cap domain. However, the central sheet can show some lateral modifications, like an extra strand S6 in some enzymes or an additional β -hairpin, thus extending the central sheet.

The cap is the most variable part of HAD family enzymes. When HADs evolved and extended, a high diversity appeared in the cap domain, thus giving flexibility for the substrate and the catalysed reaction. This part of the enzyme mediates solvent exclusion and insertion during the catalytic cycle and it determines substrate specificity and coordination (Lahiri et al., 2004; Kestler et al., 2014; Huang et al., 2015). To date there are three categories of cap domains:

- C0 also called “capless” because it is the most minimal and simple cap domain; most of the time, enzymes with a C0 domain act on macromolecular substrates like proteins or DNA.
- C1 that is inserted in the β -hairpin of the flap motif. This cap is very flexible and quickly alternates between open and closed positions of the enzyme.
- C2a/C2b caps are inserted immediately after the S3 strand. This cap is less flexible than C1, but a study of C2b-family HAD phosphatases from *Plasmodium falciparum* revealed two distinct positions (open and closed). The C2a-type caps are typical of small-metabolite targeted phosphatases and PGLP belongs to this type.

The most represented caps domain among HAD enzymes are C1 and C2 and some proteins can carry both of them (Lahiri et al., 2004).

Despite strongly different sequences and substrate specificities due to the cap domain, the high amount of HAD protein crystal structures allowed to decipher a HAD reactional mechanism (Figure 14). After entry of the substrate into the active site, the enzyme shows a closed conformation and the Mg^{2+} cation interacts with the phosphate to prepare the nucleophile attack by the first catalytic aspartate, forming a transitory acyl-phosphate with the carboxyl group of the amino acid. The enzyme then moves to the open state to allow solvent entry. Then the second catalytic amino acid, that is an aspartate for the proteins with a phosphatase activity, deprotonate a H_2O molecule to release the product (Morais et al., 2004; Burroughs et al., 2006a; Caparrós-Martín et al., 2013; Gohla, 2019)

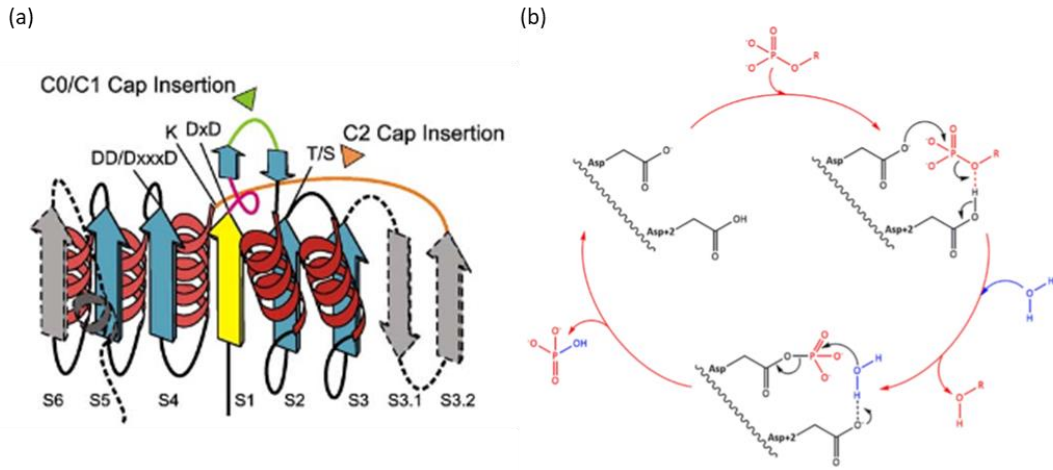


Figure 14: The phosphoglycolate phosphatase, a HAD protein

(a) Secondary structure of a classical haloacid dehalogenase protein: showing the Rossmannoid structure and Cap insertions (from Burroughs et al., 2006). (b) Reactional mechanism of the phosphoglycolate phosphatase (from Gohla, 2018).

Table 3: Phosphopeptides identified for PGLP1 in *A. thaliana* (extracted from table 2 for clarity)

Enzyme / Gene	Phosphopeptide	Biological material	Publication / Database
phosphoglycolate phosphatase <i>AtPGLP1 At5g36700</i>	LIEGVPE(pT)LDMLR	Cauline leaf, 2 months old	Aryal et al. (2012)
	TLLVLSGV(pT)SISMLESPEPK	Cauline leaf, 2 months old	Aryal et al. (2012)
	ISDFL(pS)PK	Rosette, 22 days old	Reiland et al. (2009)b
	(pT)LLVLSGVTSISMLESPEK IQPDFYTSK	Cell culture (Nitrogen starvation)	PhosPhAt

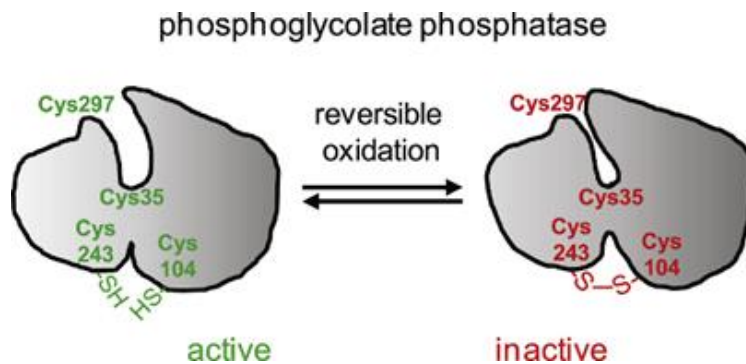


Figure 15: Hypothetic mechanism of mammalian PGP redox regulation (from Seifried et al., 2016b)

e) PGLP1 regulation

Despite the importance of PGLP in many organisms and especially plants (as seen from the phenotype of *Arabidopsis pglp1* mutants), limited information is available on how this enzyme is regulated. In the context of the phosphoregulation of photorespiration, three phospho-peptides and four potential phospho-sites have been identified in different phosphoproteomes, thus suggesting a potential regulation of AtPGLP1 by protein phosphorylation (Table 3). Interestingly, AtPGLP1 has also been identified as a target of a 2-cys-peroxiredoxin in a co-immunoprecipitation experiment (Cerveau et al., 2016) and very recently it was also identified in a tap-tag experiment with NTRC (NADPH-TRX reductase), thus implying that one level of regulation for this protein could be redox related (González et al., 2019).

As in plants, little is known about the regulation of PGLP in other organisms. However, it has recently been reported that mammalian PGP was regulated by the redox state of the cell. Mammalian PGP acts to detoxify 2-PG resulting from DNA double strand breaks caused by hydroxyl radicals and it is known that at a post-translational level, cysteines are good targets because of the thiol carried by the radical chain of this amino acid. Using methods including thiol labelling with an alkylating agent (iodoacetyl polyethylene glycol) and site-directed mutagenesis of cysteines, it was demonstrated that PGP activity could be inhibited by H₂O₂ in a reversible manner. This open/closed regulation (Figure 15) involved cysteine residues, C35, C104 and C243, while PGP oligomerization was also found to be redox-dependent *via* another cysteine C297 (Seifried et al., 2016a; Seifried et al., 2016b). These studies suggested that an oxidative stress downregulated PGP activity, but cellular antioxidant systems could counteract this by reductant-dependent PGP oligomerization that led to enzyme re-activation.

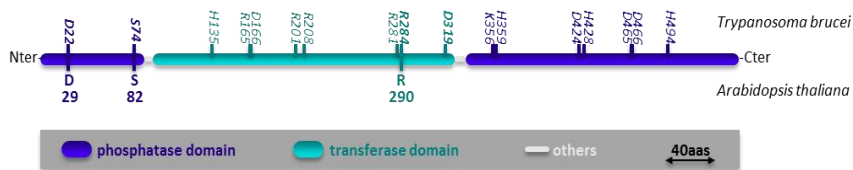
2) Cytosolic iPGAM: phosphoregulation or a transitory catalytic phosphoenzyme?

The importance of 3-PGA as a central metabolite of plant metabolism has been discussed above. This metabolite is the substrate of phosphoglycerate mutase (PGAM) that has a reaction mechanism exhibiting similarities to the previously described HAD phosphatases. Indeed, both PGAM and PGLP adopt a transient phospho-enzyme state during their catalytic reaction.

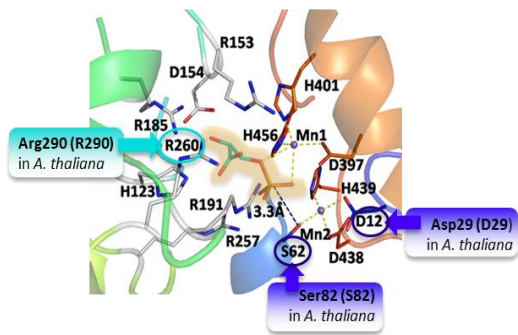
PGAM exists in almost all living organisms, and at least three distinct reactions can be catalysed by this enzyme:

- Interconversion of 1,3-bisphosphoglycerate into 2,3-bisphosphoglycerate;
- Isomerization between 3-PGA and 2-PGA (studied in my PhD work);

iPGAM		Aspartate (ASP/D)	Serine (SER/S)	Arginine (ARG/R)	Aspartate or Glutamate (ASP or Glu/D or E)
family 1	<i>Trypanosoma brucei</i>	D22	S74	R284	D319
	<i>Arabidopsis thaliana</i>	D29	S82	R290	E325
family 2	<i>Staphylococcus aureus</i>	D12	S62	R260	Does not exist
	<i>Bacillus stearothermophilus</i>	D12	S62	R264	Does not exist

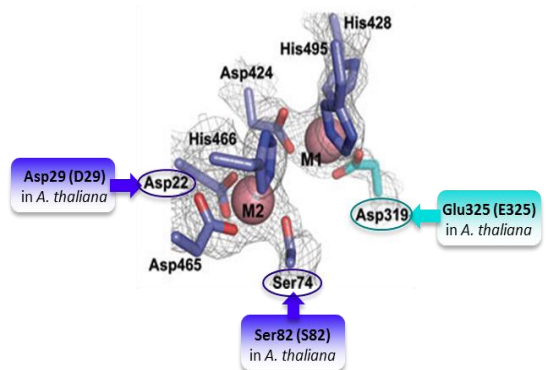


Staphylococcus aureus



According to Roychowdhury et al., FEBS Journal, 2015

Trypanosoma brucei



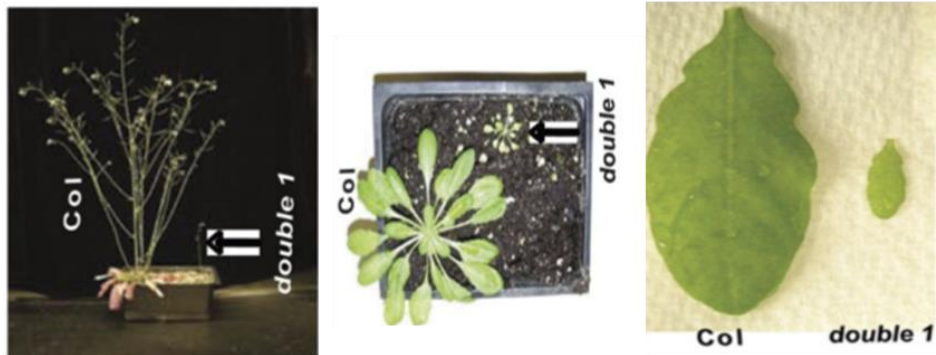
According to Mercaldi et al., FEBS Journal, 2012

Figure 16: Overview of the structure function studies in different species *Trypanosoma brucei*, *Geobacillus stearothermophilus* and *Staphylococcus aureus*

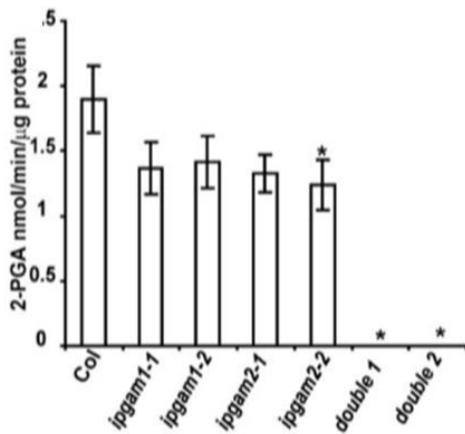
- Production of 2-PGA and 3-PGA from 2,3-bisphosphoglycerate (Fothergill-Gilmore and Watson, 1989).

Two enzymes that are not structurally, mechanistically, nor evolutionary related, can catalyze the interconversion between 3-PGA and 2-PGA. One enzyme requires 2,3-bisphosphoglycerate as a cofactor and is therefore called 2,3-bisphosphoglycerate-dependent phosphoglycerate mutase (dPGAM). This enzyme can catalyze the three reactions with different rates and besides its structure and protein sequence, it is comparable to bisphosphoglycerate mutase. The second enzyme is independent of 2,3-bisphosphoglycerate but a divalent cation is needed for its activity. It is called 2,3-bisphosphoglycerate-independent phosphoglycerate mutase (iPGAM) and it can only catalyze the 3-PGA/2-PGA isomerization reaction that transfers an internal phosphate group from the C-3 to the C-2 position (Fothergill-Gilmore and Watson, 1989; Fraser et al., 1999). Glycolysis and gluconeogenesis in all vertebrates, some fungi such as *Saccharomyces cerevisiae*, and some bacterial organisms like *Haemophilus influenzae* work with dPGAM while iPGAM is the major form found in plants, algae, nematodes, and some other fungi and bacteria like *E.coli* and *B.subtilis* (Jedrzejewski, 2000). iPGAM is a monomer in contrast to dPGAM and it is also a larger protein. Since glycolysis is essential for ATP production and cell viability and the human enzyme is completely different from certain pathogens that carry iPGAM, these proteins have been identified as good chemotherapeutic targets (Blackburn et al., 2014). This is one of the reasons why it was important to extend our knowledge about this enzyme. The dPGAM structure and reaction mechanism were discovered and well-studied by means of *S.cerevisiae* dPGAM structure (Campbell et al., 1972), but less was known about iPGAM proteins until the cloning of several *iPGAM* genes. In higher plants, knowledge about iPGAM started in castor oil plant (Leadlay et al., 1977), wheat germ (Breathnach and Knowles, 1977; Leadlay et al., 1977), maize (Grana et al., 1992; Delaossa et al., 1994) and tobacco (Huang et al., 1993) and allowed to show the high sequence conservation of iPGAM proteins among these species. Gene sequences encoding iPGAM showed some similarities with alkaline phosphatases, especially a highly conserved sequence corresponding to the metal binding domain (Kuhn et al., 1995), while dPGAM was more related to acid phosphatases (Huang et al., 1993; Graña et al., 1995). This suggested that even if dPGAM and iPGAM can catalyze the same reaction, they were evolutionary and mechanistically unrelated. The first iPGAM protein to be crystallized was from *Geobacillus stearothermophilus* and this allowed a better understanding of the reactional mechanism of this enzyme (Jedrzejewski et al., 2000a). Later, the structure of iPGAMs from several other organisms including *Leishmania Mexicana*, *Trypanosoma brucei*, *Geobacillus stearothermophilus*, *Staphylococcus aureus* and *Bacillus anthracis* was determined by crystallization (Jedrzejewski et al., 2000b; Nukui et al., 2007; Nowicki et al., 2009; Mercaldi et al., 2012). Furthermore, based on sequence comparisons, iPGAM proteins have been classified into two families. Plant and trypanosomatid iPGAMs belonged to family 1 while family 2

(a)



(b)



(c)

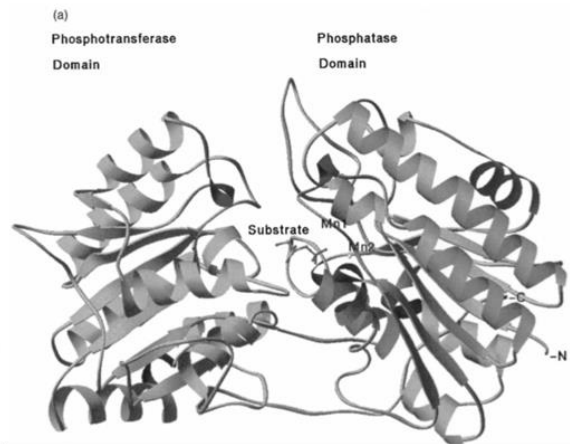


Figure 17: Impact of *AtiPGAM* on *A.thaliana* development & iPGAM protein structure
(a) Phenotype of *ipgam1* \times *ipgam2* double mutant plants (see Zhao and Assmann, 2011). (b) Comparison of leaf *AtiPGAM* activity of different genotypes (see Zhao and Assmann, 2011). (c) iPGAM structure from *Geobacillus stearothermophilus* (see Jedrzejewski et al., 2000)

contained iPGAMs from *Staphylococcus aureus* (SaiPGAM), *Bacillus anthracis* (BaiPGAM), *Geobacillus stearothermophilus* (BsiPGAM) (Blackburn et al., 2014). Even if the catalytic mechanism of iPGAM from the two families were similar, it appeared that family 1 enzymes were more activated by Mg^{2+} and Zn^{2+} than Mn^{2+} , unlike family 2 enzymes that function exclusively with Mn^{2+} (Fuad et al., 2011).

Structural determinations led to the clarification of the structure and catalytic mechanism of iPGAM in several species (Figure 16). They have a compact globular shape and can be found in open and closed monomeric forms whatever the family, since BsiPGAM was crystallized in a closed conformation, BaiPGAM in an open conformation and SaiPGAM in a partially closed conformation. These globular proteins were composed of two domains: a transferase domain and a phosphatase domain interacting with each other *via* a large surface containing hydrogen bonds and separated by two loops forming flexible bridges that held these two domains together. There was a small space between these two domains that constituted the catalytic center. Both domains were made of a central β -sheet surrounded by α -helices on the outside. The first domain, domain A, contained the substrate binding site, while the second one, the domain B, possessed the catalytic site. It was thus shown that the phosphate transfer from C-3 to C-2 of the phosphoglycerate involved a transient phospho-residue on a highly conserved serine. This reactional mechanism has been deciphered in *Geobacillus stearothermophilus* and it had a strict requirement for Mn^{2+} . This study also showed the involvement of specific residues in substrate and Mn^{2+} binding, the retention conformation, and the isomerization reaction. After the ligand binding step, the enzyme adopted a closed conformation to perform the phosphate transfer (Jedrzejewski et al., 2000a). Experiments carried out on BaiPGAM showed that the substrate ensured a link between the two domains. Since the reaction was reversible, the product needed to be released fast and this explained the low affinity of 2-PGA/3-PGA for the protein. Further information concerning the catalytic mechanism was obtained from the partially open conformation of the iPGAM structure of *Staphylococcus aureus* (SaiPGAM). It confirmed that the binding site was only located on domain A and that substrate binding occurred in the open conformation. Indeed, it was proposed that the open conformation was the prevalent state in solution. Structural analysis also showed that divalent cation binding was “sequential and cooperative” with the final exergonic reaction required for phosphate transfer to happen. Furthermore, the comparison of the three crystallized proteins allowed to calculate the hydrophobic area exposed to the solvent in the closed vs open conformations and it suggested that the increase of conserved hydrophobic residues exposed to the solvent led to the reopening of the protein to allow a new reaction cycle (Blackburn et al., 2014; Roychowdhury et al., 2014; Roychowdhury et al., 2015).

In *Arabidopsis thaliana*, a comparison of sequence similarities and electrostatic potentials suggested the presence of six genes encoding putative PGAM proteins (Mazarei et al., 2003;

Andriotis et al., 2010; Stein et al., 2010). Among these genes, only two of them, *At1g09780* (*AtiPGAM1*) and *At3g08590* (*AtiPGAM2*) shared similarities with iPGAM from other higher plants; encoding 60 kDa proteins with a 90 % identity. In the double *ipgam1ipgam2* mutant, *AtiPGAM* activity was undetectable and some drastic vegetative and reproductive developmental phenotypes were observed (Figure 17); stunted growth and an absence of pollen production leading to sterility. Moreover, in the mutant lines, stomatal movement initiated by low CO₂, blue light and ABA signaling were impaired (Zhao and Assmann, 2011). Such results pointed out the importance of this primary metabolism enzyme in plant development and adaptation to environmental changes. No developmental phenotypes were seen in the single mutants even though *AtiPGAM* activity was reduced thus suggesting a functional redundancy (Zhao and Assmann, 2011). When *AtiPGAM* activity was reduced in *Solanum tuberosum*, a 30 % accumulation of 3-PGA and a reduction of starch were detected when compared to the WT. In these plants, vegetative growth was impaired as much as the rate of photosynthesis probably because of 3-PGA accumulation that could have a negative feedback on photosynthesis (Westram et al., 2002). Although these results have underlined the importance of this enzyme, the mechanism(s) regulating plant iPGAM activity is still unclear. It has already been mentioned in the paragraph (II.3) focused on glycolysis that one level of regulation of this pathway could be the phosphoregulation of certain glycolytic enzymes (Boex-Fontvieille et al., 2014) (<http://phosphat.uni-hohenheim.de>). Among these potential phosphoproteins, a phospho-peptide containing a phosphorylated serine at position 82 of *Arabidopsis* iPGAM1/2 was highly represented in the PhosPhAt database.

V) My PhD objectives and strategies

Sessility is a major constraint that plants must deal with. Faced with numerous stresses coming from the environment, of both biotic and abiotic origins, to survive plants have no alternative but to adapt rapidly and specifically to such conditions. To do so, fast and reversible post-translational modifications are used to regulate protein activity. Among the various translational modifications available, protein phosphorylation is one of the most used by living organisms. During my PhD, a main objective was to decipher the role of the phosphorylation of two important primary metabolism enzymes:

- **AtPGLP1**, which is the first enzyme of the photorespiratory cycle where it removes toxic 2-PG to produce glycolate, transformed in the cycle to finally produce 3-PGA that can feed the CB cycle.

- **AtiPGAM**, which is involved in glycolysis, another major pathway, during which it catalyses the isomerisation between 3-PGA and 2-PGA.

- For *AtPGLP1*, three phospho-peptides and four potential phospho-sites had been identified in different phosphoproteomes: threonines in positions 103, 322, 330 (T103, T322 and T330) and serine in position 356 (S356). It should be noted that positions were calculated from the full-length polypeptide before processing of the chloroplast targeting sequence and that T322 and T330 were identified on the same phospho-peptide but never at the same time. The aim was to identify the role of each phospho-site. To achieve this, each phospho-residue was mutated by site-directed mutagenesis to either mimic a constitutive phosphorylation (by replacing the T/S with an aspartate) or to create a non-phosphorylatable enzyme (replacement with an alanine). Mutated *AtPGLP1* proteins were expressed and purified from *E. coli* cells in a recombinant protein strategy, and they were also expressing *in planta* by complementing the *Arabidopsis pglp1* mutant.

Furthermore, since mammalian PGP had recently been shown to be regulated by the redox state of the cell, a second goal of my PhD was to discover whether *Arabidopsis* PGLP1 responded to oxidation-reduction conditions. We wanted first to know if oxidation impacted *AtPGLP1* activity as seen for the mammalian PGP, and then to decipher the role of the different cysteines on *AtPGLP1* activity and structure. To do so we decided to do site-directed mutagenesis of the *Arabidopsis* PGLP1 protein at the five cysteines and investigate their role.

In order to compare *in vitro* kinetic parameters of soluble mutated *AtPGLP1* variants and WT enzyme, several recombinant protein strategies were tested to produce and purify the different *AtPGLP1* proteins, which already represented a first challenge. My next goal was to develop adapted and repeatable protocols to measure *AtPGLP1* activity in real time, using 2-PG as substrate. This included a spectrophotometric method using a coupled reaction with recombinant GOX, and two direct reactions either by NMR (to measure the production of glycolate) or by using a phosphate sensor method (to measure released inorganic phosphate).

Impact of the phospho-site mutations was then questioned through an *in planta* approach where *Arabidopsis pglp1* plants were transformed with *AtPGLP1* phospho-site mutated forms to investigate their impact on photorespiration and plant metabolism in general. This brought up the following question; under which conditions were these potential phospho-regulations necessary? In this context, it was decided to study *AtPGLP1* activity in response to day/night and different stresses including high light, different CO₂ concentrations and high temperature. The tested conditions were known to modulate photorespiration and thus could require the regulation of *AtPGLP1* activity.

- For *AtiPGAM*, the identified S82-containing phospho-peptide had been found in various phosphoproteomes. In this context, my aim was to decipher the role of this phosphorylation in

Arabidopsis thaliana. The same site-directed mutagenesis strategy was adopted, first on the detected phospho-site that was changed to either an aspartate or an alanine. This was then extended to other key amino acids chosen according to their role in the different steps of the reaction mechanism and based on data from other organisms (*Trypanosoma brucei*, *Geobacillus stearothermophilus*) to gain insights into the catalytic mechanism of the plant enzyme and to eventually determine whether S82 phosphorylation was only an indication of AtiPGAM activity.

RESULTS

CHAPTER I

Preamble

This chapter will be organized as followed:

- I) Characterization of phosphoglycerate mutase catalytic mechanism in *Arabidopsis thaliana*

This part is presented as a manuscript in preparation.

- II) Additional results

This part of the first chapter details the work following the manuscript.

- I) Characterization of phosphoglycerate mutase catalytic mechanism in *Arabidopsis thaliana*

Characterization of phosphoglycerate mutase catalytic mechanism in *Arabidopsis thaliana*

Pauline DUMINIL¹, Marlène DAVENTURE², Céline OURY¹, Michel ZIVY², Edouard BOEX-FONTVIEILLE^{1, 3}, Guillaume TCHERKEZ^{1, 4}, Michael HODGES¹, Nathalie GLAB^{1*}

¹Institute of Plant Sciences Paris-Saclay, CNRS, Université Paris-Sud, INRA, Université d'Evry, Université Paris-Diderot, Université Paris-Saclay, 91405 Orsay Cedex, France

²PAPPSO, GQE - Le Moulon, INRA, Université Paris-Sud, CNRS, AgroParisTech, Université Paris-Saclay, 91190 Gif-sur-Yvette, France

³present address: Institut National de Police Scientifique, 31 av. Franklin Roosevelt, BP30169, Ecully cedex, France

⁴ present address: Research School of Biology, Australian National University, 2601 Canberra, ACT, Australia

*Corresponding author: Tel. +33 (0)1 69153349; e-mail: nathalie.glab@u-psud.fr

Key words: Glycolysis, Phosphorylation, iPGAM, 3-phosphoglycerate, *Arabidopsis thaliana*

Abstract

The phosphoglycerate mutase (PGAM) catalyses the reversible isomerisation between the 3-phosphoglycerate (3-PGA) and the 2-phosphoglycerate (2-PGA). In the living kingdom, PGAM enzymes are divided in two families, the dPGAM present in vertebrates, some fungi and bacteria, depend on the 2,3-biphosphoglycerate as a cofactor and the iPGAM, independent of this molecule that are found in plants and some microorganisms. All glycolytic enzymes are known for a long time; however, their catalytic and regulation mechanisms are still under study. Since the plants are sessile and need to respond quickly to the environmental changes, one highly relevant level of regulation is the post-translational ones, the most significant being the protein phosphorylation. The database reserved to the *A. thaliana* phosphopeptides mentions the presence of a specific phosphopeptide for *AtiPGAM* that was never characterized. In the present work, the *AtiPGAM2* was analysed in silico and in vitro through the determination of its kinetics parameters. We then focused on the catalytic mechanism of this plant enzyme by the use of mutated enzyme forms.

Introduction

Glycolysis is a ubiquitous metabolic pathway occurring in the cytosol of all types of cells. It consists of a chemical chain reaction transforming a molecule of glucose into two three-carbon sugars, namely two pyruvates, allowing the generation of reducing power and energy as NADH and ATP, respectively. Once produced, the pyruvate can classically feed the TCA cycle in the mitochondria *via* the acetyl-CoA leading to the complete oxidation of the pyruvate linked with further chemical energy production, and also contribute to the building up of new important metabolites, such as lipids in specialized plastids (Ruan, 2014). An isoform of most cytosolic, glycolytic enzymes can be found in the chloroplast and are mainly involved in the Calvin-Benson cycle and the pentose phosphate pathway (Plaxton, 1996; Givan, 1999). A recent study has even localized a range of glycolytic enzymes in the outer membrane of mitochondria envelope (Giegé et al., 2003), allowing a directed entrance of pyruvate into the Krebs cycle. Various metabolites are exchanged between these organelles enabling reductant and phosphate homeostasis in cells (Weber and Linka, 2011). One of these glycolytic enzymes is the phosphoglycerate mutase that catalyzes the reversible isomerization of 3-phosphoglycerate (3-PGA) and 2-phosphoglycerate (2-PGA), the eighth step of the classical glycolysis. The 3-PGA is a pivotal metabolite since it is also involved in several other pathways such as: Calvin-Benson cycle, starch and serine biosynthesis.

Two evolutionary unrelated protein groups may have this mutase activity (Jedrzejewski, 2000). One of these groups needs 2,3-bisphosphoglycerate as a cofactor to be efficient and is so called 2,3 diphosphoglycerate dependent phosphoglycerate mutase (dPGAM); while the other group of enzymes only needs a divalent cation (e.g., Mg^{2+} , Mn^{2+} , Co^{2+} , Zn^{2+}) to be functional and is called 2,3 diphosphoglycerate independent phosphoglycerate mutase (iPGAM). Glycolysis and gluconeogenesis in vertebrates, some fungi and bacteria work with dPGAM, that is often the only type of PGAM, like in human (Fothergill-Gilmore and Watson, 1989); while iPGAM is predominant in plants, algae, nematodes, and some other fungi and bacteria (mainly Gram-positive), making the iPGAM a target for antibiotics. These two groups of proteins show few similarities when considering the sequence, the structure and the catalytic mechanism (Jedrzejewski, 2000). Furthermore, the iPGAM proteins are classified in two families according to their amino acid sequences. Family 1 is composed of enzymes found in trypanosomatids and plants and uses Mg^{2+}/Zn^{2+} , while the others constitute family 2 and need Mn^{2+} to be active (Fuad et al., 2011; Blackburn et al., 2014). X ray diffraction techniques led to resolve the 3D structure of some family 1 enzymes : from *Leishmania Mexicana* (LmiPGAM) and *Trypanosoma brucei* (TpiPGAM), and family 2 enzymes: from *Bacillus stearothermophilus* (BsiPGAM), *Staphylococcus aureus* (SaiPGAM) and *Bacillus anthracis* (BaiPGAM) (Jedrzejewski et al., 2000a; Nukui et al., 2007; Nowicki et al., 2009; Mercaldi et al., 2012; Roychowdhury et al., 2015). In the case of

iPGAMs such crystallographic data revealed that the monomeric, globular enzyme is made of two domains: domain A containing the substrate binding site, also called the phosphatase domain, and domain B the catalytic serine, named transferase domain. Both domains are linked by a flexible junction necessary for the enzyme to work *via* an open vs closed conformation. Moreover, it has been shown that the phosphate group transfer from one carbon to another on the substrate phosphoglycerate is based on a mechanism involving a transient phospho-serine. The position of this serine residue in the protein sequence is highly conserved, among other evolutionary preserved amino-acids essential for the catalytic cycle.

In *Arabidopsis thaliana*, using TAIR and KEGG databases, sequence similarities and electrostatic potential, six genes were suggested to encode putative PGAM proteins (Mazarei et al., 2003; Andriotis et al., 2010; Stein et al., 2010). Among these genes, only two, *At1g09780* and *At3g08590* have similarities with iPGAM from other higher plants and thus were annotated as iPGAM in both databases. These two genes, *iPGAM1* and *iPGAM2*, encode a 60 kDa phosphoglycerate mutase independent of 2,3-biphosphoglycerate sharing 90% identity between each other. In the *ipgam1ipgam2* double mutant, iPGAM activity is undetectable and plants display severely impaired vegetative and reproductive developmental phenotypes. A stunted growth and a lack of pollen production are observed leading to sterility (Zhao and Assmann, 2011). These results have pointed out the importance of this primary metabolism enzyme in plant development. Interestingly, no developmental phenotype is visible in both single mutants, even if iPGAM activity is moderately reduced, thereby suggesting a functional redundancy (Zhao and Assmann, 2011). These genetic-based results underlined the importance of these enzymes, as expected from their position in primary metabolism, however and curiously enough, the mechanism that regulates iPGAM activity in plants is still unclear. In this regard, an iPGAM phosphopeptide is found at a high occurrence in many phosphoproteomes performed from *A. thaliana*. In all experiments, and whatever the culture conditions, the serine 82 (S82) is found to be phosphorylated (<http://phosphat.uni-hohenheim.de/>). In plants, since the glycolysis rate is higher in the dark we hypothesized a day/night regulation of AtiPGAM by phosphorylation (Tcherkez et al., 2008).

Thus, the aim of our work is to clarify the role of this phosphosite in the regulatory mechanisms acting on the *A. thaliana* iPGAMs. A strategy using site-directed mutagenesis has been adopted to change, first S82 by an alanine and an aspartate, a non-phosphorylatable and a phosphiomimic amino acid respectively, then other key amino acids identified in previous studies (from other organisms: *Trypanosoma brucei*, *Geobacillus stearothermophilus*, *Staphylococcus aureus*) to finally gain insight into the catalytic mechanism of this plant enzyme.

Materials and Methods

Plant material

Arabidopsis thaliana ecotype Columbia (Col-0) was used in all experiments. Seeds are sowed on the breeding soil for at least one week for the germination and plantlets are transplanted on new individual pots for growth in short day chamber with light regime of 8h light at 175 μmol of photons. $\text{m}^{-2}.\text{s}^{-1}$ and 16h dark, 20 °C day/18 °C night and 65 % humidity.

Plasmid construction, site-directed mutagenesis

Cloning of wild type and S82A or S82D mutated iPGAM2 open reading frame (ORF) into pET16b was performed using Gibson assembly-based method (Gibson et al., 2009). For pET16b-*AtiPGAM2_{WT}*, two PCR amplified fragments were assembled, one corresponding to pET16b backbone using the primer combination [pET16b-fw+pET16b-rev] and native pET16b as template and the other to iPGAM2 ORF using the primer combination [iPGAM2-fw16b+iPGAM2-rev16b] and iPGAM2 cDNA into pUNI51 as template (obtained from ABRC ; (Yamada et al., 2003). For pET16b-*AtiPGAM2_{S82A}* and pET16b-*AtiPGAM2_{S82D}*, the same strategy was applied except that the mutated iPGAM2 ORF were obtained through the assembly of two PCR amplified fragment each obtained with the following primer combinations [iPGAM2-fw16b+iPGAM2S82Arev] and [iPGAM2S82Afwd+iPGAM2-rev16b] for *AtiPGAM2_{S82A}* and [iPGAM2-fw16b+iPGAM2S82Drev] and [iPGAM2S82Dfwd+iPGAM2-rev16b] for *AtiPGAM2_{S82D}*. To obtain pET16b-*AtiPGAM2_{D29N}* and pET16b-*AtiPGAM2_{R290L}*, the previously described pET16b-*AtiPGAM2_{WT}* was used as template for mutagenesis experiment performed with QuikChange Lightning Site-Directed Mutagenesis Kit (Agilent) and the primer combinations [563PRO+564TER] and [565PRO+566TER] respectively. All primers sequences are given in supplementary data table S1.

Purification of the recombinant proteins

E. coli BL21 cells containing either pET16b-*AtiPGAM2_{D29N}* or pET16b-*AtiPGAM2_{S82A}* or pET16b-*AtiPGAM2_{S82D}* or pET16b-*AtiPGAM2_{R290L}* have been grown in 400mL of Luria-Bertani broth supplemented with Ampicillin (50 mg.L⁻¹) at 37°C until a 0.8 OD_{600nm} and the expression was induced by addition of isopropyl -1-D-thiogalactopyranoside 500 μM final concentration overnight at 20°C. The cells are then centrifuged and resuspended in a lysis buffer (3mL for a 200mL culture pellet) containing Tris-HCl 50mM pH7.5; NaCl 300 mM; imidazole 5 mM, a protease inhibitor (Complete Mini, EDTA-free, Roche Applied Science) and the cells are ground mechanically with the French press at 3.5 MPa. After a 30 min centrifugation at 4°C and 27 000 g, the recombinant proteins are purified on His-Select nickel affinity resin (Sigma-Aldrich) according to manufacturer indications for the

“batch” technique. The washing and elution were performed with modified lysis buffer respectively at 20 mM and 250 mM imidazole. The eluate is further desalted using the PD-10 columns (GE Healthcare) previously equilibrated with Tris-HCl 50 mM at pH 7.5 following the manufacturer’s instructions. Protein concentration is determined using the Pierce™ Coomassie Plus Assay Reagent (B6916, Sigma-Aldrich).

Enzymatic assay

The enzymatic assay was carry out using a Varian Cary 50 spectrophotometer at 340 nm in a buffer containing 30 mM Tris-HCl pH 7.5, 20 mM KCl, 5 mM MgSO₄ according to (Zhang et al., 2004) with 2.5 µg of proteins.

Phosphoproteome experiments

The enzymes were incubated at 30 °C with different 3-PGA concentrations during 10 min in a 20 µL reaction buffer 30 mM Tris-HCl pH 7.5, 20 mM KCl, with or without 5 mM MgSO₄ and 2.5 µg of proteins. The reaction was stopped by adding a Laemmli buffer 4X. The protein are then separated in an electrophoresis one-dimensional polyacrylamide gel according to their molecular mass, in denaturing conditions (Laemmli, 1970). The band corresponding to iPGAM (61 kDa) was cut according to the molecular weight marker (PageRuler Prestained, Thermo Scientific). The phosphoproteome experiments from the SDS-PAGE gel cut were performed according to Hummel *et al.*, (2015). The phosphoproteome experiments on *A. thaliana* leaves were previously described by (Boex-Fontvieille et al., 2014).

Results

iPGAMs structure/ function

We first investigated the relationship between structure and function of AtiPGAM, by performing *in-silico* studies on the 3D prediction structure of the enzyme *via* SWISS MODEL. Swiss Model Repository (SMR) was recently updated to build up a structure database according to crystallized proteins from a variety of species that directly provides the best template for the 3D structure prediction of *A. thaliana* proteins (Bienert et al., 2017). The emerging PGAM sequence in this study was that of the *Leshmania mexicana*. Indeed, this enzyme (i) was crystallized in presence of the substrate 3-PGA and two divalent cations (Co²⁺), and (ii) shows a high percentage of identity between the sequences, with many conserved secondary structures (α-helix and β-sheet) (Figure 1a). The “rainbow” representation of the 3D structure allows a clear identification of the two domains A

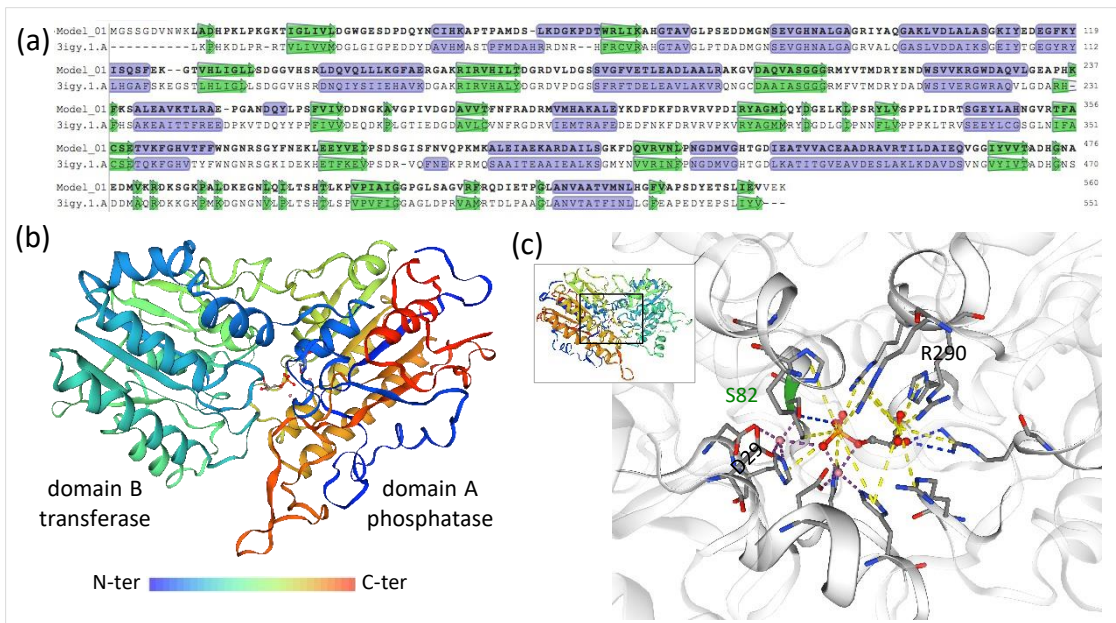


Figure 1: AtiPGAM2 3D-structure prediction.

Using both modelling and repository tool of SWISS-MODEL website the 3D structure of AtiPGAM2 was predicted. Using SWISS-MODEL workspace, several templates were found. (a) presents the alignment of AtiPGAM2 sequence (Model_01) with one of the template (3igy.1) showing 56.8% sequence identity corresponding to the sequence of the *Leshmania mexicana* co-factor independent phosphoglycerate mutase (see Figure S1 in supplementary data for its 3D-structure). Green arrows indicate α -helices and purple boxes β -sheets. (b) represents the rainbow 3D-structure of AtiPGAM2 found in SWISS-MODEL Repository database (A0A384KAQ5) also built with 3igy.1 template with a global model quality estimation (GMQE) of 0.8 (in a scale from 0 to 1). The two domains (A phosphatase and B transferase) are indicated. This structure includes two metal ions (pink balls) and 3-phosphoglycerate (see Figure S1 in supplementary data for QMEAN representation; the QMEAN score is -0.65). (c) represents the catalytic core of the enzyme. Insert shows the position of the focused region. Note that the presented view corresponds to a 180° turn compared to the one presented in (b). Reactive serine is marked in green on the chain (S82). All residues involved in metal ion and 3-PGA binding are licorice represented. Apart from S82, the two other residues studied in this work are annotated (D29 and R290; for others see Figure S1 in supplementary data). Purple lines represent the five interactions of each metal ion with both 3-PGA and the chain. Blue and yellow lines represent respectively the three hydrogen bonds and the 14 salt bridges of the 3-PGA with the chain. Each type of bonds is detailed in Figure S1 in supplementary data.

Table 1: Measurement of AtiPGAM2 kinetic parameters *in vitro*

Protein	K_m (mM)	V_{max} ($\mu\text{mol}\cdot\text{min}^{-1}\cdot\text{mg}^{-1}$ of protein)	K_{cat} (s^{-1})
pET16b-AtiPGAM2 _{WT}	0.467 ± 0.032	48.5 ± 3.3	51.3 ± 3.5

AtiPGAM2 activity can be measured by the disappearance of NADH detectable *via* the Varian Cary 50 spectrophotometer at $\Delta A_{340 \text{ nm}}$ during a coupled reaction (supplementary data Figure S2). These parameters were calculated using “Kinetic Enzyme Wizard” from Sigma-Plot (Systat Software Inc.) with molar extinction coefficient $6.22 \cdot 10^{-3} \text{ M}^{-1}\cdot\text{cm}^{-1}$. Value are means \pm SD (n=3 independent experiments)

(phosphatase domain composed of the amino and the carboxy-terminal) and B (transferase domain) (Figure 1b). A focus on the active site provided informations on the amino acids involved in the catalytic mechanism. First, the catalytic centre serine 82 (S82) interacts with the substrate 3-PGA and one of the two Cobalt ions. This cation is also connected with aspartate 29 (D29), while in the opposite transferase domain, arginine 290 (R290) bounds the carboxylic part of the 3-PGA substrate (Figure 1c and supplementary data Figure S1). It was thus needed to bring a confirmation as to the precise role of these residues in the active site of *AtiPGAM*, as deduced from the *in-silico* modelling approach. The sequence alignment of iPGAM enzymes from different species: *Staphylococcus aureus*, *Bacillus anthracis*, *Bacillus stearothermophilus* from (family 2), or *Trypanosoma brucei* and *Leshmania mexicana* (family 1), made it apparent the conservation amongst other residues of the aspartate 29 (D29) and arginine 290 (R290) (Blackburn et al., 2014). Indeed, D29 is in domain A, and corresponds in the alignment to D12 for family 1 iPGAMs, and D22 or 23 for family 2 *TbiPGAM* and *LmiPGAM*, respectively. Structural studies of the corresponding proteins from other species demonstrated that this aspartate residue is involved in orientating the second divalent cation to catalyse the phospho-transfer in a closed conformation. On the other hand, R290 from *A. thaliana* enzyme is on domain B; as are R284 (*TbiPGAM*), R285 (*LmiPGAM*) and R260/R264 (*SaiPGAM*/*BsiPGAM*, respectively). This arginine residue was shown to be necessary for the interaction between the enzyme and the carboxyl group of the substrate (Jedrzejewski et al., 2000a; Nukui et al., 2007; Nowicki et al., 2009; Mercaldi et al., 2012; Roychowdhury et al., 2015). Thus, both sequence comparison and 3D structure prediction of *AtiPGAM* (Figure 1) provided clues to hypothesize a central role of D29, S82 and R290 in the enzyme catalytic mechanism. A site directed mutagenesis approach was well adapted to investigate such a question.

AtiPGAM kinetic parameters

The activity measurement of the recombinant protein *AtiPGAM2* has never been reported so far. To this end, we adapted the coupled reaction technique described in (Zhang *et al.*, 2004; Supplementary data Figure S2) and primarily used to measure the activity of the enzyme in leaf extracts from *A. thaliana* (Zhao and Assmann, 2011). The K_m value (0.467 mM; Table 1) for the 3-PGA substrate was found to be similar to that of *L. mexicana* and *T. brucei* enzyme; in contrast the k_{cat} value was ten times lower compared to *LmiPGAM* (Guerra et al., 2004; Mercaldi et al., 2012). Indeed, looking on the databases (<https://www.brenda-enzymes.org>), the functional parameters for iPGAMs are highly variable, depending on the organisms. Few information are available for plants, except for the *Zea mays* and *Ricinus communis* enzyme whose K_m for the 3-PGA is comparable to that of *AtiPGAM* (Botha and Dennis, 1986a; Grana et al., 1989).

S82 is found to be phosphorylated in several phosphoproteomes

The serine 82 was found to be phosphorylated in different phosphoproteome experiments (<http://phosphat.uni-hohenheim.de/>) and it is known that iPGAM in both families is working *via* a transitory phosphoserine that ensures the phosphate transfer from one carbon to another. However, there is no available information about the identity of the catalytic serine in the *Arabidopsis* enzyme. Sequence alignment has shown that serine 82 of *AtiPGAM2* corresponds to S62 in *SaiPGAM* and *BsiPGAM*, and S74 in *TbiPGAM* (Blackburn et al., 2014), which have been demonstrated to be catalytic. At this stage, two hypotheses had to be considered. This *Arabidopsis* S82 has a role in catalysis; alternatively, it could be the result of a post-translational modification regulatory mechanism. It is important to note that these two hypotheses are not mutually exclusive. To test this, mutated enzymes were produced: S82D (aspartate is a phosphomimic amino acid, due to its negative charge), and S82A (alanine is a non-phosphorylatable residue). The production and purification rates were the same between the WT and the mutated recombinant proteins (supplementary data Figure S3), however the activity was completely abolished in both cases (Figure 2). These results strongly suggest the cardinal role of S82 in the enzyme catalytic mechanism.

Deciphering the reaction mechanism using mutated enzyme forms

The study of iPGAM in other species allowed us to target two other highly conserved amino acids to go further in the understanding of the reaction mechanism in *A. thaliana*. As described in the Materials and Methods, the residues have been modified by site directed mutagenesis, e.g., aspartate 29 to asparagine (D29N) and arginine 290 to leucine (R290L). These amino acids were chosen because their involvement in the open/closed conformation of the enzyme was predicted (Jedrzejewski et al., 2000a). As mentioned above, D29 in *BsiPGAM* domain A is also considered as the “metal binding domain” and is involved in positioning the substrate *via* the metal binding (Jedrzejewski et al., 2000a) while R290 in domain B (substrate binding domain) is supposed to participate in the substrate binding, and consequently the closure of the enzyme. In our experiment, none of the purified, mutated enzymes displayed a catalytic activity, thereby confirming the requirement of these residues to keep the wild type activity (Figure 2). It was demonstrated by LC-MS/MS that the abundance of phosphopeptide S82 increases with substrate amounts (Figure 3a). Thus, since there was no contaminating protein kinase in the assay, it can be concluded that the phosphate group on the S82 originates from 3-PGA. This result establishes this phosphoserine as a step in the catalytic mechanism. In next experiments the mutated enzymes D29N and R290L were used to confirm the role of S82 as a transient phosphoresidue step of the catalytic mechanism. The mutated recombinant proteins were incubated with/without a high amount of 3-PGA (2.5 mM; Figure 3b) and the phosphorylation level was measured (Figure 3). Interestingly, S82 phosphorylation only occurs in the

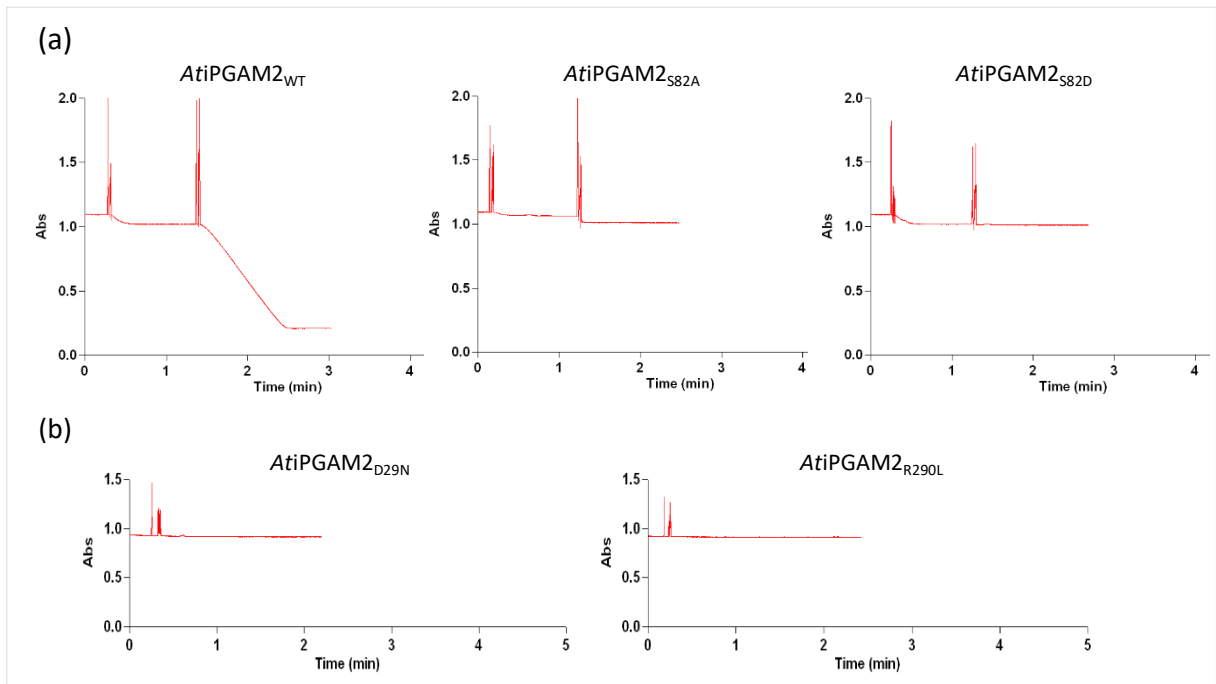


Figure 2: *AtiPGAM2* activity of the mutated recombinant proteins by comparison with the WT

Importance of specific residues for *AtiPGAM2* activity, measured *via* the coupled reaction as described in Materials and Methods using the Varian Cary 50 spectrophotometer at $\Delta A_{340\text{ nm}}$ at 1mM of substrate (3-PGA) and 2,5 μg of recombinant proteins (a) Since S82 is mutated whatever the alternative amino-acid (S82A or S82D), the activity is completely abolished in comparison with the WT. (b) When the residues predicted to be important for the *AtiPGAM2* activity (D29 and R290) are mutated (D29N and R290L), there is no more detectable activity.

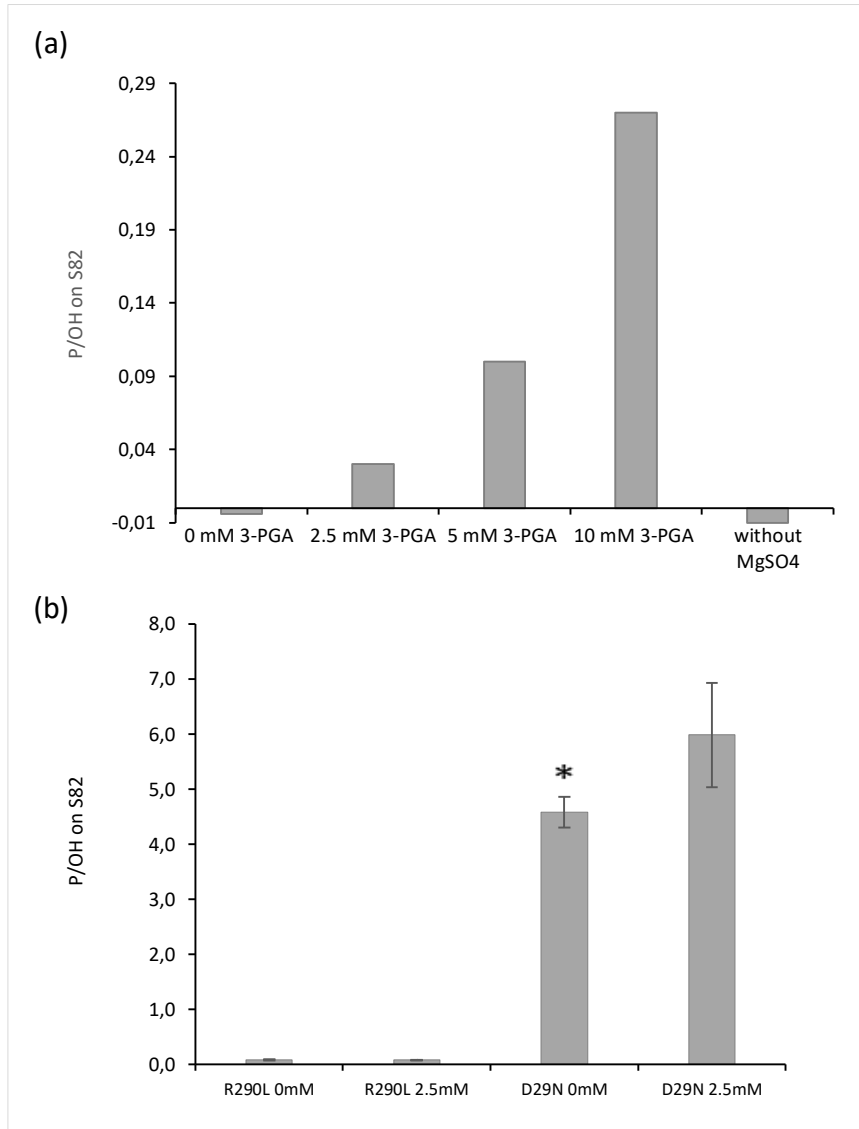


Figure 3: Phosphorylation level detected on S82 of the recombinant *AtiPGAM2*

(a) Phosphorylation level on Serine 82 (S82) on *AtiPGAM_{WT}* according to the substrate concentrations (3-PGA; from 0 to 10 mM) and the absence of Mg^{2+} (without $MgSO_4$). The bacterial contaminations are deducted from the data. **(b)** Phosphorylation level on Serine 82 (S82) with/without 3-PGA (0 mM and 2.5 mM) measured on the mutated recombinant proteins *AtiPGAM2-D29N* and *AtiPGAM2-R290L* (D29N; R290L). Value are means \pm SD (n=3 biological replicates). Statistical significance was determined by a Student's *t*-test (* $P < 0.05$).

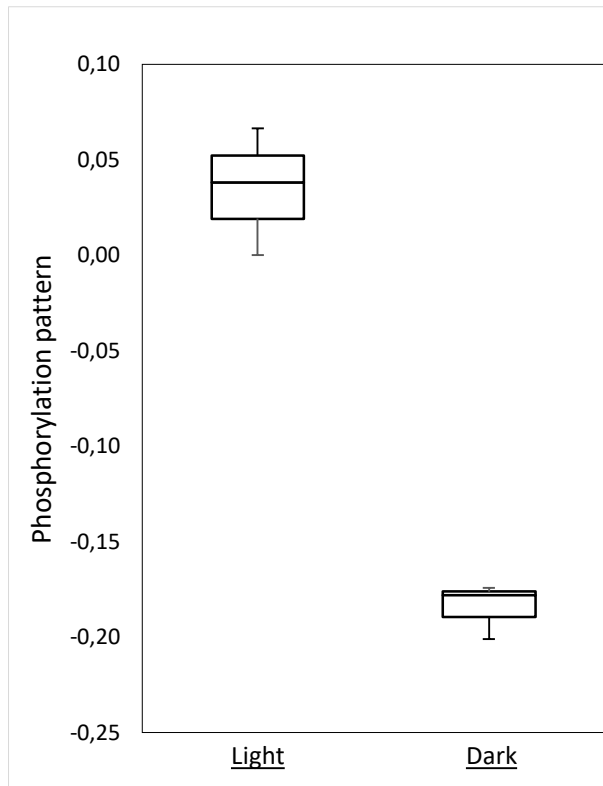


Figure 4: Day/ night phosphoproteome in leaves

Phosphorylation level of Serine 82 was measured in leaves of *Arabidopsis thaliana* plants grown in ambient air and under a 8:16 h light/dark regime (short days) at an irradiance of approximately $100 \mu\text{mol}\cdot\text{m}^{-2}\cdot\text{s}^{-1}$. This box plot was performed on $n=3$ experiments. Ordinate axis represents relative phosphorylation pattern in \log_2 .

close conformation (D29N) of the enzyme (Figure 3b). In this case, phospho-transfer to S82 occurs first, then the enzyme adopts the close conformation and the system is blocked; so that phosphoserine can be detected by LC/MS. In the R290L mutation, the substrate 3-PGA cannot bind the enzyme and thus making the phosphoserine formation impossible. (Figure 3). This is the *in vitro* confirmation that the reaction mechanism in *A. thaliana* involves an open/closed conformation and a catalytic serine carrying the phosphate during the transfer. The significant amount of S82 phosphorylated in the D29N assay in absence of the substrate indicates that the phospho-transfer occurred in the bacteria, before purification steps. However, this does not affect the conclusion.

Phosphorylation of S82 in planta

We reasoned that amounts of the phosphorylation of S82 should be significantly higher when the enzyme catalytic rate increases *in vivo*, as we previously measured this *in vitro* (see above Figure 3). By use of isotopic labelling based study the group had previously reported the higher glycolysis investment in plant metabolism during the dark phase (Tcherkez et al., 2008). The hypothesis that the glycolytic iPGAM should be more active, and thus more phosphorylated, in the darkened plant leaf was therefore investigated. A dark/light phosphoproteome was thus performed on leaf proteins of *A. thaliana* (Figure 4). Unexpectedly, it turned out that the peptide containing S82 was statistically more phosphorylated under light than in the dark conditions.

Discussion

Two types of phosphoglycerate mutase have been characterized in various organisms of the living kingdom: one is dependent on the 2,3-bisphosphoglycerate as cofactor, while the other is independent of this metabolite, instead requires a divalent cation to gain its full activity. Their involvement in the primary metabolism pathway, glycolysis, obviously makes these proteins of paramount importance. For example, in plants, which have the iPGAMS enzyme form, our data indicated that the double *A. thaliana* mutant *ipgam1ipgam2* (the two genes encoding high identity enzymes in the genome *At1g09780* and *At3g08590*) shows impaired growth and development and is completely sterile. Development is also found to be largely altered in the antisense potato *ipgam* mutants (Westram et al., 2002; Zhao and Assmann, 2011). Another example is the *in vitro* RNA silencing of *iPGAM* in *Brugia malayi* that rescues the parasite motility, while the same kind of gene silencing in *Caenorhabditis elegans* leads to a larval stage lethality (Zhang et al., 2004; Singh et al., 2013). Interestingly, vertebrates, including human, only possess dPGAM (like also yeast and some bacteria), while plants, archaea and other bacteria are performing glycolysis using iPGAM (Fothergill-Gilmore and Watson, 1989; Jedrzejewski, 2000). iPGAMs are thus perfect targets for antibiotics in

humans. In the same way dPGAMs inhibitors could even be used against plants invasion by some yeast or bacteria, such as for wheat-germ (McAleese et al., 1987).

It was therefore crucial to clarify the catalytic mechanism of these proteins and in next steps how they are regulated in the famous plant model, *Arabidopsis*. In previous works on crystallized protein from diverse organism, it was established the role of a transient phosphoserine carrying the phosphate during the isomerization, in an enzyme adopting open/close conformations and using a divalent cation Mn^{2+} , Mg^{2+} or Zn^{2+} (Jedrzejewski et al., 2000a; Nukui et al., 2007; Nowicki et al., 2009; Mercaldi et al., 2012; Roychowdhury et al., 2015). We first characterized the *in vitro* activity of a recombinant AtiPGAM to measure its kinetic parameters. Since AtiPGAM1 and AtiPGAM2 share a high sequence identity and functional redundancy, it is assumed that they are very close in terms of activity and regulatory properties (Zhao and Assmann, 2011). K_m and k_{cat} were measured using the classical coupled reaction; one conclusion is that *A. thaliana* enzymes have a relatively high K_m . This relatively low affinity for the substrate may be related to the actual concentrations of the substrate in the leaf cells. Some measurements were performed on *Solanum tuberosum* in the context of the *ipgam* antisense plant study and revealed a $0.632 \mu\text{mol.g}^{-1}$ of fresh weight (Westram et al., 2002). In *A. thaliana* leaves, the magnitude of order is the same with a concentration around $0.3 \mu\text{mol.g}^{-1}$ FW (Flügel et al., 2017).

Sequence alignments among various species showed some highly conserved residues, including the catalytic serine (Blackburn et al., 2014). Moreover, the corresponding serine in *A. thaliana* was found phosphorylated in several phosphoproteomes (<http://phosphat.uni-hohenheim.de/>), we moved our interest that specific residue and to this goal programmed site directed mutagenesis; the mutation of S82 (onto alanine, non phosphorylatable and aspartate, phosphomimic) entrained a complete loss of catalytic activity (Figure 3) thereby identifying this residue as the catalytic serine in *A. thaliana* enzyme. Further phosphoproteomic analyses on the recombinant proteins finally confirmed S82 involvement in the isomerization of the 3-PGA phosphate, as this showed that the phosphorylation level of the enzyme is dependent on the amount of substrate in the activity assay. It should be noticed that the recombinant enzyme was already partially phosphorylated; we supposed this has occurred in the bacteria before the enzyme purification (Figure 3). Altogether the data indicated the reality of an open/close mechanism for AtiPGAM as suggested in the case of the previously crystallized proteins (Jedrzejewski et al., 2000a; Nukui et al., 2007; Nowicki et al., 2009; Mercaldi et al., 2012; Roychowdhury et al., 2014). In this regard, they confirmed the importance of aspartate 29 in the catalytic process, as its mutation to asparagine keep the enzyme in the close conformation. As mentioned above, this also explains that the phosphorylated, mutated enzyme in the bacteria retained the phosphate. On the other hand, the mutation of arginine 290 completely blocks the reaction mechanism, by probably preventing the

substrate binding. Therefore, neither of these mutated proteins is active. As suggested above, the phosphate labeling of *AtiPGAM*_{D29N} without any 3-PGA in the assay is probably due to the presence of the substrate in the bacteria before the purification; it suggests the stability of the enzyme/substrate structure when D29 is mutated (Figure 3).

Glycolysis in plants is mostly active during the night, substituting to photosynthesis for energy supply to cells; there, hexoses (from sucrose and starch) fuel glycolysis for ATP synthesis and also metabolite diversification. Indeed, in the dark, the $\delta^{13}\text{C}$ value of respired CO_2 coming from ^{13}C -enriched glucose increased to more than 300 % compared to the light period (Tcherkez et al., 2008). Based on preliminary results (cf above), and because the reaction is expected to go faster during the night, our hypothesis was that the enzyme should be more phosphorylated (on S82) in dark conditions. In contrast, the leaf phosphoproteomic experiments (Figure 4) revealed that this serine was easily detectable and statistically more phosphorylated under light conditions. There is no straightforward explanation to this fact since an increase in phosphorylated S82 implies a corresponding increase in 3-PGA (thus increasing the enzyme catalytic rate and serine phosphorylation), which obviously can only occur in the activated pathway (dark). This totally unexpected result may strongly push forward the idea of an additional level of regulation acting on *iPGAM*. One obvious hypothesis is that a protein kinase phosphorylates the S82 thereby resulting in the inhibition of the catalytic process (*via* the lack of interaction with 3-PGA substrate) under light conditions when the mesophyll cell gets energy from photosynthesis. There are numerous examples of the phospho-control of several enzymes of the glycolytic pathway in plants such as the sucrose synthase in *Ricinus communis*, the glyceraldehyde-3-phosphate dehydrogenase in wheat, the pyruvate kinase in the cotton and recently the enolase in maize (Bustos and Iglesias, 2002; Fedosejevs et al., 2014; Zhang and Liu, 2017; Cao et al., 2019). This notorious post-translational modification is known to regulate other pathways, for example photorespiration (Hodges et al., 2013). This would represent an original and elegant mechanism for the control of enzyme activity *via* the phospho-enzyme step of the catalytic process. Further works may be dedicated investigating this very attractive mechanism. We could take advantage of the modified protein on D29 and R290 to see whether *AtiPGAM*_{2R290L} can still be phosphorylated *in planta*, as was the *AtiPGAM*_{2WT}; since we have demonstrated that this mutated form (inactive) cannot be phosphorylated by the substrate, this would mean that a S82 phosphorylation is occurring, which has to be performed by the requested, regulatory protein kinase. This type of experiment needs the complementation of the double mutant by the R290L mutated form. Unfortunately, the double mutant is sterile. Alternatively, the hypothesis implies that the protein kinase should be light activated (or the phosphatase light inhibited) and a variety of pharmacological experiments, both *in vitro* and *in vivo*, are available to undertake the identification of the modifying enzyme.

Acknowledgements

This work was supported by a public grant overseen by the French National Research Agency (ANR) as part of the “Investissement d’Avenir” programme, through the “Lidex-3P” project and a French State Grant (ANR-10-LABX-0040-SPS) funded by the IDEX Paris-Saclay. This work was also supported by the ANR-14-CE19-0015 grant Regul3P awarded to MH. PD was supported by a PhD grant from the French Ministry of Higher Education and Research. We would like to thank Julie Capitanio, Julie Mignon for their contributions to the experiments and Jean Vidal for his help on this manuscript. Authors declare that they have no conflicts of interest.

Supplementary Data

Figure S1: *AtiPGAM2* structure prediction.

Figure S2: *AtiPGAM2* activity measurement through a coupled reaction.

Figure S3: Purification of *AtiPGAM2*_{S82A} and *AtiPGAM2*_{S82D}.

Figure S4: Purification of *AtiPGAM2*_{WT}, *AtiPGAM2*_{D29N} and *AtiPGAM2*_{2290L}.

Figure S5: Identification of the phosphopeptide in *AtiPGAM*

Table S1: List of the primers used for the cloning and site directed mutagenesis with the corresponding names, sequences and Tm °C.

References

- Andriotis VME, Kruger NJ, Pike MJ, Smith AM. 2010.** Plastidial glycolysis in developing Arabidopsis embryos. *New Phytologist* **185**: 649–662.
- Bienert S, Waterhouse A, de Beer TAP, Tauriello G, Studer G, Bordoli L, Schwede T. 2017.** The SWISS-MODEL Repository-new features and functionality. *Nucleic acids research* **45**: 313–319.
- Blackburn EA, Fuad FAA, Morgan HP, Nowicki MW, Wear MA, Michels PAM, Fothergill-Gilmore LA, Walkinshaw MD. 2014.** Trypanosomatid phosphoglycerate mutases have multiple conformational and oligomeric states. *Biochemical and Biophysical Research Communications* **450**: 936–941.
- Boex-Fontvieille E, Davanture M, Jossier M, Zivy M, Hodges M, Tcherkez G. 2014.** Photosynthetic activity influences cellulose biosynthesis and phosphorylation of proteins involved therein in Arabidopsis leaves. *Journal of Experimental Botany* **65**: 4997–5010.
- Botha C, Dennis T. 1986.** Isozymes of Phosphoglyceromutase from the Developing Endosperm Ricinus communis : Isolation and Kinetic Properties ' of The isozymes of phosphoglyceromutase from the developing endosperm of Ricinus communis have been partially purified . The purified cyto. **245**: 96–103.
- Bustos DM, Iglesias AA. 2002.** Non-phosphorylating glyceraldehyde-3-phosphate dehydrogenase is post-translationally phosphorylated in heterotrophic cells of wheat (*Triticum aestivum*). *FEBS Letters* **530**: 169–173.
- Cao H, Zhou Y, Chang Y, Zhang X, Li C, Ren D. 2019.** Comparative phosphoproteomic analysis of developing maize seeds suggests a pivotal role for enolase in promoting starch synthesis. *Plant Science* **289**: 110243.
- Fedosejevs ET, Ying S, Park J, Anderson EM, Mullen RT, She Y-M, Plaxton WC. 2014.** Biochemical and molecular characterization of RcSUS1, a cytosolic sucrose synthase phosphorylated in vivo at serine 11 in developing castor oil seeds. *The Journal of biological chemistry* **289**: 33412–33424.
- Flügel F, Timm S, Arrivault S, Florian A, Stitt M, Fernie AR, Bauwe H. 2017.** The Photorespiratory Metabolite 2-Phosphoglycolate Regulates Photosynthesis and Starch Accumulation in Arabidopsis. *The Plant Cell* **29**: 2537–2551.
- Fothergill-Gilmore LA, Watson HC. 1989.** The phosphoglycerate mutases. *Advances in enzymology and related areas of molecular biology* **62**: 227–313.

Fuad FAA, Fothergill-Gilmore LA, Nowicki MW, Eades LJ, Morgan HP, McNae IW, Michels PAM, Walkinshaw MD. 2011. Phosphoglycerate mutase from *Trypanosoma brucei* is hyperactivated by cobalt in vitro, but not in vivo. *Metallomics : integrated biometal science* **3**: 1310–1317.

Gibson DG, Young L, Chuang R-Y, Venter JC, Hutchison CA 3rd, Smith HO. 2009. Enzymatic assembly of DNA molecules up to several hundred kilobases. *Nature methods* **6**: 343–345.

Giegé P, Heazlewood JL, Roessner-Tunali U, Harvey Millar A, Fernie AR, Leaver CJ, Sweetlove LJ. 2003. Enzymes of glycolysis are functionally associated with the mitochondrion in arabidopsis cells. *Plant Cell* **15**: 2140–2151.

Givan C V. 1999. Evolving concepts in plant glycolysis: two centuries of progress. *Biological Reviews* **74**: 277–309.

Grana X, Urena J, Ludevid D, Carreras J, Climent F. 1989. Purification, characterization and immunological properties of 2,3-bisphosphoglycerate-independent phosphoglycerate mutase from maize (*Zea mays*) seeds. *European journal of biochemistry* **186**: 149–153.

Guerra DG, Vertommen D, Fothergill-Gilmore LA, Opperdoes FR, Michels PAM. 2004. Characterization of the cofactor-independent phosphoglycerate mutase from *Leishmania mexicana mexicana*. Histidines that coordinate the two metal ions in the active site show different susceptibilities to irreversible chemical modification. *European journal of biochemistry* **271**: 1798–1810.

Hodges M, Jossier M, Boex-Fontvieille E, Tcherkez G. 2013. Protein phosphorylation and photorespiration. *Plant Biology* **15**: 694–706.

Hummel M, Dobrenel T, Cordewener J (J. HG)., Davanture M, Meyer C, Smeekens S (J. CM)., Bailey-Serres J, America T (A. HP)., Hanson J. 2015. Proteomic LC–MS analysis of *Arabidopsis* cytosolic ribosomes: Identification of ribosomal protein paralogs and re-annotation of the ribosomal protein genes. *Journal of Proteomics* **128**: 436–449.

Jedrzejak MJ. 2000. Structure, function, and evolution of phosphoglycerate mutases: Comparison with fructose-2,6-bisphosphatase, acid phosphatase, and alkaline phosphatase. *Progress in Biophysics and Molecular Biology* **73**: 263–287.

Jedrzejak MJ, Chander M, Setlow P, Krishnasamy G. 2000. Mechanism of catalysis of the cofactor-independent phosphoglycerate mutase from *Bacillus stearothermophilus*: Crystal structure of the complex with 2-phosphoglycerate. *Journal of Biological Chemistry* **275**: 23146–23153.

Laemmli UK. 1970. Cleavage of structural proteins during the assembly of the head of bacteriophage T4. *Nature* **227**: 680–685.

Mazarei M, Lennon KA, Puthoff DP, Rodermeel SR, Baum TJ. 2003. Expression of an Arabidopsis phosphoglycerate mutase homologue is localized to apical meristems, regulated by hormones, and induced by sedentary plant-parasitic nematodes. *Plant molecular biology* **53**: 513–530.

McAleese SM, Jutagir V, Blackburn GM, Fothergill-Gilmore LA. 1987. The bisphosphonomethyl analogue of 2,3-bisphosphoglycerate inhibits yeast but not wheat-germ phosphoglycerate mutase. *Biochemical Journal* **243**: 301–304.

Mercaldi GF, Pereira HM, Cordeiro AT, Michels PAM, Thiemann OH. 2012. Structural role of the active-site metal in the conformation of *Trypanosoma brucei* phosphoglycerate mutase. *The FEBS Journal* **279**: 2012–2021.

Nowicki MW, Kuaprasert B, McNae IW, Morgan HP, Harding MM, Michels PAM, Fothergill-Gilmore LA, Walkinshaw MD. 2009. Crystal Structures of *Leishmania mexicana* Phosphoglycerate Mutase Suggest a One-Metal Mechanism and a New Enzyme Subclass. *Journal of Molecular Biology* **394**: 535–543.

Nukui M, Mello L V, Littlejohn JE, Setlow B, Setlow P, Kim K, Leighton T, Jedrzejas MJ. 2007. Structure and molecular mechanism of *Bacillus anthracis* cofactor-independent phosphoglycerate mutase: a crucial enzyme for spores and growing cells of *Bacillus* species. *Biophysical journal* **92**: 977–988.

Plaxton WC. 1996. The organization and regulation of plant glycolysis. *Annual Review of Plant Physiology and Plant Molecular Biology* **47**: 185–214.

Roychowdhury A, Kundu A, Bose M, Gujar A, Mukherjee S, Das AK. 2015. Complete catalytic cycle of cofactor-independent phosphoglycerate mutase involves a spring-loaded mechanism. *The FEBS Journal* **282**: 1097–1110.

Roychowdhury A, Kundu A, Gujar A, Bose M, Das AK. 2014. Expression, purification, crystallization and preliminary X-ray diffraction studies of phosphoglycerate mutase from *Staphylococcus aureus* NCTC8325. *Acta Crystallographica Section F: Structural Biology Communications* **70**: 53–56.

Ruan Y-L. 2014. Sucrose Metabolism: Gateway to Diverse Carbon Use and Sugar Signaling. *Annual Review of Plant Biology* **65**: 33–67.

Singh PK, Kushwaha S, Mohd S, Pathak M, Misra-Bhattacharya S. 2013. In vitro gene silencing of

independent phosphoglycerate mutase (iPGM) in the filarial parasite *Brugia malayi*. *Infectious diseases of poverty* **2**: 5.

Stein M, Gabdoulline RR, Wade RC. 2010. Cross-species analysis of the glycolytic pathway by comparison of molecular interaction fields. *Molecular bioSystems* **6**: 152–164.

Tcherkez G, Bligny R, Gout E, Mahé A, Hodges M, Cornic G. 2008. Respiratory metabolism of illuminated leaves depends on CO₂ and O₂ conditions. *Proceedings of the National Academy of Sciences* **105**: 797–802.

Weber APM, Linka N. 2011. Connecting the Plastid: Transporters of the Plastid Envelope and Their Role in Linking Plastidial with Cytosolic Metabolism. *Annual Review of Plant Biology* **62**: 53–77.

Westram A, Lloyd JR, Roessner U, Riesmeier JW, Kossmann J. 2002. Increases of 3-phosphoglyceric acid in potato plants through antisense reduction of cytoplasmic phosphoglycerate mutase impairs photosynthesis and growth, but does not increase starch contents. *Plant, Cell & Environment* **25**: 1133–1143.

Yamada K, Lim J, Dale JM, Chen H, Shinn P, Palm CJ, Southwick AM, Wu HC, Kim C, Nguyen M, et al. 2003. Empirical Analysis of Transcriptional Activity in the *Arabidopsis* Genome. *Science* **302**: 842–846.

Zhang Y, Foster JM, Kumar S, Fougere M, Carlow CKS. 2004. Cofactor-independent Phosphoglycerate Mutase Has an Essential Role in *Caenorhabditis elegans* and Is Conserved in Parasitic Nematodes. *Journal of Biological Chemistry* **279**: 37185–37190.

Zhang B, Liu J-Y. 2017. Serine phosphorylation of the cotton cytosolic pyruvate kinase GhPK6 decreases its stability and activity. *FEBS open bio* **7**: 358–366.

Zhao Z, Assmann SM. 2011. The glycolytic enzyme, phosphoglycerate mutase, has critical roles in stomatal movement, vegetative growth, and pollen production in *Arabidopsis thaliana*. *Journal of experimental botany* **62**: 5179–5189.

Tables

Table 1: Measurement of AtiPGAM2 kinetic parameters *in vitro*

Protein	K_m (mM)	V_{max} ($\mu\text{mol}\cdot\text{min}^{-1}\cdot\text{mg}^{-1}$ of protein)	K_{cat} (s^{-1})
AtiPGAM2 _{WT}	0.467 ± 0.032	48.5 ± 3.3	51.3 ± 3.5

AtiPGAM2 activity was measured through the disappearance of NADH detectable using a Varian Cary 50 spectrophotometer at $\Delta A_{340\text{ nm}}$ by a coupled reaction described in material and Methods (see also supplementary data Figure S2). These parameters were calculated using “Kinetic Enzyme Wizard” from Sigma-Plot (Systat Software Inc.) with molar extinction coefficient $6.22 \cdot 10^{-3} \text{ M}^{-1}\cdot\text{cm}^{-1}$. Value are means \pm SD (n=3 independent experiments)

Figure Legends

Figure 1: AtiPGAM2 3D-structure prediction.

Using both modelling and repository tool of SWISS-MODEL website the 3D structure of AtiPGAM2 was predicted. Using SWISS-MODEL workspace, several templates were found. (a) presents the alignment of AtiPGAM2 sequence (Model_01) with one of the template (3igy.1) showing 56.8% sequence identity corresponding to the sequence of the *Leshmania mexicana* co-factor independent phosphoglycerate mutase (see Figure S1 in supplementary data for its 3D-structure). Green arrows indicate α -helices and purple boxes β -sheets. (b) represents the rainbow 3D-structure of AtiPGAM2 found in SWISS-MODEL Repository database (A0A384KAQ5) also built with 3igy.1 template with a global model quality estimation (GMQE) of 0.8 (in a scale from 0 to 1). The two domains (A phosphatase and B transferase) are indicated. This structure includes two metal ions (pink balls) and 3-phosphoglycerate (see Figure S1 in supplementary data for QMEAN representation; the QMEAN score is -0.65). (c) represents the catalytic core of the enzyme. Insert shows the position of the focused region. Note that the presented view corresponds to a 180° turn compared to the one presented in (b). Reactive serine is marked in green on the chain (S82). All residues involved in metal ion and 3-PGA binding are licorice represented. Apart from S82, the two other residues studied in this work are annotated (D29 and R290; for others see Figure S1 in supplementary data). Purple lines represent the five interactions of each metal ion with both 3-PGA and the chain. Blue and yellow lines represent respectively the three hydrogen bonds and the 14 salt bridges of the 3-PGA with the chain. Each type of bonds is detailed in Figure S1 in supplementary data.

Figure 2: AtiPGAM2 activity of the mutated recombinant proteins by comparison with the WT

Importance of specific residues for *AtiPGAM2* activity, measured *via* the coupled reaction as described in Materials and Methods using the Varian Cary 50 spectrophotometer at $\Delta A_{340\text{ nm}}$ at 1mM of substrate (3-PGA) and 2.5 μg of recombinant proteins (a) Since S82 is mutated whatever the alternative amino-acid (S82A or S82D), the activity is completely abolished in comparison with the WT. (b) When the residues predicted to be important for the *AtiPGAM2* activity (D29 and R290) are mutated (D29N and R290L), there is no more detectable activity.

Figure 3: Phosphorylation level detected on S82 of the recombinant AtiPGAM2

(a) Phosphorylation level on Serine 82 (S82) on *AtiPGAM*_{WT} according to the substrate concentrations (3-PGA; from 0 to 10 mM) and the absence of Mg^{2+} (without MgSO_4). The bacterial contaminations are deducted from the data. (b) Phosphorylation level on Serine 82 (S82) with/without 3-PGA (0 mM and 2.5 mM) measured on the mutated recombinant proteins *AtiPGAM2*-D29N and *AtiPGAM2*-R290L (D29N; R290L). Value are means \pm SD ($n=3$ biological replicates). Statistical significance was determined by a Student's *t*-test (* $P < 0.05$).

Figure 4: Day/ night phosphoproteome in leaves

Phosphorylation level of Serine 82 was measured in leaves of *Arabidopsis thaliana* plants grown in ambient air and under a 8:16 h light/dark regime (short days) at an irradiance of approximately $100\ \mu\text{mol}\cdot\text{m}^{-2}\cdot\text{s}^{-1}$. This box plot was performed on $n=3$ experiments. Ordinate axis represents relative phosphorylation pattern in \log_2 .

Supplementary data

Supplementary figure legends

Figure S1: AtiPGAM2 structure prediction.

All models presented here can be found on the website <https://swissmodel.expasy.org/interactive>. We took advantage of the SWISS-MODEL Repository entry A0A384KAQ5_ARATH_iPGAM2 in the database of annotated 3D protein structure models. From the three templates automatically proposed, two were further used because the third has a quite low QMEAN score (see (c)). **(a,b)** present the 3D-structure of these two templates used; in purple α -helices and in green β -sheets. **(a)** 3nvl.1.A corresponds to the crystal structure of the 2,3-bisphosphoglycerate-independent phosphoglycerate mutase of *Trypanosoma brucei* with one sulfate and two cobalt ions as ligands (Mercaldi et al., 2012). **(b)** 3igy.1 corresponds the crystal structure of cofactor-independent phosphoglycerate mutase of *Leishmania mexicana* with two cobalt ions and 3-phosphoglycerate as ligands (Nowicki et al., 2009) **(c)** the estimation of the modelling quality along the *A. thaliana* iPGAM2 target sequence (A0A384KAQ5) with the three templates is shown using a QMEAN scale (from red, low quality to blue high quality); from outside to the inside of the circle: with 3nvl.1.A , 3igy.1 and 5kgl.1 templates. Modelling with 5kgl.1 template that corresponds to the structure of Apo independent phosphoglycerate mutase from *Caenorhabditis elegans* (Yu et al., 2017) displays a low QMEAN score -3.34 and was not used later. **(d and e)** show the QMEAN scaled predicted structures of AtiPGAM2 using 3nvl.1.A and 3igy.1 as template respectively. **(f, g, h and i)** are details of the catalytic core in the AtiPGAM2 predicted structure based on 3igy.1 that includes two Co^{2+} ions (Co1 and Co2, pink balls) and 3-phosphoglycerate (3-PGA; grey, red and orange respectively C, O, P atoms). The reactive serine 82 (S82) is coloured in green on the chain. All residues involved in the different bonds are licorice represented. **(f)** depicts the interactions (purple lines) of the first Co^{2+} ion (Co1); three interactions with residues D431, H435 and H502 and two with 3-PGA. **(g)** depicts the interactions (purple lines) of the second Co^{2+} ion (Co2); four interactions with residues D29, S82, D472 and H473 and one with 3-PGA. **(h)** displays hydrogen bonds (blue lines) between the 3-PGA and the chain, one bond with S82 and two with R207. **(i)** shows the 14 salt bridges between 3-PGA and the following residues: H141, R171, R207, R214 (2 bonds), R287 (2 bonds), R290, K362, H365, H435 (2 bonds), H473 and H502.

Figure S2: AtiPGAM2 activity measurement through a coupled reaction.

The diagram represents the coupled reaction used to measure the AtiPGAM activity according to (Zhang *et al.*, 2004): 3-PGA: 3-phosphoglycerate; 2-PGA: 2-phosphoglycerate; PEP: phosphoenolpyruvate; iPGAM: phosphoglycerate mutase independent; ENO: Enolase; PK: Pyruvate

Kinase; LDH: lactate dehydrogenase; ADP: adenosine diphosphate; ATP: adenosine triphosphate; NADH: nicotinamide adenine dinucleotide reduced; NAD⁺: nicotinamide adenine dinucleotide. Since every step is equimolar the *AtiPGAM2* activity can be measured by the disappearance of NADH detectable *via* the Varian Cary 50 spectrophotometer at $\Delta A_{340 \text{ nm}}$.

Figure S3: Purification of *AtiPGAM2*_{S82A} and *AtiPGAM2*_{S82D}.

A SDS-PAGE gel was performed with of the protein samples collected at different steps of the purification of *AtiPGAM2*_{S82A} and *AtiPGAM2*_{S82D} and further stained with Coomassie blue. Numbers indicate the different steps of the purification as followed: (1): sample from the total bacterial protein lysate after induction using IPTG (10 μL loaded). (2): sample collected from the soluble proteins (10 μL loaded). (3): sample collected among the proteins unbound to the Ni²⁺ resin (10 μL loaded). (4): sample of proteins collected in the first washing step of the resin (20 μL loaded). (5): sample collected from the eluted proteins using 250 mM imidazole (10 μL loaded). (6): sample collected from the desalted proteins (10 μL loaded). M: molecular weight marker (5 μL loaded; PageRuler Prestained Molecular marker, Thermo Scientific)

Figure S4: Purification of *AtiPGAM2*_{WT}, *AtiPGAM2*_{D29N} and *AtiPGAM2*_{R290L}.

A SDS-PAGE gel was performed with of the protein samples collected at different steps of the purification of *AtiPGAM2*_{WT}, *AtiPGAM2*_{D29N} and *AtiPGAM2*_{R290L} and further stained with Coomassie blue. Numbers indicate the different steps of the purification as followed: (1): sample from the total bacterial protein lysate before induction using IPTG (10 μL loaded). (2): sample from the total bacterial proteins after induction using IPTG (10 μL loaded). (3): sample collected from the soluble proteins (10 μL loaded). (4): sample collected among the proteins unbound to the Ni²⁺ resin (10 μL loaded). (5): sample of proteins collected in the first washing step of the resin (20 μL loaded). (6): sample collected from the eluted proteins using 250 mM imidazole (10 μL loaded). (7): sample collected from the desalted proteins (10 μL loaded). M: molecular weight marker (5 μL loaded; PageRuler Prestained Molecular marker, Thermo Scientific)

Figure S5: Identification of the phosphopeptide in *AtiPGAM*

Spectra of phosphorylated peptides showing b in blue (N-terminal) and y in red (C-terminal) fragmentations ions from MS2. During the peptide fragmentation, the peptide bound is first cut because the N-C liaison is weaker than C-C thus producing “b ions” in blue and “y ions” in red. On the top is the phosphopeptide sequence with the red or blue squares corresponding to the attribution between the experimental ions and the theoretical mass of the amino acids. The serine 17 in the phosphopeptide (S82 in the protein) corresponds to ions b17 and y12 (matching with a 1247.55

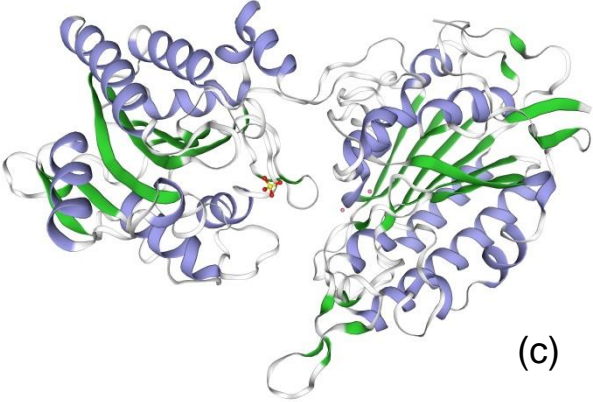
mass). By subtracting the y12 and y11 masses, we obtain 167 that corresponds to the mass of a phosphoserine.

Supplementary tables

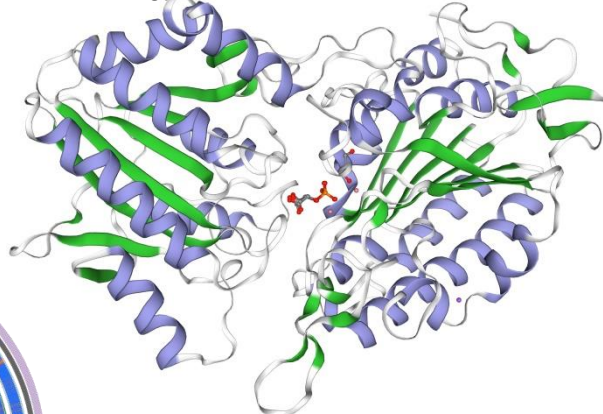
Table S1: List of the primers used for the cloning and site directed mutagenesis with the corresponding names, sequences and Tm °C.

What it is for	name	sequence 5'>3'	Tm °C
iPGAM2ORF mutagenesis			
D29N	563PRO	CTATCGGTTTGATTGTTCTCAATGGATGGGGTGAATCTGATCC	72.3
	564TER	GGATCAGATTCACCCATCCATTGAGAACAAATCAAACCGATAG	72.3
R290L	565PRO	CATTCAATTTCCGTGCTGATCTTATGGTCATGCATGCAAAGGC	72.3
	566TER	GCCTTTGCATGCATGACCATAAGATCAGCACGGAAATTGAATG	72.3
Cloning			
Cloning into pET16b (Gibson strategy)	pET16b-fw	CTCGAGGATCCGGCTGCTAA	61.4
	pET16b-rev	CTCCATATGACGACCTTCGA	57.3
	iPGAM2-rev16b	TTAGCAGCCGGATCCTCGAGTCACTTCTCGACGACTTCGATC	76.3
	iPGAM2-fw16b	TCGAAGGTCGCATATGGAGGGTAGCTCCGGCGACGTT	75.9
S82A	iPGAM2S82Afw	GGGAAACAGTGAAGTTGGCCACAATGCTCTTGG	70.7
	iPGAM2S82Arev	CAACTTCACTGTTTCCCATGTCGTCTTCGCTG	69.5
S82D	iPGAM2S82Dfw	GGGAAACGATGAAGTTGGCCACAATGCTCTTGG	70.7
	iPGAM2S82Drev	CAACTTCATCGTTTCCCATGTCGTCTTCGCTG	69.5

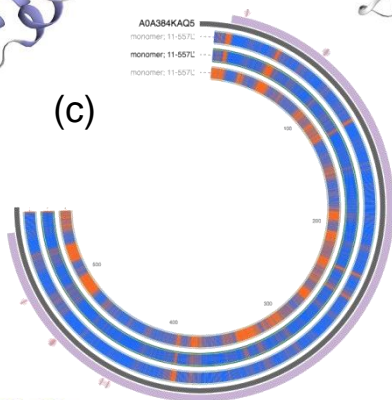
(a) 3nvl.1.A *Trypanosoma brucei*



(b) 3igy.1 *Leishmania mexicana*

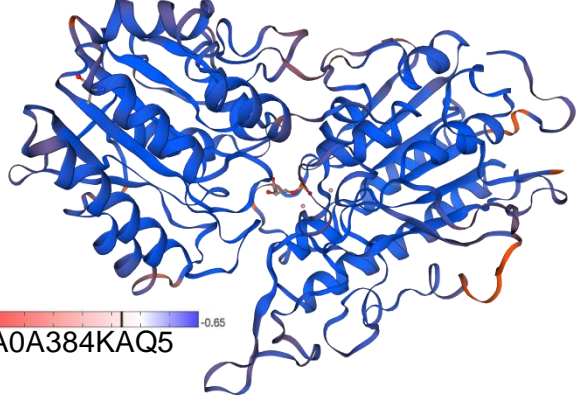
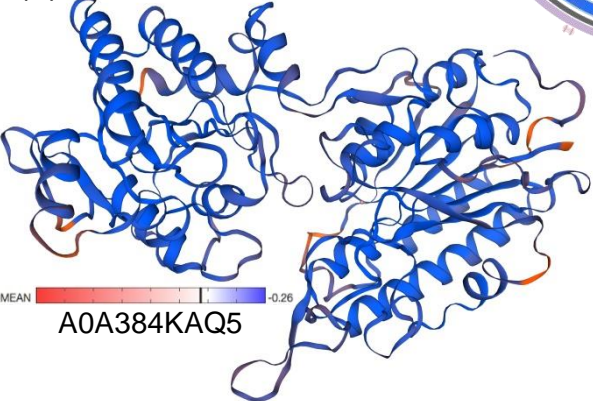


(c)

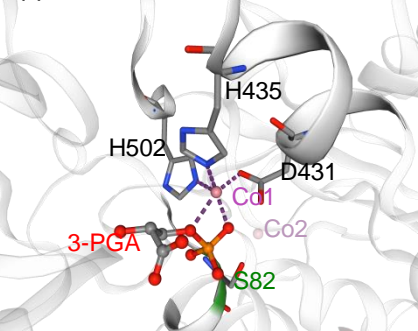


low quality high quality

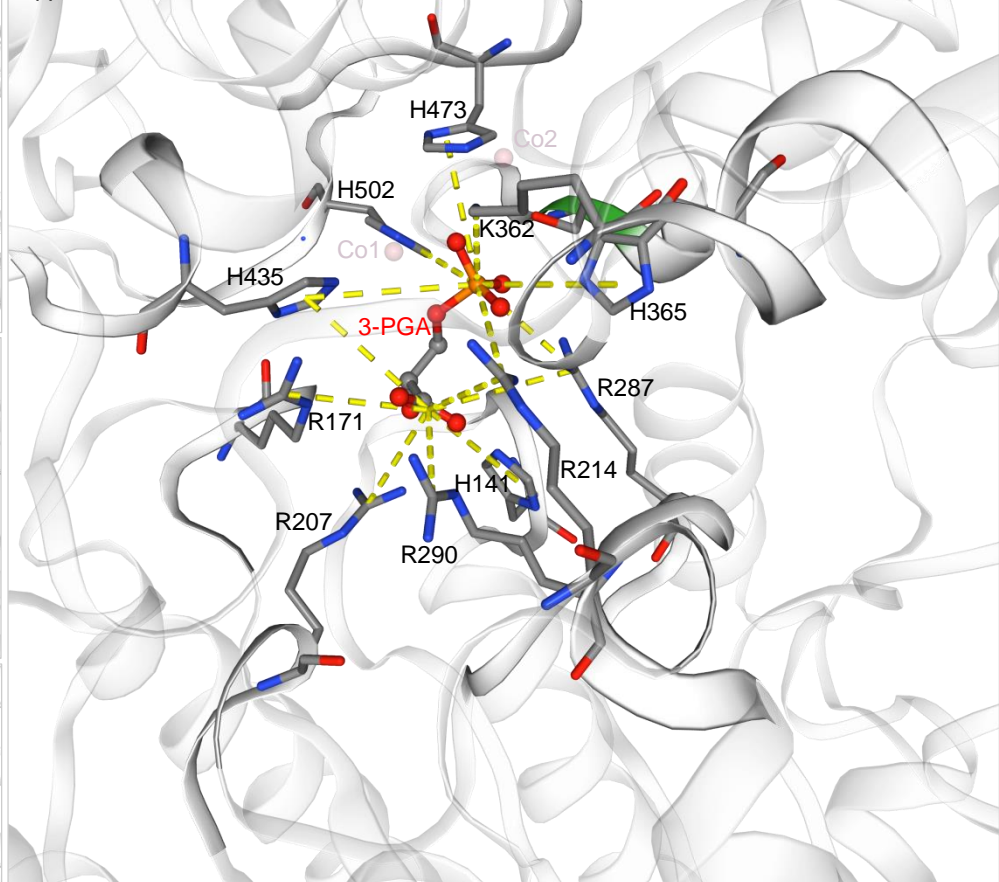
(d)



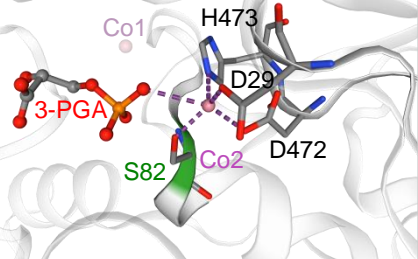
(f)



(i)



(g)



(h)

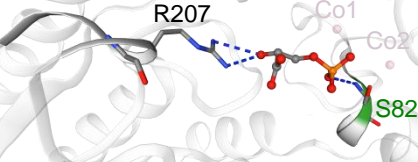


Figure S1: AtiPGAM2 structure prediction.

All models presented here can be found on the website <https://swissmodel.expasy.org/interactive>. We took advantage of the SWISS-MODEL Repository entry A0A384KAQ5_ARATH_iPGAM2 in the database of annotated 3D protein structure models. From the three templates automatically proposed, two were further used because the third has a quite low QMEAN score (see (c)). (a,b) present the 3D-structure of these two templates used; in purple α -helices and in green β -sheets. (a) 3nvl.1.A corresponds to the crystal structure of the 2,3-bisphosphoglycerate-independent phosphoglycerate mutase of *Trypanosoma brucei* with one sulfate and two cobalt ions as ligands (Mercaldi et al., 2012). (b) 3igy.1 corresponds the crystal structure of cofactor-independent phosphoglycerate mutase of *Leishmania mexicana* with two cobalt ions and 3-phosphoglycerate as ligands (Nowicki et al., 2009). (c) the estimation of the modelling quality along the *A. thaliana* iPGAM2 target sequence (A0A384KAQ5) with the three templates is shown using a QMEAN scale (from red, low quality to blue high quality); from outside to the inside of the circle: with 3nvl.1.A , 3igy.1 and 5kg1.1 templates. Modelling with 5kg1.1 template that corresponds to the structure of Apo independent phosphoglycerate mutase from *Caenorhabditis elegans* (Yu et al., 2017) displays a low QMEAN score -3.34 and was not used later. (d and e) show the QMEAN scaled predicted structures of AtiPGAM2 using 3nvl.1.A and 3igy.1 as template respectively. (f, g, h and i) are details of the catalytic core in the AtiPGAM2 predicted structure based on 3igy.1 that includes two Co^{2+} ions (Co1 and Co2, pink balls) and 3-phosphoglycerate (3-PGA; grey, red and orange respectively C, O, P atoms). The reactive serine 82 (S82) is coloured in green on the chain. All residues involved in the different bonds are licorice represented. (f) depicts the interactions (purple lines) of the first Co^{2+} ion (Co1); three interactions with residues D431, H435 and H502 and two with 3-PGA. (g) depicts the interactions (purple lines) of the second Co^{2+} ion (Co2); four interactions with residues D29, S82, D472 and H473 and one with 3-PGA. (h) displays hydrogen bonds (blue lines) between the 3-PGA and the chain, one bond with S82 and two with R207. (i) shows the 14 salt bridges between 3-PGA and the following residues: H141, R171, R207, R214 (2 bonds), R287 (2 bonds), R290, K362, H365, H435 (2 bonds), H473 and H502.

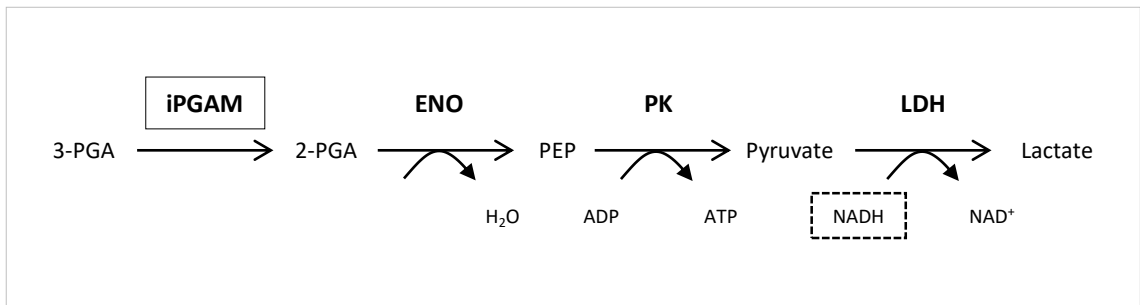


Figure S2: *AtiPGAM2* activity measurement through a coupled reaction.

The diagram represents the coupled reaction used to measure the *AtiPGAM* activity according to (Zhang *et al.*, 2004): 3-PGA: 3-phosphoglycerate; 2-PGA: 2-phosphoglycerate; PEP: phosphoenolpyruvate; iPGAM: phosphoglycerate mutase independent; ENO: Enolase; PK: Pyruvate Kinase; LDH: lactate dehydrogenase; ADP: adenosine diphosphate; ATP: adenosine triphosphate; NADH: nicotinamide adenine dinucleotide reduced; NAD⁺: nicotinamide adenine dinucleotide. Since every step is equimolar the *AtiPGAM2* activity can be measured by the disappearance of NADH detectable *via* the Varian Cary 50 spectrophotometer at $\Delta A_{340\text{ nm}}$.

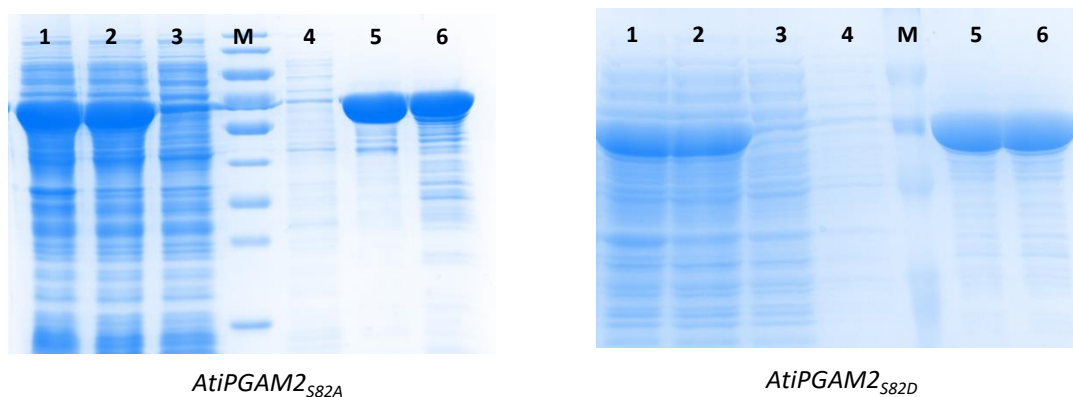
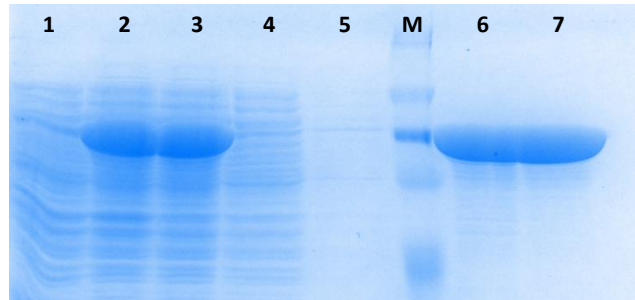
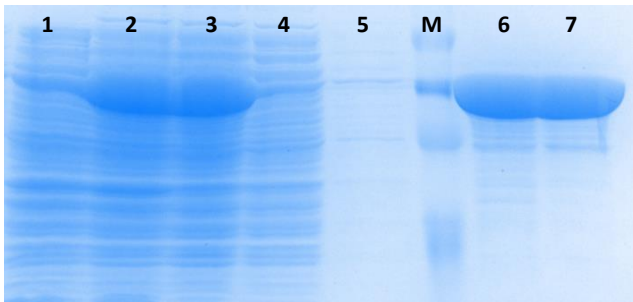


Figure S3: Purification of *AtiPGAM2*_{S82A} and *AtiPGAM2*_{S82D}.

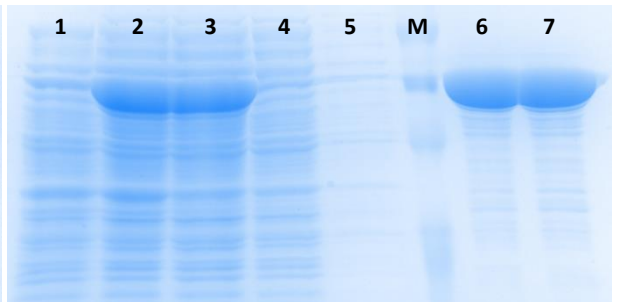
A SDS-PAGE gel was performed with of the protein samples collected at different steps of the purification of *AtiPGAM2*_{S82A} and *AtiPGAM2*_{S82D} and further stained with Coomassie blue. Numbers indicate the different steps of the purification as followed: **(1)**: sample from the total bacterial protein lysate after induction using IPTG (10 μ L loaded). **(2)**: sample collected from the soluble proteins (10 μ L loaded). **(3)**: sample collected among the proteins unbound to the Ni²⁺ resin (10 μ L loaded). **(4)**: sample of proteins collected in the first washing step of the resin (20 μ L loaded). **(5)**: sample collected from the eluted proteins using 250 mM imidazole (10 μ L loaded). **(6)**: sample collected from the desalted proteins (10 μ L loaded). M : molecular weight marker (PageRuler Prestained Molecular marker, Thermo Scientific)



AtiPGAM2_{WT}



AtiPGAM2_{D29N}



AtiPGAM2_{R290L}

Figure S4: Purification of *AtiPGAM2_{WT}*, *AtiPGAM2_{D29N}* and *AtiPGAM2_{R290L}*.

A SDS-PAGE gel was performed with of the protein samples collected at different steps of the purification of *AtiPGAM2_{WT}*, *AtiPGAM2_{D29N}* and *AtiPGAM2_{R290L}* and further stained with Coomassie blue. Numbers indicate the different steps of the purification as followed: **(1)**: sample from the total bacterial protein lysate before induction using IPTG (10 μ L loaded). **(2)**: sample from the total bacterial proteins after induction using IPTG (10 μ L loaded). **(3)**: sample collected from the soluble proteins (10 μ L loaded). **(4)**: sample collected among the proteins unbound to the Ni²⁺ resin (10 μ L loaded). **(5)**: sample of proteins collected in the first washing step of the resin (20 μ L loaded). **(6)**: sample collected from the eluted proteins using 250 mM imidazole (10 μ L loaded). **(7)**: sample collected from the desalted proteins (10 μ L loaded). M: molecular weight marker (5 μ L loaded; PageRuler Prestained Molecular marker, Thermo Scientific)

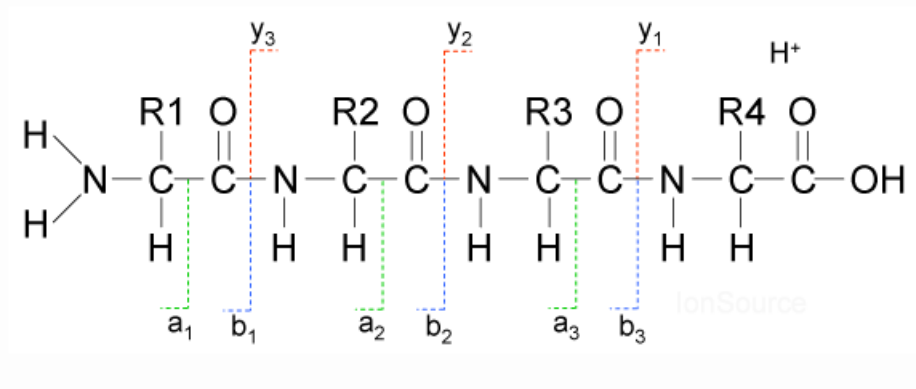
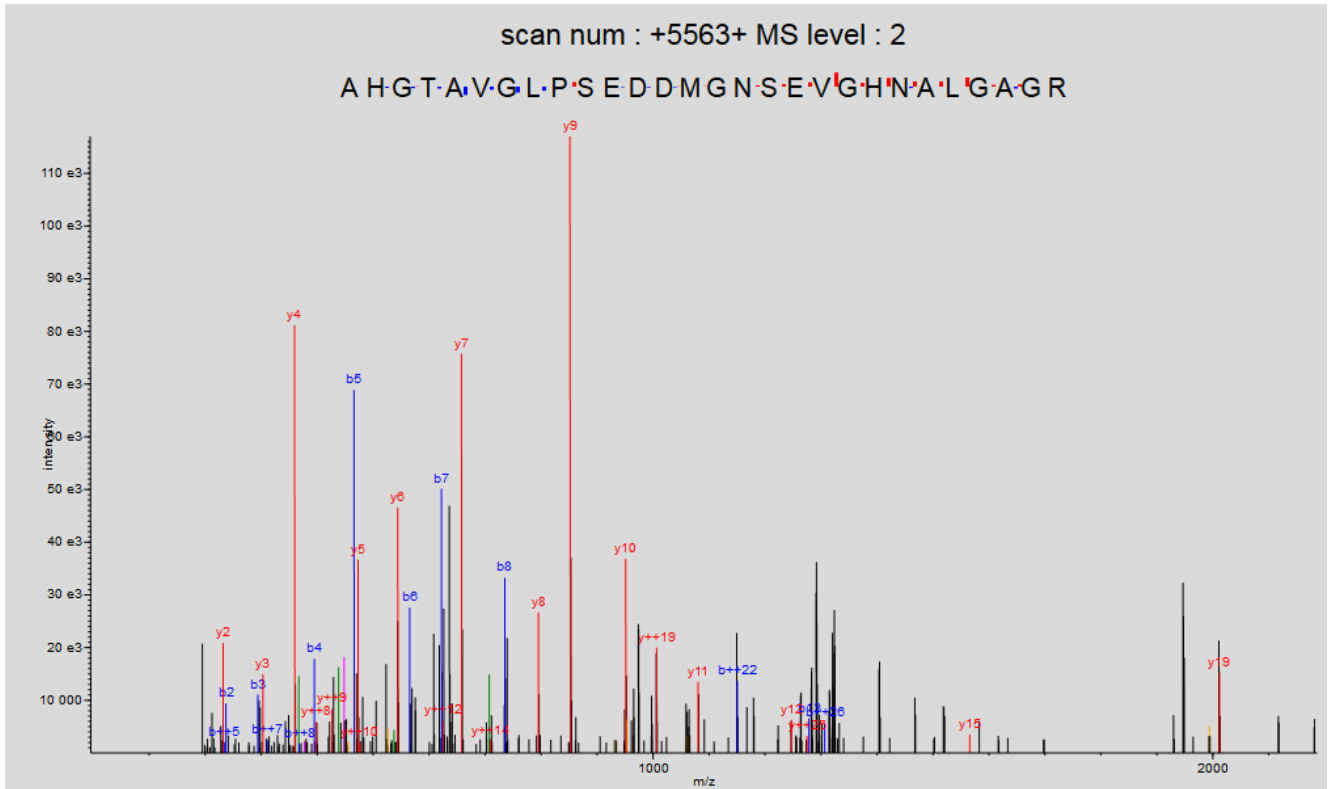


Figure S5: Identification of the phosphopeptide in AtiPGAM

Spectra of phosphorylated peptides showing b in blue (N-terminal) and y in red (C-terminal) fragmentations ions from MS2. During the peptide fragmentation, the peptide bound is first cut because the N-C liaison is weaker than C-C thus producing “b ions” in blue and “y ions” in red. On the top is the phosphopeptide sequence with the red or blue squares corresponding to the attribution between the experimental ions and the theoretical mass of the amino acids. The serine 17 in the phosphopeptide (S82 in the protein) corresponds to ions b17 and y12 (matching with a 1247.55 mass). By subtracting the y12 and y11 masses, we obtain 167 that is corresponding to the mass of a phosphoserine.

Table S1: List of the primers used for the cloning and site directed mutagenesis with the corresponding names, sequences and Tm °C.

What it is for:	name	sequence 5'>3'	Tm °C
iPGAM2ORF mutagenesis			
D29N	563PRO	CTATCGGTTTGATTGTTCTCAATGGATGGGGTGAATCTGATCC	72.3
	564TER	GGATCAGATTCACCCCATCCATTGAGAACAATCAAACCGATAG	72.3
R290L	565PRO	CATTCAATTTCCGTGCTGATCTTATGGTCATGCATGCAAAGGC	72.3
	566TER	GCCTTTGCATGCATGACCATAAGATCAGCACGGAAATTGAATG	72.3
Cloning			
Cloning into pET16b (Gibson strategy)	pET16b-fw	CTCGAGGATCCGGCTGCTAA	61.4
	pET16b-rev	CTCCATATGACGACCTTCGA	57.3
	iPGAM2-rev16b	TTAGCAGCCGGATCCTCGAGTCACTTCTCGACGACTTCGATC	76.3
	iPGAM2-fw16b	TCGAAGGTCGTCATATGGAGGGTAGCTCCGGCGACGTT	75.9
S82A	iPGAM2S82Afwd	GGGAAACAGTGAAGTTGGCCACAATGCTCTTGG	70.7
	iPGAM2S82Arev	CAACTTCACTGTTTCCCATGTGCTCTTCGCTG	69.5
S82D	iPGAM2S82Dfwd	GGGAAACAGTGAAGTTGGCCACAATGCTCTTGG	70.7
	iPGAM2S82Drev	CAACTTCATCGTTTCCCATGTGCTCTTCGCTG	69.5

II) Additional results

This part of the first chapter details the work following the manuscript on *AtiPGAM2* mechanism and regulation that was not included in because the results were not clear enough. However, we think that the strategy we develop is still a possible way to decipher the remaining question of the phosphoregulation of the enzyme by a kinase *in vivo*.

To assess the existence of a putative phosphorylation event by a kinase, we wanted to take advantage of our work performed *in vitro* using *AtiPGAM2*_{D29N} and *AtiPGAM2*_{R290L}. However, since these enzymes display no activity *in vitro* and probably neither *in vivo*, we can't consider the functional complementation of the mutant with the mutated genes occluding these proteins as an option to go further *in planta* understanding of the catalytic process of *AtiPGAM2*. Indeed, the double mutant *ipgam1/ipgam2* displays a highly impaired development and is sterile. Therefore, we decided to transform Col-0 plants with a modified gene encoding a protein labeled in the phosphopeptide that includes the reactive serine 82 *via* a potential silent mutation. In this respect, the serine 75 was converted into threonine that is comparable to serine in the conformation and the modified proteins should thus become identifiable during the phosphoproteomic experiments. Furthermore, this residue was chosen because some plants already display a threonine at this position instead of a serine like *A. thaliana*.

The activity and rate of complementation is the same for AtiPGAM2_{WT} and AtiPGAM2_{S75T} in vitro and in vivo

Before transforming the Col-0 plants it was necessary to figure out if the labelling mutation S75T was not changing the *AtiPGAM2* activity *in vitro* or *in vivo*. The activity was measured the same way than *AtiPGAM2*_{WT} using the coupled reaction previously described and the recombinant protein displays the same kinetic parameters (Figure 18).

Moreover, the serine 82 phosphorylation of the recombinant protein is still quantifiable and correlated with the amount of 3-PGA while S75 is changed into threonine. During this experiment, we just increased the 3-PGA concentrations to see if the phosphorylation state still increases or if there is a saturation effect. Indeed, in presence of 100 mM of substrate the phosphorylation rate of S82 continue to increase (Figure 19a). Finally, the D29N and R290L mutations added to the S75T one has the same effect on the activity (data not shown). We did the exact same experiments with the double mutated recombinant enzymes *AtiPGAM2*_{S75T/D29N} and *AtiPGAM2*_{S75T/R290L} with and without substrate. The results were the same than the WT protein, the mutation of R290 makes the phosphoserine formation nearly impossible while the mutation of D29 keep the enzyme in a close conformation without releasing the catalytic phosphate on S82 (Figure 19b). However, in contrast with the *AtiPGAM2*_{D29N} protein, when the S75 is mutated into threonine, the presence or absence of substrate doesn't significantly change the level of phosphorylation. It is probably not due to the

AHGTA**V**GLP**T**EDDMGN**S**EVGHNALGAGR

Protein	K_m (mM)	V_{max} ($\mu\text{mol}\cdot\text{min}^{-1}\cdot\text{mg}^{-1}$ of protein)	K_{cat} (s^{-1})
pET16b-AtiPGAM2 _{WT}	0.467 ± 0.032	48.5 ± 3.3	51.3 ± 3.5
pET16b-AtiPGAM2 _{S75T}	0.37 ± 0.018	50.45 ± 0.95	53.4 ± 1

Figure 18: Comparison of kinetic parameters of AtiPGAM2_{WT} and AtiPGAM2_{S75T}

These parameters were calculated using “Kinetic Enzyme Wizard” from Sigma-Plot (Systat Software Inc.) with molar extinction coefficient $6.22 \cdot 10^{-3} \text{ M}^{-1}\cdot\text{cm}^{-1}$. Value are means \pm SD (n=3 independent experiments)

Above the table is the phosphopeptide found for AtiPGAM2 from PhosphAt 4.0 database. The threonine in red indicates the position of the serine 75 that has been mutated to discriminate the phosphopeptide *in planta*, while the green serine is the one, which is phosphorylated (S82)

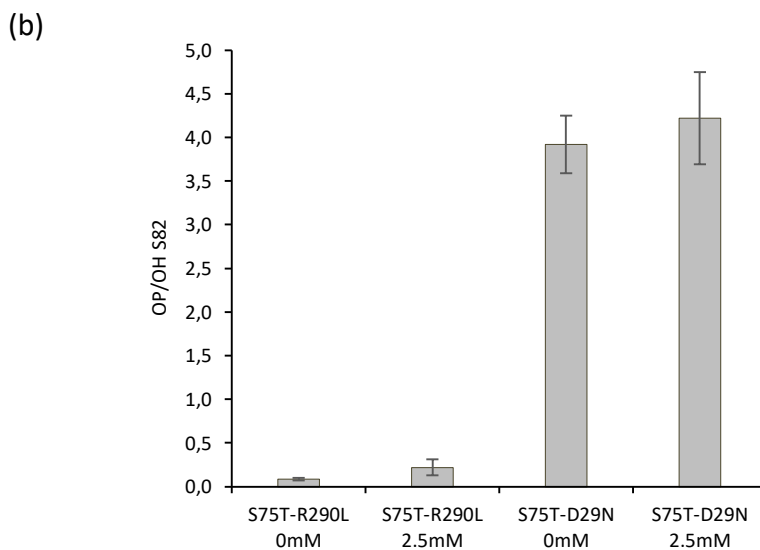
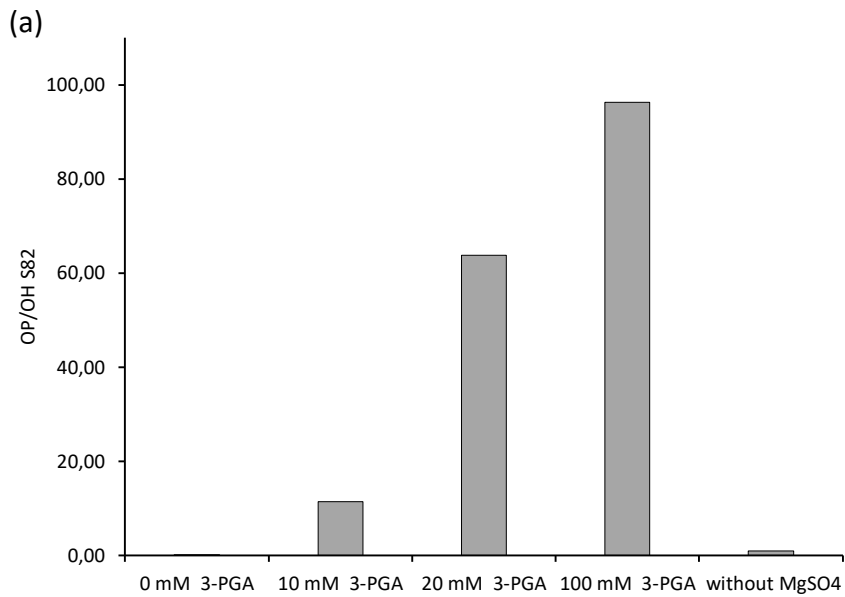


Figure 19: The *AtiPGAM2*_{S75T} has the same phosphorylation pattern as *AtiPGAM2*_{WT}

(a) Increase of S82 phosphorylation correlated with the substrate concentration 3-PGA between 0 mM and 100 mM of 3-PGA and without Mg²⁺. (b) Phosphorylation level of *AtiPGAM2*_{S75T/D29N} and *AtiPGAM2*_{S75T/R290L} with/without 3-PGA 0 mM and 2.5 mM). Value are means ± SD (n=3 biological replicates).

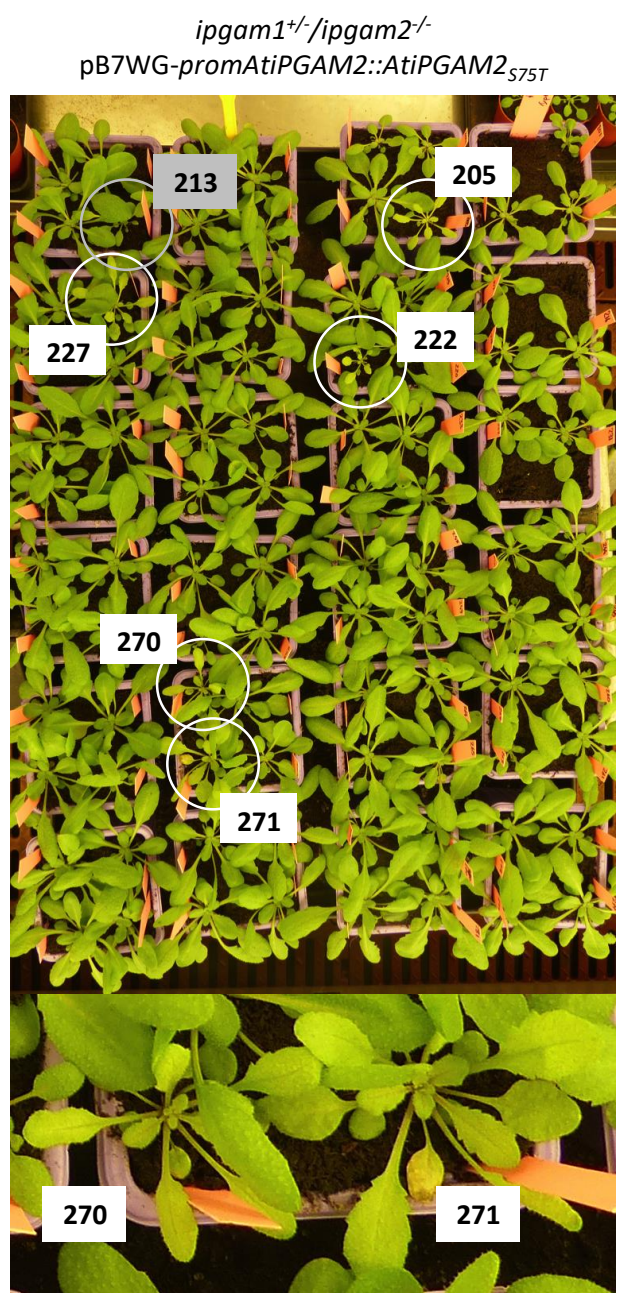
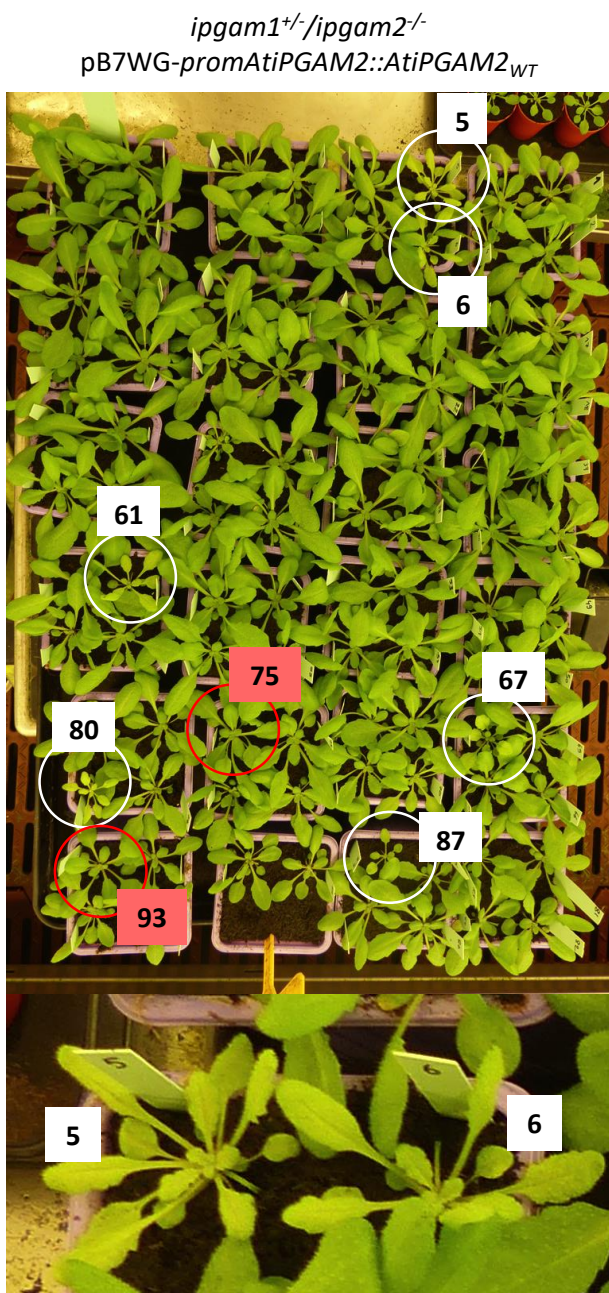


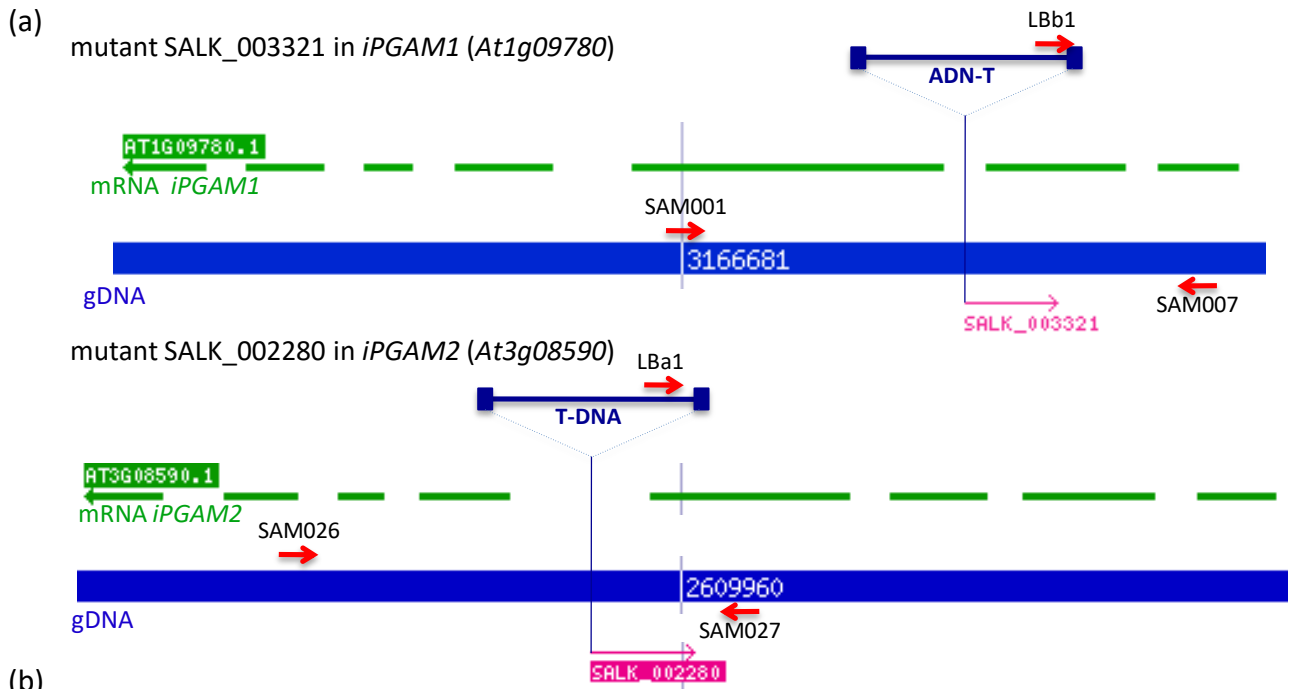
Figure 20: Functional complementation of *ipgam1^{+/-} ipgam2^{-/-}* sesquimutant.

Sesquimutant plants previously validated by genotyping (*ipgam1^{+/-} ipgam2^{-/-}*) were transformed via *A.tumefaciens* either with pB7WG-promAtiPGAM2::*AtiPGAM2_{WT}* or with pB7WG-promAtiPGAM2::*AtiPGAM2_{S75T}* (as indicated above the pictures). After selection, primary transformants were transplanted in soil and grown under short day conditions. Pictures correspond to 5 week-old plants that were further sampled for DNA extraction to perform genotype analysis. Plants circled in white and numbered display a growth delay (numbers correspond to these used in Figure 21). Note that the plant #213 is circled in grey because it is small but has not the same phenotype as the others. Red circles indicate the plant used as control in Figure 21. For each transformation, a detailed view of one pot that contains by chance two primary transformants with a growth delay is shown.

mutation but experiment dependent, the protein was already highly phosphorylated in the bacteria as previously discussed.

We just confirmed that the *AtiPGAM2*_{S75T} mutated proteins doesn't change *in vitro* the behavior of the protein, concerning the activity or the phosphorylation state. However, before transforming the Col-0 plants with gene encoding this tagged protein, we must also verify its expression in plants is able to functionally complement the double mutant *ipgam1ipgam2*. To do so, since the double mutant show very important growth delays and sterility, we decided to complement the sesquimutant *ipgam1^{+/-}/ipgam2^{-/-}* and select the double homozygous mutant subsequently transformed plants among the primary transformant population (Figure 20). The double mutants *ipgam* are not fully complemented by the addition of neither *AtiPGAM2*_{WT} nor *AtiPGAM2*_{S75T} under the control of the *iPGAM2* promotor region since these plants are already detectable *via* their developmental phenotype (Figure 20) and were further confirmed to correspond to the *bona fide* double *ipgam1^{-/-}/ipgam2^{-/-}* mutants harboring the transgene *promAtiPGAM2::AtiPGAM2*_{WT} or *S75T* (Figure 21). However, both forms are complementing with the same level confirming the results obtained *in vitro*, which demonstrated that the mutation of serine 75 into a threonine doesn't change the protein activity. The complementation is high enough to do a complete development cycle and produce seeds (data not shown).

We then transformed the Col-0 plants with the *iPGAM2* ORF with site directed mutation(s) encoding the *AtiPGAM2*_{S75T}, *AtiPGAM2*_{S75T/D29N} and *AtiPGAM2*_{S75T/R290L} proteins to evaluate *in planta* the phosphorylation level of the different proteins. Indeed, since the mutation of R290L prevents the protein to bind the substrate, if this form is phosphorylated *in vivo*, it would suggest that *AtiPGAM2* could be regulated by phosphorylation by kinase and phosphatase activities. For this purpose, the leaves were collected in 2 am and 2 pm and the soluble proteins were extracted to measure the phosphorylation level of S82 in the different samples by LC-MS (as described in Materials and Methods section 5) Phosphopeptide measurements by PAPPSON). After a trypsin digestion, the phosphopeptides were enriched in a TiO₂ column. However, even with this method it was difficult to detect the tagged phosphopeptide. Nevertheless, four replicates for each condition (day/night) and genotype (*AtiPGAM2*_{S75T}, *AtiPGAM2*_{S75T/D29N}, *AtiPGAM2*_{S75T/R290L}) were constituted and each sample corresponds to a mix of leaves from 12 different plants. Unfortunately, among all these samples, the phosphopeptide was only detectable and quantifiable in one sample in the day condition and one sample in the night condition on *AtiPGAM2*_{S75T/R290L} and *AtiPGAM2*_{S75T} respectively. This difficult detection of the modified phosphopeptide could come from the low expression level of the transgene due to the *iPGAM2* promoter region. Indeed we previously observed that even if the complementation was high enough to recover fertility, the complemented double mutants displayed



(b)

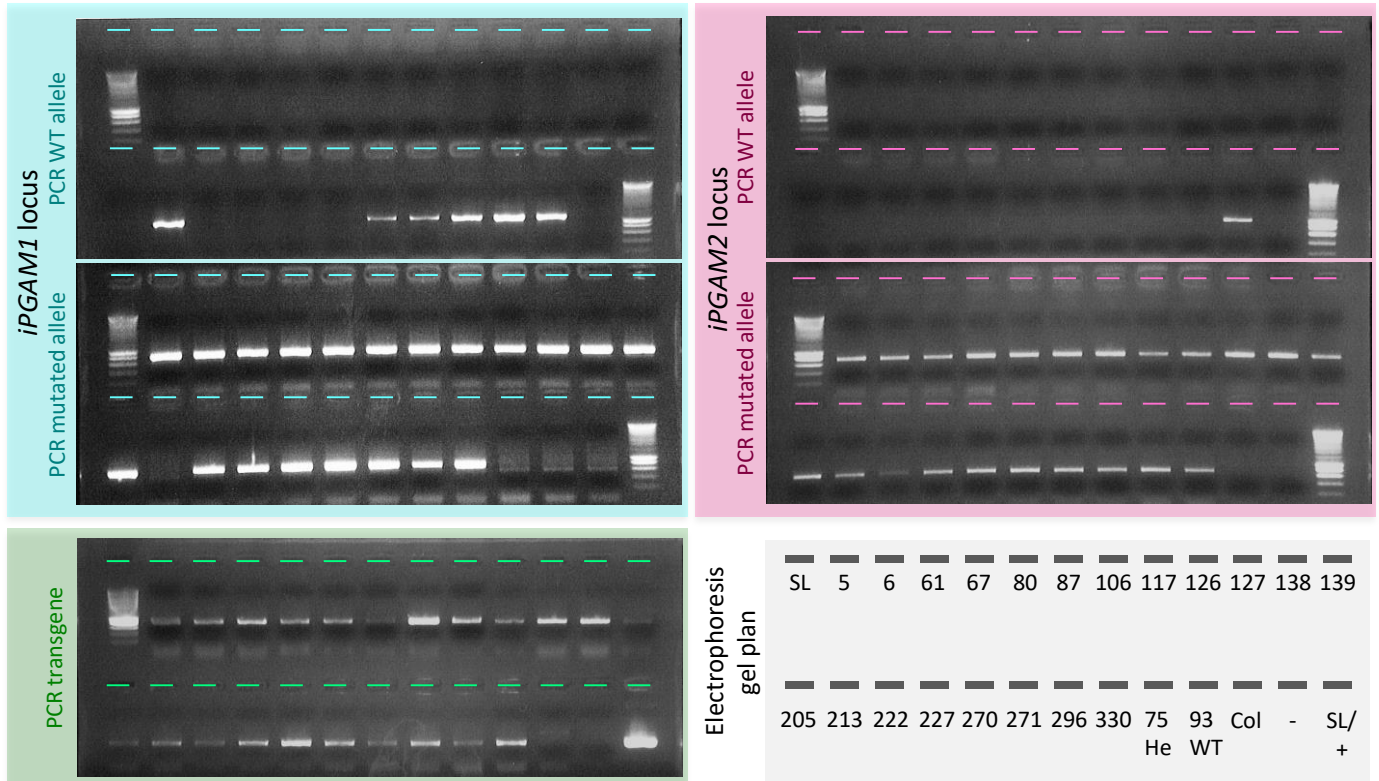


Figure 21: Determination of primary transformant genotype.

(a) position of T-DNA insertion at both *iPGAM1* and *iPGAM2* loci. The sesquimutant used for transformation is *ipgam1*^{-/-} *ipgam2*^{-/-}. Red arrows indicate the position of the primer used for PCR in (b). (b) Five PCRs are performed to determine the genotype of the primary transformants, which some are shown in white circles in Figure 7 (and red for He and WT control at the *iPGAM1* locus). Each PCR was run following the same gel plan. For each locus one PCR determines the presence of the WT allele ([SAM001+SAM007], 1184 bp expected for *iPGAM1* and [SAM026+SAM027], 1021 bp expected for *iPGAM2*) and the other determines the presence of the mutated allele ([LBb1+SAM007], 788bp expected for *iPGAM1* and [LBa1+SAM027], 824 bp expected for *iPGAM2*). The presence of the transgene is assessed in a PCR with the primer [596PRO+597TER]; a 727 bp fragment is expected with the transgene as template while a 1330 bp fragment is expected with gDNA as template. In this PCR the original plasmid used for plant transformation is used as positive control (+). (SL) is the molecular marker Smart Ladder (Eurogentec).

a developmental phenotype and thus are not fully restored by the level of expression. It could also be a problem of phosphopeptide identification. Since only one amino acid is different and we tried to choose another residue that has approximately the same design and charges, it remains possible that the m/z of the tag peptide was not different enough to distinguish it from the WT. However, the fact that even with these difficulties, we detected a phosphopeptide for the *AtiPGAM2*_{S75T/R290L} is a good sign not to refute the hypothesis of a kinase regulating iPGAM in *A. thaliana* even if several technical issues need to be fix.

CHAPTER II

***In vitro* characterization of *Arabidopsis thaliana* phosphoglycolate phosphatase 1 (AtPGLP1) activity and potential post-translational regulations**

Pauline DUMINIL¹, Caroline MAUVE¹, Céline OURY¹, Michael HODGES¹, Nathalie GLAB^{1*}

¹Université Paris-Saclay, CNRS, INRAE, Univ Evry, Institute of Plant Sciences Paris-Saclay (IPS2), 91405 Orsay, France.

*Author for correspondence: Tel. +33(0)169153349 ; e-mail: nathalie.glab@u-psud.fr

Word count: 6542

Introduction: 1048

Materials and Methods: 1643

Results: 1933

Discussion: 1828 (27.9 % of total word count)

Number of figures: 4

Number of tables: 3

Supporting Information:

Number of figures: 8

Number of tables: 1

Running title Deciphering AtPGLP1 regulation *in vitro*

Summary

Photorespiration is initiated by the oxygenase activity of ribulose-1,5-bisphosphate carboxylase oxygenase (RuBisCO) that produces toxic 2-phosphoglycolate (2-PG) in the chloroplast. This molecule is dephosphorylated by phosphoglycolate phosphatase 1 (PGLP1), the first enzyme of the photorespiratory cycle. Here we focus on *Arabidopsis thaliana* PGLP1 (AtPGLP1) activity and its post-translational regulation by protein phosphorylation and oxidation-reduction. Four potential phosphosites were studied by comparing wild-type, phospho-mimetic and non-phosphorylatable recombinant AtPGLP1 proteins. Only the mutation of either threonine 103 or threonine 322 to aspartate decreased *in vitro* AtPGLP1 activity, suggesting a potential phospho-inhibition of the enzyme. On the other hand, mutation at either threonine 320 or serine 356 had no effect on the measured kinetic parameters. AtPGLP1 activity was also impacted negatively when oxidized by H₂O₂ while DTT reduction had no effect. It was found that AtPGLP1 homodimerization was required for enzymatic activity and several cysteines and structural regions were identified as important for homodimer formation as seen from yeast two-hybrid assays.

(158 words)

Key words: AtPGLP1, NMR, Oxidation-reduction, Photorespiration, Protein phosphorylation

Introduction

Photorespiration is initiated by the oxygenase activity of the ribulose-1,5-bisphosphate (RuBP) carboxylase/oxygenase (RuBisCO) and thus occurs in all oxygenic photosynthetic organisms. The photorespiratory cycle requires eight core enzymes and four subcellular compartments (chloroplasts, mitochondria, peroxisomes and the cytosol) (Bauwe *et al.*, 2010). The oxygenation of RuBP leads to the production of a molecule of 3-phosphoglycerate (3-PGA) and 2-phosphoglycolate (2-PG), the latter being considered toxic because of its ability to inhibit certain enzymes of glycolysis and the Calvin-Benson cycle: triose phosphate isomerase (TPI), phosphofructokinase (PFK) and sedoheptulose-1,7-bisphosphate phosphatase (SBPase) (Anderson, 1971; Kelly and Latzko, 1976; Flügel *et al.*, 2017). Therefore, the photorespiratory cycle is crucial for air-grown plants since it has both a detoxifying and a C-salvaging role. This is highlighted by the observed growth phenotypes of

photorespiratory enzyme-lacking mutants (Timm & Bauwe, 2013). The first enzyme of the cycle is phosphoglycolate phosphatase (PGLP; E.C. 3.1.3.18) that dephosphorylates 2-PG to produce glycolate in the chloroplast. In *Arabidopsis thaliana*, two genes encode proteins exhibiting PGLP activity, *AtPGLP1* (At5g36700) and *AtPGLP2* (At5g47760) but only *AtPGLP1* is involved in photorespiration. Indeed, the *pglp1* knock-out mutant of *A. thaliana* showed a 97 % decrease of leaf PGLP activity and a lethal phenotype when grown in ambient air (0.038 % CO₂) while 2 % CO₂ was required for it to grow (Schwarte & Bauwe, 2007). A similar phenotype had been observed already for a *pglp* knock-down mutant of barley (RPr84/90) (Blackwell *et al.*, 1988). Moreover, a recent study has indicated a major role for PGLP in C₄ plants since RNAi lines targeting a *PGLP* gene of *Flaveria bidentis* exhibited a photorespiratory phenotype (Levey *et al.*, 2019). These mutants highlight the importance of a functional PGLP enzyme to metabolize 2-PG in plant chloroplasts.

Biochemical studies of PGLP purified from spinach, maize, barley, tobacco, *Chlamydomonas reinhardtii*, *Anacystis nidulans* and *Coccochloris peniocyctis* showed that this enzyme is 2-PG specific and required a divalent cation and a chloride anion, as well as homodimerization, for full activity (Richardson & Tolbert, 1961; Christeller & Tolbert, 1978a,b; Husic & Tolbert, 1984; Hardy & Baldy, 1986; Hall *et al.*, 1987; Norman & Colman, 1991; Mamedov *et al.*, 2001). The K_m for 2-PG was found to be species dependent; 26 μM (tobacco and spinach), 40 μM (pea) and 30 μM (bean) with values of 140 μM for *Chlamydomonas*, 220 μM for *C. peniocyctis* and 570 μM for maize (Christeller & Tolbert, 1978c,a; Husic & Tolbert, 1984; Hardy & Baldy, 1986; Belanger & Ogren, 1987; Huh *et al.*, 1989; Norman & Colman, 1991). The highest activities were measured in the presence of either Mg²⁺ or Co²⁺ while Ca²⁺ appeared to inhibit the PGLP reaction (Husic & Tolbert, 1984).

PGLP is a member of the haloacid dehalogenase family (HAD), a very large family of enzymes that can be found in all three super-kingdoms of life, with about 80 000 members that regroup a high range of biological functions including phosphatases, dehalogenases, phosphoamidases, phosphoglucomutase, ATPases, and phosphonates (Allen & Dunaway-Mariano, 2004, 2016; Burroughs *et al.*, 2006; Huang *et al.*, 2015). HAD proteins are made of a core domain containing four highly conserved motifs and a typical Rossmannoid structure (Rao & Rossmann, 1973) and a variable cap domain that defines substrate specificity (Seifried *et al.*, 2013). PGLP1 belongs to the phosphatase group of HAD proteins and it is related to phosphoglycolate phosphatase (PGP) enzymes found in mammals, human, yeast,

and bacteria. In many of these organisms, the role of PGP is also to detoxify 2-PG (Zecher & Wolf, 1980; Lyngstadaas *et al.*, 1999; Kim *et al.*, 2015; Collard *et al.*, 2016; Segerer *et al.*, 2016; Nagappa *et al.*, 2019) and they share certain similarities with plant PGLP such as a requirement for a divalent cation and chloride (Rose *et al.*, 1986; Lyngstadaas *et al.*, 1999; Teresa Pellicer *et al.*, 2003; Kim *et al.*, 2004; Segerer *et al.*, 2016; Xu *et al.*, 2016; Krocová *et al.*, 2019). The catalytic mechanism of the PGP reaction has been deciphered thus showing that 2-PG dephosphorylation is achieved *via* the formation of a transitory phosphoenzyme on a highly conserved aspartate (Seifried *et al.*, 2013). Mammalian PGP was shown to be regulated by oxidation mainly *via* disulphide bridge formation that altered activity and oligomerization state (Seifried *et al.*, 2016).

In plants, while the core photorespiratory enzymes and their genes have been identified and well characterized, little is known about their regulation. Some evidence suggests that photorespiratory genes are regulated during a day/night cycle and that this could be controlled by serine levels (Timm *et al.*, 2013). Post-translational modifications of certain photorespiratory enzymes have also been reported. Indeed, several mitochondrial photorespiratory proteins (glycine decarboxylase (GDS)-H/-P/-T and serine hydroxymethyl transferase (SHMT1)) were seen to interact with thioredoxin (Balmer *et al.*, 2004) and recently a thioredoxin-dependent redox regulation of GDC activity has been shown to occur (Fonseca-Pereira *et al.*, 2019; Reinholdt *et al.*, 2019). Redox-associated modifications of photorespiratory enzymes by either glutathionylation or S-nitrosylation have also been reported. Pea glycolate oxidase (GOX) activity was inhibited by S-nitrosylation while serine:glyoxylate aminotransferase and hydroxypyruvate reductase were identified as S-nitrosylated proteins (Ortega-Galisteo *et al.*, 2012). Mitochondrial GDC was found to be regulated by both S-nitrosylation and glutathionylation (Palmieri *et al.*, 2010). Interestingly, PGLP1 has been found also to be a S-nitrosylated protein (Hu *et al.*, 2015) and it was identified in Arabidopsis 2-cys peroxiredoxin (Cerveau *et al.*, 2016) and NADH-thioredoxin reductase C (NTRC) (González *et al.*, 2019) interaction studies. That said, the most prevalent post-translational regulation is reversible protein phosphorylation that can modify protein conformation, stability, activity, localization as well as protein/protein interactions. Interestingly, all but one of the eight-core photorespiratory enzymes have been associated with at least one phospho-peptide identified by phosphoproteomic studies (see Hodges *et*

al., 2013) thus suggesting that protein phosphorylation may be an important regulatory mechanism of photorespiration.

The aim of this work was to characterize the enzymatic properties of *A. thaliana* PGLP1 and to understand the effect of potential post-translational modifications on *AtPGLP1* activity. The impact of four PGLP1 phosphorylation sites identified in various phosphoproteomes were evaluated by characterizing the kinetic and oligomeric properties of wild-type, phosphorylation-mimetic and non-phosphorylatable recombinant *AtPGLP1* proteins. The importance of *AtPGLP1* dimerization and oxido-reduction status on *in vitro* enzymatic activity was also investigated. During the course of this work, three methods to measure *in vitro* PGLP1 activity were developed.

Materials and methods

Cloning of the PGLP1 ORF into pET16b and pDEST-His₆MBP

First strand cDNA was obtained by reverse transcription of *A. thaliana* leaf total RNA performed with ImProm-IITM reverse transcriptase (Promega) and used to PCR-amplify *AtPGLP1* ORF cDNA without the DNA sequence encoding the chloroplast targeting peptide using *PfuI* polymerase (Promega) and primers 535PRO and 536TER (see Table S1 for all primer sequences) designed to introduce *NdeI* and *XhoI* restriction sites. The amplified sequence was transiently cloned into pGEM[®]-T Easy for sequencing (by EurofinsTM) and then into pET16b to generate pET16b-*AtPGLP1*_{WT} using the restriction sites. The *AtPGLP1* cDNA in pGEM[®]-T Easy was then used as a template to add *attB* sites for Gateway[®] cloning by a first PCR using 598PRO and 599TER primers followed by a second PCR reaction using GW-FORWARD and GW-REVERSE primers. The resulting DNA fragment was cloned into pGEM[®]-T Easy for verification before being transferred to pDONR207 *via* a BP recombination reaction. The generated plasmids, pDONR207-*AtPGLP1*_{WT} and pET16b-*AtPGLP1*_{WT}, were used to carry out site-directed mutagenesis with the QuikChange[®] II XL Site-Directed Mutagenesis Kit (Agilent Technology) according to the manufacturer's instructions and suitable primers (see Table S1). In this way, pET16b-*AtPGLP1*_{T330A}, pET16b-*AtPGLP1*_{T330D}, pET16b-*AtPGLP1*_{S356A}, pET16b-*AtPGLP1*_{S356D} as well as pDONR207-*AtPGLP1*_{C86A}, pDONR207-*AtPGLP1*_{T103A}, pDONR207-*AtPGLP1*_{T103D}, pDONR207-*AtPGLP1*_{T322A}, and pDONR207-*AtPGLP1*_{T322D} were obtained. Using the same approach, two deletions were produced: DEL1 corresponding to the deletion of the sequence encoding amino acids 219 to 224 (RYFNYY) and DEL2

corresponding to the sequence encoding amino acids 263 to 268 (SMVGAL). After validation of the mutations/deletions, WT and mutated *AtPGLP1* sequences were introduced into pDEST-His₆MBP *via* LR Clonase Gateway® recombination reactions thus generating pDEST-His₆MBP-*AtPGLP1*_{WT}, pDEST-His₆MBP-*AtPGLP1*_{C86A}, pDEST-His₆MBP-*AtPGLP1*_{T103A}, pDEST-His₆MBP-*AtPGLP1*_{T103D}, pDEST-His₆MBP-*AtPGLP1*_{322A}, pDEST-His₆MBP-*AtPGLP1*_{T322D}, pDEST-His₆MBP-*AtPGLP1*_{DEL1} and pDEST-His₆MBP-*AtPGLP1*_{DEL2}. The pET16b and pDEST-His₆MBP *AtPGLP1* constructs were used for production and purification of *AtPGLP1* recombinant proteins by affinity chromatography.

Cloning AtPGLP1 ORF into yeast two hybrid plasmids

The plasmid pDONR207-*AtPGLP1*_{WT} was used again as a template to carry out site-directed mutagenesis using appropriate primers (see Table S1) to obtain the mutation of cysteines 86, 232, 239, 302, 320 to alanines and the double 232/239 mutation. For the double 302/320 mutation, pDONR207-*AtPGLP1*_{C302A} was used as the template for mutagenesis. The WT and mutated (C86A, T103A, T103D, C232A, C239A, C232/239A, C302A, C320A, C302/320A, DEL1, DEL2) versions of *AtPGLP1* in pDONR207 were transferred into both pDEST-AD and pDEST-BD (Dreze *et al.*, 2010) using LR Clonase Gateway® reactions according to the manufacturer's instructions. After validation, AD and BD plasmid combinations were co-transformed into *Saccharomyces cerevisiae* strain Y8930 using a simplified protocol (Gietz *et al.*, 1992).

Recombinant protein purification

A 3 mL overnight preculture of *E. coli* BL21(DE3) cells containing either a pET16b or pDEST-His₆MBP plasmid with the *AtPGLP1* ORF (WT or mutated) was diluted into 200 mL of Luria-Bertani broth containing ampicillin (50 mg L⁻¹) and grown at 37 °C under shaking at 180 rpm until a OD_{600nm} of 0.8 was reached. *AtPGLP1* expression was induced by addition of 500 µM isopropyl -1-D-thiogalactopyranoside and further cultured for 4 h at 37 °C. Cells were pelleted by centrifugation and resuspended in 3 mL of lysis buffer (50 mM Tris-HCl pH 7.5, 150 mM NaCl, 10 mM MgSO₄, antiproteases (cOmplete™ Mini, EDTA-free Protease Inhibitor Cocktail Tablets provided in EASY packs by Sigma-Aldrich; 1 tablet in 50 mL) and either 5 mM imidazole for the expression using pDEST-His₆MBP or 10 mM when using pET16b. Bacterial cells were broken *via* a French press (3 times at 3.5 MPa). After a 30 min centrifugation at 4 °C and 27 000 g, recombinant proteins were batch-purified using His-Select nickel affinity

resin (Sigma-Aldrich) according to the manufacturer's instructions. Washing was performed with 45 mL of lysis buffer containing either 20 mM imidazole (for pDEST-His₆MBP expression) or 75 mM imidazole (for pET16b expression). Recombinant proteins were eluted with 3 mL of lysis buffer containing 250 mM imidazole. A desalting step was added using PD-10 columns (GE Healthcare) equilibrated with Tris-HCl 50 mM at pH 7.5 according to the manufacturer's instructions. Protein concentration was measured using PierceTM Coomassie Plus Assay Reagent (Sigma-Aldrich) according to the manufacturer's instructions.

Purification of recombinant GOX

The production and purification of recombinant Arabidopsis GOX protein (*AtGOX1*) were performed according to Dellero *et al.*, (2015) and it was used to measure *AtPGLP1* activity in the coupled reaction protocol described below.

AtPGLP1 activity measurement by a coupled enzymatic reaction

The enzymatic activity of *AtPGLP1* recombinant proteins was measured *via* a coupled reaction (see Figure S1) using a Varian Cary 50 spectrophotometer at $A_{440\text{ nm}}$ that allowed the detection of oxidized *o*-dianisidine production, in the presence of 5 μg of purified recombinant *AtPGLP1*, 40 μg of purified recombinant *AtGOX1*, 2 U of horseradish peroxidase (HRP; Sigma-Aldrich), 400 μM *o*-dianisidine dihydrochloride ($\geq 95\%$; Sigma-Aldrich) and various concentrations (0.01 μM to 5 mM) of 2-phosphoglycolic acid (lithium salt $\geq 95.0\%$; Sigma-Aldrich), in a 1 mL final volume of reaction buffer (50 mM Tris-HCl pH 8, 10 mM MgSO_4 and cCompleteTM anti-proteases). The reaction was initiated by the addition of *AtPGLP1* protein and measured at 30 °C by following the $\Delta A_{440\text{ nm}}$ in real time. The effect of different cations on *AtPGLP1* activity was tested using recombinant *AtPGLP1* purified in the absence of cations by the addition of 10 mM of either Mg^{2+} , Mn^{2+} , Co^{2+} , Ca^{2+} or Zn^{2+} (chloride salt) to the reaction buffer.

AtPGLP1 activity measurement by phosphate sensor

AtPGLP1 activity was measured in 384-well black plates (Greiner Bio-One) in a 20 μL final volume containing between 0.01 μM and 5 mM of phosphoglycolic acid (lithium salt $\geq 95.0\%$), 0.25 ng of *AtPGLP1* recombinant protein, and 1 mM phosphate sensor (Invitrogen). The reaction buffer contained 50 mM Tris pH 7.5, 0.05 % Triton X-100, 10 mM MgSO_4 and

20 mM NaCl. The increase of phosphate sensor fluorescence was measured during 30 min at 30 °C using a Tecan Infinite M200.

AtPGLP1 activity measurement by ¹H-NMR

For NMR activity measurements, 2.5 µg of recombinant AtPGLP1 was used in a 1 mL reaction buffer (50 mM Tris-HCl pH 8, 10 mM MgSO₄ and cOmplete™ anti-proteases). The produced glycolate and the remaining 2-PG were measured after 10 s of reaction performed at 30 °C and stopped by addition of 30 µL of 14.3 M hydrochloric acid. To test the impact of the reduced/oxidized state of the protein on PGLP activity, recombinant protein was incubated for 10 min at 30 °C with two concentrations (1 mM and 10 mM) of either H₂O₂ or dithiothreitol (DTT). The reaction was initiated by the addition of the pre-incubated recombinant protein. ¹H-NMR experiments were performed using an Ascend 400 MHz NanoBay instrument equipped with an AVANCE III HD console and a Prodigy BBO cryoprobe (³¹P-¹⁵N) (Bruker). Analyses were done at 277 K without tube spinning, using water suppression and excitation sculpting with gradients. To obtain a good signal-to-noise ratio, 128 scans were carried out, representing an acquisition time of 9.5 min per sample. The reference was 3-(trimethylsilyl) propionic-2,2,3,3-d₄ acid because of its solubility in water. Data were analysed using TopSpin software (Bruker). The free induction decay signal was processed by performing exponential line broadening, calculating the Fourier transformation, adjusting the phase and applying a baseline correction. The attribution of each peak to glycolate and 2-PG was done using analytical standards (phosphoglycolic acid lithium salt ≥95.0%, glycolic acid **ReagentPlus® 99%**, both from Sigma-Aldrich). Calibration curves with known concentrations confirmed that data acquisition was quantitative since peak areas were proportional to the amount of molecules in the sample ($R^2 > 0.98$ for glycolate and $R^2 > 0.96$ for 2-PG). For DTT and H₂O₂ experiments, 2-PG and glycolate signals were not modified.

Determination of kinetic parameters

Kinetic parameters of AtPGLP1 recombinant proteins were calculated using the Michaelis-Menton equation of Sigma-Plot “Kinetic Enzyme Wizard” (Systat Software). This was repeated three times, on three different recombinant protein productions and purifications for each AtPGLP1 form tested.

Yeast two-hybrid assays

The day before transformation, a culture in YPDA medium was started with 3-4 of isolated yeast colonies and agitated at 200 rpm overnight at 30 °C. Cells were harvested (7 min, 1250 g, room temperature), washed with sterile H₂O, then washed and concentrated twice with TE/LiAc buffer (TE buffer: 10 mM Tris-HCl pH 7.5, 1 mM EDTA; LiAc buffer: 0.1 M lithium acetate pH 7.5 adjusted with 5 % acetic acid (v/v)). For each AD+BD combination, 1 mL of cell suspension was centrifuged and to the cell pellet was sequentially added: 100 µg of salmon sperm carrier DNA previously denatured 30 min at 95 °C and placed immediately on ice, 1 µg of each type of plasmid DNA (AD and BD) and 220 µL of PEG/TE/LiAc/DMSO buffer (10 mL freshly prepared buffer contained 5 g PEG 3350, 1 mL 10xTE, 1 mL 10xLiAc, adjusted to 10 mL with H₂O; sterilized by filtration before the addition of DMSO (final concentration of 10 % v/v)). The mixture was vortexed, and shaken at 200 rpm at 30 °C for 30-40 min. A heat shock was performed at 42 °C for 15 min after which the mixture was placed on ice for 3 min then 1 mL of cold sterile water was added. Cells were pelleted (3 min 1810 g room temperature) and re-suspended in TE buffer before plating on SD-Leu-Trp. After 3-4 days incubation at 30 °C, a dozen isolated colonies were picked and mixed in sterile water, the OD_{600 nm} was adjusted to 2 and serial dilutions were performed. 20 µL drops of each dilution were deposited on three different media: SD-Leu-Trp (permissive medium), SD-Leu-Trp-His and SD-Leu-Trp-His+3-AT 1 mM (interaction selective media). Growth was recorded after 7 days of incubation at 30 °C.

Modelling the 3D structure of AtPGLP1

AtPGLP1 3D structure predictions were performed using the modelling workspace of SWISS-MODEL (<https://swissmodel.expasy.org/interactive>). The target sequence was the AtPGLP1 polypeptide without the chloroplast signal peptide. The template was PBD 4BKM corresponding to the crystal structure of the murine AUM (phosphoglycolate phosphatase) capping domain as a fusion protein with the catalytic core domain of murine chronophin (pyridoxal phosphate phosphatase).

Results

The kinetic properties and divalent cation requirements of recombinant AtPGLP1

Since the reported K_m values for 2-PG of PGLP appeared to depend on species (see Introduction), it was decided to measure this kinetic parameter using our recombinant *AtPGLP1_{WT}* protein. To do this, three different methods were developed; a coupled reaction using recombinant *AtGOX1*, a commercial phosphate sensor and $^1\text{H-NMR}$ (see Materials and methods section). In the presence of Mg^{2+} cations, the three methods gave similar K_m 2-PG values of 0.34 ± 0.03 mM (coupled), 0.27 ± 0.03 mM (sensor) and 0.42 ± 0.0015 mM (NMR) and k_{cat} values of 19.7 ± 2.5 s^{-1} (coupled), 18.0 ± 0.5 s^{-1} (sensor) and 17.2 ± 1 s^{-1} (NMR). These data validated our coupled reaction protocol and it was selected as our method of choice to measure *AtPGLP1* activity when possible.

Since PGLP activity has been shown to depend on the presence of a divalent cation and that maximal activities were affected by the specific cation used, it was decided to test the impact of a number of divalent cations (Mg^{2+} , Mn^{2+} , Co^{2+} , Zn^{2+} and Ca^{2+}) on recombinant *AtPGLP1* activity. To do this, divalent cations were omitted during the recombinant protein purification procedure. Table 1 shows the effect of divalent cations on the calculated K_m 2-PG, V_{max} and k_{cat} values of *AtPGLP1_{WT}*. It can be seen that there was no detectable *AtPGLP1* activity in the presence of Zn^{2+} while maximal activity was observed when Mg^{2+} was added to the reaction buffer. As already reported, Ca^{2+} inhibited PGLP activity as seen by the approx. 9-fold decrease of V_{max} and k_{cat} while increasing the K_m 2-PG by 4-fold. On the other hand, when compared to Mg^{2+} , both Mn^{2+} and Co^{2+} led to a similar 2-fold decrease of K_m 2PG however the decrease of V_{max} and k_{cat} was different with Mn^{2+} giving rise to a 5-fold decrease while Co^{2+} reduced these parameters by only approx. 2-fold. Therefore, Mg^{2+} was clearly the most efficient divalent cation for maximal *AtPGLP1* activity (Table 1) and therefore it was decided to carry out all *AtPGLP1* activity measurements in the presence of this cation.

AtPGLP1 protein contained HAD family member motifs

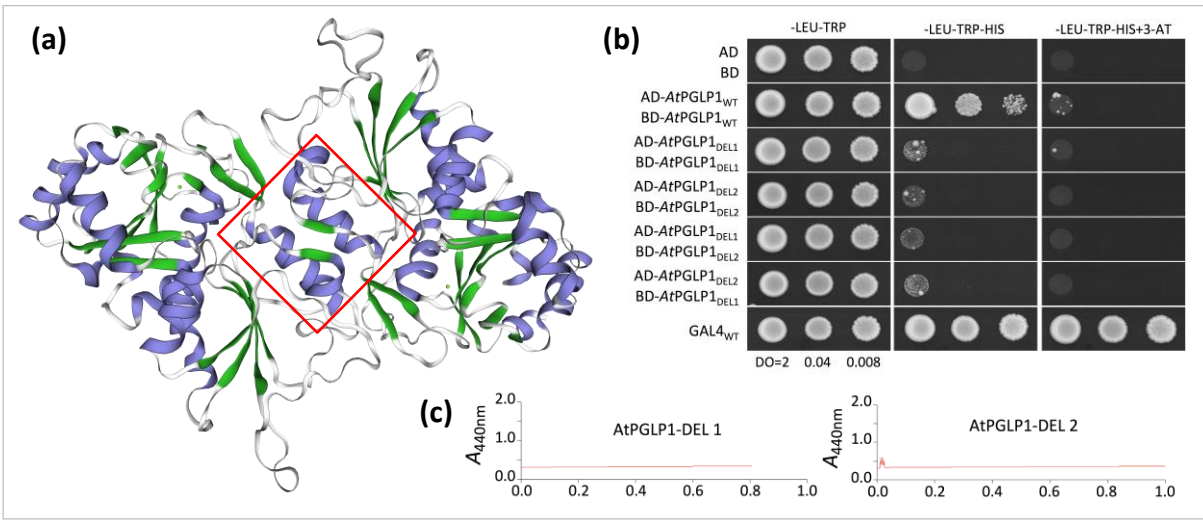
Haloacid dehalogenase (HAD) family proteins are characterized by a very low sequence identity across species, but they maintain conserved structural domains and several important motifs (Motif I to IV; Figure 1a). Sequence alignments of *AtPGLP1* with other HAD phosphatase family members indicated that *AtPGLP1* protein contained each of the four highly conserved HAD phosphatase motifs: The catalytic DxD at the end of the S1 strand, a threonine and a serine at the end of the S2 strand, a conserved lysine at the N-terminus of the helix located upstream of the S4 strand and a terminal GDxxxxD acidic group of residues

Table 1: The effect of divalent cations on the kinetic parameters of recombinant AtPGLP1 measured using the GOX-coupled reaction.

Divalent cation	K_m (mM)	V_{max} ($\mu\text{mol of glycolate.mg}^{-1}$ of prot.min $^{-1}$)	k_{cat} (s $^{-1}$)
Mg $^{2+}$	0.34 \pm 0.03	29.4 \pm 3.7	19.7 \pm 2.5
Mn $^{2+}$	0.18 \pm 0.02	6.1 \pm 0.8	4.1 \pm 0.6
Co $^{2+}$	0.15 \pm 0.01	17.5 \pm 0.1	11.7 \pm 0.1
Ca $^{2+}$	1.37 \pm 0.22	3.5 \pm 0.3	2.3 \pm 0.2
Zn $^{2+}$	-	0	-

Kinetic parameters were calculated using “Kinetic Enzyme Wizard” of Sigma-Plot (Systat Software Inc.) with activities recorded using a range of 2-PG from 0.01 mM to 5 mM. The reaction was started with 5 μg of recombinant protein while all the other enzymes were in excess (2U HRP and 40 μg GOX). Values are means \pm SD (n=3 independent experiments)

Figure 2: Duminil et al.



(Figure 1a, Figure S2). We then generated a predicted model of AtPGLP1 3D structure using SWISS MODEL (<https://swissmodel.expasy.org/interactive>) and the structure of murine AUM PGP capping domain as a fusion protein with the catalytic core domain of murine chronophin (pyridoxal phosphate phosphatase) (PBD 4BKM). The model showed the catalytic residues and the typical Rossmannoid fold organisation of repeated α and β units forming a parallel central sheet of five strands (from S1 to S5) that sometimes includes S6 (Figure 1b and c) and indicated regions involved in AtPGLP1 dimer formation (Figure S3). Information from this structural model was used to study the role of AtPGLP1 dimerization and the mutation of cysteine residues and phospho-sites on AtPGLP1 activity.

Homodimerization and PGLP1 activity

The predicted 3D structure of AtPGLP1 indicated two motifs that appeared to be involved in homodimer formation: an α -helix (from G261 to S271) and a β -strand (from R219 to K225) (Figure S3). It was thus decided to perform deletions in these putative contact domains to determine their involvement in AtPGLP1 homodimerization and the effect on enzymatic activity. To do so, AtPGLP1 was mutagenized to generate AtPGLP1-DEL1 where amino acids R219 to Y224 of the β -sheet were removed (see Figure 1a) and AtPGLP1-DEL2 where amino acids S263 to L268 were deleted from the α -helix (see Figure 1a), then homodimer formation was tested by a yeast two-hybrid assay (Figure 2b). Indeed, when either of the selected regions was suppressed, protein interactions were highly impaired thus suggesting an important role of each region for AtPGLP1 homodimerization (Figure 2). To check the stability of both AtPGLP1-DEL proteins, they were expressed and purified as MBP-His-fusion proteins in *E. coli*. SDS-PAGE confirmed that they were produced and stable (Figure S4) however they showed no PGLP activity in the coupled reaction assay using a saturating 1 mM 2-PG concentration (Figure 2c). Therefore, it appeared that AtPGLP1 must form at least a homodimer to be active.

Oxidation of AtPGLP1 inhibited enzyme activity

Recent studies have shown a thioredoxin-dependent redox regulation of photorespiratory GDC activity (Fonseca-Pereira *et al.*, 2019; Reinholdt *et al.*, 2019), while mammalian PGP activity was found to be sensitive to oxidation (Seifried *et al.*, 2016) and Arabidopsis PGLP1 appeared to interact with a 2-cys peroxiredoxin (Cerveau *et al.*, 2016). Therefore, it was

Figure 3: Duminil et al.

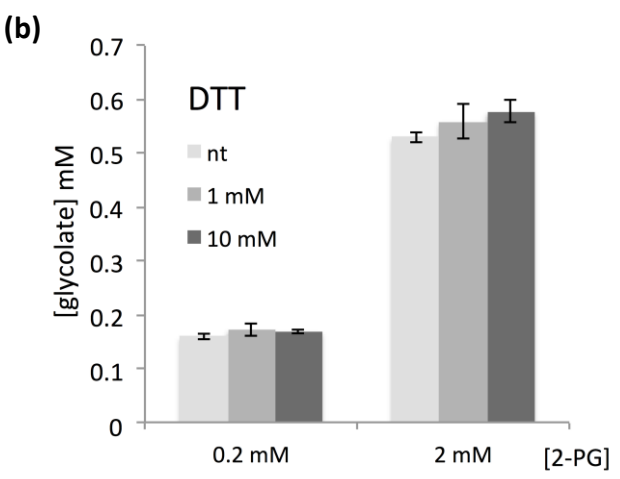
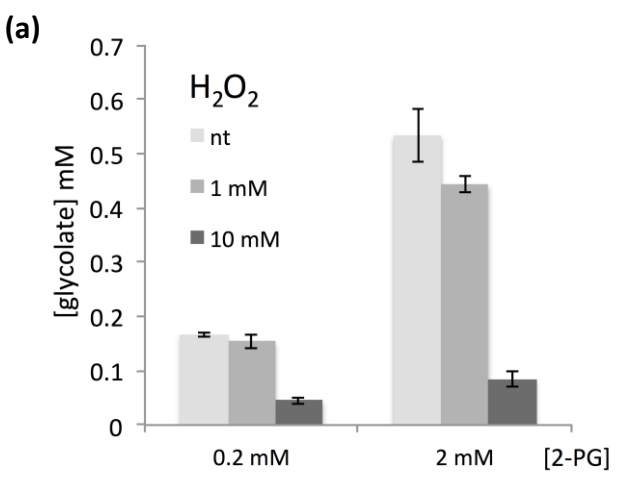


Table 2: The role of cysteines in AtPGLP1 dimerization using a yeast two-hybrid test

Interaction tested	-LEU-TRP-HIS	LEU-TRP-HIS+3AT
AD-AtPGLP1 _{WT} /BD-AtPGLP1 _{WT}	+++++	+
AD-AtPGLP1 _{C86A} /BD-AtPGLP1 _{C86A}	+++++	+
AD-AtPGLP1 _{C232A} /BD-AtPGLP1 _{C232A}	++++	+/-
AD-AtPGLP1 _{C239A} /BD-AtPGLP1 _{C239A}	+++++	+/-
AD-AtPGLP1 _{C232A} /BD-AtPGLP1 _{C239A}	+++++	-
AD-AtPGLP1 _{C239A} /BD-AtPGLP1 _{C232A}	+++	-
AD-AtPGLP1 _{C232/239A} /BD-AtPGLP1 _{C232/239A}	-	-
AD-AtPGLP1 _{C302A} /BD-AtPGLP1 _{C302A}	++	-
AD-AtPGLP1 _{C320A} /BD-AtPGLP1 _{C302A}	-	-
AD-AtPGLP1 _{C302A} /BD-AtPGLP1 _{C320A}	+	-
AD-AtPGLP1 _{C320A} /BD-AtPGLP1 _{C320A}	+++++	+
AD-AtPGLP1 _{C302/320A} /BD-AtPGLP1 _{C302/320A}	+	-

The importance of each cysteine of AtPGLP1 was by a two-hybrid assay to determine a role in AtPGLP1 homodimerization. Two double mutants were also generated to study the possible interaction between different cysteines. The + and – represents the intensity of the two-hybrid interaction when compared with the wild-type (see Supplementary Figure 6). $\Delta A_{600\text{ nm}}$ was measured and adjusted to 2 units and serial dilutions were performed. 20 μL drops of each dilution were deposited on three different media (LEU-TRP data not shown because this corresponds to the permissive medium; LEU-TRP-HIS; -LEU-TRP-HIS+3-AT). Four replicates were performed.

decided to test the redox sensitivity of AtPGLP1 activity by carrying out DTT and H₂O₂ treatments. Since our coupled reaction involved the measurement of H₂O₂ production by AtGOX1, and the Pi sensor method was based on a link between a fluorophore and a bacterial protein *via* a cysteine, we developed a quantitative ¹H-NMR approach for activity measurements. First it was verified that the protein, buffer, substrate and product did not produce overlapping spectra signals and that the reaction was linear during the selected 10 s reaction time. NMR spectra showed the glycolate signal to be a singlet because detected protons were equivalent on the molecule, while the 2-PG signal formed a doublet because the sensed protons were coupled with atoms carried by the phosphate (Figure S5a). Although the 2-PG signal was less intense because it was divided, curves of decreasing 2-PG and increasing glycolate were symmetrical during the reaction (Figure S5b). It was decided to measure AtPGLP1 activity by following glycolate production (Figures S5b and S5c). This method was used to determine the kinetic parameters of AtPGLP1_{WT} (K_m 2-PG of 0.42 mM, V_{max} of 25.6 $\mu\text{mol}\cdot\text{mg}^{-1}$ of protein $\cdot\text{min}^{-1}$ and a k_{cat} of 17.2 s^{-1}), and it allowed us to study the impact of H₂O₂ and DTT on AtPGLP1 activity at both limiting (0.2 mM) and saturating (2 mM) 2-PG concentrations. The addition of DTT did not alter AtPGLP1 activity while the oxidative treatment with H₂O₂ led to a severe inhibition of enzyme activity (Figure 3).

Involvement of cysteines in AtPGLP1 homodimerization

Since AtPGLP1 activity appeared to be modified by oxidation, it was decided to study the role of the cysteine residues of the mature AtPGLP1 protein (Figure 1a, Figure S2). Therefore, we carried out site-directed mutagenesis to test the effect of replacing each cysteine by an alanine on homodimer formation using our yeast two-hybrid assay. It was possible that oxidation of the active site cysteine 86 situated in between the catalytic aspartate residues of the conserved motif (DxD) of the HAD family might be responsible for the observed inhibition. Although this cysteine had been shown to be required for mammalian PGP activity (Seifried *et al.*, 2016), surprisingly, the AtPGLP1_{C86A} protein was still active and exhibited similar kinetic parameters to those of AtPGLP1_{WT} (see Table 3). It was also possible that oxidation of cysteines could alter AtPGLP1 conformation, dimerization or oligomerization. As expected, the mutation of cysteine 86 showed that it was not involved in homodimer formation (Table 2, Figure S6). A second conserved cysteine between mammalian PGP and Arabidopsis PGLP1 was cysteine 239 corresponding to cysteine 193 of

the mouse enzyme. Since this residue had been found not to regulate murine PGP (Seifried *et al.*, 2016), it was decided to only test whether one or more of the remaining 3 cysteines of the mature *AtPGLP1* protein were involved in dimer formation. The yeast two-hybrid assay showed that cysteine 302 was important for the interaction between *AtPGLP1* monomers to occur (Table 2, Figure S6) as an interaction was not observed in the case of simple and double mutations involving cysteine 302 and when the C302A mutation was carried by either the AD or BD vectors. On the other hand, the single mutation of either cysteine 232 or cysteine 239 did not appear to impact monomer interactions, while this was not the case for the double C232A/C239A mutation (Table 2, Figure S6). Therefore, together these two cysteine residues appeared to be important to allow dimer formation.

Phosphoregulation of AtPGLP1 activity

Protein phosphorylation is a major regulatory post-translational mechanism and four phosphosites have been identified (at threonine 103, 322, 330 and serine 356) on three different *AtPGLP1* phosphopeptides (see Hodges *et al.*, 2013; PhosPhAt database). PGLP protein sequence alignments showed that these four amino acids were highly conserved among numerous plant species including C₄ plants like maize and also prokaryotes (Figure S2). However, they were not completely preserved in mammalian PGPs (Figure 1a), perhaps suggesting a specific role in photosynthetic organisms to regulate photorespiration. In order to decipher the function of each phosphosite, the *AtPGLP1* ORF was modified by site-directed mutagenesis to produce either a non-phosphorylatable enzyme (mutated to give an alanine) or a constitutive phosphorylation-mimetic form (mutated to give an aspartate). In all cases, recombinant *AtPGLP1* protein was produced and purified with an N-terminal poly-histidine tag (see Figures S7 and S8). In specific cases, the recombinant protein was also fused to the maltose binding protein (MBP) to enhance solubility in *E. coli* cells (see Figure S8). Indeed, in the absence of the MBP, *AtPGLP1*_{T103D} was completely insoluble whereas *AtPGLP1*_{T103A} was not, thus suggesting a modification in the conformation of the phosphorylation-mimetic form. Solubility problems also occurred for T322-mutated *AtPGLP1*, whatever the alternative residue. After production and affinity purification, *in vitro* PGLP activity was measured in the presence of Mg²⁺ and kinetic parameters were calculated. To do so, a procedure was developed to allow real time measurements of PGLP activity using a coupled reaction with recombinant *AtGOX1* (Dellero *et al.*, 2015), the second enzyme of

Figure 4: Duminil et al.

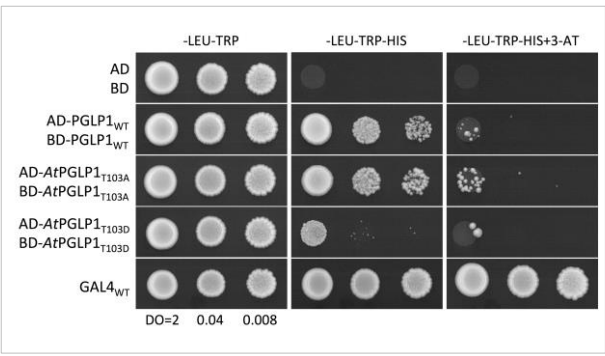


Table 3: The kinetic properties of phospho-mimetic AtPGLP1 and motif I mutated AtPGLP1

Protein form	K_m (mM)	V_{max} ($\mu\text{mol of glycolate}\cdot\text{mg}^{-1}$ of prot. $\cdot\text{min}^{-1}$)	k_{cat} (s^{-1})
AtPGLP1 _{WT} [◦]	0.34 ± 0.03	29.5 ± 3.7	19.7 ± 2.5
AtPGLP1 _{WT} [*]	0.31 ± 0.04	31.9 ± 1.8	21.3 ± 1.2
AtPGLP1 _{T103A} [*]	0.30 ± 0.04	32.3 ± 0.9	21.7 ± 0.6
AtPGLP1 _{T103D} [*]	-	-	-
AtPGLP1 _{T322A} [*]	0.29 ± 0.01	30.7 ± 1	20.6 ± 0.7
AtPGLP1 _{T322D} [*]	0.33 ± 0.04	2.2 ± 0.1	1.5 ± 0.04
AtPGLP1 _{T330A} [◦]	0.28 ± 0.02	25.9 ± 0.9	17.4 ± 0.6
AtPGLP1 _{T330D} [◦]	0.40 ± 0.06	24.9 ± 3.1	16.7 ± 2
AtPGLP1 _{S356A} [◦]	0.34 ± 0.03	22.8 ± 1.4	15.3 ± 1
AtPGLP1 _{S356D} [◦]	0.30 ± 0.02	22.4 ± 1.6	15.0 ± 1
AtPGLP1 _{C86A} [*]	0.4 ± 0.04	22.3 ± 2.15	14.9 ± 1.44

Kinetic parameters of wild-type AtPGLP1_{WT} and mutated (AtPGLP1_{T103A}; AtPGLP1_{T103D}; AtPGLP1_{T322A}; AtPGLP1_{T322D}; AtPGLP1_{T330A}; AtPGLP1_{T330D}; AtPGLP1_{S356A}; AtPGLP1_{S356D}; AtPGLP1_{C86A}) were calculated using “Kinetic Enzyme Wizard” of Sigma-Plot (Systat Software Inc.) with activities recorded using a range of 2-PG from 0.01 mM to 5 mM. The reaction was started with 5 μg of recombinant protein while all the other enzymes were in excess (2U HRP and 40 μg GOX). Values are means \pm SD (n=3 independent experiments)

* Indicates recombinant proteins produced using pDEST-His₆MBP

◦ Indicates recombinant proteins produced using pET16b

the photorespiratory cycle that releases H₂O₂ during glycolate oxidation that was quantified in the presence of o-dianisidine and horseradish peroxidase (see Figure S1). This coupled reaction was used to measure the kinetic parameters of our different recombinant AtPGLP1 proteins. When compared to AtPGLP1_{WT}, mutation of either threonine 330 or serine 356 did not change significantly the kinetic parameters (K_m 2-PG, V_{max} and k_{cat}) of the enzymes, whatever the mutation (Table 3). When threonine 103 was mutated, the kinetic parameters of MBP-fused AtPGLP1_{T103A} remained unchanged compared to the WT protein, while the soluble MBP-fused version of phosphorylation-mimetic AtPGLP1_{T103D} was inactive (Table 3). The production of this inactive MBP-fused form as well as MBP-fused AtPGLP1_{T332D} and AtPGLP1_{T332A} proteins and the MBP-fused version of AtPGLP1_{WT} were checked by SDS-PAGE (Figure S8). Perhaps surprisingly, recombinant AtPGLP1_{T322A} exhibited WT kinetic parameters while the phosphorylation-mimetic AtPGLP1_{T322D} showed a 13-fold decrease in k_{cat} and V_{max} values although the K_m 2-PG remained unaltered (Table 3). Therefore, it appeared that phosphorylation at T103 and T322 could have a role in regulating AtPGLP1 activity.

Phosphoregulation of AtPGLP1 and homodimerization

Since phosphorylation-mimetic AtPGLP1_{T103D} showed altered protein solubility in *E.coli* cells and it was inactive compared to AtPGLP1_{WT} and AtPGLP1_{T103A} recombinant proteins, we decided to test whether it was capable of forming homodimers using the yeast two-hybrid assay. This showed that the interaction between AtPGLP1_{T103D} was significantly weakened when compared to the other AtPGLP1 proteins tested (Figure 4). Such observations suggested that the absence of AtPGLP1_{T103D} activity was associated with a modification of monomer interactions that probably impeded dimer formation (Table 3 and Figure 4).

Discussion

Recombinant AtPGLP1 has a high K_m for 2-PG

PGLP1 is the first enzyme of the photorespiratory cycle and it is involved in removing toxic 2-PG molecules that are known to inhibit TPI, SBPase and PFK (Anderson, 1971; Kelly and Latzko, 1976; Flügel et al., 2017). The reported K_i values of 2-PG are low; 15 μ M (pea TPI, (Anderson, 1971)), 50 μ M (spinach PFK, (Kelly & Latzko, 1976)) and 10 μ M (Arabidopsis SBPase, (Flügel et al., 2017)) and therefore, the calculated K_m for 2-PG of our recombinant AtPGLP1 of between 0.27 mM and 0.42 mM (depending on the assay method) was

surprisingly high. Indeed, K_m 2-PG values from PGLP purified from extracts of photosynthetic organisms were much lower (e.g. 26-40 μM for spinach, tobacco, pea and bean PGLP, and 140 μM for *Chlamydomonas* PGLP (see Introduction). However, the *AtPGLP1* K_m 2-PG value was in the same range as that found for the C_4 plant, *Zea mays*, of 0.57 mM, even though it might be expected that the C_4 -enzyme would have a lower affinity for 2-PG due to the low photorespiratory activity of C_4 plants compared to C_3 plants. That said, Arabidopsis and maize photorespiratory GOX enzymes were found to have very similar K_m glycolate values (Dellero *et al.*, 2015). The unexpected high K_m for 2-PG of our recombinant *AtPGLP1* compared to PGLP extracted and purified from leaves of several species might indicate that *in planta* PGLP1 had undergone some post-translational modifications that improved its kinetic properties or that PGLP1 interacts with protein partners or unknown cofactors that are missing when measuring an *in vitro* activity with bacterial produced recombinant *AtPGLP1*.

Divalent cation and AtPGLP1 activity

AtPGLP1 belongs to the HAD family of enzymes that uses a Mg^{2+} cation in the active site to coordinate 2-PG and allow phosphate transfer to the first aspartate of the conserved motif 1 (Burroughs *et al.*, 2006). Even if the requirement of a divalent cation for a full plant PGLP activity is well documented, the efficiency of different cations appeared to be species dependent. Recombinant *AtPGLP1* showed a higher activity with Mg^{2+} (Table 1) as was the case for maize and *Anacystis* PGLP while Co^{2+} gave the highest activity in spinach and *Chlamydomonas* (see Introduction). The presence of Ca^{2+} was less efficient, increasing the K_m 2-PG and reducing the k_{cat} (Table 1) and low PGLP activities associated with this divalent cation has already been reported. The importance of $\text{Mg}^{2+}/\text{Mn}^{2+}$ as a cofactor for PGLP1 has recently been discussed with respect to photorespiration (Bloom & Lancaster, 2018). It was proposed that the carboxylase/oxygenase activity ratio of RuBisCO was altered by the chloroplastic $\text{Mg}^{2+}/\text{Mn}^{2+}$ ratio with a lower carboxylase activity when Mn^{2+} was bound to RuBisCO thus increasing the proportion of oxygenase activity. Therefore, within the framework of this model it might be expected that PGLP1 activity would be favored by Mn^{2+} compared to Mg^{2+} but this is clearly not the case as the k_{cat} was 5-fold reduced, although the K_m 2-PG was halved (Table 1). On the other hand, light is known to lead to an increase of Mg^{2+} concentration in the chloroplast stroma and the magnitude of this change between

dark and light was seen to be sufficient to regulate biological processes such as CO₂ fixation (Portis & Heldt, 1976; Portis, 1981). Since the need of PGLP1 activity is more important in the light, this could be a regulatory mechanism.

AtPGLP1 dimerization is required for enzyme activity

Gel filtration chromatography using purified plant PGLP has shown that the enzyme is a homodimer (e.g. Mamedov *et al.*, 2001). The 3D structural model of AtPGLP1 (Figure 1) indicated that an α -helix and a β -sheet were probably involved in homodimer formation (Figure S3). This was confirmed by the absence of yeast two-hybrid interactions between AtPGLP1 proteins when either one or both of these regions were deleted (Figure 2). Interestingly, the deletions did not appear to alter AtPGLP1 protein stability since they could be produced and purified from transformed *E. coli* cells (Figure S4) however these AtPGLP1-DEL proteins showed no activity thus indicating that a PGLP1 homodimer was the minimal functional organization. This conclusion was confirmed by observations made with the inactive AtPGLP1_{T103D} protein that did not show homodimer formation by our yeast two-hybrid assay (Figure 4 and Table 3).

Cysteine residues are important for AtPGLP1 dimerization

Mammalian PGP has been shown to be regulated by reversible oxidation involving a number of cysteine residues (Seifried *et al.*, 2016) and plant photorespiratory enzymes have been associated with post translational regulations associated with cysteine residues (Keech *et al.*, 2017; Fonseca-Pereira *et al.*, 2019; Reinholdt *et al.*, 2019), 2-cys peroxiredoxin (Cerveau *et al.*, 2016), NTRC (González *et al.*, 2019), and nitrosylation (Hu *et al.*, 2015; Dei *et al.*, 2019). Indeed, many chloroplast proteins are known to be regulated by thioredoxin-dependent redox modifications in the light including many photosynthesis-related enzymes (Geigenberger *et al.*, 2017). Since AtPGLP1 activity was not highly modified by DTT addition (Figure 3), it seems that the reduction of disulfide bonds is not a regulatory mechanism of this enzyme. However, as with mammalian PGP, oxidation reduced AtPGLP1 activity. After a pre-treatment with 10 mM of H₂O₂ there are 73 % and 84 % decreases of activity with 0.2 mM and 2 mM respectively of 2-PG as a substrate (Figure 3). If AtPGLP1 is susceptible to oxidation stress *in planta* this could explain why it was identified as a 2-cys peroxiredoxin-interacting protein (Cerveau *et al.*, 2016). AtPGLP1 contains 5 cysteines residues that are

well-conserved between plant PGLP proteins (Figure S2) while only 2 of them were conserved with respect to mammalian PGP (Figure 1). The cysteine of the first conserved HAD family motif (C86 of AtPGLP1) was shown to be crucial for mammalian PGP activity since when mutated to alanine the enzyme displayed no measurable activity (Seifried *et al.*, 2016). Surprisingly, this was not the case for AtPGLP1 since our AtPGLP1_{C86A} protein exhibited K_m , V_{max} and k_{cat} values similar to the WT enzyme (Table 3), thus indicating that while the plant enzyme shared the conserved motif I there are some unexplained differences in the importance of certain residues. Even if not all cysteine residues were conserved between the plant and mammalian PGLP proteins, cysteines 302, and together 232 and 239 of AtPGLP1 appeared to play a role in dimer interactions (Table 2 and Figure S6), that we found to be important for enzyme activity (see above). Surprisingly, these cysteines were not found directly in the structures shown to be important for dimer interactions (see Figure S3). However, the AtPGLP1 structural model indicated a hydrogen bond between C232 and C239 that could be important to maintain protein conformation between the α -helix containing C232 and the β -sheet of C239 that are part of the cap domain. These cysteine-containing structures are also close to the observed subunit interaction region and therefore they could impact dimer formation if the double mutation induced a conformational change. That said, if the H-bond was important it might be expected to affect dimer formation even with single mutations, but this was not observed (Table 2). Although C302 reduced the strength of the dimer interaction as indicated from the yeast two-hybrid assay and the C302/C320 double mutant showed a further reduced dimer interaction (Table 2 and Figure S3), this is difficult to explain from the AtPGLP1 model since these two cysteines are not in the vicinity of the dimer interface and they are not predicted to interact together *via* neither hydrogen nor disulphide bonds. Interestingly, C320 has been found to be nitrosylated in a large-scale Arabidopsis study (Hu *et al.*, 2015) and *Lotus japonicus* PGLP was also found S-nitrosylated (Matamoros *et al.*, 2019) thus showing that it is an important regulatory residue and that perhaps nitrosylation impedes homodimer formation and PGLP1 activity.

Phospho-mimetic AtPGLP1 exhibits altered properties

Phosphoproteomics studies suggested that AtPGLP1 could be regulated by protein phosphorylation (Heazlewood *et al.*, 2008; Reiland *et al.*, 2009; Aryal *et al.*, 2012) however

the relevance of each phosphosite and the impact of each phosphorylation on enzyme properties was lacking. Here, we characterized individual recombinant phospho-mimetic AtPGLP1 proteins and clearly showed that in certain cases enzyme activity could be modified while in other cases no effect on activity was observed. The most abundant phospho-peptide found in the PhosPhAt database contained phosphorylated S356 located at the C-terminus of AtPGLP1 (see Figure 1). It was therefore surprising to find that phospho-mimetic AtPGLP1_{S356D} exhibited similar K_m 2-PG and k_{cat} values as the WT protein (Table 3). However, it is possible that S356 phosphorylation could regulate AtPGLP1 interactions with other chloroplastic proteins, or perhaps its stability *in planta*. An absence of altered AtPGLP1 kinetic parameters was also observed for AtPGLP1_{T330D}. This threonine residue was located on the same phospho-peptide as T322 but never found at the same time so perhaps it might have been misidentified as the phospho-threonine on the peptide. Enzyme activity was absent or severely decreased in phospho-mimetic AtPGLP1_{T103D} and AtPGLP1_{T322D} proteins, both of which showed solubility problems when produced in *E. coli* cells and required to be produced fused to MBP. When T322 was mutated to an alanine to produce a non-phosphorylatable AtPGLP1, the resulting protein was also insoluble (this was not the case for AtPGLP1_{T103A}) thus suggesting that T322 was an important residue in maintaining AtPGLP1 either conformation or stability. Phospho-mimetic AtPGLP1_{T322D} exhibited a low PGLP activity and k_{cat} while K_m 2-PG remained unchanged, thus suggesting that phosphorylated T322 would not alter 2-PG binding but somehow it could slow down the phospho-transfer reaction. This residue is situated in a β -sheet directly linked to the region containing the acidic motif IV involved in divalent cation coordination at the active site (Burroughs *et al.*, 2006) and therefore a slight T322 phosphorylation-induced conformational change could hinder PGLP1 activity. Phospho-mimetic AtPGLP1_{T103D} was completely inactive (Table 3) and as mentioned earlier it appeared to be correlated to an absence of AtPGLP1 dimer formation (Figure 4). This residue is located within an α -helix of the Rossmannoid fold structure that is directly linked to a β -sheet containing a catalytic site threonine residue involved in enzyme activity (T118). This α -helix is also in close proximity to a small C-terminus α -helix containing S356 however neither of these phosphorylated residues are found close to the dimer interaction interface. Due to the location of T103 it is difficult to explain why the phospho-mimetic form of AtPGLP1 no longer interacts in the yeast two-hybrid assay. On the other hand, a phosphorylation-induced conformation change could displace the active site T118

thus leading to an inactive *AtPGLP1*_{T103D} enzyme. Indeed, the solubility problem of *AtPGLP1*_{T103D} suggests that this mutation leads to a conformational change that could destabilize the protein and lead to aggregation in *E.coli* cells.

Taken together, our work indicates that *AtPGLP1* could undergo multi-level post-translational regulations and that homodimerization appears to be crucial for PGLP activity. Further work is now required to better understand the physiological relevance of *AtPGLP1* phosphorylation and oxidation, of which both appear to either reduce or inhibit PGLP activity *in vitro*.

Acknowledgements

This work was supported by a public grant overseen by the French National Research Agency (ANR) as part of the “Investissement d’Avenir” programme, through the “Lidex-3P” project and a French State Grant (ANR-10-LABX-0040-SPS) funded by the IDEX Paris-Saclay. This work was also supported by the ANR-14-CE19-0015 grant Regul3P awarded to MH. PD was supported by a PhD grant from the French Ministry of Higher Education and Research. We would like to thank Mathieu Jossier for providing *AtGOX1*-pET28a, Emeline Thuleau and William Rietmeyer for their contributions to the experiments. Authors declare that they have no conflicts of interest.

Supporting Informations

Figure S1: Scheme of the coupled reaction used to measure *AtPGLP1* activity.

Figure S2: Multiple sequence alignments of PGLP proteins.

Figure S3: Focus on the predicted contact points of *AtPGLP1* homodimer.

Figure S4: SDS-PAGE of samples collected during the purification of recombinant proteins: pDEST-His₆MBP-*AtPGLP1*_{C86A}; pDEST-His₆MBP-*AtPGLP1*_{DEL1} and pDEST-His₆MBP-*AtPGLP1*_{DEL2}.

Figure S5: Quantification of glycolate and 2-PG by nuclear magnetic resonance (¹H-NMR).

Figure S6: Involvement of cysteines in *AtPGLP1* homodimerization.

Figure S7: Stained SDS-PAGE gels of collected fractions during the purification of recombinant *AtPGLP1* using pET16b.

Figure S8: SDS-PAGE gel comparison of collected fractions during the purification of recombinant *AtPGLP1* using pET16b compare to pDEST-His₆MBP.

Table S1: List of the primers used for site-directed mutagenesis (phosphosites and cysteines) and for cloning. In this table is indicated: primer use, name, sequence and Tm (°C)

What it is for :	name	sequence 5'>3'	Tm °C
PGLP1 ORF mutagenesis			
C86A	665PRO	GAAACTTTTATCTTCGATGCTGATGGTGTGATTTGGAAG	68.4
	666TER	CTTCAAATCACACCATCAGCATCGAAGATAAAAGTTTC	68.4
T103A	541PRO	GATAGAGGGAGTTCCTGAAGCTCTTGATATGCTTCGTGCC	73.5
	542TER	GGCACGAAGCATATCAAGAGCTTCAGGAACTCCCTCTATC	73.5
T103D	539PRO	GATAGAGGGAGTTCCTGAAGATCTTGATATGCTTCGTGCC	72.5
	540TER	GGCACGAAGCATATCAAGATCTTCAGGAACTCCCTCTATC	72.5
C232A	667PRO	ATTCAGTATGGAACACTCGCTATCCGTGAAAACCCGGGG	73.7
	668TER	CCCCGGGTTTTACGGATAGCGAGTTCCTACTGAAT	73.7
C239A	669PRO	ATCCGTGAAAACCCGGGGCTTTTCATCGCTACAAAC	73.7
	670TER	GTTTGTAGCGATGAAAAGAGCCCCGGGTTTTACGGAT	73.7
C232/239A	671PRO	CAGTATGGAACACTCGCTATCCGTGAAAACCCGGGGCTTTTCATCGCTACA	>75
	672TER	TGTAGCGATGAAAAGAGCCCCGGGTTTTACGGATAGCGAGTGTCCACTACTG	>75
C302A	673PRO	ATCCAAAAGTCACAGATAGCCATGGTTGGTGATAGATTG	69.5
	674TER	CAATCTATCAACCAACATGGCTATCTGTGACTTTTGGAT	69.5
C320A	675PRO/684PRO	TTCGGGCAGAAATGGCGGTGCTAAGACTCTACTCGTCTCTC	>75
	676TER/685TER	GAGGACGAGTAGAGTCTTAGCACCCGCATTCTGCCCGAA	>75
T322A	545PRO	GCAGAAATGGCGGTTGTAAGGCTCTACTCGTCTCTCGGGTG	>75
	546TER	CACCCGAGAGGACGAGTAGAGCCTTACAACCGCCATTCTGC	>75
T322D	543PRO	GCAGAAATGGCGGTTGTAAGGATCTACTCGTCTCTCGGGTG	>75
	544TER	CACCCGAGAGGACGAGTAGATCCTTACAACCGCCATTCTGC	>75
T330A	549PRO	CTCGTCTCTCGGGTGTGCTCAATCTCTATGTTGGAAAG	73.4
	550TER	CTTTCAAACATAGAGATTGAAGCAACCCGAGAGGACGAG	73.4
T330D	547PRO	CTCGTCTCTCGGGTGTGATTCAATCTCTATGTTGGAAAG	72.4
	548TER	CTTTCAAACATAGAGATTGAATCAACCCGAGAGGACGAG	72.4
T322/330A	557PRO	GAATGGCGGTTGTAAGGCTCTACTCGTCTCTCGGGTGTGCTTCAATCTCTATGTTG	>75
	558TER	CAACATAGAGATTGAAGCAACCCGAGAGGACGAGTAGAGCCTTACAACCGCCATTCT	>75
T322/330D	555PRO	GAATGGCGGTTGTAAGGATCTACTCGTCTCTCGGGTGTGATTCAATCTCTATGTTG	>75
	556TER	CAACATAGAGATTGAATCAACCCGAGAGGACGAGTAGATCCTTACAACCGCCATTCT	>75
S356A	553PRO	GCAAGATCTCCGATTTTCTGGTCCGAAAGCCGCAACTG	74.7
	554TER	CAGTTGCGGCTTTCGGAGCCAGAAAATCGGAGATCTTGC	74.7
S356D	551PRO	GCAAGATCTCCGATTTTCTGGATCCGAAAGCCGCAACTG	73.7
	552TER	CAGTTGCGGCTTTCGGATCCAGAAAATCGGAGATCTTGC	73.7
DEL1	677PRO	GCTGTTGTGGTTGATTTGAT-deletion 18nt-AAAATTCAGTATGGAACACTC	69.4
	678TER	GAGTGTCCATACTGAATTTT-deletion 18nt-ATCAAATCCAACCAACAGC	69.4
DEL2	679PRO	CTCAAGAATGGGAGGTGGTGGC-deletion 18nt-GTTGGATCCACTCAACGTGAGCC	>75
	680TER	GGCTCACGTTGAGTGGATCCAAC-deletion 18nt-GCCACCACCTGCCATTCTTGAG	>75
PGPL1 cloning			
PGLP1mat ORF into pET [NdeI-XhoI]	535PRO	GACATATGACGAGTTCCAATATTACACCAAGAG	65.8
	536TER	GTCTCGAGTTATACAGTTGCGGCTTTCGGAG	69.5
PGLP1mat ORF_ Gateway adaptable (2018)	598PRO	TACAAAAAGCAGGCTTCACGAGTTCCAATATTACACCAAGAG	70.4
	599TER	CAAGAAAGCTGGGTCTTATACAGTTGCGGCTTTCGGAG	72.7
cloning into yeast two hybrid pDEST vectors	AD-FW/pDEST-AD	CGCGTTTGAATCACTACAGGG	62.1
	BD-FW/pDEST-BD	GGCTTCAGTGGAGACTGATATGCTC	66.4
	B2-STOP/pDEST-Y2H	GGAGACTTGACAAAACCTCTGGCG	66.1
cloning into pGEM-T	Direct	ACGACGTTGAAAACGACGGCCAG	53.9
	Reverse	CAGGAAACAGCTATGACCATGATTACG	53.1
PCR fragment for Gateway BP reaction	GW-FORWARD	GGGGACAAGTTTGTACAAAAAAGCAGGCTTC	66.8
	GW-REVERSE	GGGGACCACTTTGTACAAAAAAGCTGGGTC	69.5
cloning into pET	PromT7-PRO	TAATACGACTCACTATAGGG	53.2
	TermT7-TER	GCTAGTTATTGCTCAGCGGT	57.3

References

- Allen KN, Dunaway-Mariano D. 2004.** Phosphoryl group transfer: evolution of a catalytic scaffold. *Trends in Biochemical Sciences* **29**: 495–503.
- Allen KN, Dunaway-Mariano D. 2016.** Catalytic scaffolds for phosphoryl group transfer. *Current Opinion in Structural Biology* **41**: 172–179.
- Anderson LE. 1971.** Chloroplast and cytoplasmic enzymes II. Pea leaf triose phosphate isomerases. *Biochimica et Biophysica Acta (BBA) - Enzymology* **235**: 237–244.
- Aryal UK, Krochko JE, Ross ARS. 2012.** Identification of Phosphoproteins in Arabidopsis thaliana Leaves Using Polyethylene Glycol Fractionation, Immobilized Metal-ion Affinity Chromatography, Two-Dimensional Gel Electrophoresis and Mass Spectrometry. *Journal of Proteome Research* **11**: 425–437.
- Balmer Y, Vensel WH, Tanaka CK, Hurkman WJ, Gelhaye E, Rouhier N, Jacquot J-P, Manieri W, Schürmann P, Droux M, et al. 2004.** Thioredoxin links redox to the regulation of fundamental processes of plant mitochondria. *Proceedings of the National Academy of Sciences of the United States of America* **101**: 2642–2647.
- Bauwe H, Hagemann M, Fernie AR. 2010.** Photorespiration: players, partners and origin. *Trends in Plant Science* **15**: 330–336.
- Belanger FC, Ogren WL. 1987.** Phosphoglycolate phosphatase: purification and preparation of antibodies. *Photosynthesis Research* **14**: 3–13.
- Bienvenut WV, Scarpelli J-P, Dumestier J, Meinel T, Giglione C. 2017.** EnCOUNTER: a parsing tool to uncover the mature N-terminus of organelle-targeted proteins in complex samples. *BMC bioinformatics* **18**: 182.
- Blackwell RD, Murray AJS, Lea PJ, Kendall AC, Hall NP, Turner JC, Wallsgrave RM. 1988.** The value of mutants unable to carry out photorespiration. *Photosynthesis Research* **16**: 155–176.
- Bloom AJ, Lancaster KM. 2018.** Manganese binding to Rubisco could drive a photorespiratory pathway that increases the energy efficiency of photosynthesis. *Nature Plants* **4**: 414–422.
- Burroughs AM, Allen KN, Dunaway-Mariano D, Aravind L. 2006.** Evolutionary Genomics of the HAD Superfamily: Understanding the Structural Adaptations and Catalytic Diversity in a

Superfamily of Phosphoesterases and Allied Enzymes. *Journal of Molecular Biology* **361**: 1003–1034.

Carveau D, Kraut A, Stotz HU, Mueller MJ, Couté Y, Rey P. 2016. Characterization of the *Arabidopsis thaliana* 2-Cys peroxiredoxin interactome. *Plant Science* **252**: 30–41.

Christeller JT, Tolbert NE. 1978a. Phosphoglycolate phosphatase. Purification and properties. *The Journal of biological chemistry* **253**: 1780–1785.

Christeller JT, Tolbert NE. 1978b. Mechanism of phosphoglycolate phosphatase. Studies of hydrolysis and transphosphorylation, substrate analogs, and sulfhydryl inhibition. *The Journal of biological chemistry* **253**: 1791–1798.

Christeller JT, Tolbert NE. 1978c. Phosphoglycolate phosphatase. Effect of cation and pH on activity. *The Journal of biological chemistry* **253**: 1786–1790.

Collard F, Baldin F, Gerin I, Bolsée J, Noël G, Graff J, Veiga-Da-Cunha M, Stroobant V, Vertommen D, Houddane A, et al. 2016. A conserved phosphatase destroys toxic glycolytic side products in mammals and yeast. *Nature Chemical Biology* **12**: 601–607.

Dellero Y, Mauve C, Boex-Fontvieille E, Flesch V, Jossier M, Tcherkez G, Hodges M. 2015. Experimental evidence for a hydride transfer mechanism in plant glycolate oxidase catalysis. *The Journal of biological chemistry* **290**: 1689–1698.

Dreze M, Monachello D, Lurin C, Cusick ME, Hill DE, Vidal M, Braun PBT-M in E. 2010. Chapter 12 - High-Quality Binary Interactome Mapping. In: *Guide to Yeast Genetics: Functional Genomics, Proteomics, and Other Systems Analysis*. Academic Press, 281–315.

Enzymes C. (u.s.A.). 22: 237–244.

Flügel F, Timm S, Arrivault S, Florian A, Stitt M, Fernie AR, Bauwe H. 2017. The Photorespiratory Metabolite 2-Phosphoglycolate Regulates Photosynthesis and Starch Accumulation in *Arabidopsis*. *The Plant Cell* **29**: 2537–2551.

Fonseca-Pereira P, Souza PVL, Hou L, Schwab S, Geigenberger P, Nunes-Nesi A, Timm S, Fernie AR, Thormählen I, Araújo WL, et al. 2019. Thioredoxin h2 contributes to the redox regulation of mitochondrial photorespiratory metabolism. *Plant, Cell & Environment*: 1–21.

Geigenberger P, Thormählen I, Daloso DM, Fernie AR. 2017. The Unprecedented Versatility of the Plant Thioredoxin System. *Trends in Plant Science* **22**: 249–262.

Gietz D, St Jean A, Woods RA, Schiestl RH. 1992. Improved method for high efficiency transformation of intact yeast cells. *Nucleic acids research* **20**: 1425.

Gohla A. 2019. Do metabolic HAD phosphatases moonlight as protein phosphatases?

Biochimica et Biophysica Acta - Molecular Cell Research **1866**: 153–166.

González M, Delgado-Requerey V, Ferrández J, Serna A, Cejudo FJ. 2019. Insights into the function of NADPH thioredoxin reductase C (NTRC) based on identification of NTRC-interacting proteins in vivo. *Journal of Experimental Botany* **70**: 5787–5798.

Hall NP, Kendall AC, Lea PJ, Turner JC, Wallsgrove RM. 1987. Characteristics of a photorespiratory mutant of barley (*Hordeum vulgare* L.) deficient in phosphoglycollate phosphatase. *Photosynthesis research* **11**: 89–96.

Hardy P, Baldy P. 1986. Corn phosphoglycolate phosphatase: purification and properties. *Planta* **168**: 245–252.

Heazlewood JL, Durek P, Hummel J, Selbig J, Weckwerth W, Walther D, Schulze WX. 2008. PhosPhAt: a database of phosphorylation sites in *Arabidopsis thaliana* and a plant-specific phosphorylation site predictor. *Nucleic acids research* **36**: 1015–1021.

Hodges M, Jossier M, Boex-Fontvieille E, Tcherkez G. 2013. Protein phosphorylation and photorespiration. *Plant Biology* **15**: 694–706.

Hu J, Huang X, Chen L, Sun X, Lu C, Zhang L, Wang Y, Zuo J. 2015. Site-specific nitrosoproteomic identification of endogenously S-nitrosylated proteins in *Arabidopsis*. *Plant Physiology* **167**: 1731–1746.

Huang H, Pandya C, Liu C, Al-Obaidi NF, Wang M, Zheng L, Toews Keating S, Aono M, Love JD, Evans B, et al. 2015. Panoramic view of a superfamily of phosphatases through substrate profiling. *Proceedings of the National Academy of Sciences of the United States of America* **112**: 1974–1983.

Huh DH, Kursell A V, Husic HD. 1989. Kinetic properties of phosphoglycollate phosphatase from *Pisum sativum* and *Phaseolus vulgaris*. *Phytochemistry* **28**: 719–720.

Husic HD, Tolbert NE. 1984. Anion and divalent cation activation of phosphoglycollate phosphatase from leaves. *Archives of Biochemistry and Biophysics* **229**: 64–72.

Inhibition of spinach-leaf phosphofructokinase by 2-phosphoglycollate. 1976. *FEBS Letters* **68**: 55–58.

Keech O, Gardeström P, Kleczkowski LA, Rouhier N. 2017. The redox control of photorespiration: from biochemical and physiological aspects to biotechnological considerations. *Plant Cell and Environment* **40**: 553–569.

Kelly GJ, Latzko E. 1976. Inhibition of spinach-leaf phosphofructokinase by 2-phosphoglycollate. *FEBS Letters* **68**: 55–58.

- Kim SR, Xu H, Lesmana A, Kuzmanovic U, Au M, Florencia C, Oh EJ, Zhang G, Kim KH, Jin Y-S. 2015.** Deletion of PHO13, encoding haloacid dehalogenase type IIA phosphatase, results in upregulation of the pentose phosphate pathway in *Saccharomyces cerevisiae*. *Applied and environmental microbiology* **81**: 1601–1609.
- Kim Y, Yakunin AF, Kuznetsova E, Xu X, Pennycooke M, Gu J, Cheung F, Proudfoot M, Arrowsmith CH, Joachimiak A, et al. 2004.** Structure- and function-based characterization of a new phosphoglycolate phosphatase from *Thermoplasma acidophilum*. *The Journal of biological chemistry* **279**: 517–526.
- Krocová E, Neradová S, Kupcik R, Janovská S, Bílková Z, Heidingsfeld O. 2019.** PHO15 genes of *Candida albicans* and *Candida parapsilosis* encode HAD-type phosphatases dephosphorylating 2-phosphoglycolate. *FEMS yeast research* **19**: 112.
- Levey M, Timm S, Mettler-altmann T, Borghi GL, Koczor M, Arrivault S, Weber APM, Bauwe H, Gowik U, Westhoff P. 2019.** Efficient 2-phosphoglycolate degradation is required to maintain carbon assimilation and allocation in the C4 plant *Flaveria bidentis*. **70**: 575–587.
- Liu Y, Mauve C, Lamothe-Sibold M, Guérard F, Glab N, Hodges M, Jossier M. 2019.** Photorespiratory serine hydroxymethyltransferase 1 activity impacts abiotic stress tolerance and stomatal closure. *Plant, Cell & Environment* **42**: 2567–2583.
- Lyngstadaas A, Løbner-Olesen A, Grelland E, Boye E. 1999.** The gene for 2-phosphoglycolate phosphatase (gph) in *Escherichia coli* is located in the same operon as *dam* and at least five other diverse genes. *Biochimica et Biophysica Acta (BBA) - General Subjects* **1472**: 376–384.
- Mamedov TG, Suzuki K, Miura K, Kucho K, Fukuzawa H. 2001.** Characteristics and Sequence of Phosphoglycolate Phosphatase from a Eukaryotic Green Alga *Chlamydomonas reinhardtii*. *Journal of Biological Chemistry* **276**: 45573–45579.
- Matamoros MA, Cutrona MC, Wienkoop S, Begara-Morales JC, Sandal N, Orera I, Barroso JB, Stougaard J, Becana M. 2019.** Altered plant and nodule development and protein S-nitrosylation in *Lotus japonicus* mutants deficient in S-nitrosoglutathione reductases. *Plant and Cell Physiology* **1**: 1–44.
- Nagappa LK, Satha P, Govindaraju T, Balaram H. 2019.** Phosphoglycolate phosphatase is a metabolic proofreading enzyme essential for cellular function in *Plasmodium berghei*. *Journal of Biological Chemistry* **294**: 4997–5007.
- Norman EG, Colman B. 1991.** Purification and characterization of phosphoglycolate phosphatase from the cyanobacterium *Coccochloris peniocyctis*. *Plant Physiology* **95**: 693–

698.

Ortega-Galisteo AP, Rodríguez-Serrano M, Pazmiño DM, Gupta DK, Sandalio LM, Romero-Puertas MC. 2012. S-Nitrosylated proteins in pea (*Pisum sativum* L.) leaf peroxisomes: changes under abiotic stress. *Journal of experimental botany* **63**: 2089–2103.

Palmieri MC, Lindermayr C, Bauwe H, Steinhauser C, Durner J. 2010. Regulation of plant glycine decarboxylase by s-nitrosylation and glutathionylation. *Plant physiology* **152**: 1514–1528.

Portis AR. 1981. Evidence of a Low Stromal Mg²⁺ Concentration in Intact Chloroplasts in the Dark. *Plant Physiology* **67**: 985–989.

Portis AR, Heldt HW. 1976. Light-dependent changes of the Mg²⁺ concentration in the stroma in relation to the Mg²⁺ dependency of CO₂ fixation in intact chloroplasts. *Biochimica et Biophysica Acta (BBA) - Bioenergetics* **449**: 434–446.

Rao ST, Rossmann MG. 1973. Comparison of super-secondary structures in proteins. *Journal of molecular biology* **76**: 241–256.

Reiland S, Messerli G, Baerenfaller K, Gerrits B, Endler A, Grossmann J, Gruissem W, Baginsky S. 2009. Large-scale Arabidopsis phosphoproteome profiling reveals novel chloroplast kinase substrates and phosphorylation networks. *Plant physiology* **150**: 889–903.

Reinholdt O, Schwab S, Zhang Y, Reichheld J-P, Fernie AR, Hagemann M, Timm S. 2019. Redox-Regulation of Photorespiration through Mitochondrial Thioredoxin o1. *Plant Physiology* **181**: 442–457.

Richardson KE, Tolbert NE. 1961. Phosphoglycolic Acid Phosphatase. *Journal of Biological Chemistry* **236**: 1285–1290.

Rose ZB, Grove DS, Seal SN. 1986. Mechanism of activation by anions of phosphoglycolate phosphatases from spinach and human red blood cells. *Journal of Biological Chemistry* **261**: 10996–11002.

Schwarte S, Bauwe H. 2007. Identification of the Photorespiratory 2-Phosphoglycolate Phosphatase, PGLP1, in Arabidopsis. *Plant Physiology* **144**: 1580–1586.

Segerer G, Hadamek K, Zundler M, Fekete A, Seifried A, Mueller MJ, Koentgen F, Gessler M, Jeanclos E, Gohla A. 2016. An essential developmental function for murine phosphoglycolate phosphatase in safeguarding cell proliferation. *Scientific Reports* **6**: 1–13.

Seifried A, Bergeron A, Boivin B, Gohla A. 2016. Reversible oxidation controls the activity and oligomeric state of the mammalian phosphoglycolate phosphatase AUM. *Free Radical*

Biology and Medicine **97**: 75–84.

Seifried A, Schultz J, Gohla A. 2013. Human HAD phosphatases: Structure, mechanism, and roles in health and disease. *FEBS Journal* **280**: 549–571.

Teresa Pellicer M, Felisa Nuñez M, Aguilar J, Badia J, Baldoma L. 2003. Role of 2-phosphoglycolate phosphatase of *Escherichia coli* in metabolism of the 2-phosphoglycolate formed in DNA repair. *Journal of bacteriology* **185**: 5815–5821.

Timm S, Bauwe H. 2013. The variety of photorespiratory phenotypes - employing the current status for future research directions on photorespiration. *Plant Biology* **15**: 737–747.

Timm S, Florian A, Wittmiß M, Jahnke K, Hagemann M, Fernie AR, Bauwe H. 2013. Serine Acts as a Metabolic Signal for the Transcriptional Control of Photorespiration-Related Genes in *Arabidopsis*. *Plant Physiology* **162**: 379–389.

Xu H, Kim S, Sorek H, Lee Y, Jeong D, Kim J, Oh EJ, Yun EJ, Wemmer DE, Kim KH, et al. 2016. PHO13 deletion-induced transcriptional activation prevents sedoheptulose accumulation during xylose metabolism in engineered *Saccharomyces cerevisiae*. *Metabolic engineering* **34**: 88–96.

Zecher R, Wolf HU. 1980. Partial purification and characterization of human erythrocyte phosphoglycolate phosphatase. *The Biochemical journal* **191**: 117–124.

Tables

Table 1: The effect of divalent cations on the kinetic parameters of recombinant AtPGLP1 measured using the GOX-coupled reaction.

Divalent cation	K_m (mM)	V_{max} ($\mu\text{mol of glycolate}\cdot\text{mg}^{-1}$ of prot. $\cdot\text{min}^{-1}$)	k_{cat} (s^{-1})
Mg^{2+}	0.34 ± 0.03	29.4 ± 3.7	19.7 ± 2.5
Mn^{2+}	0.18 ± 0.02	6.1 ± 0.8	4.1 ± 0.6
Co^{2+}	0.15 ± 0.01	17.5 ± 0.1	11.7 ± 0.1
Ca^{2+}	1.37 ± 0.22	3.5 ± 0.3	2.3 ± 0.2
Zn^{2+}	-	0	-

Kinetic parameters were calculated using “Kinetic Enzyme Wizard” of Sigma-Plot (Systat Software Inc.) with activities recorded using a range of 2-PG from 0.01 mM to 5 mM. The reaction was started with 5 μg of recombinant protein while all the other enzymes were in excess (2U HRP and 40 μg recombinant AtGOX1). Values are means \pm SD (n=3 independent experiments).

Table 2: The role of cysteines in AtPGLP1 dimerization using a yeast two-hybrid test

Interaction tested	-LEU-TRP-HIS	LEU-TRP-HIS+3AT
AD-AtPGLP1 _{WT} /BD-AtPGLP1 _{WT}	+++++	+
AD-AtPGLP1 _{C86A} /BD-AtPGLP1 _{C86A}	+++++	+
AD-AtPGLP1 _{C232A} /BD-AtPGLP1 _{C232A}	++++	+/-
AD-AtPGLP1 _{C239A} /BD-AtPGLP1 _{C239A}	+++++	+/-
AD-AtPGLP1 _{C232A} /BD-AtPGLP1 _{C239A}	+++++	-
AD-AtPGLP1 _{C239A} /BD-AtPGLP1 _{C232A}	+++	-
AD-AtPGLP1 _{C232/239A} /BD-AtPGLP1 _{C232/239A}	-	-
AD-AtPGLP1 _{C302A} /BD-AtPGLP1 _{C302A}	++	-
AD-AtPGLP1 _{C320A} /BD-AtPGLP1 _{C320A}	-	-
AD-AtPGLP1 _{C302A} /BD-AtPGLP1 _{C320A}	+	-
AD-AtPGLP1 _{C320A} /BD-AtPGLP1 _{C302A}	+++++	+
AD-AtPGLP1 _{C302/320A} /BD-AtPGLP1 _{C302/320A}	+	-

The importance of each cysteine of AtPGLP1 was tested using a two-hybrid assay to determine their role in AtPGLP1 homodimerization. Two double mutants were also generated to study the involvement of two cysteines at once. The + and – represents the intensity of the two-hybrid interaction when compared with the wild-type (see Figure S6). $\Delta A_{600\text{ nm}}$ of yeast cell suspensions was measured and adjusted to 2 units and serial dilutions were performed. 20 μL drops of each dilution were deposited on three different media (LEU-TRP data not shown because this corresponds to the permissive medium; LEU-TRP-HIS; -LEU-TRP-HIS+3-AT). Four replicates were performed.

Table 3: The kinetic properties of phospho-mimetic AtPGLP1 and motif I mutated AtPGLP1

Protein form	K_m (mM)	V_{max} ($\mu\text{mol of glycolate}\cdot\text{mg}^{-1}$ of prot. $\cdot\text{min}^{-1}$)	k_{cat} (s^{-1})
$^{\circ}$ AtPGLP1 _{WT}	0.34 ± 0.03	29.5 ± 3.7	19.7 ± 2.5
* AtPGLP1 _{WT}	0.31 ± 0.04	31.9 ± 1.8	21.3 ± 1.2
* AtPGLP1 _{T103A}	0.30 ± 0.04	32.3 ± 0.9	21.7 ± 0.6
* AtPGLP1 _{T103D}	-	-	-
* AtPGLP1 _{T322A}	0.29 ± 0.01	30.7 ± 1	20.6 ± 0.7
* AtPGLP1 _{T322D}	0.33 ± 0.04	2.2 ± 0.1	1.5 ± 0.04
$^{\circ}$ AtPGLP1 _{T330A}	0.28 ± 0.02	25.9 ± 0.9	17.4 ± 0.6
$^{\circ}$ AtPGLP1 _{T330D}	0.40 ± 0.06	24.9 ± 3.1	16.7 ± 2
$^{\circ}$ AtPGLP1 _{S356A}	0.34 ± 0.03	22.8 ± 1.4	15.3 ± 1
$^{\circ}$ AtPGLP1 _{S356D}	0.30 ± 0.02	22.4 ± 1.6	15.0 ± 1
* AtPGLP1 _{C86A}	0.4 ± 0.04	22.3 ± 2.15	14.9 ± 1.44

Kinetic parameters of wild-type AtPGLP1_{WT} and mutated (AtPGLP1_{T103A}; AtPGLP1_{T103D}; AtPGLP1_{T322A}; AtPGLP1_{T322D}; AtPGLP1_{T330A}; AtPGLP1_{T330D}; AtPGLP1_{S356A}; AtPGLP1_{S356D}; AtPGLP1_{C86A}) were calculated using “Kinetic Enzyme Wizard” of Sigma-Plot (Systat Software Inc.) with activities recorded using a range of 2-PG from 0.01 mM to 5 mM. The reaction was started with 5 μg of recombinant protein while all the other enzymes were in excess (2U HRP and 40 μg AtGOX1). Values are means \pm SD (n=3 independent experiments). (*) indicates recombinant proteins produced using pDEST-His₆MBP and ($^{\circ}$) indicates recombinant proteins produced using pET16b as vector.

Figure Legends

Figure 1: AtPGLP1 belongs to the HAD family

(a) Amino acid sequence alignment of phosphoglycolate phosphatases from human (Human_PGP), mouse (Murine_PGP) and *A. thaliana* (*AtPGLP1*). The cap domain is in italic, in grey are represented the HAD family motifs with key amino acids in dark red. Cysteines are in orange. The green amino acids of the *AtPGLP1* sequence correspond to the chloroplast addressing peptide and amino acids in blue have been identified as being phosphorylated in *AtPGLP1*. Position numbers above are given for the *A. thaliana* sequence. DEL1 and DEL2 indicate the position of the two deletions described in Figure 2 and Figure S3. (b) Represents the rainbow scale (Nter to Cter) homodimer 3D-structure of *AtPGLP1*_{WT} built from 4bkm.1 (Swiss Model Template Library ID or PDB 4BKM) as template with a global model quality estimation (GMQE) of 0.68 (on a 0 to 1 scale). The shaded part represents the region of interest where the requires residues for activity are indicated. (c) Flat structure of *AtPGLP1* showing a typical Rossmannoid organisation with the arrows corresponding to β -strands (S1 to S6) and the α -helices in between. Studied residues are indicated with the same colours as in (a) and (b).

Figure 2: Impact of two structural deletions on AtPGLP1 homodimerization

(a) Represents an alternative view of the predicted 3D structure of homodimeric *AtPGLP1*_{WT} that focuses on the potential structural elements involved in monomer contacts; in purple α -helices and in green β -strands (see Figure S3 for more details). (b) Yeast two-hybrid assay focusing on the interaction of *AtPGLP1* deleted in predicted regions involved in the dimer interface. $\Delta A_{600\text{ nm}}$ of yeast cell suspensions was adjusted to 2 units and serial dilutions were performed. The different AD+BD combinations are indicated. 20 μL drops of each dilution were deposited on three different media (LEU-TRP; LEU-TRP-HIS; -LEU-TRP-HIS+3-AT). Negative (AD+BD) and positive (GAL4_{WT}) are given. Four replicates were done; the photos were taken 7 days after incubation at 30 °C. (c) Activity of *AtPGLP1* deleted in two different contact regions (DEL1; DEL2 described in Figure 1a and S3) for dimer formation was measured, using the GOX-coupled reaction with 1 mM 2-PG and 5 μg of recombinant proteins. The absence of signal at 440 nm shows an absence of *AtPGLP1* activity.

Figure 3: The effect of a pre-treatment with either H₂O₂ or DTT on AtPGLP1 activity

AtPGLP1 (2.5 µg) was incubated for 30 min in the presence of either 0.2 mM or 2 mM 2-PG at 30 °C. The glycolate concentration was measured using the ¹H-NMR as described in materials and methods. Values are means ± SD (n=3 independent experiments). The amount of glycolate was recorded after an AtPGLP1 pre-treatment with (a) H₂O₂ or (b) DTT at two concentrations (1 mM and 10 mM).

Figure 4: Yeast two-hybrid assay comparing the homo-dimer interaction of phospho-mimetic AtPGLP1_{T103D} with that of AtPGLP1_{WT} and AtPGLP1_{T103A}

ΔA_{600 nm} of yeast cell suspensions was adjusted to 2 units and serial dilutions were performed. The different AD+BD combinations are indicated. 20 µL drops of each dilution were deposited on three different media (LEU-TRP; LEU-TRP-HIS; -LEU-TRP-HIS+3-AT). Negative (AD+BD) and positive (GAL4_{WT}) are given. Four replicates were done; the photos were taken 7 days after incubation at 30 °C

Supporting information

Supporting figure legends

Figure S1: Scheme of the coupled reaction used to measure AtPGLP1 activity

This coupled enzymatic reaction used AtGOX1 and took advantage of the work using recombinant GOX proteins by (Dellero *et al.*, 2015). The detected product was oxidized o-dianisidine recorded by spectrophotometry at A_{440 nm}. HRP= horseradish peroxidase.

Figure S2: Multiple sequence alignments of PGLP proteins

Multiple sequence alignments of PGLP proteins performed with Clustal Omega (1.2.4) and the following sequences: A.thaliana, *Arabidopsis thaliana*, NP_001190427; P.patens, *Physcomitrella patens*, XP_024393628; O.sativa, *Oryza sativa*, XP_015636788; S.bicolor, *Sorghum bicolor*, XP_002448095; Z.mays, *Zea mays*, AQK44460; S.lycoper, *Solanum lycopersicum*, XP_004250073; B.napus, *Brassica napus*, XP_013706932; G.max, *Glycine max*, NP_001276320; M.trunca, *Medicago truncatula*, AES80436; G.hirsut, *Gossypium hirsutum*, XP_016722161; P.tricho, *Populus trichocarpa*, XP_024463546; T.pseudo, *Thalassiosira pseudonana*, XP_002297210; O.tauri, *Ostreococcus tauri*, OUS46983; C.reinha,

Chlamydomonas reinhardtii, XP_001703502 ; *V. carter*, *Volvox carteri f.nagariensis*, EFJ42912 ; *C. aeropho*, Candidatus *Aerophobetes bacterium*, TKJ44102 ; *Bacillus*, *Bacillus* sp.FJAT-22090, WP_144538556 ; *Clostrid*, *Clostridium* sp. CL-2, WP_032118399 ; *Phycisph*, *Phycisphaera* sp. TMED151, OUW04164.

Indicated on the *A. thaliana* sequence: green, chloroplastic targeting sequence experimentally determined (Bienvenut *et al.*, 2017); orange bold, cysteines; blue, sequence of identified phosphopeptides in PhosPhAt 4.0; blue bold, residues identified as phosphorylated. Indicated on the complete alignment: grey shade, conserved motifs of the HAD phosphatase family numbered from I to IV, dark red bold, residues highly conserved and required for phosphatase activity (Gohla, 2019), orange bold, conserved cysteines compared to *AtPGLP1*; orange, other cysteines; blue bold conserved or similar residues compared to phosphosites identified in *A. thaliana*.

Figure S3: Focus on the predicted contact points of *AtPGLP1* homodimer

The predicted 3D rainbow structure of *AtPGLP1* was determined using SWISS-model *via* the crystalized structure of the murine phosphoglycolate phosphatase cap domain and the murine pyridoxal phosphate phosphatase core domain. Focus is made on the predicted contact points with the numbered residues that led us to choose the deletions, DEL1 and DEL2.

Figure S4: SDS-PAGE of samples collected during the purification of recombinant proteins *His₆MBP-AtPGLP1_{C86A}*, *His₆MBP-AtPGLP1_{DEL1}* and *His₆MBP-AtPGLP1_{DEL2}*

C86A is the mutation of cysteine 86 into alanine while DEL1 and DEL2 correspond to deletions of the DNA sequence encoding amino acids 219 to 224 (RYFNYY) and 263 to 268 (SMVGAL), respectively from *AtPGLP1* sequence (see Figure 1a). (1) crude extract after the French press step, (2) soluble fraction collected after centrifugation of the total extract, (3) proteins collected after elution from the Nickel affinity column; (M) molecular weight markers (PageRuler Prestained Protein Ladder, Thermo Scientific).

Figure S5: Quantification of glycolate and 2-PG by nuclear magnetic resonance (¹H-NMR)

(a) NMR spectra with 2 mM 2-PG and glycolate; 2.5 μg of *AtPGLP1* and 50 mM Tris-HCl. The focus on the spectra was done between 4 and 5 ppm, where both 2-PG (green) and glycolate

(black) signals are detectable and separated. **(b)** Appearance of glycolate (in black) and disappearance of 2-PG (in green; 2 mM initial) between 0 and 300 s using 2.5 μ g of recombinant *AtPGLP1_{WT}*. **(c, left)** Spectra after 10 s of reaction performed with 2.5 μ g of proteins and a range of 2-PG concentrations (from 0 mM, 0.01 mM, 0.35 mM, 0.7 mM, 1 mM and 5 mM, in that order from the bottom to the top). **(c, right)** Measurement of *AtPGLP1* activity using NMR. Each point corresponds to the V_i detected between 0-10 s in the presence of 2.5 μ g of recombinant protein and a range of substrate concentrations (2-PG; from 0 mM to 5 mM). Value are means \pm SD (n=3 independent experiments).

Figure S6: Involvement of cysteines in *AtPGLP1* homodimerization.

(a) The predicted 3D structure of *AtPGLP1* (using SWISS-model) is represented as a homodimer. The cysteines in gold are circled and numerated on one monomer. **(b)** and **(c)** represents the yeast two-hybrid experiments performed with the mutated *AtPGLP1* on various cysteines. $A_{600\text{ nm}}$ of yeast cell suspensions was measured and adjusted to 2 units and serial dilutions were performed. 20 μ L drops of each dilution were deposited on three different media (LEU-TRP; LEU-TRP-HIS; -LEU-TRP-HIS+3-AT) represented by the three columns. Four replicates were performed; images were acquired after 7 days of incubation at 30 °C.

Figure S7: Stained SDS-PAGE gels of collected fractions during the purification of recombinant *AtPGLP1* using pET16b

Here are represented soluble mutated proteins using pET16b. Fractions were deposited in the following order: **(1)** total proteins from IPTG-induced bacteria collected after the French press, **(2)** soluble proteins harvested after centrifugation, **(3)** pass-through proteins that did not link to the Nickel affinity resin, **(4)** proteins collected after the first washing step, **(5)** proteins eluted from the Nickel affinity resin using 250 mM imidazole, **(6)** proteins after desalting, **(M)** molecular weight markers (PageRuler Prestained Protein Ladder, Thermo Scientific).

Note that the molecular weight markers are not always in the same place due to the different migration time of the gels. The black box shows the zone where recombinant *AtPGLP1* was located.

Figure S8: SDS-PAGE gel comparison of collected fractions during the purification of recombinant AtPGLP1 using pET16b compare to pDEST-His₆MBP.

Fractions were deposited in the following order: (1) total proteins from IPTG-induced bacteria collected after the French press, (2) soluble proteins harvested after centrifugation, (3) pass-through proteins that did not link to the Nickel affinity resin, (4) proteins collected after the first washing step, (5) proteins eluted from the Nickel affinity resin using 250 mM imidazole, (6) proteins after desalting, (M) molecular weight markers (PageRuler Prestained Protein Ladder, Thermo Scientific). Note that the molecular weight markers are not always in the same place due to the different migration time of the gels. The black box shows the zone where recombinant AtPGLP1 was located.

Figure S1: Duminil et al.

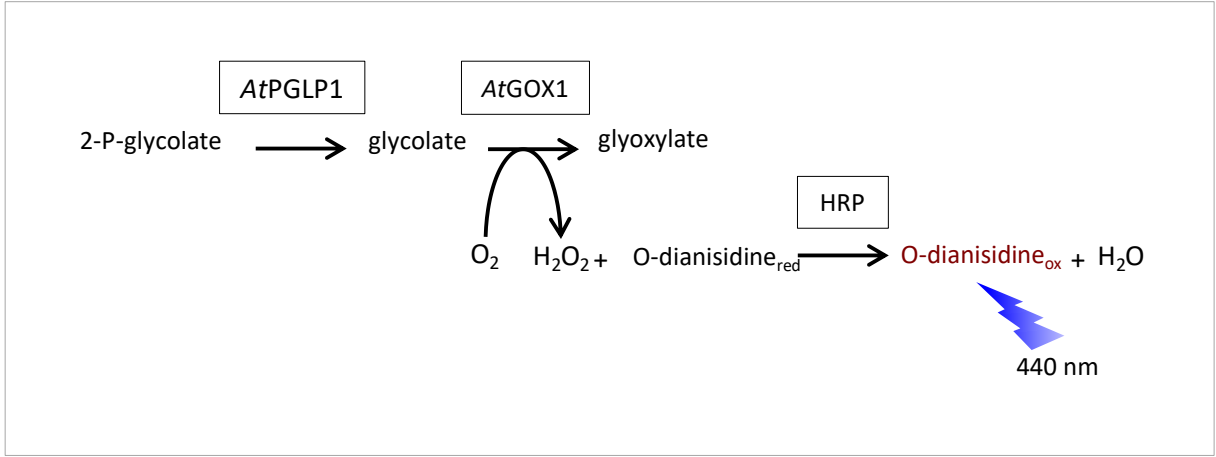


Figure S2: Duminil et al.

A.thaliana	- MLSR ----- SVASAV ---- TPVS - SSSLL -- PNSKPIFCLKTL SGYRS ----- S	37
P.patens	MAICVAPFRSLSSPLLRSAAAPPCTAKSVVFGCPSLRNLVKQ-----QLTSRPMVSSS	54
O.sativa	MLLTR-----ASPTFLPSTSAASPSPQ-QAPSS--PTF-GRSQYR-----RGGGLVSVS	45
S.bicolor	MLQVR-----ASPTFLPSTSSSSS----QA--PTHSPF-SGKSQR-----RGGLAAAP	41
Z.mays	MLQVR-----ASSAFLPSTSSPSPSSSQAPAPAPFRL-SGKSQR-----RGGLIAVP	47
S.lycoper	- MLS ----- IR-VT-ATISSSSTLFFTN-SK ----- KISNKFSYISNPLK-NS	38
B.napus	- MLNR ----- T---TL ----- VSSS-SVSL -- PNSKPF SVKAFSGFRS ----- S	34
G.max	- MLRS ----- STLTQS-VTVTCVRHSHRQWFQSI PV ----- NYR-FFDAARNSLSSPN	45
M.trunca	MMLRS ----- SS-TIA-ATSVGVCHTQRLW SHSVTL ----- NYR-LSQFAGNPLL-SN	44
G.hirsut	- MATK ----- AAVSVA-ASVTAASSSSSKFVINTPHRFLCLKRLSS FSSFSASAL --- A	49
P.tricho	- MLSR ----- TVVSVS-AVSTSTSTS ----- LSRFLCKVNQTI PKFLGQKLSHNF	44
T.pseudo	-----	0
O.tauri	----- MSYSVQ RS GATRAAVSRA	18
C.reinha	----- MLSLK	5
V.carter	----- MQALQR	6
C.aeropho	-----	0
Bacillus	-----	0
Clostrid	-----	0
Phycispha	-----	0
I 86		
A.thaliana	SFCGGCIRKIN --- HKPLRMTSSNITPRAMATQ QLENADQLIDSVETFI DCD GVIWKGD	94
P.patens	G----- GRMNCSAQVETEATASAPFLTDHAKLIDSVETFI DCD GVIWKGD	100
O.sativa	SPVAGQR--- CAA-RRRSVM AAA ---- GAVPAAKLENADALIDSVETFI DCD GVIWKGD	97
S.bicolor	SA----- NRV-ARRSGVMA ---- AAAAAAKLEDADALIDSVETFI DCD GVIWKGD	88
Z.mays	QA----- SRV-ARRSVM AAAGAAAA PAAAKLEDADALIDSVETFI DCD GVIWKGD	98
S.lycoper	SKPIKWNC----- KNSRMESKSSSFVTKASAQPLTNPAELIDSVETFI DCD GVIWKGD	92
B.napus	SFSGGIVRRID--- HKPLRVMTPNLT PRAMAAQ QLENADQLIDSVETFI DCD GVIWKGD	91
G.max	SAIFKWKRKANYNRHSS-G-- M-GTFTTRALAQPPQNADELIDSVETFI DCD GVIWKGD	101
M.trunca	SAFVKWKRNISSNKNN-R---- FRMATKALAQPLQNADELIDSVETFI DCD GVIWKGD	99
G.hirsut	IKCTISISN-- CSPNK SARSM EG - FTTRTKASAQPLENADELIASVETFI DCD GVIWKGD	106
P.tricho	TNCTTWNKNLNLNRKCSTRMDN- FTTKASAAAQPLTNADELIGSVETFI DCD GVIWKGD	103
T.pseudo	----- MSMRPKDLLPGVDVFI DCD GVIWRGD	27
O.tauri	E-VPRARTQSARAVRRTRRGESIA-M NAKASRLGESEAKALV DATETFI DCD GVIWKGD	76
C.reinha	Q-LPSARC-AARVPRVRRMVA QASARPI -- ATNEQKLELLK VECFI DCD GVIWLGD	61
V.carter	S-VPSARA-GARAVRPARKM VCTAASRPI PRATNEQKLDLLK VECFI DCD GVIWLGD	64
C.aeropho	----- MSLYVFDLD GVIYRGE	16
Bacillus	----- MNGYIFDLD GTYIDN	16
Clostrid	----- MKSIDDLKCFILDM DGTIYLG N	22
Phycispha	----- MKDVQFINNFINNFEVFLNCD GVIWNGN	29
. : : : * * . * : :		
103 II		
A.thaliana	KLIEGVPE TL DMLRAK GKRLVF TNNSTKSRKQY GKKFETLGLNV NEEEIFASSFAAAAY	154
P.patens	SLIEGVPE TL DMLRSM GKRLVF TNNSTKSRKQY GKKFESLGLSV SEEEIFASSFAAAAY	160
O.sativa	KLIDGVPE TL DMLRSK GKRLVF TNNSTKSRKQY GKKFETLGLNV NEEEIFASSFAAAAY	157
S.bicolor	KLIDGVPE TL DLRSK GKRLVF TNNSTKSRKQY GKKFETLGLMS IDEEEIFASSFAAAAY	148
Z.mays	KLIDGVPE TL DLRSK GKRLVF TNNSTKSRKQY GRKFETLGLSV DDEEIFASSFAAAAY	158
S.lycoper	KLIDGVPE TL DLREK GKRLVF TNNSTKSRKQY GKKFETLGLSV NEEEIFASSFAAAAY	152
B.napus	KLIEGVPE TL DMLRAK GKRLVF TNNSTKSRKQY GKKFETLGLNV NEEEIFASSFAAAAY	151
G.max	KLIDGVPE TL DMLRSK GKRLVF TNNSTKSRKQY GKKFETLGLNV SEEEIFASSFAAAAY	161
M.trunca	SLIEGVPE TL DMLRSK GKRLVF TNNSTKSRKQY GKKFETLGLNV NAEEIFASSFAVAAY	159
G.hirsut	KLIDGVPE TL DMLRSK GKRLVF TNNSTKSRKQY GKKFETLGLNV NEEEIFASSFAAAAY	166
P.tricho	KLIDGVPE TL DMLRSR GKRLVF TNNSTKSRKQY GKKFESLGLDV SEEEIFASSFAAAAY	163
T.pseudo	SVIPGIPQ TL EKLRL ALGK KMYF TNNSTKSRAGY KKKFDSLGLNV PAEEIFSSSFAAAAY	87
O.tauri	SLIEGVPE TL DLRSM GKRLVF TNNSTKSRAGY TKKFESLGLKVN AAEEIFSSSFAAAAY	136
C.reinha	KVIEGVPE TL DMLRGM GKRVF TNNSTKSRAGY MSKFQSLGLNV KAEEIYSSSYAAAAAY	121
V.carter	KVIDGVPE TL DMLRGM GKRVF TNNSTKSRAGY MSKFQSLGLDV KAEEIYSSSYAAAAAY	124
C.aeropho	RLLPGVKE TL TKLRK RGNQ VSFL TNNSTLSRSGFQ KKLTQMGIEVH LEDLFPSSHLAAIY	76
Bacillus	EIIAGVPE AIKSLK ARGDKVI FL TNKS IASR KDY EKLLKLDIEV KEEVINSNYI TAHY	76
Clostrid	EIIDGAE IFINTIK SMG KEYI FL TNNS SKNR KVY KEKLDRL GFDIDE EIFT SGEATI IY	82
Phycispha	TAIHKASE VINFLK SIK QLYFI TND C SKSR FAFINK FKEFG ININESEI IC SSFLAAY	89
: : : : . . * : * * . . * : * : : : . : * . . *		

A.thaliana	LQSIDFPK-DKKVYVIGEEGILKELELAGFYLGPPDDGKRQIELKPGFLMEHDHVDGAV	213
P.patens	LKSIKFPK-DKKVYIIGEAGIQLELQAGINYYIGGPEDGDKRIDLAPGQLMEHDHVDGAV	219
O.satviva	LQSIDFPK-DKKVYVIGEDGILKELELAGFYLGPPSDGDKKIELKPGFYMEDHDKVDGAV	216
S.bicolor	LQSIDFPK-DKKVYVIGEEGILKELELAGFYLGPPDGDGKKIELKPGFLMEHDHVDGAV	207
Z.mays	LQSIDFPK-DKKVYVIGEEGILKELELAGFYLGPPDGDGKKIELKPGFLMEHDHVDGAV	217
S.lycoper	LKSIDFPK-DKKVYVIGEDGILKELELAGIQYLGPPEDGDKKIELKPGYMMEQDKVDGAV	211
B.napus	LQSIDFPK-DKKVYVIGEEGILKELDLAGFYLGPPDDGKKQIELKPGFLMEHDHVDGAV	210
G.max	LKSIDFPK-DKKVYVIGEDGILKELELAGYQYLGPPEDGGKQIELKPGFLMEHDHVDGAV	220
M.trunca	LKSIDFPK-DKKVYVIGEDGILKELELAGYQYVGGPEDGGKQIELKPGFLMEHDHVDGAV	218
G.hirsut	LKSIDFPK-DKKVYVIGEDGILKELELAGFYLGPPEDGGKQIELKPGFLMEHDHVDGAV	225
P.tricho	LKSIDFPK-DKKVYVIGEDGILKELELAGFYLGPPEDGGKQIELKPGFLMEHDHVDGAV	222
T.pseudo	LEQSKFKETGKKVYVVEVGIQEELDLIGVPHFGPPEDANKQPDMPGPGCMVEHDHVDGAV	147
O.tauri	LESIDFK---KKAYVIGETGILEELDNVGVKHIGGESDADKQVTLKSGELMHHDHVDGAV	193
C.reinha	LESINFN---KKVYVIGETGILEELDLKGIHVGGPGDADKKVTLKSGEFMEHDHVDGAV	178
V.carter	LESINFQ---KKVYVIGETGILEELDMKGIHVGGPSDADKRVTLRSGEFMEHDHVDGAV	181
C.aeropho	LGHKTKNK-NIKVLVFGEEGLFEELRQARIKLT-----TSKDANYV	117
Bacillus	LKKVMKP--EDSVYVIGEAPLFEELRGENIKLAE-----CSARASHV	116
Clostrid	LNSIKSN---SKVFLLGTEYLKEEFLNAGFNITD-----RYENNIDFV	122
Phycispha	LKQKKN---KTAYIIGEGLLLEFDKMNKIYIYIETDNNNE--MNKDLILNIHNNIGAV	144

* . . . * : *

232 239

A.thaliana	VVGFDRYFNYYKIQYGTLCIRENPGCLFIATNRDAVTHLTDQEWAGGGSMVVALVGSQT	273
P.patens	VVGFDRYLNYYKLQYATLCIRENPGCMFIATNCDAVTHLTDQEWAGGGSMVGAIKGSTK	279
O.satviva	VVGFDRYFNYYKVQYGTLCIRENPGCLFIATNRDAVTHLTDQEWAGGGSMVGAAILGSTK	276
S.bicolor	VVGFDRYFNYYKVQYGTLCIRENPGCLFIATNRDAVTHLTDQEWAGGGSMVGAAILGSTK	267
Z.mays	VVGFDRYFNYYKVQYGTLCIRENPGCLFIATNRDAVTHLTDQEWAGGGAMVGAALLGSTK	277
S.lycoper	VVGFDRYFNYYKIQYATLCIRENPGCLFIATNRDAVTHLTDQEWAGGGSMVGAAILGSTK	271
B.napus	VVGFDRYFNYYKIQYGTLCIRENPGCLFIATNRDAVTHLTDQEWAGGGSMVVALVGSQC	270
G.max	VVGFDRYFNYYKIQYGTLCIRENPGCLFIATNRDAVTHLTDQEWAGGGSMVVALVGSQT	280
M.trunca	VVGFDRYFNYYKVQYGTLCIRENPGCLFIATNRDAVTHLTDQEWAGGGSMVVALVGSQT	278
G.hirsut	VVGFDRYFNYYKVQYGTLCIRENPGCLFIATNRDAVTHLTDQEWAGGGSMVGAICGSTQ	285
P.tricho	VVGFDRYFNYYKVQYGTLCIRENPGCLFIATNRDAVTHLTDQEWAGGGSMVGAIFVGSQT	282
T.pseudo	VVGFDRNINYYKIQAQALCINENPGCEFIATNTDAVTHLTDQEWAGNGSMVGAIKGCTG	207
O.tauri	IVGFDRNINYYKIQAATLCIRENPGCMFIATNTDAVTHLTDQEWAGNGSMVGAIKGSTK	253
C.reinha	VVGFDRYVNYKIQAATLCIRENPGCMFIATNRDAVTHLTDQEWAGNGSMVGAIVGSKT	238
V.carter	VVGFDRYINYYKIQAATLCIRENPGCLFIATNRDAVTHLTDQEWAGNGSMVGAIVGSKT	241
C.aeropho	VVGMDRKFNFEKLLAYEAIL--NGAKFVATNKDVTYPTTEEG-TVPAAGAIKALEVSTH	174
Bacillus	VLGWRDRFTYDKLNQAYQAWK--NGAEIATNPDRTPVREG-DIPDCGAMIGALEGTTG	173
Clostrid	VLGFDTTLTYNKLWIACDIIR--EGVTYIATHPDKNCPLENGKYPDTGAIIEIYSSSTG	180
Phycispha	VVGFDRNISYNKIEYARIAL-ENPQCMILIVTNRDAKTYLTESQYLAGTGSMIGAVEGCTN	203

::* * . . : * : . . . * : * . . . * : :

III 302 IV 320 322 330

A.thaliana	RE-PLVVGKPSFMMDYLA-DKFGIQKSQICMVGDRDLTDILFGQNGGCKTLLVLSGVTS	331
P.patens	KE-PLVVGKPSFMMDYLA-SEFNIKTSQICMVGDRDLTDILFGQNGGCATLLVLSGVTT	337
O.satviva	QE-PLVVGKPSFMMDYLA-KKFGITTSQICMVGDRDLTDILFGQNGGCKTLLVLSGVTS	334
S.bicolor	QE-PLVVGKPSFMMDYLA-KKFGITTSQICMVGDRDLTDILFGQNGGCKTLLVLSGVTS	325
Z.mays	QE-PLVVGKPSFMMDYLA-KKFGITTSQICMVGDRDLTDILFGQNGGCKTLLVLSGVTS	335
S.lycoper	RE-PLVVGKPSFMMDYLA-DKFKIQKSQICMVGDRDLTDIVFGQNGGCKTLLVLSGVTS	329
B.napus	RE-PLVVGKPSFMMDYLA-DKFGIEKSQICMVGDRDLTDILFGQNGGCKTLLVLSGVTS	328
G.max	RE-PLVVGKPSFMMDYLA-NKFGISKSQICMVGDRDLTDILFGQNGGYKTLLVLSGVTT	338
M.trunca	RE-PLVVGKPSFMMDYLA-NEFGISKSQICMVGDRDLTDILFGQNGGCKTLLVLSGVTT	336
G.hirsut	RE-PLVVGKPSFMMDYLA-NKFGILKSQICMVGDRDLTDILFGQNGGCKTLLVLSGVTN	343
P.tricho	RE-PLVVGKPSFMMDYLA-NKFGILKSQICMVGDRDLTDILFGQNGGCKTLLVLSGVTS	340
T.pseudo	RE-PTVVGKPSPLMIDYLC-DKLGIDRGRICMVGDRDLTDILFGSDNGLKSLVLSGVTT	265
O.tauri	RE-PIVVGKPAAFMLDYIA-NKFNIRKQITMVGDRDLTDILFGNDGGLNLLVLSGVTT	311
C.reinha	RE-PIVVGKPSDFMLKNIS-ASLGLRPDQIAMVGDRDLTDIMFGKNGGLTALVLSGVTT	296
V.carter	RE-PTVVGKPSDFMLKNIS-ASLGLRPDQICMVGDRDLTDIMFGKNGGLTSLVLSGVTT	299
C.aeropho	KR-ALLLGKPHLFLGKTVM-KSKGYTSADTILVGDGLETDLVGRKRLKIVTVLVLSGITL	232
Bacillus	EPIKLITGKPSLSMANYVLDVLMQEASNCYMI GDRLETDIKMGNDAGMHSVLVMTGITTT	233
Clostrid	KK-PYIIGKPNKEIINSIC-KKYSVNKRDMIAIVGDRLYTDIKTGENSGISIIVLVSGETT	238
Phycispha	RT-ATLVGKPSNFLNLL-----ININPEKCLIVGDKLIDILFANTNIPSCVLVSGATI	257

. : *** . . . : ** * * * . . : ** : * *

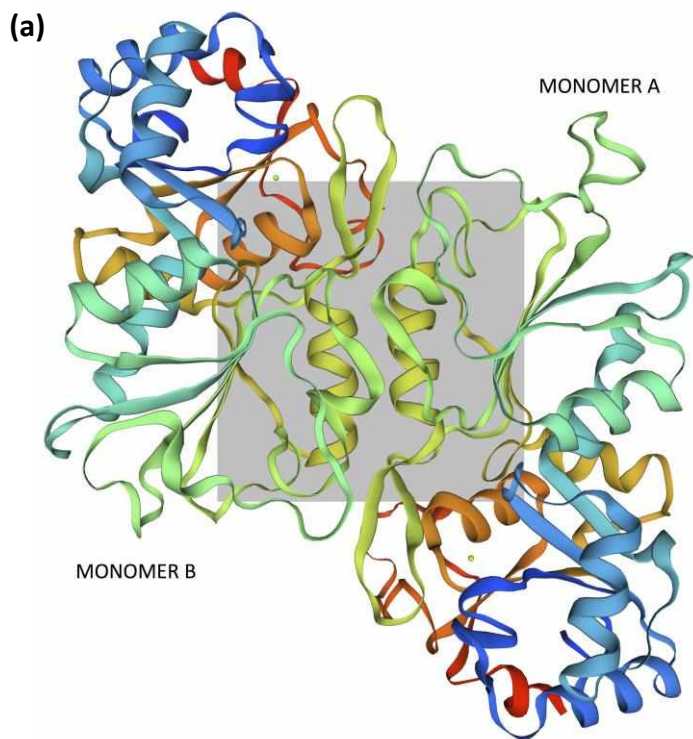
356

A.thaliana	ISMLESPEKNIQPDFYTSKISDFLSPKAATV-----	362
P.patens	LETLQSPENKIQPDFYTTKISDLLAAKKVASA-----	369

O.sativa	VQMLQSPDNSIQPDFYTNQISDFL T LKAATV-----	365
S.bicolor	LQTLQSPDNSIQPDFYTNQLSDFL T LKAATV-----	356
Z.mays	LQTLQSPDNSIQPDFYTNQISDFL T LKAATV-----	366
S.lycoper	LSMLQDPSNSTQPDFYANKISDFL S IKAAAV-----	360
B.napus	ISMLESPEENKIQPDFYTSKISDFL S LKAAAV-----	359
G.max	LAMLQSPNNSIQPDFYTNKISDFL S LKAAAV-----	369
M.trunca	LPVLQSPNNSIQPDFYTNKISDFL S LKAAAV-----	367
G.hirsut	LSMLQSPNSIQPDFYTNKISDFL S IKTATV-----	374
P.tricho	LSMLQSPNSIKPDFYTNKISDFL S LKASAV-----	371
T.pseudo	EEKLLSQENVITPDYADSIIVDFVVDENAKVGA-----	298
O.tauri	KEML C SDDNTIAPTNYTDKLADLL C VGKVPA-----	342
C.reinha	PEVLNSPDNKVHPDFVLNSLPDLL S VKEKAMVAA-----	330
V.carter	EEVLNSPENKVIPDYVLSKLPDLL T VKEVAMVAA-----	333
C.aeropho	EKMLQKAPPSLKPDYVIQSLDL S LKIGHGYKLVSSIDTL	274
Bacillus	LNMLE--NPVHKPKYIILESVRDIL T L-----	257
Clostrid	IEEYNE--SKIKADFVYKSVKEINEELLK-----	265
Phycispha	LNDLELFPREKLPTFFARSIADFIHNIQK-----	286

. : ::

Figure S3: Duminil et al.



(b)

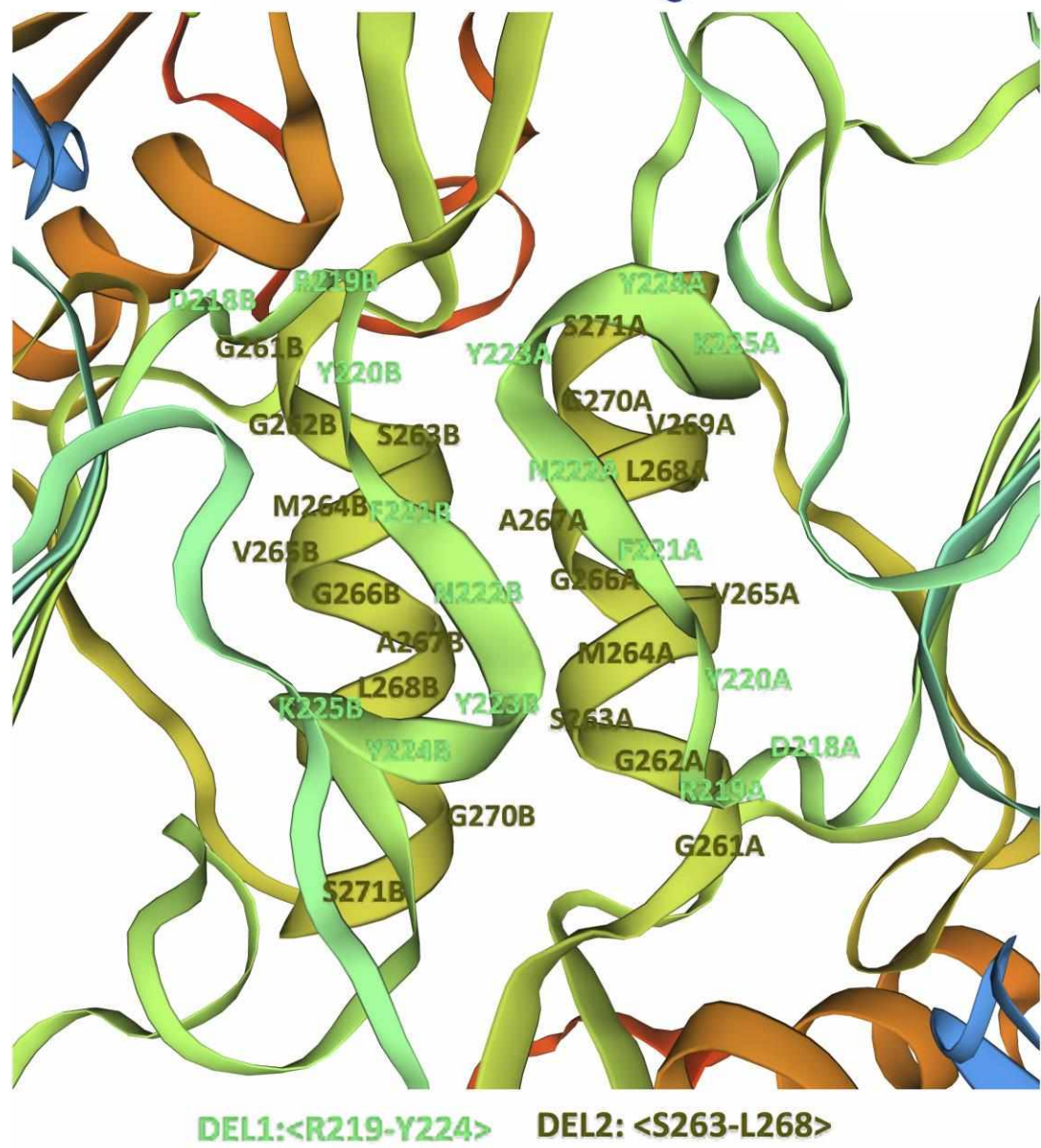


Figure S4: Duminil et al.

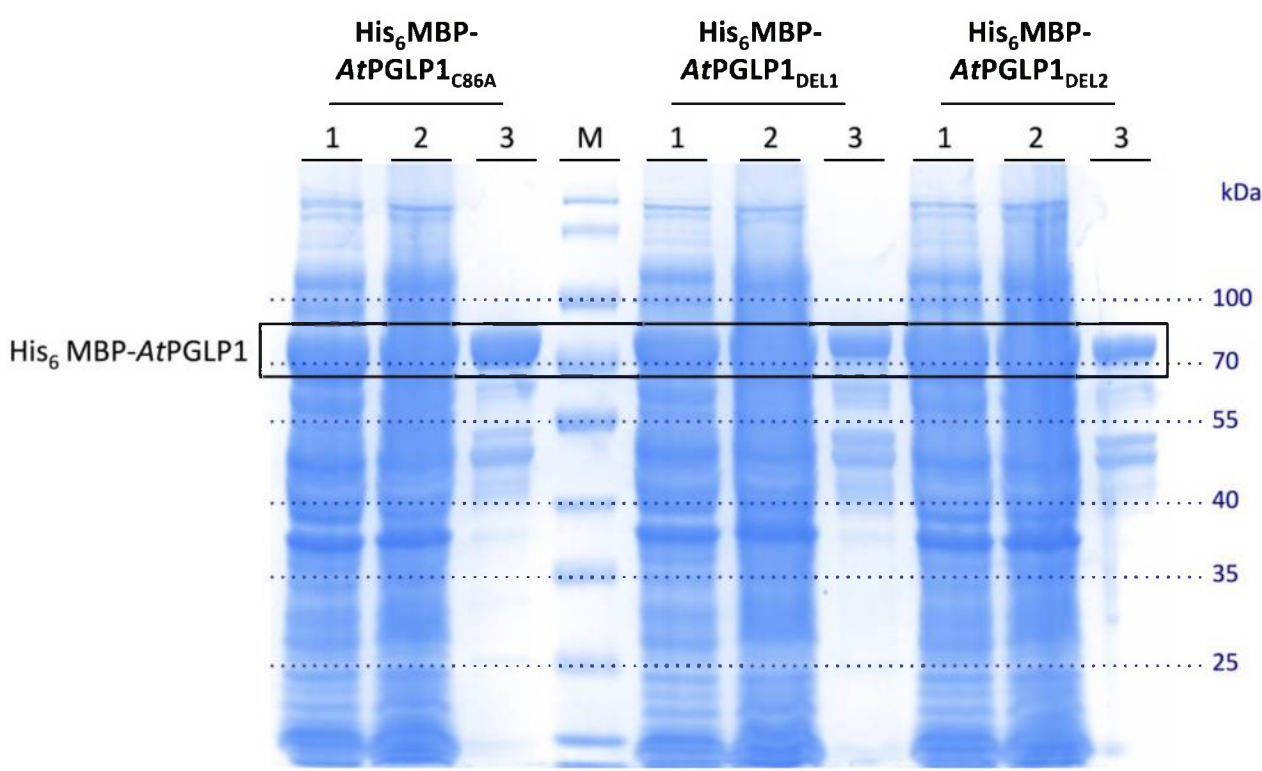


Figure S5: Duminil et al.

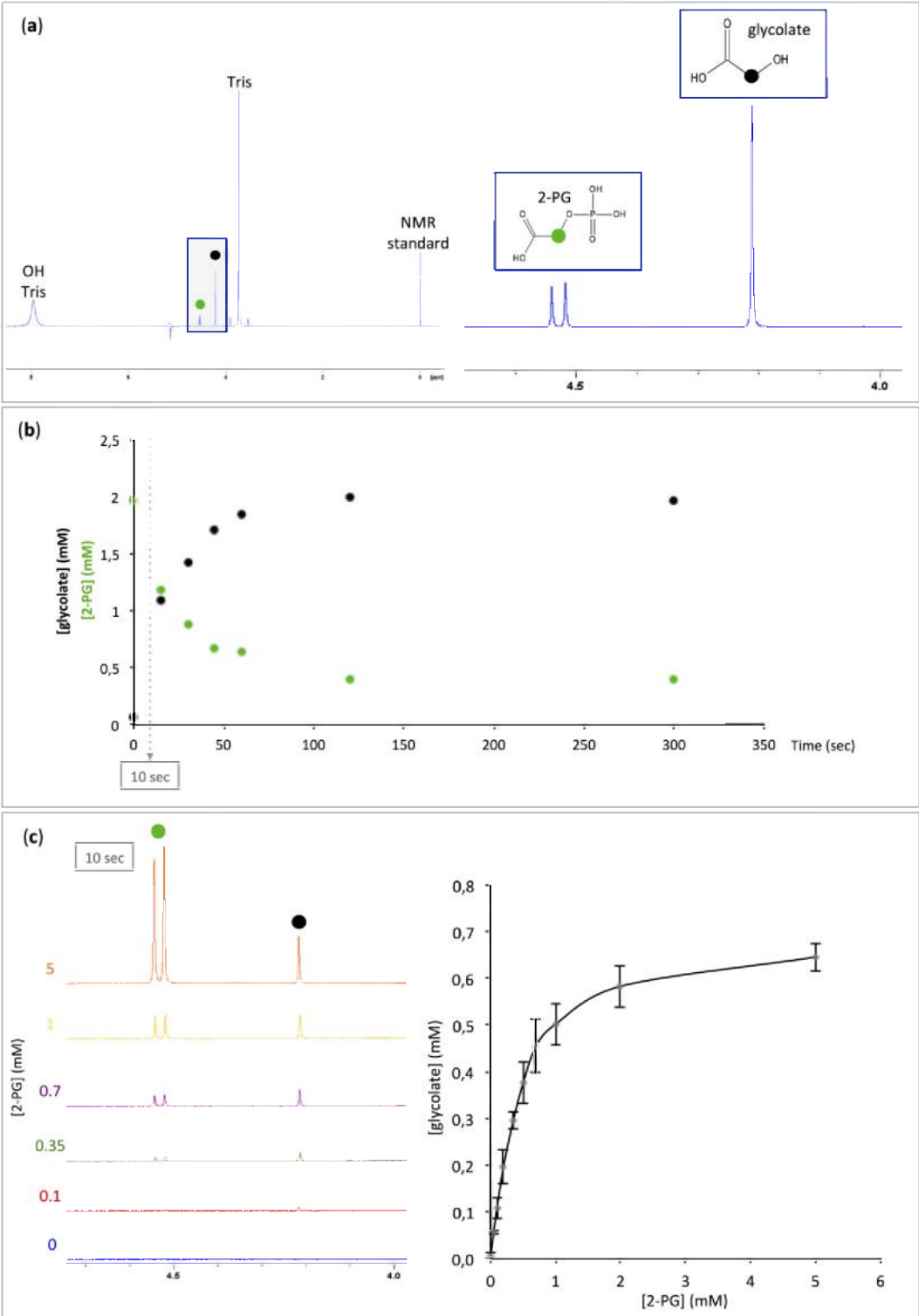
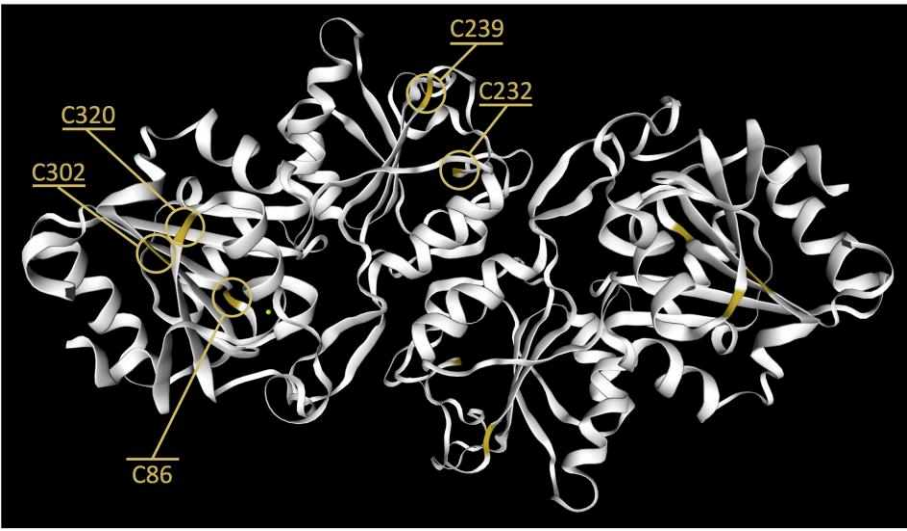
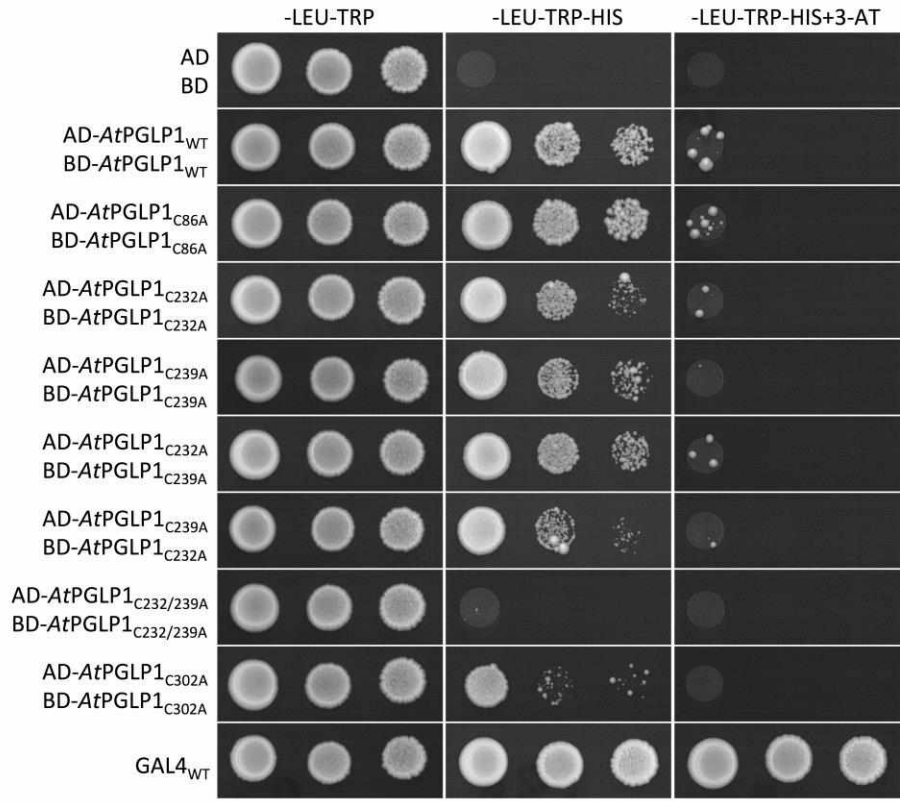


Figure S6: Duminil et al.

(a)



(b)



(c)

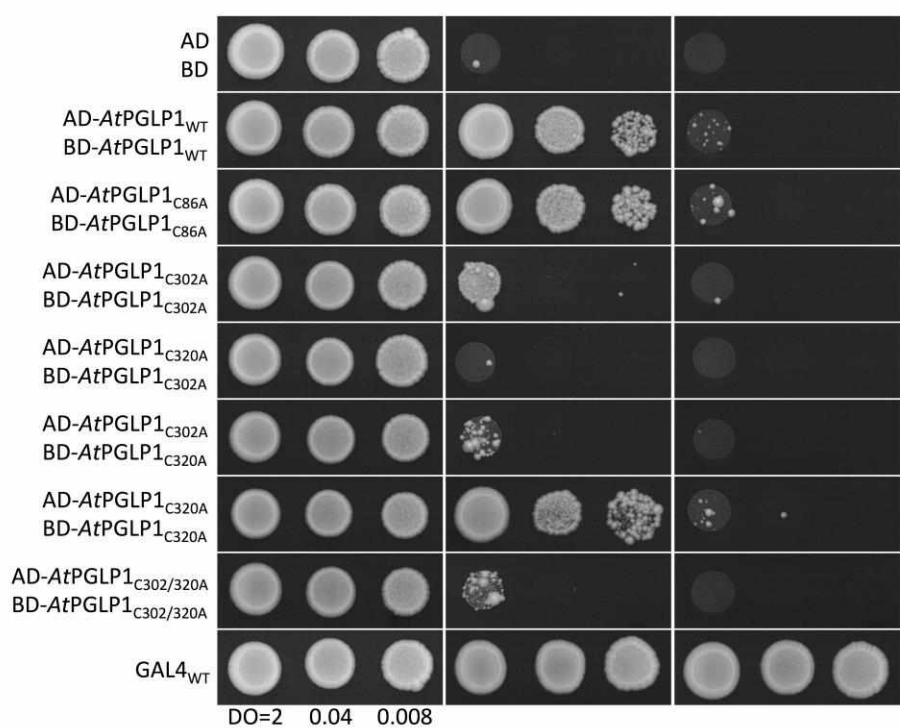


Figure S7: Duminil et al.

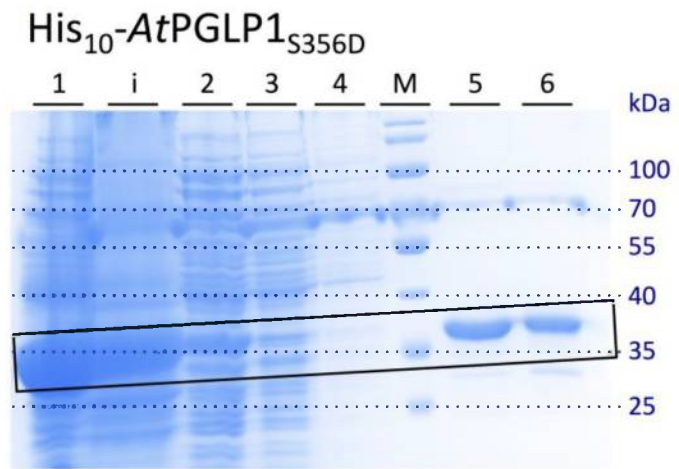
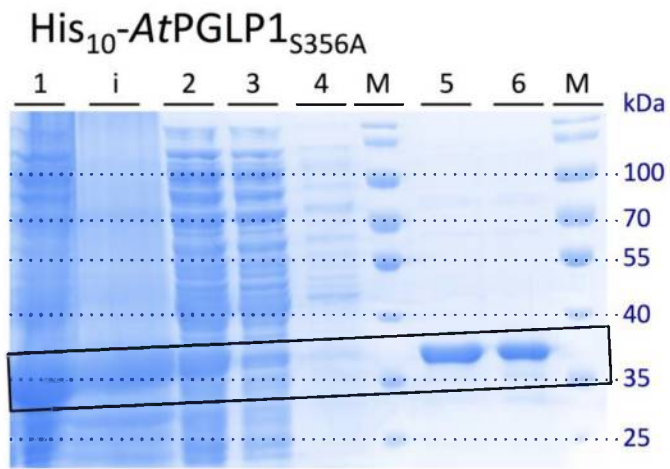
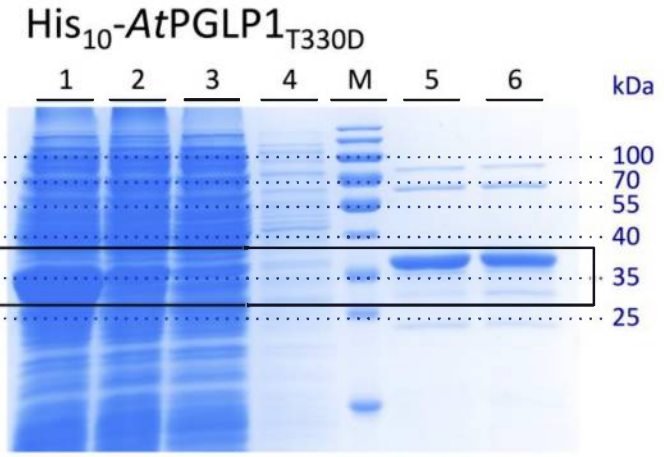
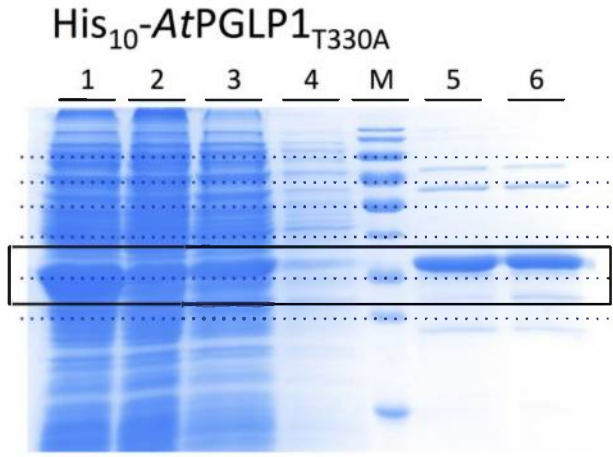
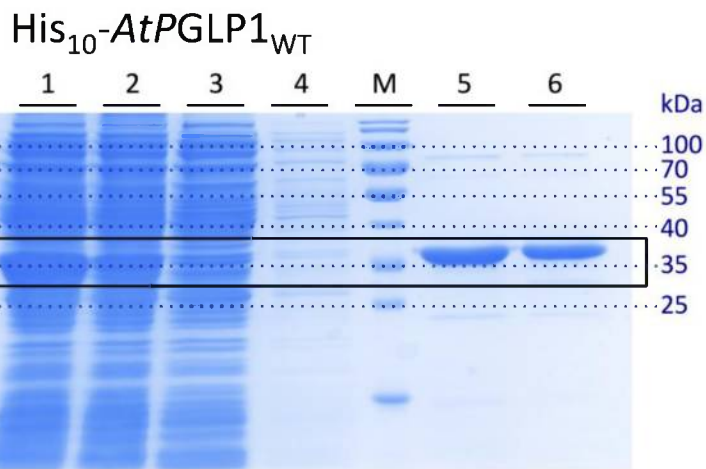
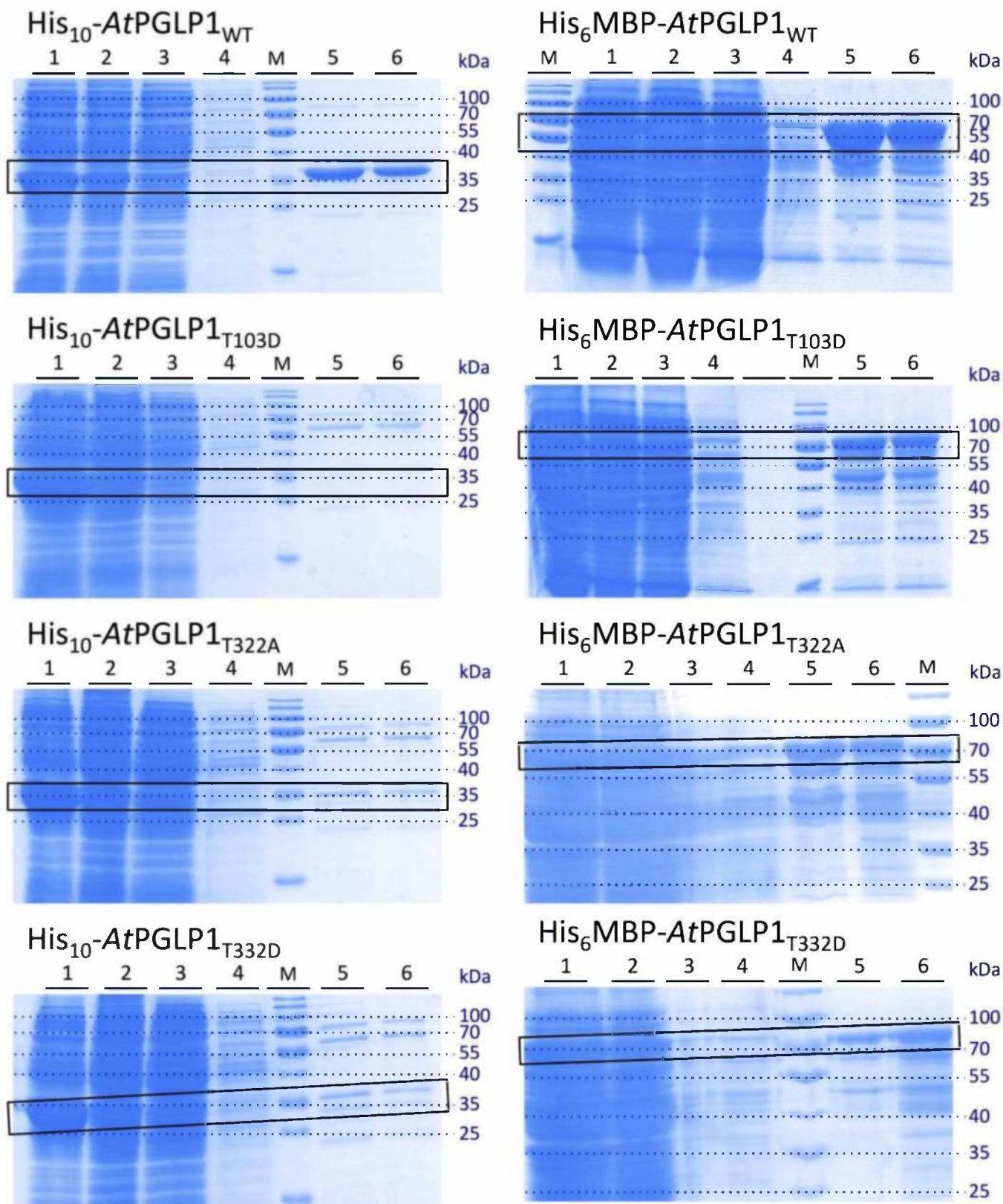


Figure S8: Duminil et al.



CHAPTER III

Preamble

After the work focused on recombinant *AtPGLP1 in vitro* and its activity and regulation, this chapter is dedicated to my *AtPGLP1 in planta* work corresponding to plant experiments performed during my PhD project. Since these results are either too preliminary or need to be completed, this chapter will not be presented as a manuscript.

This chapter is divided into two parts:

The first concerns the characterization of leaf *AtPGLP1* activity of wild type Col-0 plants, depending on daytime and several environmental treatments known to modulate photorespiratory activity; high temperature, high light and elevated CO₂. The second part is focused on an Arabidopsis *pglp1* mutant and its functional complementation with different *AtPGLP1-GFP* versions; wild-type *AtPGLP1_{WT}-GFP* and mutated *AtPGLP1-GFP* at selected potential phosphosites to produce either phosphorylation-mimetic (*AtPGLP1_{T103D}-GFP*, *AtPGLP1_{S356D}-GFP*) or non-phosphorylatable (*AtPGLP1_{T103A}-GFP*, *AtPGLP1_{S356A}-GFP*) forms. The choice of these two phosphosites will be justified later in the second part of this chapter. *AtPGLP1* fused to the GFP was used to eventually test, later, whether mutations could affect PGLP1 subcellular localization. It should be noted that recombinant *AtPGLP1_{WT}-GFP* was purified from *E. coli* cells and shown not to alter the kinetic properties of the protein (data not shown).

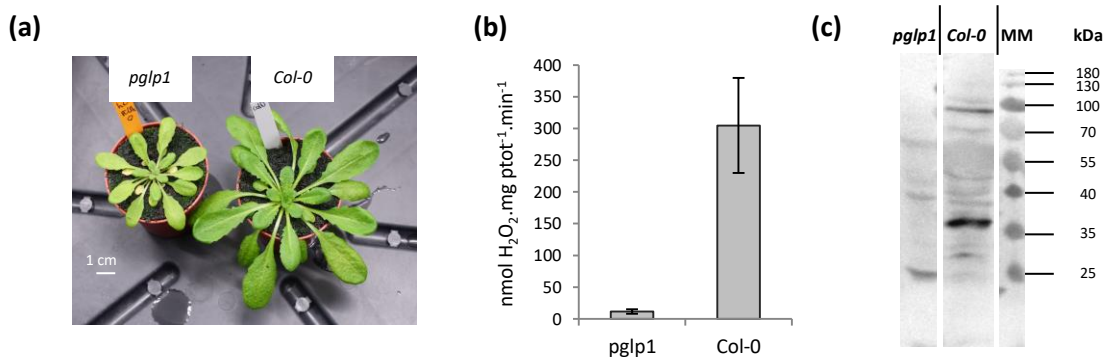


Figure 22: *pglp1* homozygous mutant phenotype and leaf PGLP activity and protein

(a) Phenotype of the *Arabidopsis* *pglp1* homozygous mutant after 6 weeks in 1 % CO₂ and short day conditions. (b) *AtPGLP1* activity of soluble proteins extracted from *pglp1* and Col-0 leaves. The reaction was carried out with the recombinant *AtGOX1* coupled reaction using 50 µg of soluble leaf proteins and 1mM 2-PG. (c) Western blot of soluble proteins extracted from *pglp1* and Col-0 using 5 µg of proteins and our anti-*AtPGLP1* serum.

I) AtPGLP1 activity in plants

1) Introduction

The results described in the preceding chapter suggested that one level of AtPGLP1 regulation was post-translational whether by protein phosphorylation or redox modulation at some specific amino acids. Thus, it seemed reasonable to investigate the existence of such regulations *in planta*. First it was decided to study whether leaf AtPGLP1 activity was modulated when Arabidopsis Col-0 plants were submitted to treatments expected to either increase or decrease photorespiratory activity. The 2C-cycle is highly responsive to environmental changes (light, temperature, drought, etc) as previously described in the introduction of my thesis. In the first part of this chapter we will thus analyse AtPGLP1 activity of total soluble proteins from Col-0 leaf extracts during a day/night cycle, under two abiotic stresses (high temperature and high light) and when transferred from air to elevated 1 % CO₂. The level of AtPGLP1 protein was evaluated to identify if any activity changes could be correlated with variations at the AtPGLP1 protein level or if the enzyme was just more/less active. In the previous chapter, we described the development of a coupled reaction using recombinant AtGOX1 to measure recombinant AtPGLP1 activity and this technique was used also to perform enzymatic activity assays with soluble proteins extracted from Arabidopsis leaves. AtPGLP1 protein levels were estimated by Western blots either using antibodies raised in rabbits against our purified recombinant AtPGLP1 protein or commercial anti-GFP antibodies when AtPGLP1 was fused to the GFP.

2) Results

Since the measurement of leaf extract PGLP activity using our GOX-coupled reaction had never been described before, we first tested this technique by comparing PGLP activities measured with total soluble proteins extracted from an Arabidopsis homozygous *pglp1* mutant and Col-0 leaves. PGLP activity was measured using rosette leaf extracts of plants grown at 1 % CO₂ since the Arabidopsis *pglp1* mutant was unable to grow under normal ambient air (see Figure 26). Furthermore, even at 1 % CO₂ this mutant still displayed a growth delay compared to WT, Col-0 plants (Figure 22a). This suggested that even at this elevated CO₂ level in the atmosphere there was still some RuBisCO oxygenase activity occurring and the production of toxic 2-PG although it could also be that AtPGLP1 is involved in another crucial pathway independent of photorespiration and therefore the growth phenotype could not be rescued by high CO₂. That said, there is a good correlation between the quasi-absent PGLP activity in *pglp1* mutant leaves (Figure 22b) and the

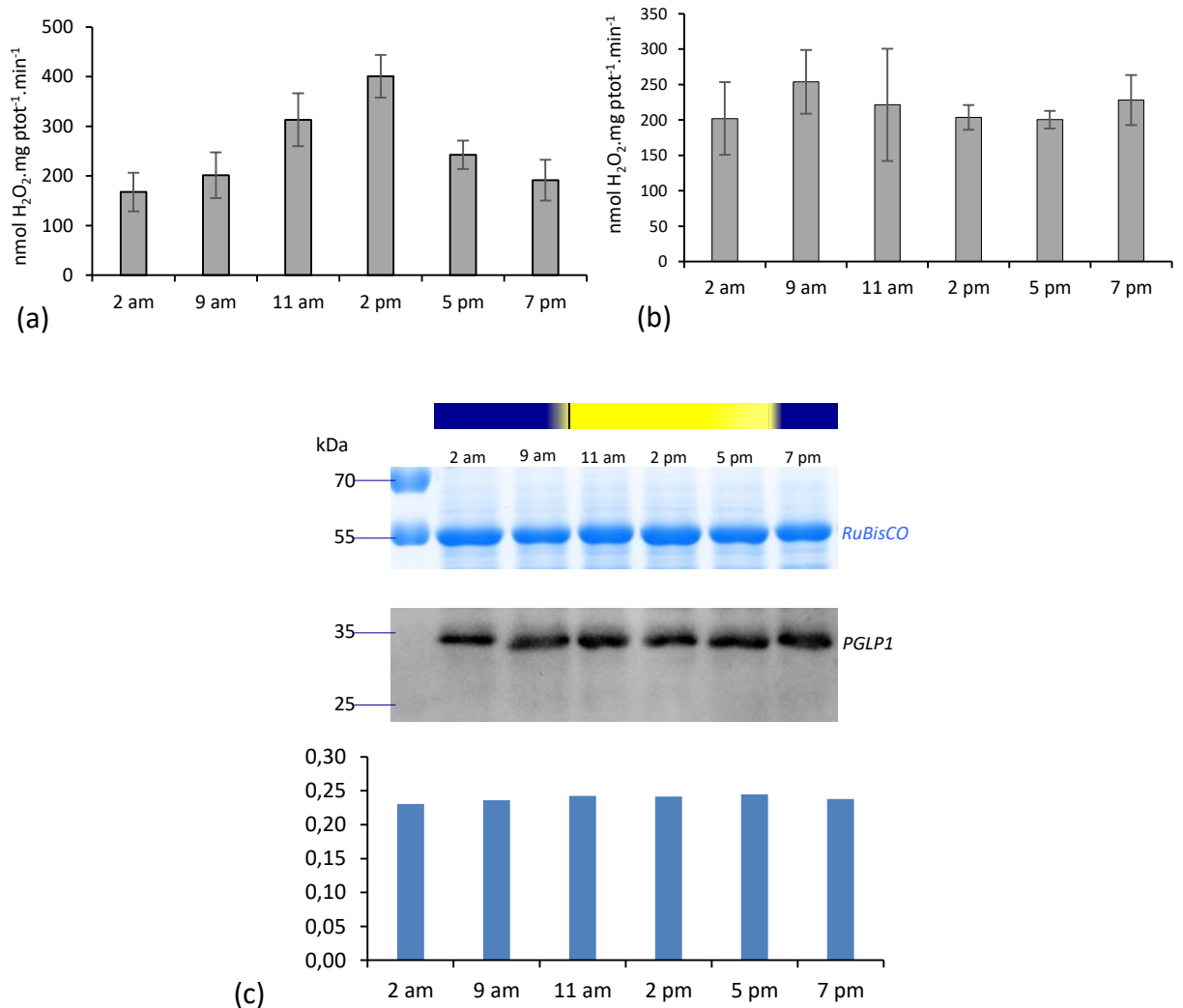


Figure 23: AtPGLP1 activity is cycling according to the day/night conditions

(a and b) AtPGLP1 activity measurement using the coupled reaction initiated by the addition of 50 µg of soluble proteins extracted from leaves. Value are means ± SD (n=3 independent samples). **(a)** in ambient air (0.04 % of CO₂); **(b)** in high CO₂ (1 %).

(c) Western blots performed with the same protein extraction used for activity measurement (4 µg). The AC I (our anti-AtPGLP1 serum) was used at 1:250 and the AC II (HRP conjugated anti-rabbit IgG, A6154 Sigma) at 1:10 000. The membrane was exposed for 45 s. The histograms show AtPGLP1 quantification and were done using Image J software. The histogram corresponds to the ratio between RuBisCO and AtPGLP1 quantifications.

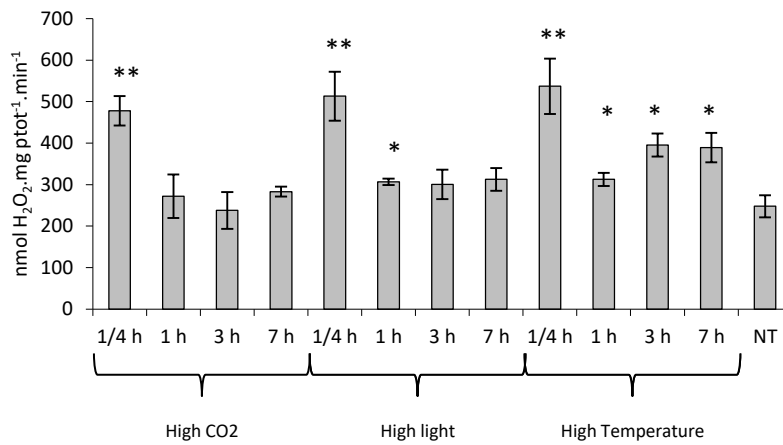
absence of AtPGLP1 protein as seen from the western blot using our anti-AtPGLP1 serum (Figure 22c). Therefore, these results validate the GOX-coupled reaction as a method to measure PGLP activity in plant leaves.

Once the PGLP activity measurement method had been validated, and since photorespiration only occurs in the light during the day, we decided to characterize leaf AtPGLP activity during a day/night cycle. To achieve this, leaves of air-grown 5-week-old Arabidopsis Col-0 plants were collected at different times during a 24 h period at 2 am, 9 am, 11 am, 2 pm, 5 pm and 7 pm (it should be noted that the 8 h-long light period started at 10 am and ended at 6 pm) and at each time rosettes from 5 plants were pooled. From these samples, total soluble proteins were extracted (see Materials and methods, section 4 “Extraction of leaf soluble proteins for AtPGLP activity measurements”) and 50 µg were used to measure leaf PGLP activities. At each time point, three independent samples (of 5 rosettes) were measured, and three independent light/dark cycles of different sets of plants were performed (see Figure 23). PGLP activity was measured after desalting the leaf soluble protein extracts and the reaction was carried out in the presence of 10 mM MgCl₂ (as for recombinant AtPGLP1 activity measurements). The final detected product of oxidized o-dianisidine was measured in real-time at A_{440nm} using a Varian Cary 50 spectrophotometer.

The CO₂ concentration in normal ambient air is widely considered to be 0.04 %, however in the IPS2 building with human activity, it was measured at around 0.05 %. Therefore, in normal air, it was observed that AtPGLP1 activity was cycling during the day/night cycle and displayed its highest activity in the middle of the light period at 2 pm. This activity gradually decreased until 2 am during the dark period, to increase again in the light (Figure 23). Interestingly, these experiments indicated that PGLP activity could be modulated while PGLP1 protein levels remained unchanged thus inferring that leaf AtPGLP1 was undergoing a post translational regulation(s). Furthermore, it seemed that leaf PGLP activity responded to conditions that increased/decreased photorespiration. At 1 % CO₂, required for Arabidopsis *pglp1* mutant growth, leaf PGLP activity did not show any significant changes during the day and night (Figure 23b). At this CO₂ concentration, photorespiration is very low compared to normal air and AtPGLP1 activity may not require to be regulated. Interestingly, the activity level of leaf PGLP in high CO₂ conditions was the same as that during the night in ambient air grown Arabidopsis plants; this could constitute a basal extractable leaf PGLP activity for low photorespiratory conditions.

Since PGLP activity responded to day/light conditions that modulate photorespiration, we decided to investigate how AtPGLP1 enzymatic activity reacted to environmental conditions known to impact photorespiration. Thus 5 week-old control Col-0 plants grown in short-day conditions in ambient air were submitted to two different stress treatments, either high temperature (40 °C) or high light (475 µmol.m⁻².s⁻¹) and to a transfer from ambient air to high CO₂ (1 %). Samples were taken

(a)



(b)

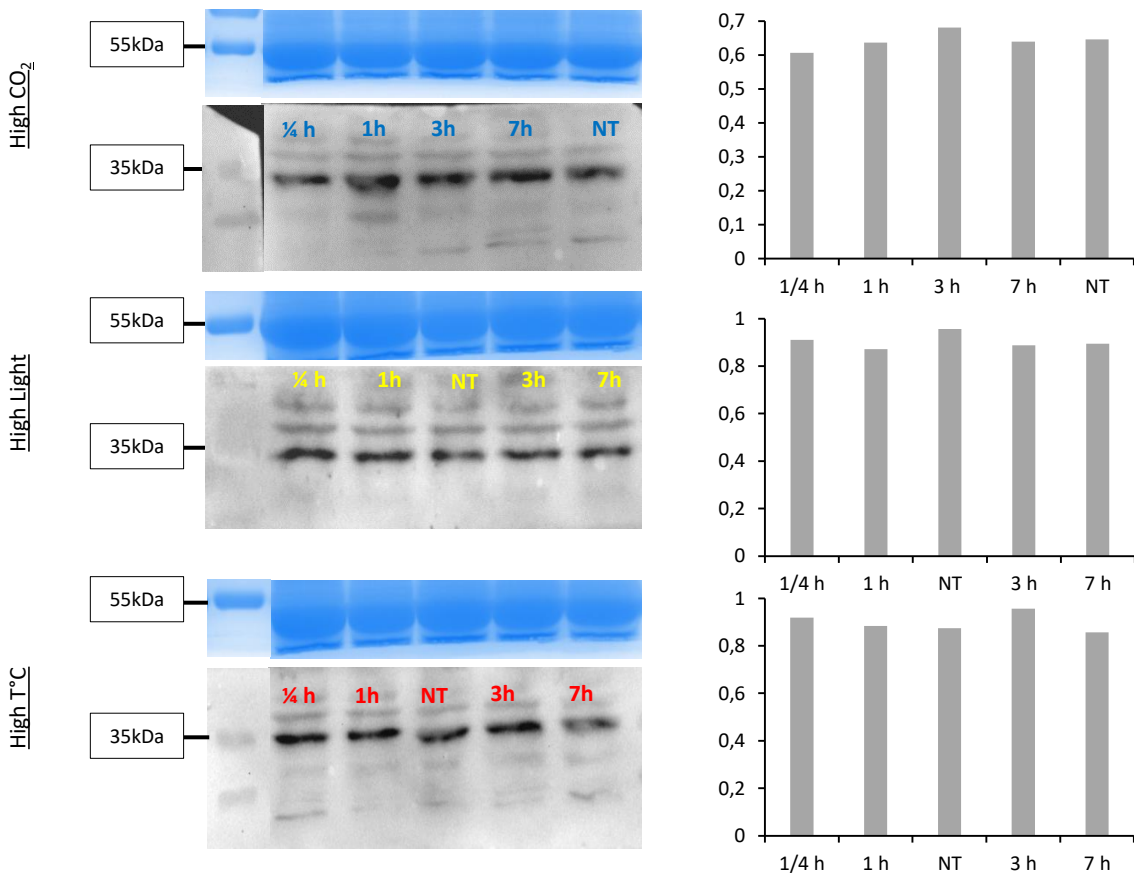


Figure 24: AtPGLP1 activity is changing under stresses since ¼ h of exposure compare to non-treated samples (NT)

(a) Measurement of AtPGLP1 activity using the coupled reaction. Time point correspond the activity measured with soluble protein extracted from plants sampled after ¼ h, 1 h, 3 h and 7 h of exposure to different stresses high light (475 $\mu\text{mol.m}^{-2}.\text{s}^{-1}$), high temperature (40 °C) and high CO₂ (1 %). Statistical significance was determined by a Student's *t*-test comparing different conditions to the non-treated samples (*P < 0.05 and **P < 0.005). (b) Western blots performed with the same protein extraction used for activity measurement. The AC I (anti-PGLP1 serum) was used at 1:250 and the AC II (HRP conjugated anti-rabbit IgG, A6154 Sigma) at 1:10 000. The membrane was exposed for 45 s. The histograms show AtPGLP1 quantification and were done using Image J software (ratio between RuBisCO and AtPGLP1 quantifications). The RuBisCO in the Coomassie gel is used as a gel-loading control

after ¼ h, 1 h, 3 h and 7 h of exposure to the treatment and five independent plants were pooled to constitute three replicates. Again, in these experiments we wanted to determine whether leaf PGLP activity (using our GOX-coupled reaction) responded to an environmental stimuli and if any changes in measured activity could be correlated or not to AtPGLP1 protein levels (as determined by Western blots using our AtPGLP1 antibody serum) so as to get more insights into a potential post-translational regulation of AtPGLP1 *in planta*.

As shown in Figure 24a, leaf AtPGLP activity increased after only a ¼ h of exposure to whatever the environmental condition considered (high light, high temperature, high CO₂). Since these conditions impact photorespiration, the observed fast response provides a good indication that one level of AtPGLP1 activity regulation could occur through post-translational modifications (PTMs) whether by protein phosphorylation, protein oxidation-reduction or a yet to be identified PTM. This conclusion was strengthened by the fact that amount of PGLP1 protein was not seen to be significantly modified during the time course of the different treatments (Figure 24b). In each case, after 1 h of exposure, leaf AtPGLP activity returned to the level observed for control plants submitted to no treatment (NT). Both high light and high temperature are expected to increase photorespiration. The fact that PGLP activity rapidly and transiently increased could reflect the slower kinetics of other processes to occur that facilitate plant acclimation in response to these stressful environmental conditions. Surprisingly after ¼ h exposure to 1 % CO₂ (Figure 24a), AtPGLP1 activity also increased whereas a decrease would be predicted since the photorespiratory cycle is expected to be downregulated by a higher CO₂/O₂ ratio leading to a lower RuBisCO oxygenase activity. As previously mentioned, photorespiration and photosynthesis are intimately linked and the increased PGLP activity after ¼ h in high CO₂ could be related to an enhancement of photosynthesis requiring a higher RuBisCO activation level and thus also allowing for more oxygenase activity to take place before the plants could adjust to the new environmental conditions, for instance *via* the occurrence of CO₂-induced stomatal closure. After an hour in high CO₂, the measured leaf PGLP activity decreased and returned to a similar level observed in normal air, thus probably reflecting photosynthetic acclimation to such conditions.

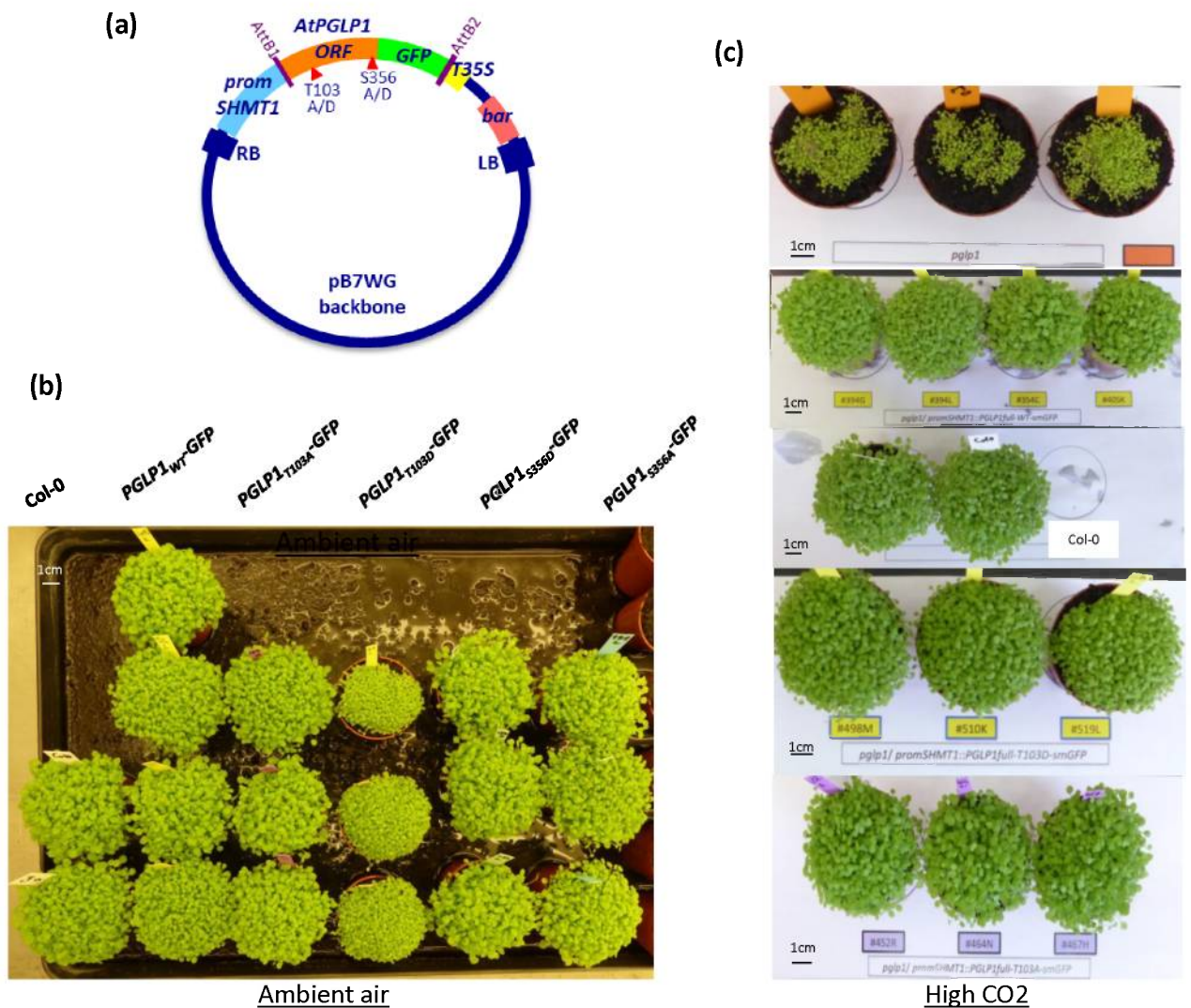


Figure 25: Functional complementation of *pglp1* homozygous mutant with the gene encoding modified proteins on potential phosphosites T103 and S356

(a) Schematic diagram of constructions prepared for generating *pglp1*-complemented transgenic lines. RB and LB are respectively the right and left border of TDNA-region; *promAtSHMT1* refers to the sequence of the *SHMT1* promoter region and *bar* is the gene that confers the resistance to the herbicide glufosinate-ammonium in plants. Red arrows represent the point mutation into alanine and aspartate on the resulting enzyme on residues T103 and S356. (b) Growth phenotype in normal air of the three (or four for *AtPGLP1*_{WT}-GFP) independent lines, homozygous with one insertion, selected for each complementation. The seedlings are two weeks old on the picture and have been cultivated in short day conditions. (c) Growth phenotype in high CO₂ (1 %) of the *pglp1* mutant and the complemented lines with *promAtSHMT1::AtPGLP1*_{WT}-GFP; *promAtSHMT1::AtPGLP1*_{T103D}-GFP; *promAtSHMT1::AtPGLP1*_{T103A}-GFP in that order from the top to the bottom. The same three independent lines as in (b) are shown, four for the WT form together with two Col-0 control seedlings.

II) Functional complementation of a homozygous *pglp1* mutant

1) Introduction

The PGLP1 activity and protein experiments performed on Arabidopsis Col-0 plants reinforced our hypothesis about a post-translational regulation of AtPGLP1. As previously mentioned, phosphoregulation of the 2C-cycle has already been suggested from phosphoproteomics data (see Hodges et al., 2013) and even tested on other photorespiratory enzymes (Hodges et al., 2013; Liu et al., 2019; Liu, 2019). Moreover, in our *in vitro* experiments, the analysis of the four potential phosphosites identified so far for AtPGLP1 (T103, T322, T330 and S356) showed that in two cases (T103 and T322) the activity of the phospho-mimetic enzymes was severely inhibited. However, considering the strong developmental phenotype of the homozygous *pglp1* mutant and the allocated time during a PhD, we decided to focus on two phosphosites for the *in planta* mutant functional complementation studies. In these experiments, the *pglp1* mutant was transformed by agroinfiltration with the AtPGLP1 ORF that included the sequence encoding the chloroplast targeting signal peptide and different mutations (done by site-directed mutagenesis) to produce modified chloroplastic PGLP1 proteins fused to the GFP (green fluorescence protein). The expression of AtPGLP1_{WT}-GFP and modified AtPGLP1-GFP was under the control of the photorespiratory *AtSHMT1* promoter (Hodges et al., 2013; Deller et al., 2016a; Liu et al., 2019). For each transformation, three independent homozygous lines with one insertion were *in vitro* selected using the *bar* gene that conferred resistance to glufosinate-ammonium as selection marker. Furthermore, all mutated AtPGLP1-GFP versions once introduced into *pglp1* plants were sequenced to validate the presence of the mutated form in each line.

The previous chapter showed that the mutation T103 to an alanine (a non phosphorylatable residue) had no impact on the kinetic parameters of recombinant AtPGLP1_{T103A} and its ability to form a homodimer, while the mutation to an aspartate that mimics a constitutive phosphorylation at this position completely abolished the activity of phospho-mimetic AtPGLP1_{T103D}, while rendering the recombinant protein insoluble. The yeast two-hybrid assay also showed that AtPGLP1_{T103D} homodimerization became very weak when compared to the WT protein. Taking into account all of these results, it was obvious that phosphorylation of T103 could have an important role *in planta* and therefore it was chosen as a phosphosite to further investigate by complementation of the Arabidopsis *pglp1* mutant with either AtPGLP1_{T103A}-GFP or AtPGLP1_{T103D}-GFP.

Although the phospho-peptide containing phosphorylated S356 had been found frequently in phosphoproteomics analyses, the other AtPGLP1 phospho-peptides have been found only once (see PhosPhAt 4.0 <http://phosphat.uni-hohenheim.de/>; (Heazlewood et al., 2008; Durek et al., 2010).

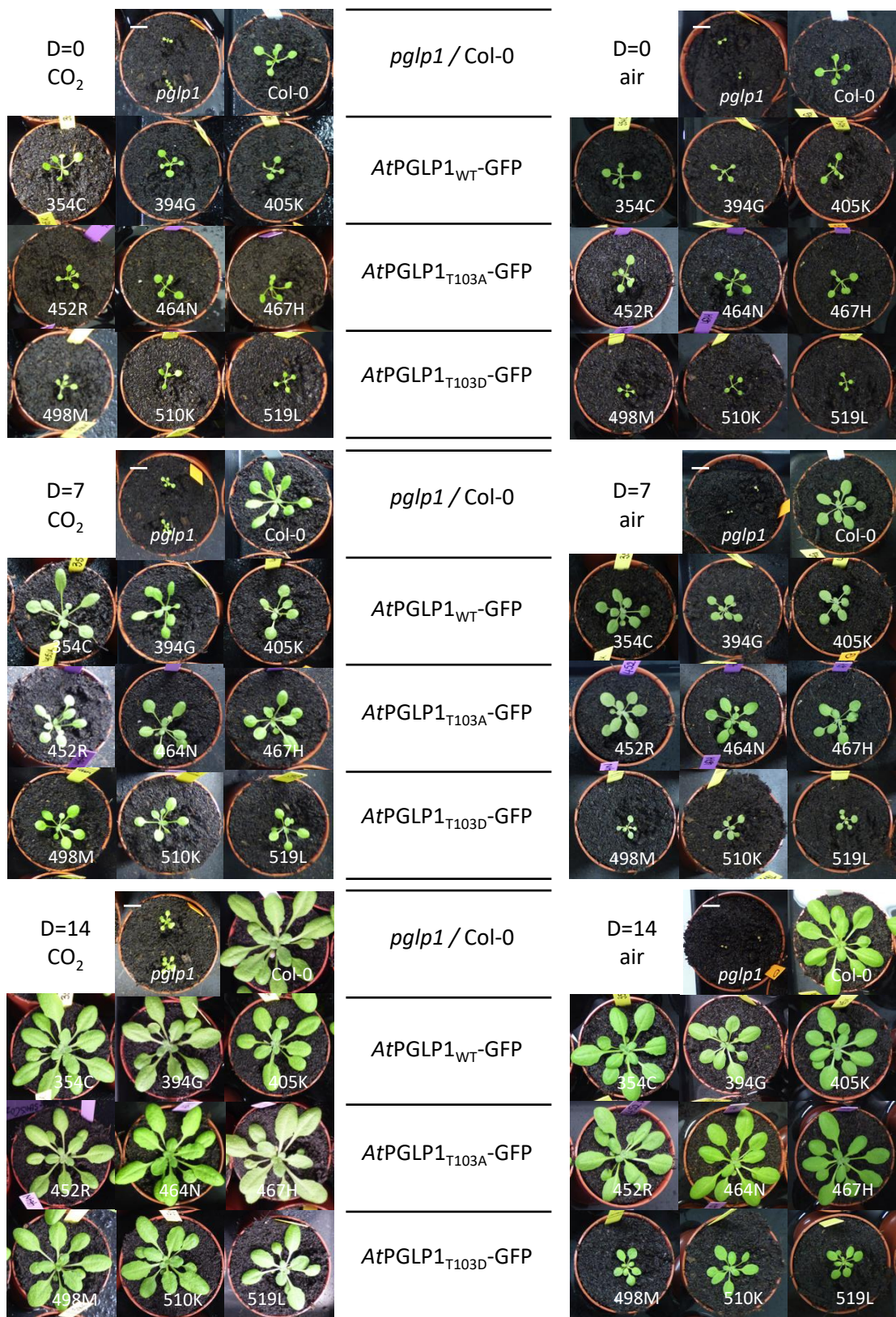


Figure 26: Growth phenotype of *pglp1* mutant and complemented lines by *AtPGLP1*_{T103A}-GFP; *AtPGLP1*_{T103D}-GFP; *AtPGLP1*_{WT}-GFP and Col-0 are controls

Three independent homozygous lines for the insertion of *AtPGLP1*_{T103A} or *D*-GFP transgene were analysed together with three independent lines for the insertion of *AtPGLP1*_{WT}-GFP, Col-0 control and the *pglp1* mutant. Young plantlets were obtained in high CO₂ (1 %) after germination in air. Then after the transfer into individual pots (time D=0) half remains for two weeks in high CO₂ (1 %; CO₂) in short day conditions and the other half is transferred in normal air (air) and short day conditions. Plants were pictured at D=0, 7 days after (D=7) and 14 days after (D=14). 354C, 394G, 405K: *pglp1*/ prom*AtSHMT1*::*AtPGLP1*_{WT}-GFP; 452R, 464N, 467H: *pglp1*/ prom*AtSHMT1*::*AtPGLP1*_{T103A}-GFP; 498M, 510K, 519L: *pglp1*/ prom*AtSHMT1*::*AtPGLP1*_{T103D}-GFP

Perhaps surprisingly, when S356 was mutated (S356D and S356A) this did not change either *AtPGLP1* activity or its homodimerization (as seen from two-hybrid assays but data not given in Chapter II). It is thus possible that this specific phosphosite, which is in an exposed C-terminus location in the predicted *AtPGLP1* 3D structure, could be involved in regulating *AtPGLP1* subcellular location or its interaction with other partners in the chloroplast, two features that were not ascertainable *in vitro*.

Furthermore, since the measured kinetic parameters of the recombinant *AtPGLP1* protein might not reflect the *in planta* reality (high K_m 2-PG for such an important enzyme, compared to the reported K_i 2-PG values for the inhibition of TPI, SBPase and PFK), because of the lack of putative cofactor(s) or a protein interactor(s), for example, it was possible that either S356A or S356D mutations could affect *AtPGLP1* *in planta* and thus impact the complementation of the *pglp1* mutant phenotype. Therefore, complementation of *pglp1* was also performed with the GFP-fused versions of *AtPGLP1*_{S356A/S356D} in order to decipher the role of this highly represented phosphosite. The second part of this chapter is thus focused on comparing the growth phenotype of the different Arabidopsis lines in either 1 % CO₂ or normal air.

2) Results

The Arabidopsis homozygous *pglp1* mutant can only grow under very high concentrations of CO₂. Even under 1 % CO₂, it still displayed a strong developmental phenotype (Figure 25c, first row). Interestingly, germination was possible and more efficient in ambient air, but for further growth, *pglp1* plants needed to be cultivated in high CO₂ where it still showed slower growth and a yellowish phenotype (Figure 25c; also Figure 22a). We thus tried to complement this mutant to see if a wild-type phenotype was recovered with our different *AtPGLP1*-GFP forms. At the seedling stage in ambient air, it was found that only the *AtPGLP1*_{T103D}-GFP lines still displayed a growth delay with smaller leaflets (Figure 25b), while this phenotype was absent in high CO₂ suggesting that the high amount of CO₂ in the chamber was enough to rescue the phenotype observed in ambient air (Figure 25c, row 4). Since the complementation appeared to be incomplete with *AtPGLP1*_{T103D}-GFP, it was decided to obtain a clearer phenotype in ambient air compared to high CO₂ by studying single plants in individual pots (Figure 26). First, this confirmed the severe *pglp1* mutant growth phenotype of small plants even in 1 % CO₂, while in ambient air the mutant died 7 days after sub-culturing in short day conditions. The complemented lines with *AtPGLP1*_{WT}-GFP and *AtPGLP1*_{T103A}-GFP displayed a developmental phenotype comparable to that of WT Col-0 control plants. On the contrary, the three independent lines carrying the phospho-mimetic *AtPGLP1*_{T103D}-GFP variant were smaller in normal air since day 0 although they were still able to develop (Figure 26, right side). The developmental delay persisted over the growing period since *AtPGLP1*_{T103D}-GFP plants remained smaller, even if the

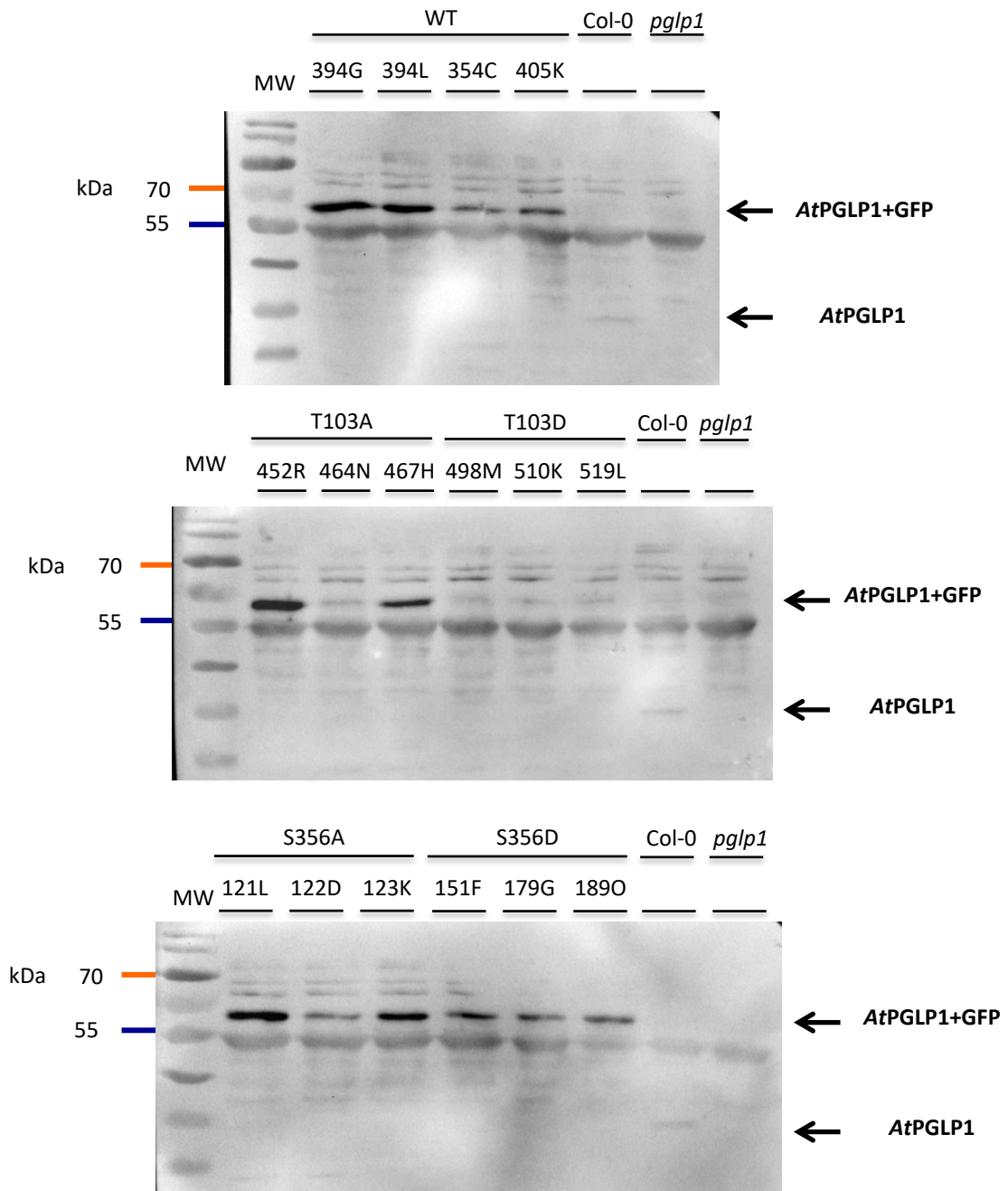


Figure 27: Amount of AtPGLP1 protein in complemented lines

Western blot performed as described in the Materials and Methods on proteins (8 μ g) extracted from leaves sampled at 2pm with AC I (our anti-AtPGLP1 serum) at 1:250 and AC II (HRP conjugated anti-rabbit IgG, A6154 Sigma) at 1:10000. The westerns were done on three independent lines for AtPGLP1_{T103A}GFP, AtPGLP1_{T103D}GFP, AtPGLP1_{S356A}GFP, AtPGLP1_{S356D}GFP and four independent lines for AtPGLP1_{WT}GFP. Col-0 and *pglp1* homozygous mutant were used as controls. The membrane was exposed for 45 s.

phenotype was less drastic than the *pglp1* mutant. When *AtPGLP1*_{T103D}-GFP plants were cultivated in high 1 % CO₂ and short day conditions, only a very slight growth delay was observed, and they almost completely recovered a WT phenotype (Figure 26, left side). Since lines expressing either *AtPGLP1*_{S356A}-GFP or *AtPGLP1*_{S356D}-GFP exhibited a WT growth phenotype in ambient and high CO₂ air, this suggested that S356 phosphorylation might not have a significant role under controlled growth conditions.

Unfortunately, the end of my thesis work suffered from a lack of 2-PG at the IPS2 since it had become extremely difficult to purchase this PGLP1 substrate due to the absence of stocks at all usual European suppliers. As a consequence of this, leaf PGLP activity measurements of the different lines could not be performed. Nonetheless, to start the characterization of our complemented plants, Western blot analyses were performed to evaluate *AtPGLP1* protein amounts in rosettes of each line. This was performed using either the serum containing antibodies directed against recombinant *AtPGLP1* or antibodies against GFP, with Col-0 and homozygous mutant plants used as controls. After confirming the absence of the *AtPGLP1*-GFP protein in the *pglp1* mutant and Col-0 leaves (Figure 27), we effectively detected this protein in leaves of *pglp1* plants transformed with *AtPGLP1*_{WT}-GFP using the anti-*AtPGLP1* serum (and also using anti-GFP but not presented here), and even if the amount of protein was not constant from one line to another a signal between 55 kDa and 70 kDa could be detected in all lines (Figure 27, top). This molecular mass corresponded to the *AtPGLP1* protein fused to GFP (*AtPGLP1*-GFP theoretical MW: 61 kDa). This protein was also detected in the three transgenic lines that expressed *AtPGLP1*_{T103A}-GFP, while the protein band corresponding to *AtPGLP1*-GFP in the plants transformed with *AtPGLP1*_{T103D}-GFP were seen to be very weak and this was the case for all of our three independent lines (Figure 27, middle). This could indicate that the phospho-mimetic *AtPGLP1* protein was unstable or/and quickly degraded. Nevertheless, it also strongly suggested that even a low amount of PGLP1 protein in *A. thaliana* is sufficient to allow plant survival even with a growth delay and to partially rescue the phenotype by comparison to the *pglp1* mutant (see Figures 25 and 26). However, that said, it was a surprise to see a partial complementation of the *pglp1* mutant with this *AtPGLP1* form since the recombinant protein purified from *E. coli* cells showed no measurable activity in our *in vitro* GOX-coupled reaction assay conditions. Finally, a PGLP1-GFP protein band was also visible in extracted proteins from plants complemented with *AtPGLP1*_{S356A}-GFP and *AtPGLP1*_{S356D}-GFP even if once again the amount of protein was not comparable among the different lines (Figure 27, bottom). In all cases, this could reflect a variation of the expression level of the *AtPGLP1*-GFP transgene due to a positional effect of the insertion in each independent line.

Photorespiration is dependent on the CO₂/O₂ ratio surrounding the RuBisCO and this can be affected by stomatal movements. By studying photorespiratory mutants, a link between stomatal

(a)

pB7WG-promAtSHMT1::PGLP1 _{WT} -GFP	<i>pglp1</i>
pB7WG-promAtSHMT1::PGLP1 _{T103D} -GFP	Col-0
pB7WG-promAtSHMT1::PGLP1 _{T103A} -GFP	



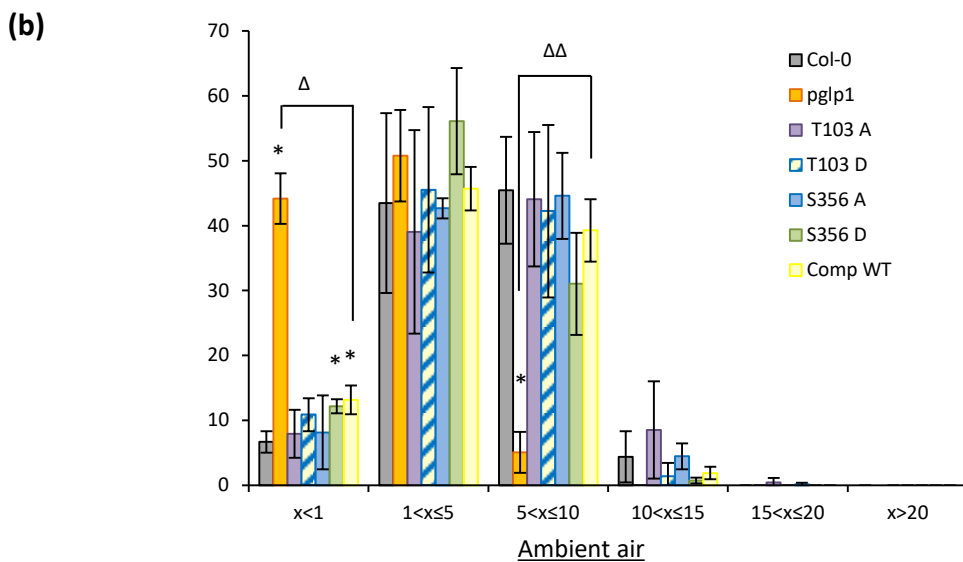
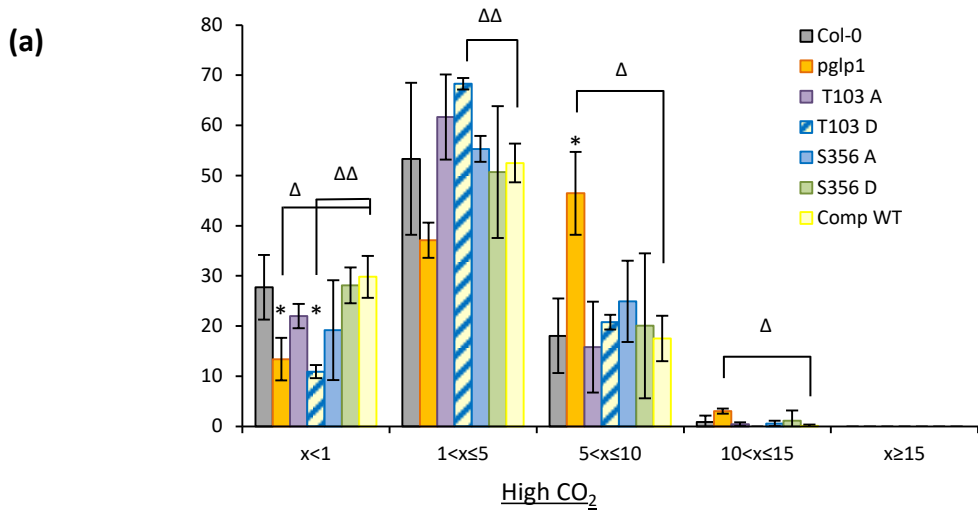
(b)

pB7WG-promAtSHMT1::PGLP1 _{WT} -GFP	<i>pglp1</i>
pB7WG-promAtSHMT1::PGLP1 _{S356D} -GFP	Col-0
pB7WG-promAtSHMT1::PGLP1 _{S356A} -GFP	



Figure 28: Growth phenotype of the complemented lines in high CO₂ (1 %) after 8 weeks in short days

(a) Homozygote transgenic lines transformed with *promAtSHMT1::AtPGLP1_{T103A}-GFP* : 452R, 464N, 467H; and with *promAtSHMT1::AtPGLP1_{T103D}-GFP* : 498M, 510K, 519L. Homozygote transgenic lines transformed with *promAtSHMT1::AtPGLP1_{WT}-GFP* : 354C, 394L, 405K ; Col-0 and *pglp1* mutant are used as controls. (b) Homozygote transgenic lines transformed with *promAtSHMT1::AtPGLP1_{S356A}-GFP* : 121L, 122D, 123K ; and with *promAtSHMT1::AtPGLP1_{S356D}-GFP* : 151F, 179G, 189O. Homozygote transgenic lines transformed with *promAtSHMT1::AtPGLP1_{WT}-GFP* : 354C, 394L, 405K; Col-0 and *pglp1* mutant are used as controls.



(c)

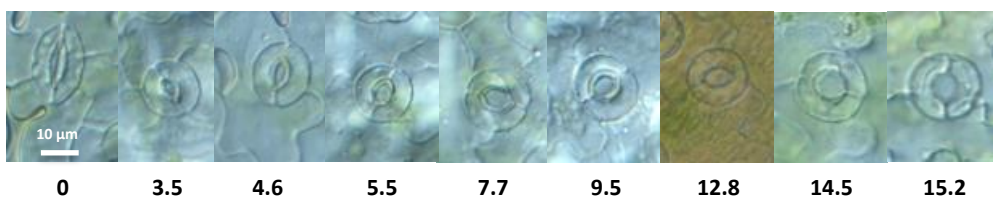


Figure 29: Stomatal movement in complemented lines in ambient air compared to high CO₂ (1%)

(a and b) Graphs representing the stomata repartition according to the percentage of stomatal aperture, for all transgenic lines transformed either by *AtPGPL1_{WT}-GFP*, *AtPGPL1_{T103A}-GFP*, *AtPGPL1_{T103D}-GFP*, *AtPGPL1_{S356A}-GFP*, *AtPGPL1_{S356D}-GFP*. Col-0 plant and *pglp1* mutant are used as controls. For every genotype, three independent lines were analysed and for each line between 200 and 300 stomata were quantified (measurement of ostiole and guard cell surface). Statistical significance was determined by a Student's *t*-test (**P*<0.05 by comparison with the Col-0; ^Δ*P*<0.01; ^{ΔΔ}*P*<0,001 by comparison to the complemented WT). (a) Leaves were collected on plants grown in high CO₂ and (b) leaves were collected on plants 24 h after the transfer from high CO₂ to ambient air. (c) Pictures reflecting the gradual stomatal aperture. Numbers under the pictures indicate the percentage of stomatal aperture calculated for the stomata shown above from closed (left) to opened (right) stomata. Photographs were taken with a microscope Axio-Imager Z2 (Zeiss).

movements and a blocked photorespiratory cycle has been reported, and although the exact mechanism was not elucidated it might be linked to ABA (Eisenhut et al., 2017; Liu et al., 2019). It should be noted that the potential phosphosite S356 was found in a phosphoproteome study that tried to get more insight on ABA signalisation (Umezawa et al., 2013). By indirectly measuring stomatal aperture *via* leaf transpiration, Eisenhut et al., (2017) proposed that Col-0 plants and the weak photorespiratory *hpr1* mutant had their stomata more closed in high CO₂ and more open after one day of transfer to normal air when compared to strong photorespiratory mutants including *pglp1* that exhibited opposite transpirational features.

Before measuring the stomatal movements of our transgenic and control lines, their growth phenotype after 8 weeks in 1 % CO₂ short-day conditions was noted. No obvious growth phenotype of the different complemented lines (including the T103D lines) was observed with only the *pglp1* mutant exhibiting retarded growth (Figure 28). We then measured stomatal aperture size of the complemented lines *AtPGLP1_{WT}-GFP*; *AtPGLP1_{T103A}-GFP*; *AtPGLP1_{T103D}-GFP*; *AtPGLP1_{S356A}-GFP*; *AtPGLP1_{S356D}-GFP* and compared their behaviour to Col-0 control plants and the homozygous *pglp1* mutant. To express the results, stomatal aperture of fixed epidermal strips was calculated as the percentage of the ostiole area with respect to the whole stomata surface (of the two guard cells) and values were ordered according to different classes (Figure 29). When the percentage $x < 1$, stomata were considered as closed and when $15 < x < 20$ they were considered to be fully open (Figure 29c). In our experiments, the *pglp1* mutant displayed the expected stomatal behaviour as previously suggested from the measurement of transpiration rate (Eisenhut et al., 2017). Indeed, the stomata of the *pglp1* mutant were statistically more open than those of control Col-0 plants and complemented transgenic lines transformed with *AtPGLP1_{WT}-GFP* when the epidermal strips were fixed under high CO₂. However, after a 24 h transfer to normal air, there was an increase in the number of more closed stomata of mutant leaves compared to the control Col-0 and *AtPGLP1_{WT}-GFP* complemented lines (Figure 29). At 1 % CO₂, although the stomatal aperture in the transgenic lines transformed with *AtPGLP1_{T103D}-GFP* showed a similar low number of “closed” stomata ($x < 1$) as the *pglp1* mutant, it did not appear to be affected as much since the majority of their stomata were found in the more open categories. On the contrary, after transfer to ambient air where the mutant displayed a pronounced massive closure of their stomata, the transgenic lines that expressed *AtPGLP1_{T103D}-GFP* behaved as Col-0 plants and *AtPGLP1_{WT}-GFP* complemented lines with stomata of *AtPGLP1_{T103D}-GFP* leaves being more opened than closed (Figure 29). Regarding the other transgenic lines (T103A, S356A and S356D), no overall differences in stomatal behaviour were observed compared to control Col-0 plants and *AtPGLP1_{WT}-GFP* complemented lines. Perhaps, as shown in Figure 29, transgenic lines transformed with *AtPGLP1_{S356D}-GFP* displayed a slightly ‘more closed stomata’ phenotype compared to Col-0 plants when transferred to ambient air since there were statistically more completely closed

stomata and they tended to be more represented in the class $1 < x < 5$ than $5 < x < 10$ compared to Col-0 and several other genotypes. Finally, since these transfer experiments were only repeated once for all transgenic lines, they need to be replicated to obtain more robust data.

As for the growth phenotype, the stomatal behaviour of AtPGLP1_{T103D}-GFP transgenic lines suggested that the mutant phenotype was not fully complemented in these lines. They displayed a developmental delay in ambient air that was rescued by 1 % CO₂ however this was not the case for *pglp1*. Concerning stomatal movements, AtPGLP1_{T103D}-GFP stomata tended to be slightly more closed than for the other transgenic lines while the short-term adaptation during a transfer to normal air did not appear to be problematic since stomatal aperture values were comparable to Col-0. On the other hand, AtPGLP1_{T103A}-GFP lines did not show any differences in growth and stomatal behaviour when compared to either Col-0 or AtPGLP1_{WT}-GFP complemented lines. Therefore, if there was a negative regulation of AtPGLP1 by T103 phosphorylation, the impossibility to phosphorylate the protein at this site *in planta* was not detrimental for plant growth and stomatal movements in our controlled conditions. Finally, despite its frequent abundance in the PhosPhAt database, the role of AtPGLP1 S356 phosphorylation still remains to be elucidated.

GENERAL DISCUSSION AND PERSPECTIVES

I) Reminder of the scientific background

In the literature, most primary metabolism pathways are well-described in plants, with characterized mutants. However, a lot of knowledge is still lacking with respect to the regulation of these metabolic routes. Since there are major cross-talks between different metabolic pathways, it still represents a major challenge to gather strong evidence regarding the regulation of plant metabolism. During my PhD I had the opportunity to study post-translational regulations of enzymes belonging to two major metabolic pathways; glycolysis occurring in all living organisms, and photorespiration that is necessary for air-grown photosynthetic organisms.

1) Investigation of the *At*iPGAM reaction mechanism, a glycolytic enzyme

Glycolysis has been known and studied for a very long time (see Givan, 1999). It is believed to occur more at night to generate energy and reducing power in the cytosol, in the absence of photosynthesis, from starch and sugars synthesized and accumulated during the day (see Tcherkez et al., 2008). Since glycolysis is ubiquitous in the living kingdoms, I took advantage of our knowledge from other organisms to decipher the reaction mechanism of *At*iPGAM that catalyses the C3 to C2 transfer of the phosphate of 3-PGA to produce 2-PGA in the cytosol. This reaction is reversible and depends on the presence of divalent cations (Jedrzejewski et al., 2000; Nowicki et al., 2009; Mercaldi et al., 2012; Roychowdhury et al., 2015). Since the regulation of plant iPGAM had not been extensively studied, it was interesting to find a highly occurring iPGAM phosphopeptide in a substantial number of *A. thaliana* phosphoproteomes (see PhosPhAt 4.0 at <http://phosphat.uni-hohenheim.de/>). However, these large-scale experiments bring only a limited amount of information about specific regulation processes, and therefore the principal aim of my work concerning this enzyme was to investigate the significance of this phosphosite. Indeed, it could have been either the result of a classical PTM by protein phosphorylation *via* a protein kinase, or a catalytic intermediate associated with the phosphate transferred from one carbon to another during the enzymatic reaction. Interestingly these two hypotheses were not mutually exclusive.

2) Analyses of post-translational regulations of AtPGLP1, a photorespiratory enzyme

Several photorespiratory mutants were initially identified in *A. thaliana* through the development of the famous screen led by Somerville and his co-workers (Somerville and Ogren, 1979; Somerville and Ogren, 1980c; Somerville and Ogren, 1980a; Somerville and Ogren, 1981; Somerville et al., 1982; Somerville and Ogren, 1982; Somerville and Ogren, 1983). Since then, the identification of photorespiratory cycle genes has been achieved mainly due to the complete sequencing of the Arabidopsis genome, the generation of T-DNA mutant libraries and the characterization of identified mutants using the classical “Somerville” photorespiratory screen of a retarded growth phenotype in air that is rescued in high CO₂ (see the list of mutants and the respective publications in Table 1, section “Introduction paragraph III”). Identified mutants were then used to further investigate photorespiration and its interactions with leaf metabolism. In photosynthetic organisms, photorespiration works side by side with photosynthesis, and when the photorespiratory cycle becomes limited it can have an inhibitory effect on both the light and dark sides of photosynthesis (Dellero et al., 2015b; Dellero et al., 2016a). Since photorespiration interacts with several important metabolic pathways (Hodges et al., 2013) we believed that it must be finely regulated however a lot of knowledge was still lacking in this area. During my PhD I focused on the post-translational regulation of the first photorespiratory enzyme in *A. thaliana*, PGLP1. As sessile organisms, plants need to quickly integrate and react to various environmental stimuli and therefore it seemed consistent to investigate this type of regulation. Interestingly, phosphopeptides for all but one (GLYK) of the core photorespiratory enzymes had been found in diverse phosphoproteomes before the start of my PhD project (see Hodges et al., 2013). Therefore, my task consisted of obtaining more insights into the role of the four potential phosphosites identified for AtPGLP1 ((Reiland et al., 2009; Aryal et al., 2012); PhosphAt 4.0). Furthermore, it was known that the chloroplast is susceptible to oxidation-reduction changes arising from the redox reactions occurring during photosynthesis. Moreover, it had been shown that photorespiratory enzymes undergo redox-related post-translational modifications (Palmieri et al., 2010; Ortega-Galisteo et al., 2012; Camejo et al., 2013; Keech et al., 2017) including thioredoxin-dependent modifications in mitochondria (Marchand et al., 2004; Fonseca-Pereira et al., 2019; Reinholdt et al., 2019). Finally, since mammalian PGP had been shown to be redox regulated (Seifried et al., 2016), we wanted to establish whether AtPGLP1 could be regulated by its oxidation-reduction status.

II) Catalytic mechanism of the phosphoglycerate mutase

The phosphoglycerate mutase converts 3-PGA to 2-PGA during glycolysis; however the reaction is reversible. As previously mentioned, two forms of PGAM exist in living organisms namely the dPGAMs and the iPGAMs (dependent or independent of 2,3-biphosphoglycerate as a cofactor, respectively). Since vertebrates only possess dPGAM enzymes while many of their parasites perform glycolysis with iPGAM, this latter enzyme constituted a target of choice for the development of antibiotics and therefore knowledge of their reaction mechanism and regulation were of great use to achieve this aim (Fothergill-Gilmore and Watson, 1989). The strong developmental phenotype of the *ipgam1ipgam2* double mutant of *A. thaliana* and *ipgam* antisense of potato demonstrated the requirement of at least one functional iPGAM gene in the plant (Westram et al., 2002; Zhao and Assmann, 2011). The iPGAM reaction had been shown to be highly dependent on the presence of two divalent cations, Mg^{2+} in our case, and it was possible *via* an open/close conformation of the protein by the concerted action of specific catalytic residues that led to an intermediary transient phospho-serine (Jedrzejewski et al., 2000a). During my PhD, the work I performed on the *A. thaliana* enzyme suggested that the plant iPGAM reaction mechanism involved the transient phosphorylation of serine 82 during the isomerisation of phosphoglycerate. Indeed, this serine residue was found to be phosphorylated on a relatively abundant phosphopeptide present in PhosPhAt 4.0. However, we surprisingly found that the quantity of this phosphopeptide was statistically higher in the light when compared to dark conditions in Arabidopsis leaves, while it had already been established that glycolysis in plants was more active during the night (see Tcherkez et al., 2008). It thus seemed that a regulatory mechanism could be occurring, and our working hypothesis was that *AtiPGAM* phosphorylation by a protein kinase occurred during the day and obstructed the catalytic serine, preventing the fixation of the substrate. Unfortunately, this remained difficult to test for several reasons. We wanted to take advantage of the characterized enzyme forms *AtiPGAM*_{D29N} (blocked in a closed conformation, therefore no formation of 2-PGA = higher amounts of phosphoserine 82) and *AtiPGAM*_{R290L} (no 3-PGA binding, therefore no phosphotransfer from the substrate = no phosphoserine 82, see results “Chapter I”) *in planta* to test our hypothesis. However, both of these enzymes were inactive and, since the double *ipgam* mutant was sterile, and its development highly impaired (Zhao and Assmann, 2011), functional complementation was thus not possible with these mutated *AtiPGAM* forms. We tried to circumvent this problem and transformed WT, Col-0 plants with a phosphopeptide containing an additional mutation (a threonine instead of a serine at position 75 that was shown not to affect iPGAM activity) to allow its discrimination with respect to endogenous *AtiPGAM*. At this point, we were faced with a second challenge that was the limitation

of detecting the different peptides (phosphorylated or not) by (phospho)proteomics. Indeed, even if the accuracy of the methods in that domain has increased over the years, there are still a number of technical constraints. First, the m/z that is supposed to be characteristic of each peptide is dependent on the analytic machine. Therefore, previous data cannot be used from one laboratory to another. Moreover, since peptide identification is mainly based on m/z values it is possible that labelling used for *in planta* experiments does not modify enough this parameter to allow identification of the modified phosphopeptide. In our case, different phosphoproteome analyses were never carried out in the same way by PAPPISO either due to technical advances or due to technical problems. Furthermore, phosphopeptides are prone to be falsely discovered and false discovery rates (FDR) are often not taken into account, while most analyses are not quantitative. Surprisingly, one analysis carried out by PAPPISO identified our mutated phosphopeptide in plants that did not contain it. Our study of *AtiPGAM* tended to show that phosphoproteomic experiments should be interpreted with care for another reason since the identification of the *iPGAM* phosphopeptide did not necessarily mean that it was phosphoregulated. This possibility still needs to be confirmed with supplemental experiments. Another issue in phosphoproteomics studies, as in most large-scale analyses, is that highly abundant peptides make low abundance peptides difficult to detect and to quantify. This is a recurrent problem when experiments are carried out on plant extracted proteins. A possible way to circumvent this problem is to specifically extract the protein of interest by immunoprecipitation. Unfortunately, in our case, specific *AtiPGAM* antibodies were not available. Therefore, a short-term perspective for this project could be either to use His-tag purified *AtiPGAM* to make antibodies, or to transform *Arabidopsis Col-0* plants to express *AtiPGAM_{D29N}* and *AtiPGAM_{R290L}* proteins fused to a tag. In this way, *AtiPGAM* immunoprecipitation could be performed with commercial antibodies raised against the chosen tag. The advantage of the latter method would be that endogenous *AtiPGAM* proteins are no longer a problem and only the introduced modified protein would be analysed in the down-stream proteomics analyses. Using this strategy, we believe it would be possible to see whether *AtiPGAM_{R290L}* could be phosphorylated and if this depended on environmental conditions. In this way, we can confirm or invalidate the possible regulation of *AtiPGAM* by a kinase-dependent protein phosphorylation during the day since we have already shown that *in vitro* recombinant *AtiPGAM_{R290L}* displayed no S82 phosphopeptide. Alternatively, we also have to consider the possibility that the more important phosphorylation during the day (due to more S82 phosphopeptide) is not the result of a phosphoregulation by a kinase but due to a higher daytime *iPGAM* activity compared to the night even if it is not consistent with the literature. Indeed, it has been demonstrated that glycolysis mainly occurs at night and thus *iPGAM* as a glycolytic enzyme would be expected to be more active during this period. However, *iPGAM* activity may be important in other processes occurring during the daytime. It is also possible that 3-PGA and 2-PGA

are not the only substrates of this enzyme. Finally, we can also consider that AtiPGAM is less active during day and that it becomes more 'blocked' with the substrate inside the catalytic centre and therefore the phosphopeptide is more abundant.

It was mentioned above that some vertebrates only have dPGAM while some human pathogens only possess iPGAM (Fothergill-Gilmore and Watson, 1989), and therefore iPGAM became a target to develop drugs to inhibit its activity. Successful examples include *P. falciparum* that causes malaria in humans and several microorganisms/nematodes that are human pathogens (Sharma et al., 2013; Crowther et al., 2014; Timson, 2016; Ríos-Soto et al., 2018). In *A. thaliana*, it is still not clear if there is also a dPGAM isoform and what would be its role(s) since the *ipgam1ipgam2* double mutant has a severe growth delay and sterility problems. Therefore, the same logic could be applied to fight against plant pathogens that only have dPGAM, and indeed this was experimented on wheat germ more than 40 years ago (McAleese et al., 1987) with an inhibitor that selectively targeted the yeast protein. A major problem of this strategy is that if the molecule inhibits dPGAM then it could also be detrimental for vertebrates including humans.

III) Phosphoglycolate phosphatase activity and regulation in *A. thaliana*

1) AtPGLP1 activity

In plants, 2-PG is considered toxic because of its inhibitory action towards several important enzymes; PFK, TPI, SBPase (Anderson, 1971; Kelly and Latzko, 1976; Flügel et al., 2017). Therefore, the role of photorespiratory PGLP in photosynthetic organisms is thus major (cf the strong developmental mutant phenotype, Schwarte and Bauwe, 2007) and we believe that the gene/protein probably undergoes various regulations to maintain the required enzymatic activity. As mentioned before, we focused on the post-translational regulation of the AtPGLP1 protein. Indeed, clues from literature indicated a potential phospho-regulation/redox regulation of this important enzyme (Hodges et al., 2013; Hu et al., 2015) and the rapid increase of AtPGLP activity (without any change in AtPGLP1 protein amount) in Col-0 leaves after a 1/4 h exposure to environmental conditions affecting photorespiration (high light, high temperature, elevated CO₂) is another observation in favour of a post-translational regulation (see Chapter III).

During my PhD, I did not only investigate AtPGLP1 regulation but also its activity using *in vitro* methods. The measured K_m for 2-PG was found to be surprisingly high for this enzyme although in the same order of magnitude as the PGLP of *Zea mays*, a C₄ plant (Hardy and Baldy, 1986). Even if studies on photorespiration in C₄ plants (*Flaveria bidentis* and *Zea mays*) showed the need for a

functional 2C-cycle (Zelitch et al., 2009; Levey et al., 2019), we might have expected a different K_m 2-PG for the enzyme of C_3 plants because of a more active 2C-cycle. The higher than expected K_m was not due to the method used to measure AtPGLP1 activity since similar values were obtained with our GOX-coupled reaction, the phosphate sensor method and by NMR. This high K_m appeared to be incompatible with the low reported K_i of 2-PG with respect to TPI, PFK and SBPase inhibition (Anderson, 1971; Kelly and Latzko, 1976; Flügel et al., 2017) and suggested that perhaps the measured K_m 2-PG of our recombinant AtPGLP1 did not reflect the value for the protein *in planta*. Indeed, the K_m 2-PG measured using PGLP purified from photosynthetic organisms was often an order of magnitude lower than our recombinant protein. This incoherence needs to be resolved and therefore a very short-term perspective would be to investigate the kinetic parameters of AtPGLP1 present in leaf extracts. As stated earlier, this was not possible to do at the end of my thesis work due to problems in world-wide 2-PG supplies. The difference between our recombinant AtPGLP1 and plant purified PGLP could be due to the lack of an element in the reaction buffer such as another cofactor, an activating protein or even a post-translational regulation that is present or has occurred *in planta*.

During our characterization of recombinant AtPGLP1, the requirement of specific divalent cations was tested, and it was found that Mg^{2+} was the most efficient for *in vitro* AtPGLP1 activity while Mn^{2+} was less efficient leading to a lower k_{cat} . Interestingly, the chloroplastic stromal Mn^{2+}/Mg^{2+} ratio has been suggested to influence the balance between the carboxylase and oxygenase activities of RuBisCO with a lower carboxylase activity proposed when Mn^{2+} is bound to the enzyme (Bloom and Lancaster, 2018). In this context, AtPGLP1 might be expected to be more active in the presence of Mn^{2+} as a cofactor however in the tested conditions during my PhD this was not the case (Bloom and Lancaster, 2018b). Moreover it has been suggested that a light-induced increase in Mg^{2+} concentration in the chloroplast stroma could be sufficient to regulate certain physiological processes including photosynthesis (Portis and Heldt, 1976; Portis, 1981). Therefore a possible cation-dependent regulation of AtPGLP1 activity might take place in the light in chloroplasts however this cation-dependence was also seen in non-photosynthetic HAD family enzymes. This will be discussed later.

2) AtPGLP1 phosphoregulation

Our *in vitro* GOX-coupled reaction method allowed us to measure a highly decreased specific activity for phospho-mimetic AtPGLP1_{T322D} compared to the WT protein and AtPGLP1_{T322A}. Interestingly, the K_m 2-PG of AtPGLP1_{T322D} remained unchanged and similar to that of AtPGLP1_{WT}. This result suggested that the eventual phosphorylation of this residue would not change the affinity

between the protein and its substrate but only the rate of the enzymatic activity, and thus a reduced specific activity. On the other hand, the phospho-mimetic *AtPGLP1*_{T103D} did not show any activity until 1 mM 2-PG was added to the reaction medium whereas *AtPGLP1*_{T103A} activity and K_m 2-PG were identical to those of the WT protein. It would be interesting to examine whether the phosphosite mutated recombinant proteins had an altered divalent cation dependency that could explain their reduced activities. Furthermore, the mutation of *AtPGLP1*_{T103D} not only abolished enzymatic activity, but also strongly affected its solubility and decreased its ability to form homodimers. These observations make us believe that protein conformation and/or stability was impaired with just this point mutation. The mutation of T322 (to an alanine or to an aspartate) also made both recombinant proteins difficult to purify, again suggesting that this residue was important for protein stability and/or conformation however only *AtPGLP1*_{T322D} displayed a lower k_{cat} .

My study of *AtPGLP1* phosphoregulation also included *in vivo* complementation of the homozygous *pglp1* mutant by the expression of the following proteins: *AtPGLP1*_{T103A}; *AtPGLP1*_{T103D}; *AtPGLP1*_{S356A}; *AtPGLP1*_{S356D} all fused to the GFP. Western blots performed on leaf extracts containing *AtPGLP1*_{T103D} suggested that the phospho-mimetic mutation affected protein stability/turnover since less *AtPGLP1* was detected in the three independent lines when compared to *AtPGLP1*_{WT} containing plants. A similar protein stability effect was proposed for phospho-mimetic SHMT1 lines during a salt stress in *A. thaliana* (Liu et al., 2019). Unexpectedly, given the low protein levels in the complemented lines and the lack of activity of the recombinant *AtPGLP1*_{T103D} enzyme, the restoration of the *pglp1* growth phenotype of our *AtPGLP1*_{T103D} complemented lines, whether partial in ambient air or complete in 1 % CO₂ was surprising. The incoherence between our *in vitro* and *in vivo* results concerning *AtPGLP1*_{T103D} again suggested that the *in vitro* activity measurements might not reflect what was occurring *in planta* since apparently, *AtPGLP1*_{T103D} activity was sufficient to improve plant growth in ambient air. Therefore another short-term perspective is to measure *AtPGLP* activity of leaf protein extracts from our different complemented lines and to compare them with the activity of Col-0 leaf extracts.

A link between stomatal movements and photorespiratory cycle activity was observed in experiments carried out during my PhD where a comparison of stomatal aperture size of high CO₂ grown plants and plants transferred to normal air for 24 h using our different lines was carried out. In this way, we found that *pglp1* stomata were more open in high CO₂ and more closed in ambient air, compared to Col-0 and *AtPGLP1*-GFP-complemented lines. These results confirmed similar conclusions made from the indirect transpiration rate results of *pglp1* plants (Eisenhut et al., 2017). Finally, stomatal aperture appeared to be partially affected in *AtPGLP1*_{T103D} lines, and perhaps expected since the growth phenotype was only partially rescued in ambient air. Therefore, our results strengthened the notion that photorespiratory processes are somehow involved in controlling

stomatal movements and more work is required to better understand how this is achieved. For instance, it would be interesting to find out whether this relies on guard cell metabolism by specifically down-regulating the photorespiratory cycle either in guard cells or in mesophyll cells. The involvement of specific stomatal signaling pathways should also be investigated for instance by crossing known signaling mutants with photorespiratory mutants.

Another surprising result was that mutation of serine 356 did not affect either *AtPGLP1* activity or the phenotype of completed *pglp1* lines while this phosphosite had been found in many distinct phosphoproteomes. However, since phosphorylation is a rapid, temporary and reversible response to specific stimuli, it is possible that conditions required for S356 phosphorylation to have an important role were not used in my PhD work. We can also consider the possibility that this phosphosite does not have a regulatory role and it is just the consequence of a non-specific kinase activity due to a weak consensus kinase motif at the identified phosphosite (Reiland et al., 2009). It is also a possibility that S356 phosphorylation can regulate *AtPGLP1* subcellular localization although this is probably not the case since RuBisCO is uniquely in plastids and toxic 2-PG must be rapidly metabolized to stop Calvin cycle enzyme inhibition. That said, PGLP1 might be able to act in the cytosol *via* the diffusion or an active transport of 2-PG across the chloroplast envelope, perhaps *via* either TPT, PLGG1 or BASS6. In our cloning strategy, we adopted to complement the *pglp1* mutant with *AtPGLP1*-GFP fusion proteins with the aim to investigate by confocal microscopy whether subcellular localization was altered in phosphosite-mutated *AtPGLP1*. This will be done in the near future.

Protein phosphoregulation studies are now often initiated by the identification of one or more phosphopeptide(s) in one or several large-scale phosphoproteome(s). Unfortunately, this approach is prone to significant false discovery rates that lead to the misidentification of phosphopeptides. This is why we tried to confirm *AtPGLP1* phosphorylation *in planta* by immunoprecipitation of *AtPGLP1* from leaf extracts followed by mass spectroscopy. This was performed using plants exposed to environmental changes impacting photorespiration with the aim of validating published *AtPGLP1* phosphosites and to identify conditions leading to *AtPGLP1* phosphorylation. Unfortunately, as seen from western blots in Chapter III, our *AtPGLP1* antibody serum recognized many other leaf proteins. Therefore, after immunoprecipitation the samples were not pure enough to detect *AtPGLP1* phosphopeptides. This problem could be eventually circumvented because *pglp1* was complemented to produce *AtPGLP1*-GFP fusion proteins. Therefore, commercial antibodies directed against GFP can be used for future immunoprecipitation assays. Alternative methods are also available to confirm, at least, that a protein is phosphorylated. In our case, the complemented plants would be helpful to confirm *AtPGLP1* phosphorylation either by using radiolabeled-ATP and leaf extracts and/or percoll-purified intact chloroplasts containing mutated proteins at specific phosphorylation sites, or by

Western blotting either using antibodies directed against phospho-serine or phospho-threonine or after Phos-tag SDS-PAGE. Although such experiments would not provide the exact phosphorylation site, the use of plants containing phosphosite mutated proteins would help. For instance, if the antibody binds to AtPGLP1 from WT plants but not to AtPGLP1 from either the T103 or S356 lines, it would validate a specific phosphosite. The same reasoning would apply when using radiolabeled-ATP.

After validating AtPGLP1 phosphosites, the ultimate step of our phosphoregulation studies would be the identification of the protein kinase(s) involved in the regulatory process. To date, nothing is currently known about a potential kinase targeting AtPGLP1. Taking into account the number of kinases in *A. thaliana* (around 1050), it was estimated that 80 of them would be chloroplastic (Schönberg and Baginsky, 2012). However, only about twenty protein kinases are currently chloroplast-located in *A. thaliana*, with perhaps the best characterized being STN7, STN8 and cpCK2 (Baginsky and Gruissem, 2009; van Wijk et al., 2014). STN7 and STN8 are thylakoid associated proteins shown to regulate short-term acclimation of plants to changing light conditions by phosphorylating light-harvesting antenna proteins of PSII (LHCII) during state transitions (STN7) and PSII core proteins (STN8) thus controlling both linear and cyclic photosynthetic electron transfer (Schönberg et al., 2017). Phosphoproteomes performed on *stn7* and *stn8* mutants suggested that AtPGLP1 was not a STN7/8 target (Reiland et al., 2011; Schönberg et al., 2017). Another well-known kinase in the chloroplast is called the chloroplast sensor kinase (CSK) and it responds to cell redox changes (Puthiyaveetil et al., 2008). The non-exhaustive list of chloroplastic kinases includes ABCK1-3 kinases (some being light regulated), some MAP kinases and calcium dependent kinases (Ytterberg et al., 2006; Bayer et al., 2012). Since we have currently no idea about the kinase(s) regulating AtPGLP1 and kinase sequence recognition motifs surrounding the AtPGLP1 phosphosites do not clearly indicate any specific class of protein kinases, it will be necessary to get more insights into the conditions that lead to AtPGLP1 phosphorylation to help select promising kinases to carry out *in vitro* and *in planta* assays. Meanwhile, future phosphoproteomes of known chloroplast kinase mutants could allow the discovery of an AtPGLP1 kinase.

3) AtPGLP1 and HAD proteins family

HAD protein family phosphatases, as previously mentioned, share some common amino acid sequences (four conserved motifs, all found in AtPGLP1), the Rossmannoid structure, and a cap domain that is more variable and depends on the substrate and the reaction mechanism (Seifried et al., 2013). Moreover, these proteins are depend on Mg^{2+} to perform the phospho-transfer from 2-PG

to the catalytic site aspartate (Rose et al., 1986). It was previously shown that most HAD proteins were stable as homodimers in mammals and most of the phosphatases could oligomerize *via* cap/cap domain interactions (Seifried et al., 2013; Kestler et al., 2014; Seifried et al., 2016a). Our yeast two-hybrid assays performed with AtPGLP1 confirmed its ability to form a homodimer and this by virtue of at least two structures of the cap domain (one α -helix and one β -strand). The deletion of these structures led to the complete abolition of enzyme activity suggesting that homodimerization was a prerequisite for AtPGLP1 activity. The many common features found between the mammalian and *A. thaliana* proteins led us to wonder if besides its role in photorespiration, plant PGLP could have other functions. Indeed, in non-photosynthetic organisms such as mammals, bacteria and yeast, PGP is involved in the detoxification of 2-PG produced during DNA double strand break repair processes (Teresa Pellicer et al., 2003; Collard et al., 2016a; Segerer et al., 2016). We hypothesized that the strong developmental phenotype of *pglp1* even in high 1 % CO₂ could be the consequence of its involvement in metabolic processes other than photorespiration. Some preliminary experiments were carried out to test this idea, and included the application of a UV-light treatment to Col-0 plants, and treatments with chemicals inducing double strand breaks in nuclear and chloroplastic DNA (bleomycin and ciprofloxacin, respectively), followed by the measurement of AtPGLP activity. As yet, the results were not conclusive and it remains a hypothesis to consider in the future.

Such considerations also lead us to question the role of AtPGLP2. It was mentioned in the introduction that two PGLP proteins are present in *A. thaliana*. It has been shown that AtPGLP2 is a cytosolic enzyme, the KO mutant did not exhibit any growth phenotype and it was responsible for only 3 % of total PGLP activity in *A. thaliana* leaves (Schwarte and Bauwe, 2007). Since AtPGLP2 does not seem to have a major role in photorespiration, it might be interesting to further characterize the *pglp2* mutant and recombinant AtPGLP2 kinetic properties. We cannot exclude the involvement of this protein in the dephosphorylation of 2-PG during DNA double strand break repair. It would also be interesting to explore the behavior of a double *pglp1pglp2* mutant to see whether plant growth and development are further impaired in high CO₂.

4) AtPGLP1 and regulation by oxidation-reduction

The chloroplast is an organelle that undergoes redox changes that depend on their photosynthetic activity. Since AtPGLP1 was found to be S-nitrosylated (a redox-mediated PTM) and mammalian phosphoglycolate phosphatase was seen to be highly sensitive to its oxidized/reduced state (Hu et al., 2015; Seifried et al., 2016a), it was decided to investigate the sensitivity of AtPGLP1 activity and homodimerization to oxidation-reduction. Since the techniques developed during my thesis work to measure AtPGLP1 activity could not be used because the spectrophotometric GOX-

couple reaction involved H₂O₂ production while the direct fluorimetric phosphate sensor was redox-sensitive, we thus developed a third method by ¹H-NMR. An NMR approach had been previously used in our laboratory to study another enzymatic reaction catalysed by the glutamine synthetase (GS1) of *A. thaliana* (Mauve et al., 2016). This analytical method allowed the quantification of the disappearing substrate and the appearance of the product at the same time. Unfortunately, although it was a suitable method to analyse recombinant AtPGLP1 activity, it was not feasible to apply this technique to leaf extracts because of the complexity of overlapping signals, especially since we used the magnetic properties of protons that are highly represented in biological molecules. The redox state of AtPGLP1 seemed to be important for enzyme activity and dimer formation. Indeed, an oxidation treatment with high levels of H₂O₂ strongly impaired AtPGLP1_{WT} activity, while the mutation of specific cysteines (redox-sensitive amino acids) such as C302 and C232/C239 weakened the interaction between AtPGLP1 monomers as judged by yeast two-hybrid assays. Since these cysteines appeared to be important for homodimer formation they probably affect enzyme activity and this should be tested. C302 is near to a conserved HAD protein motif, and it is possible that its mutation to an alanine interfered with either enzyme stability or conformation. On the other hand, C232 and C239 are located in the cap domain and could play a role not only in homodimerization but also substrate accessibility to the catalytic centre as described by Seifried et al., (2016). A conserved cysteine among mammalian PGP, and located in motif I of HAD phosphatases, was shown to be necessary for enzyme activity (Seifried et al., 2016a). Surprisingly, the mutation of the corresponding residue of AtPGLP1 (C86) did not change enzyme activity. Therefore, even if the mammal and *A. thaliana* proteins share many common features, their involvement in distinct pathways might lead to certain specificities.

To go further in the study of AtPGLP1 redox regulation, several experiments are possible. First, we can consider measuring the activity of enzymes mutated in different cysteines and for those that are still active, test using our NMR method whether H₂O₂ sensitivity is maintained. It is also possible to perform a redox western blot to evaluate the reduced state of the cysteines. This method consists of blocking reduced cysteines during plant protein extraction using an alkylating agent (like a maleimide) to avoid oxidation. This agent is linked to a molecule like polyethylene glycol to create a shift during the migration on SDS-PAGE gels and then the protein of interest is detected *via* western blotting (Go and Jones, 2009). The extent of the shift can give information about the number of reduced cysteines. This would allow us to begin *in planta* investigations of the oxidation-reduction state of AtPGLP1.

Chloroplasts/plastids contain a large diversity of thioredoxin proteins that are involved in the redox-regulation of several processes including the activation of Calvin cycle enzymes in the light (Chibani et al., 2010; Meyer et al., 2012). However, AtPGLP1 has never been identified as a

thioredoxin target and since we saw that DTT addition did not alter *AtPGLP1* activity, it is perhaps unlikely to be thioredoxin-regulated. On the other hand, *AtPGLP1* was found to interact with a 2-cys-peroxiredoxin (2-cys-PRX) in an immunoprecipitation/mass spectroscopy analysis (Cerveau et al., 2016). This protein is a thiol dependent peroxidase (reducing H₂O₂) that can have a chaperone and signalling role in several organisms and it can protect against photo-oxidative stress. In *A. thaliana* chloroplasts, two, almost identical, 2-cys-PRXs named A and B have been identified (Puerto-Galán et al., 2013). In the study of Cerveau et al., (2016), the double *Arabidopsis 2-cys-prx a/b* mutant was used as a control. Since confirmed 2-cys-PRX targets were still identified after immunoprecipitation using this double mutant, a threshold of 5 (for the amount of target in WT to mutant ratio) was decided to justify relevant interactions. This ratio for *AtPGLP1* was 8, thus supporting an interaction between the two proteins. Furthermore, both 2-cys-PRX A and B are known to be major targets of NADPH thioredoxin reductase C (NTRC) that possesses both NADPH-dependent thioredoxin reductase and thioredoxin activities (Pérez-Ruiz and Cejudo, 2009; Pulido et al., 2010). The overexpression of NTRC in *A. thaliana* resulted in a two-fold increase of biomass and starch accumulation under moderate light (Toivola et al., 2013). In a recent work that investigated NTRC partners, *AtPGLP1* was identified suggesting either a very strong interaction between 2-cys-PRX and *AtPGLP1* leading to the co-elution of *AtPGLP1* with 2-cys-PRX (known to interact with NTRC); or an *AtPGLP1* regulation involving both partners (González et al., 2019). This regulatory element could be one of the factors that were missing *in vitro* when measuring recombinant *AtPGLP1* kinetic parameters. To test this hypothesis, we could perform activity measurements in the presence of one or both 2-cys-PRX proteins and/or NTRC and reductant. It may also be interesting to go further in the study of these interactions revealed by large scale experiments, by undertaking bimolecular fluorescence complementation (BiFC), and yeast two-hybrid assays with both NTRC and 2-cys-PRX proteins.

IV) Photorespiration and plant yield improvement

The constant increase of the human population and the concomitant decrease of cultivable land places plant yield improvement at the heart of the concerns of plant scientists. Photorespiration is a major primary metabolism cycle for photosynthetic organisms and it is interconnected to many indispensable pathways: photosynthesis, Calvin-Benson cycle, nitrogen metabolism, Krebs cycle, 1C metabolism and amino acid biosynthesis. However, photorespiration competes with photosynthetic CO₂ assimilation at the RuBisCO active site and it consumes energy and can lead to C and N losses and therefore it became a target to improve plant yield. To achieve this, a complete understanding of

the photorespiratory cycle could be beneficial. Although the eight core photorespiratory enzymes have been identified and characterized, there is still a lot to discover including metabolite transporters and C2 cycle regulation. Some transporters have been already identified over the years: DiT1, DiT2.1 et DiT2.2 (Somerville and Ogren, 1983; Taniguchi et al., 2002; Renné et al., 2003), PLGG1 (Pick et al., 2013), BASS6 (South et al., 2017) and BOU (Eisenhut et al., 2013b; Samuilov et al., 2018). However, these are probably just a few of the transporters involved in the photorespiratory cycle. The lack of identified photorespiratory transporters could be due to various things. First, a functional redundancy does not allow the identification of photorespiratory phenotypes when a single transporter gene is knocked-out. This was seen for GOX in *Arabidopsis* (Dellero et al., 2016). Second, it is plausible that transporters are involved in various metabolic routes and their identification using a co-expression strategy (see Eisenhut et al., 2013b) is not possible. Third, perhaps in certain cases photorespiratory metabolites enter/leave a subcellular compartment either *via* diffusion or by a pore and therefore they do not require a transporter.

A second gap left to fill is the identification of photorespiration regulatory processes. New insights continue to emerge about post-translational regulation of photorespiratory enzymes and their interaction with proteins such as thioredoxins (Fonseca-Pereira et al., 2019; Reinholdt et al., 2019). The more we know about how and when the photorespiratory cycle is regulated to alleviate limiting steps and to maximise photorespiratory fluxes and metabolic pathway interactions, the more efficient we will become to devise strategies to target this cycle to improve plant yield.

That said, already the introduction of alternative glycolate metabolizing pathways directly inside the chloroplast has been shown to be efficient in the plant model *A. thaliana* with a 50 % increase of dry weight (Kebeish et al., 2007), and in *S. tuberosum* with a 2-3 fold increase of tuber yield (Nölke et al., 2014). It was also demonstrated to be effective in *Camelina sativa* with a 50 % increase of biomass and seed yield (Dalal et al., 2015) and more recently with tobacco where an additional reduction of glycolate export from the chloroplast was included by knocking down *PGGL1* (South et al., 2019). Another strategy has been to target limiting steps by the overexpression of a photorespiratory gene. This was successfully achieved with the H subunit of the GDC complex in both *A. thaliana* and tobacco with an improvement of plant yield under field conditions (Timm et al., 2012a; López-Calcagno et al., 2019). The overexpression of *SHMT1* in *O.sativa* produced a better photosynthetic efficiency and an increase of biomass as well as a better resistance to salt-stress (Wu et al., 2015; Mishra et al., 2016). When PGLP1 was overexpressed in *A. thaliana*, plants displayed an increase of dry and fresh weight (Flügel et al., 2017). Since the introduction of bypasses and the generation of overexpressing plants both relied on the creation of GMOs that are not welcome in Europe, an alternative strategy must be found. We can imagine finding mutations (natural or chemically induced) leading to the overexpression of rate-limiting photorespiratory genes. To do so,

plants transformed with a reporter gene (such as luciferase) under the control of the promoter of the gene of interest would undergo chemical mutagenesis, for instance by using ethyl methanesulfonate (EMS). Mutations leading to the overexpression of the reporter gene will allow the identification of plants where the promoter has been deregulated. After crossing with WT plants, the mutation can be identified in the following offspring by sequencing of their genomic DNA. Similar mutations in the corresponding genes of crop plants can thus be found in the Targeting Induced Local Lesion IN Genomes (TILLING) libraries or be generated by CRISPR-Cas 9 to target a specific locus (although this method is still labelled GMO in Europe).

In conclusion, new techniques and insights are emerging every day in the field of plant sciences and they are opening new doors for scientists to make the Earth a healthier environment while trying to feed the ever increasing population in a sustainable and ecological-friendly way.

MATERIALS AND METHODS

I) Materials

1) Plant material

Arabidopsis thaliana ecotype Columbia (Col-0) was used as wild type control plants in all experiments. The SALK_130837 mutant has a T-DNA insertion in the 8th intron of the *AtPGLP1* gene (*At5g36700*) and homozygous seeds for this insertion line were kindly provided by Professor Herman Bauwe (University of Rostock, Plant Physiology Department, Germany).

2) Growth conditions

In vivo

For *in vivo* experiments, seeds were sown on breeding soil for at least 1 week for germination and plantlet acquisition. Even when the culture was done in high CO₂, germination was done in ambient air because it was more efficient than in 1 % CO₂. Plantlets were transplanted in new individual pots to grow in short days (8 h light/16 h dark, 175 μmol of photons.m⁻².s⁻¹, 65 % humidity, 20 °C day/18 °C night) either in ambient air (CO₂ concentration around 400 μL.L⁻¹) or high CO₂ (CO₂ concentration around 10 000 μL.L⁻¹ or 1 %). To obtain new seeds, plants were transferred to long day chambers (16 h light/8 h dark, 175 μmol of photons.m⁻².s⁻¹, 65 % humidity, 20 °C day/18 °C night), either in normal air or high CO₂.

In vitro

For *in vitro* growing, seeds were sterilized and sown on a ½ MS (Murashige et Skoog, 1962) medium containing 0.8 % (w/v) of agar and a herbicide, glufosinate ammonium -PESTANAL® 15 μg/μL (45520, Sigma-Aldrich), to select resistant plants. Plants were grown in short days (8h light/16h dark, 100 μmol of photons.m⁻².s⁻¹, 65 % humidity, 20 °C day/18 °C night). For seed sterilization, about 20 mg of seeds were dipped into 1 mL of an ethanol 95 % (v/v) / sodium hypochlorite 7.5 % (w/v) solution for 6 min and then they were washed 3 times with a 100 % ethanol solution, then dried overnight on a flow-bench.

3) Plasmids

pGEM®-T Easy: The commercial pGEM®-T Easy vector (Promega) is a 3015 bp vector carrying the *bla* gene that confers ampicillin resistance to bacteria. It is linearized DNA with an additional 3'-terminal thymidine at each end which facilitates the cloning of PCR products generated by *Taq* polymerase that add a single 5'-terminal adenosine. pGEM®-T possesses a multiple cloning site

region within the α -peptide encoding region of the β -galactosidase enzyme. The galactose analogue in the medium (5-bromo-4-chloro-3-indolyl- β -D-galactopyranoside or X-gal) can be metabolized by bacteria containing this vector thus forming blue colonies. During the cloning, the inserted DNA interrupts the coding sequence and inactivates α -peptide production and the recombinant colonies appear white. This vector was used as a temporary vector for most of the cloning strategies.

pB7WG: The 9915 bp pB7WG binary vector carrying the *bar* gene and an *aad* gene confers resistance to the herbicide ammonium-glufosinate in plants and spectinomycin resistance in bacteria, respectively. It also contains the bacterial suicide gene *ccdB* that can stop bacterial growth by targeting the gyrase enzyme. This gene is found in between recombination sites *attR1* and *attR2* necessary for Gateway® cloning technology. This vector backbone was used to transform homozygous *pglp1* plants and *ipgam2^{-/-}/ipgam1^{+/-}* sesquimutants using *Agrobacterium tumefaciens* for complementation experiments.

Before the beginning of my PhD, a pGEM®-T Easy plasmid containing the promoter region of the photorespiratory enzyme *SHMT1* (about 1 kb) was already available in the team. The *SHMT1* promoter was introduced into pB7WG vector as a *SpeI-HindIII* cassette upstream from the Gateway recombination region *attR1*.

pB7WG-promAtSHMT1: This 10 789 bp plasmid corresponds to the sequence of the *SHMT1* promoter in pB7WG and was used to drive the expression of an open reading frame cDNA inserted using Gateway® technology.

pB7WG-promAtiPGAM2: This 11012 bp plasmid corresponds to the sequence of the *iPGAM2* promoter in pB7WG and was used to drive the expression of an open reading frame cDNA inserted using Gateway® technology.

pB7WG-promAtiPGAM2::AtiPGAM2_{WT}: This 11043 bp plasmid carries the *iPGAM2* ORF, mutated or not, first cloned into pDONR207 to allow recombination into pB7WG-promAtiPGAM2. Site directed mutagenesis was therefore performed on pDONR207::*iPGAM2_{WT}* to build the following plasmids:

- pB7WG-promAtiPGAM2::AtiPGAM2_{S75T};
- pB7WG-promAtiPGAM2::AtiPGAM2_{S75T/D29N};
- pB7WG-promAtiPGAM2::AtiPGAM2_{S75T/R290L};

pB7WG-promAtSHMT1::PGLP1_{WT}-GFP: This 10946 bp plasmid carries the *PGLP1* ORF, mutated or not. It includes the sequence encoding the chloroplast targeting signal peptide and it is fused in frame at the 3' end with the sequence encoding the soluble mutated GFP (smGFP). This chimeric ORF was inserted into pB7WG-prom*SHMT1* by recombination. Plasmids carrying point mutations changing T103 and S356 into either aspartate or alanine in the corresponding proteins were also used. To do so, site directed mutagenesis (see protocol in Methods) was done using pDONR207::*PGLP1_{WT}*-GFP, and the resulting plasmids were used for insertion by recombination into pB7WG-prom*AtSHMT1* to produce:

- pB7WG-prom*AtSHMT1*::*PGLP1_{T103A}*-GFP;
- pB7WG-prom*AtSHMT1*::*PGLP1_{T103D}*-GFP;
- pB7WG-prom*AtSHMT1*::*PGLP1_{S356A}*-GFP;
- pB7WG-prom*AtSHMT1*::*PGLP1_{S356D}*-GFP.

pBi/smGFP: This 4 506 bp plasmid carries the sequence encoding the soluble mutated GFP (Davis and Vierstra, 1998) under the control of the CaMV35S promoter. Few restriction sites are located upstream from the GFP coding sequence. The *bla* gene allows resistance to ampicillin in bacteria. This vector was used to insert the *GFP* sequence into various plasmids.

pDONR207: This 5585 bp vector carries the *aacC* gene that confers gentamicin resistance to bacteria. It is a Gateway® cloning system donor plasmid containing *attP1* and *attP2* recombination sites. Situated in between these sites are the bacterial suicide gene *ccdB* and the *cat* gene that confers chloramphenicol resistance to bacteria. This vector was used to clone the *PGLP1* ORF with the sequence encoding its chloroplast targeting signal peptide and with or without the GFP encoding sequence into pB7WG-prom*AtSHMT1* for plant transformation and the *PGLP1* ORF only into **pDEST-His₆MBP** to produce recombinant proteins. The corresponding plasmids were: pDONR207::*AtPGLP1_{WT}*-GFP; pDONR207:: *AtPGLP1_{full}*; pDONR207::*AtPGLP1_{WT}*.

This vector was also used to clone the *iPGAM2* ORF into pB7WG-prom*AtiPGAM2* thus producing the following plasmid: pDONR207::*AtiPGAM2_{WT}*. The site directed mutagenesis was done when the different genes were in pDONR207.

pET16b: This 5711 bp vector carries the *bla* gene that confers ampicillin resistance to bacteria. It has an N-terminal poly-histidine tag sequence followed by a multiple cloning site region and expression is controlled by the T7 promoter. It also contains a ribosome binding site (*rbS*) and a T7 termination sequence. This plasmid allows the production of a recombinant protein with a His-tag in a bacterial strain like BL21 (DE3) that can produce a T7 RNA polymerase, a very selective and active

enzyme. The pET16b plasmid also possesses both the lac operator *LacO* downstream from the T7 promoter and the *LacI* repressor gene that together allow the induction of recombinant protein production, using a lactose analogue, the isopropyl β -D-1-thiogalactopyranoside (IPTG). In the absence of IPTG, the *LacI* gene product binds to the *LacO* operator sequence and prevents transcription of the recombinant protein. When added, IPTG interacts with the repressor and allows T7 RNA polymerase driven transcription of the inserted sequence fused to the 10-His tag. This plasmid was used to produce AtPGLP1 recombinant proteins without the chloroplast targeting signal peptide and AtiPGAM2 recombinant proteins.

pET16b-AtPGLP1_{WT}: This 6638 bp plasmid corresponds to the ORF of *AtPGLP1* gene devoid of its sequence encoding the chloroplast targeting signal peptide cloned into pET16b. It was also used as a template to perform site-directed mutagenesis at T330 and S356 to either aspartate or alanine; producing

- pET16b-*AtPGLP1*_{S356A};
- pET16b-*AtPGLP1*_{S356D};
- pET16b-*AtPGLP1*_{T330A};
- pET16b-*AtPGLP1*_{T330D}.

pET16b-AtiPGAM2_{WT}: This 7394 bp plasmid corresponds to the ORF of *iPGAM2* cloned into pET16b. It was used as a template to perform site directed mutagenesis at D29, S75, S82 and R290 generating:

- pET16b-*AtiPGAM2*_{D29N};
- pET16b-*AtiPGAM2*_{S75T};
- pET16b-*AtiPGAM2*_{S82A};
- pET16b-*AtiPGAM2*_{S82D};
- pET16b-*AtiPGAM2*_{R290L}

pDEST-His₆MBP: This 6000 bp vector has the *bla* gene that confers ampicillin resistance to bacteria. Like pET28a (see below) and pET16b described below, it allows IPTG inducible production of recombinant proteins *via* the same system. In addition, *attR1* and *attR2* sites make it a destination vector for the Gateway® cloning system. The resulting recombinant protein will have an N-terminal 6-His-tag fused to the maltose binding protein (MBP). Since one of the most important problems during recombinant protein production in *E.coli* is the accumulation of the protein in the form of insoluble and inactive aggregates known as inclusion bodies, the MBP is added to enhance fusion

protein solubility (Nallamsetty et al., 2005). This plasmid was used to produce AtPGLP1 recombinant proteins without the chloroplast targeting signal peptide.

pDEST-His₆MBP-AtPGLP1_{WT}: This 7557 bp plasmid corresponds to the ORF of *PGLP1* without the sequence coding for its chloroplast targeting signal peptide cloned into **pDEST-His₆MBP**. It was used as a template for site-directed mutagenesis of T103 and T322 to either aspartate or alanine:

- pDEST-His₆MBP-AtPGLP1_{T103A};
- pDEST-His₆MBP-AtPGLP1_{T103D};
- pDEST-His₆MBP-AtPGLP1_{T322A};
- pDEST-His₆MBP-AtPGLP1_{T322D}.

This plasmid has also been used to produce the recombinant protein mutated on C86 in alanine and the deletions: DEL1 corresponding to the deletion of the sequence encoding amino acids 219 to 224 (RYFNYY) and DEL2 corresponding to the sequence encoding amino acids 263 to 268 (SMVGAL), thus producing:

- pDEST-His₆MBP-AtPGLP1_{C86A}
- pDEST-His₆MBP-AtPGLP1_{DEL1}
- pDEST-His₆MBP-AtPGLP1_{DEL2}

pET28a: This 5369 bp vector confers kanamycin resistance to bacteria and it was used to produce recombinant GOX protein with an N-terminal 6-His tag.

pET28a-AtGOX1: This plasmid corresponds to the *A.thaliana* *GOX1* ORF cloned into pET28a and it made in our laboratory by Mathieu JOSSIER (Dellero et al., 2015c).

4) Bacterial strains

Escherichia coli

DB3.1: F- *gyrA462 endA1 glnV44 Δ(sr1-recA) mcrB mrr hsdS20(r_B⁻, m_B⁻) ara14 galK2 lacY1 proA2 rpsL20(Sm^r) xyl5 Δleu mtl1*.

This strain was used to propagate the Gateway® vectors containing the *ccdB* bacterial suicide gene. The product of this gene inhibits bacterial growth by interacting with DNA gyrase, but this strain possesses a mutation in the *gyrA* gene that renders the gyrase resistant to *cddB* toxin and thereby can grow when transformed with these plasmids.

DH5 α : F⁻ *endA1 glnV44 thi-1 recA1 relA1 gyrA96 deoR nupG purB20 ϕ 80dlacZ Δ M15 Δ (lacZYA-argF)U169, hsdR17(rK-mK+), λ -.*

This strain was used to replicate plasmids during cloning strategies.

BL21 (DE3): F⁻ *ompT gal dcm lon hsdSB(r_B⁻ m_B⁻) λ (DE3 [*lacI lacUV5-T7 gene 1 ind1 sam7 nin5*]) [*malB*⁺]_{K-12}(λ ^S).*

This strain was used to produce recombinant proteins since it can produce the T7 RNA polymerase needed for transcription after induction with the lactose analog IPTG.

C41 (DE3): This strain (Lucigen) is derived from BL21 (DE3) but contains at least one uncharacterized mutation that prevents cell death when the expressed recombinant protein is toxic or insoluble. This strain was used instead of BL21 (DE3) to help produce recombinant proteins that were poorly soluble.

Agrobacterium tumefaciens

GV3101::pMP90: This strain of *A.tumefaciens* possesses the rifampicin resistance gene on its chromosome and the Ti plasmid pMP90 (pTiC58 Δ T-DNA) that carries the gentamycin resistance gene as well as the *vir* gene that allows T-DNA transfer into plants however this plasmid has no functional T-DNA of his own thus it was used for plant transformation/complementation experiments.

5) Yeast Strain

Y8930 : the genotype of *Saccharomyces cerevisiae* strain Y8930 is MAT α *leu2-3,112 trp1-901 his3-200 ura3-52 gal4 Δ gal80 Δ GAL2-ADE2 LYS2::GAL1-HIS3 MET2::GAL7-lacZ cyh2^R* (Dreze et al., 2010). It was used to carry out the two hybrid experiments.

6) Culture Media

For Yeast

YPDA medium: 20 g.L⁻¹ bacto-peptone, 10 g.L⁻¹ yeast extract (18 g.L⁻¹ bacto-agar if needed), 800 mL H₂O was added, and the medium was adjusted to pH 5.8 and autoclaved, cooled, then dextrose 2 % v/v final was added (from 40 % stock solution separately autoclaved) and adenine 1x final (from 100x stock solution, 1 % w/v, separately autoclaved) and the volume medium was adjusted to 1L with sterile H₂O.

SD medium: 6.7 g.L⁻¹ yeast nitrogen base without amino acids, was added by 800 mL of H₂O, and adjusted to pH 5.8, then added by 18 g.L⁻¹ bacto-agar and autoclaved, cooled, before dextrose 2 % v/v final was added (from 40 % stock solution separately autoclaved), appropriate dropout 1x final was added (from 10x dropout stock solution), 3-amino-1,2,4-triazole (3-AT) if needed (from a stock solution prepared in H₂O and sterilized by filtration) and volume was adjusted to 1L with sterile H₂O.

10x Dropout solution: 300 mg.L⁻¹ L-Isoleucine, 1 500 mg.L⁻¹ L-Valine, 1 000 mg.L⁻¹ L-Adenine hemisulfate salt, 200 mg.L⁻¹ L-Arginine HCl, 200 mg.L⁻¹ L-Histidine HCl monohydrate, 1 000 mg.L⁻¹ L-Leucine, 300 mg.L⁻¹ L-Lysine HCl, 200 mg.L⁻¹ L-Methionine, 500 mg.L⁻¹ L-Phenylalanine, 2 000 mg.L⁻¹ L-Threonine, 200 mg.L⁻¹ L-Tryptophan, 300 mg.L⁻¹ L-Tyrosine, 1 000 mg.L⁻¹ L-Uracil were mixed and autoclaved.

For SD-Leu-Trp medium, 10x dropout solution without L-Leucine and L-Tryptophan was prepared and for SD-Leu-Trp-His medium, 10x dropout solution without L-Leucine, L-Tryptophan and L-Histidine HCl monohydrate was prepared.

For bacteria

LB: LB Broth (Sigma L3022) used at 20 g.L⁻¹. For LB solid medium, 32 g.L⁻¹ of agar (Sigma A5306) was added.

For *in vitro* plants

MS_{1/2}/agar: Murashige & Skoog medium including vitamins (Duchefa M0222) (2.2 g.L⁻¹) was complemented with 7 g.L⁻¹ of agar (Duchefa NP696) (see Murashige and Skoog, 1962).

II) Methods

1) Molecular biology

- RNA extraction and reverse transcription

Beforehand, about 100 mg of *A.thaliana* leaves were collected in a tube containing 2 iron beads, immediately frozen in liquid nitrogen, and kept at -80 °C if necessary. Samples were ground using a ball mill. The total RNA extraction was performed using the Promega ReliaPrep™ RNA Cell Miniprep System following the manufacturer instructions. First 500 µL of BL+TG buffer (4 M

guanidine thiocyanate; 0.01 M Tris pH 7.5; 2 % 1-thioglycerol (v/v)) was added to the ground material, and centrifuged 5 min at 14000 g and 4 °C. The supernatant was then transferred to a new tube and ribonucleotides were precipitated by adding 170 µL of isopropanol 100 %. The mixture was loaded onto a ReliaPrep™ Minicolumn and washed with RNA wash solution (60 mM potassium acetate; 10 mM Tris-HCl pH 7.5 and 60 % ethanol (v/v)). To ensure that extracted RNA was not contaminated with DNA, a DNase I solution was added to the column (0.9 M MnCl₂; DNase I lyophilized; yellow Core buffer [0.0225 M Tris-Hcl pH 7.5; 1.125 M NaCl; 0.0025 % yellow dye (w/v)]). Following a centrifugation step, RNA elution was carried out in a final volume of 30 µL, using RNase free water, again by centrifugation.

mRNAs are polyadenylated at their 3' end and therefore cDNA were made using a poly-dT primer of about 15 nucleotides that anneal to the polyA tail. To destabilize mRNA stem-and-loop structures, the total RNA solution was incubated at 70 °C for 10 min then rapidly cooled on ice. Then cDNA synthesis was performed at 42 °C, with a reverse transcriptase (IM-PromII™, Promega), in a solution containing 0.5 mM of oligodT, 0.5 mM of each dNTP (dATP, dTTP, dGTP et dCTP), 5 mM of MgCl₂, 1 U of the enzyme in a final volume of 20 µL containing IM-PromII™ buffer according to the recommendations of the manufacturer. Finally, the Reverse transcriptase was inactivated by a 15 min incubation at 70 °C.

- Polymerase chain reaction (PCR)

PCR was used to exponentially amplify double stranded DNA using a DNA polymerase, and it relies on thermal cycling. Most of the time, DNA polymerase from *Thermus aquaticus* (*Taq* polymerase), prepared in the laboratory according to the protocol described in literature (Desai and Pfaffle, 1995) was used. When a high fidelity was needed, the *Pfu* DNA polymerase isolated from *Pyrococcus furiosus* (Promega) was used. Typically, the final mix contained 0.1 µM of each primer, 100 µM of each dNTP (dATP, dTTP, dGTP and dCTP), 1.5 mM of MgCl₂, 1x *Taq* polymerase buffer (from a 10x stock composed of 10 mM Tris pH 7.8; 50 mM KCl; 0.1 % (v/v) Triton), a DNA template and 0.5 U of *Taq* polymerase in a final volume of 20 µL. Almost all PCR reactions started with a denaturation step of 5 min at 94 °C. Then there was between 25 and 35 thermal cycles: 30 s of denaturation at 94 °C, 30 s of annealing at the hybridization temperature (T_h°C) depending on the primers used, 1 min per kb of sequence to amplify of elongation at 72 °C (2 min for *PfuI* polymerase), a final step of 5 min elongation also at 72 °C, and then the mix was then cooled to 15 °C.

- Agarose gel electrophoresis

Agarose gel electrophoresis is used to separate nucleic acid fragments. The nucleic acids were mixed with a colored loading buffer to track DNA migration and to help sample deposition in the wells of the gel. Its composition was as follows: 10 mM Tris-HCl pH 7.6; 60 mM EDTA; 0.03 % bromophenol blue (w/v); 0.03 % xylene cyanol FF (w/v), 60 % glycerol (v/v). The gel was composed of 1 % agarose (w/v) dissolved in 0.5 X TAE buffer (20 mM Tris pH 8.3; 10 mM acetic acid; 0.5 mM EDTA) and ethidium bromide was added at 100 $\mu\text{g}\cdot\text{L}^{-1}$. The running buffer was 0.5x TAE. Nucleic acid fragments were separated according to their size during between 20 min and 30 min (depending on the resolution needed) under a 100 V voltage. Molecular size markers were migrated in parallel to compare with the samples.

- DNA purification from agarose gel

After migration, DNA fragments were excised from the agarose gel under UV light and they were purified using the « Wizard® SV and PCR Clean-UP System » kit (Promega) according to the protocol of the manufacturer.

- Ligation of a DNA fragment into a vector

Each DNA fragment was inserted into a vector by a ligation reaction that involved a ligase from the bacteriophage T4 (3U). The final volume was 20 μL and contained enzyme buffer with the final composition: 30 mM Tris-HCl pH 7.8; 10 mM MgCl_2 ; 10 mM DTT; 1 mM ATP. The ligase reaction was incubated in a melting ice-bath until room temperature was reached, generally overnight. Most of the time the vector was bigger than the insert, and for optimal ligation an insert: vector molecular ratio of 3:1 to 10:1 was applied.

- Bacterial transformation by electroporation

The transformation requires electro-competent bacteria that were already available in the laboratory. To avoid an electric arc during the electroporation, the transforming DNA solution (either ligation, recombination reactions...) needs to be free of any salt. For that purpose, a cellulose membrane (VS 0.025 μm , Millipore) was deposited on distilled water in a Petri dish and 20 μL of the DNA reaction mixture was carefully dropped onto the membrane and recovered after 1 h.

Then the protocol was the same for every plasmid. Electro-competent bacteria and plasmid were mixed and placed inside a 1 mm electroporation cuvette and a 1.8 kV electrical pulse was applied for a few microseconds. This process disturbs the phospholipid bilayer of the membrane and produces some temporary pores. The electric potential across the cell allows the charged DNA to enter into the cells (Shigekawa and Dower, 1989). Immediately after the pulse, 700 μL of liquid medium (LB + 3 % (w/v) glucose) were added to the cuvette and the bacteria were transferred to an Eppendorf™ tube and incubated at the optimal temperature for bacterial growth (30 °C for *A. tumefaciens* and 37 °C for *E. coli*) for at least 1 h to allow the cells to recover and the resistance gene to be expressed. Finally, each bacterial culture was plated onto solid medium (LB + agar) containing the appropriate antibiotic (different dilutions were used to obtain isolated colonies). The plates were incubated overnight at either 30 °C or 37 °C depending on the bacteria. After one night, antibiotic-resistant transformed *E. coli* bacteria produced colonies. For *A. tumefaciens*, 48 h were necessary.

- Bacterial liquid cultures

First, to prepare a pre-culture an isolated bacterial colony obtained on solid medium (LB + agar) was used to inoculate 3 mL liquid medium of LB supplemented with an antibiotic to select bacteria containing a plasmid. The pre-culture was incubated overnight at the optimal temperature according to the experiment and the bacteria under a mechanical agitation.

A bacterial pre-culture can have several goals; it can be used to inoculate a larger volume of bacterial culture (e.g. 3 mL of pre-culture for 200 mL of bacterial culture with the same antibiotic) to either produce a recombinant protein or to perform a maxi extraction of plasmid.

- Plasmid DNA extraction from a bacterial pre-culture

From a 3 mL pre-culture, 2 mL were collected and centrifuged 5 min at 19 000 g at room temperature and the supernatant was discarded. The pellet was re-suspended with 100 μL of the first buffer (25 mM Tris-HCl pH 8; 10 mM EDTA; 50 mM glucose; 0.5 $\text{mg}\cdot\text{mL}^{-1}$ RNase). The mix was left at room temperature for 10 min. Then, 200 μL of the second buffer (0.2 N; NaOH SDS 0.1 % (v/v)) was added to lyse the cells, and gently homogenized. Finally, 150 μL of the third buffer (stock solution: 5 M potassium acetate; 11.5 % glacial acetic acid (v/v)) was added to neutralize the mix and left during 10 min on ice. The mix was centrifuged for 10 min at 19 000 g and at room temperature. The supernatant was transferred to a clean tube and emulsified with 200 μL of phenol/chloroform/isoamyl alcohol solution (25:24:1 v/v/v). After a 5 min centrifugation 19 000 g, the aqueous phase was collected and 1 mL of 100 % ethanol was added, homogenized and incubated

1 h at -20 °C to precipitate plasmid DNA. After a 20 min centrifugation at 19 000 g and room temperature, the pellet was washed with 1 ml of 70 % ethanol and finally dissolved in 20-30 µL of sterile pure H₂O slightly pre-warmed to help resuspension. During cloning experiments, each time a new plasmid was produced during cloning experiments, it was amplified in *E. coli* DH5α and purified.

- Measurement of nucleic acid concentrations

This was performed using a NanoDrop™ spectrophotometer. The absorbance was measured at 260 nm with 2 µL of either DNA or RNA extract, eventually diluted. One unit of OD corresponds to 50 µg.µL⁻¹ of DNA and 40 µg.µL⁻¹ of RNA.

- Enzymatic digestion of plasmid DNA

Restriction enzymes can cut a DNA molecule at specific sites. One unit of enzyme was for each µg of DNA, with a restriction buffer recommended by the manufacturer (Promega). All digestions were performed for 1 h at 37 °C.

- Site directed mutagenesis

For mutagenesis, the QuikChange Lightning Site-Directed Mutagenesis kit (Agilent) was used. It allows the introduction of point mutation(s), small deletions or the addition of nucleotides that result in one or several amino-acid modifications, insertions or deletions in the amino acid sequence of proteins. The kit uses a high-fidelity DNA polymerase called *PfuUltra*.

To do so, two complementary oligonucleotides with the desired mutation in the middle flanked by unmodified nucleotide sequence were designed and then produced by Eurofins genomics (at 100 µM). Primers were between 25 and 45 bases with a T_m ≥ 78 °C. The PCR-based extension of the oligonucleotide primers generated a mutated plasmid. The reaction was performed in a final volume of 50 µL with 50 ng of template DNA, 125 ng of each primer, 1 µL of dNTP mix from the kit, 3 µL of the QuickSolution that improves the linear amplification, and enzyme buffer. Before starting the reaction, QuikChange Lightning DNA polymerase was added (1 µL at 2.5 U/µL per reaction). The PCR program was as followed: a denaturation pre-step of 5 min at 95 °C, then 18 to 22 cycles composed of 30 s of denaturation at 95 °C, 20 s of annealing at, 30 s of elongation at 68 °C for each kb of sequence to amplify, a 7 min of final elongation at 68 °C, and the mix was then cooled to 15°C. At the end of the PCR, the reaction was treated with 2 µl of *Dpn* I (enzyme of unknown concentration included in the kit) at 37 °C for 10 min before being cooled on ice. *Dpn* I is an endonuclease that only

targets (5'-Gm6ATC-3') of the template plasmid. Indeed this plasmid was produced in *E. coli* and thus *dam* methylated while the neo-synthesized DNA was not. This step allowed the positive selection of mutation-containing plasmid. The mixture was then desalted and used to transform *E. coli* DH5 α competent cells (see the "Bacterial transformation section").

2) Cloning experiments

- Cloning of *AtPGLP1* ORF without the sequence encoding its chloroplast targeting peptide into pET16b \rightarrow pET16b-*AtPGLP1*_{mat}

The ORF of *AtPGLP1* was amplified using cDNA as template (see "RNA extraction and reverse transcription"), the *Pfu* DNA polymerase (Promega) and two specific primers (535PRO/536TER) that allowed the amplification of the *AtPGLP1* ORF without the sequence encoding its chloroplast targeting peptide and the addition of two flanking restriction sites, *NdeI* and *XhoI*. The PCR was performed in a final volume of 50 μ l containing the cDNA, each primer at 0.1 μ M, 0.1 mM of each dNTP, the enzyme buffer recommended by the manufacturer containing 20 mM MgSO₄ and 2U *Pfu* DNA polymerase. The PCR product was separated on an agarose gel electrophoresis and the DNA fragment was purified from an excised agarose slice and cloned into the pGEM-T Easy[®] plasmid to be sequenced. To do so, the purified DNA fragment was previously treated with *Taq* polymerase to add a deoxyadenosine to the 3'-ends of the amplified fragment. After DH5 α transformation, plasmid DNA mini-preparation and sequencing, the validated plasmid and the pET16b vector were *XhoI* and *NdeI* digested. After restriction enzyme digestion and agarose gel electrophoresis, pET16b and *AtPGLP1* ORF were purified and ligated together. The desalted ligation product was used to transform electro-competent *E. coli* DH5 α cells and transformed bacteria were selected on ampicillin (50 mg.L⁻¹) containing LB medium. In some of the resistant colonies, the transformation was still checked by PCR and analytic digestions.

The resulting plasmid was used as a template for directed mutagenesis of potential phospho-sites. Each plasmid was then used to produce the corresponding recombinant proteins (see Materials).

- Cloning of *AtPGLP1* ORF without the sequence encoding its chloroplast targeting peptide to a *GFP* ORF \rightarrow pET16b-*AtPGLP1*_{mat}*GFP*

To clone the *AtPGLP1* ORF fused to a DNA sequence encoding GFP into pET16, pET16b-*AtPGLP1*_{mat} was used as a template for a PCR using *Pfu* DNA polymerase and specific primers

(580PRO/581TER) that added *Xba*I and *Sal*I restriction sites to clone the resulting fragment into pBi/smGFP. The PCR fragment was transitory ligated into pGEM[®]-T Easy to be sequenced but unfortunately the *Xba*I restriction was not functional. Therefore, the plasmid pGEM-T-*AtPGLP1_{mat}* was alternatively digested with *Sph*I (upstream from the *Xba*I) and *Sal*I and inserted into pBismGFP to insert *PGLP1* in the correct frame with *GFP*. pBismGFP-*AtPGLP1_{mat}* was then used as a template for a new PCR (using 582PRO/583TER), to add *Xho*I restriction sites at both ends of the *AtPGLP1_{mat}::GFP* cassette to clone it into pET16b, previously linearized with *Xho*I and dephosphorylated (with a phosphatase) to avoid recircularization. After *E. coli* DH5 α transformation with the desalted ligation reaction and plasmid DNA mini preparation of isolated colonies previously checked by PCR, a restriction analysis was performed with several enzymes to validate the orientation of the *AtPGLP1_{mat}GFP* insert (since both ends were flanked with the same restriction site). This plasmid was then used to produce recombinant protein and to verify that the *AtPGLP1_{mat}* C-terminal GFP fusion protein did not alter *AtPGLP1* activity.

- Cloning the *SHMT1* promoter into pB7WG \rightarrow pB7WG-prom*AtSHMT1*

The promoter region of the *AtSHMT1* gene encoding photorespiratory *AtSHMT1* was previously cloned into pGEM[®]-T Easy in our laboratory. Both pGEM-T-prom*AtSHMT1* and pB7WG were digested by *Hind*III and *Spe*I, both vector and insert were purified after electrophoresis and they were ligated together. After transformation, plasmid DNA extraction, this new vector was checked by a *Hind*III/*Eco*RI double digestion. This promoter had been shown to be efficient during the study of Arabidopsis GOX (Dellero et al., 2016) and during work on the *shmt1* mutant by Weber's team in Germany.

- Gateway[®] cloning of the full-length *AtPGLP1* ORF into pB7WG-prom*AtSHMT1* \rightarrow pB7WG-prom*AtSHMT1::AtPGLP1_{full}*

The full-length *AtPGLP1* ORF was amplified as above (see “pET16b-*AtPGLP1_{mat}* cloning section”) using cDNA (see “RNA extraction and reverse transcription”) as template, by PCR with specific primers (537PRO/538TER) and the result of this reaction was used as a template for the following PCR with GW-FORWARD/GW-REVERSE as primers in order to add *attB* sites for Gateway[®] cloning. After subcloning the purified PCR fragment into pGEM[®]-T Easy for sequencing, the full length *AtPGLP1* ORF was introduced into the vector pDONR207 by recombination *via* the added *attB* sites and the *attP* sites of pDONR207 using the BP Clonase acting overnight at 25 °C. This reaction

produced *attL* sites. It was performed in a 10 μL final volume with 150 ng of vector and 150 ng of insert (the *PGLP1* fragment subcloned in pGEM[®]-T Easy), 2 μL of BP Clonase mix (Gateway[®], Thermo Fisher Scientific) and QS 10 μL of TE buffer (10 mM Tris-HCl pH 7.5; 1 mM EDTA). Enzymes were inactivated with 1 μL of proteinase K (2 $\mu\text{g}\cdot\mu\text{L}^{-1}$) at 37 °C for 10 min. The desalted reaction mixture was used to transform *E. coli* DH5 α cells (see “Bacterial transformation by electroporation”) and transformants were selected on gentamycin (50 $\text{mg}\cdot\text{L}^{-1}$) containing LB medium. Plasmid DNA was extracted (see “Plasmid DNA extraction from bacterial pre-culture”), validated by restriction analysis and used in a LR Gateway[®] reaction to transfer the full-length *PGLP1* ORF in pB7WG-prom*AtSHMT1*. The LR recombination reaction involved using the *attR* sites of pB7WG-prom*AtSHMT1* and the *attL* sites generated in the BP reaction. As above for the BP reaction, this was performed in a 10 μL final volume with 200 ng of pB7WG-prom*AtSHMT1* and 150 ng of pDONR207-*AtPGLP1*_{full}, 2 μL of LR Clonase mix (Thermo Fisher Scientific) QS 10 μL of TE buffer and incubated overnight at 25 °C. After validation, this plasmid was introduced into *A. tumefaciens* and used to transform homozygous *pglp1* mutant plants to assess the ability of the transgene (*AtPGLP1* ORF under the control of the *AtSHMT1* promoter) to complement the *pglp1* mutation.

- Gateway[®] cloning of the full-length *AtPGLP1* ORF fused to a GFP coding sequence into pB7WG-prom*AtSHMT1* → pB7WG-prom*AtSHMT1*::*AtPGLP1*

The plasmid pDONR207-*AtPGLP1*_{full} was used as template for a PCR using specific primers (584PRO/581TER) and *Pfu* DNA polymerase to add flanking *XbaI* and *SaII* restriction sites to the full-length *AtPGLP1* ORF. The resulting PCR fragment, treated with *Taq* polymerase, was cloned into pGEM[®]-T Easy for sequencing. The *XbaI* and *SaII* restriction sites were used to clone the sequence into pBismGFP digested with the same enzymes. The full-length *AtPGLP1*_{fullWT} ORF was inserted in frame with the *GFP* sequence and this was further amplified by PCR (using first 585PRO/586TER then GW-FORWARD/GW-REVERSE) to generate *AtPGLP1*_{full}-*GFP* flanked by *attB* sites for Gateway[®] cloning of the resulting sequence cassette into pDONR207 via its *attP* sites and BP clonase thus forming *attL* sites. The pDONR207-*AtPGLP1*_{fullWT}-*GFP* plasmid thus created was used as a template to effectuate site directed mutagenesis and produce:

- pDONR207-*AtPGLP1*_{T103A}-*GFP*;
- pDONR207-*AtPGLP1*_{T103D}-*GFP*;
- pDONR207-*AtPGLP1*_{S356A}-*GFP*;
- pDONR207-*AtPGLP1*_{S356D}-*GFP*.

After sequence validation, LR clonase recombination was performed to clone each mutated *AtPGLP1*-*GFP* DNA sequence into pB7WG-prom*AtSHMT1* (the protocol being the same as previously

described). Once validated, the resulting plasmids were individually introduced into *A. tumefaciens*, used to transform homozygous *pglp1* mutant plants to assess the ability of the transgene (full-length PGLP1 ORF fused to GFP under the control of the *AtSHMT1* promoter) to complement the *pglp1* growth phenotype. The different plasmids used to complement *pglp1* were:

- pB7WG-prom*AtSHMT1*::*AtPGLP1_{WT}*GFP;
- pB7WG-prom*AtSHMT1*::*AtPGLP1_{T103A}*GFP;
- pB7WG-prom*AtSHMT1*::*AtPGLP1_{T103D}*GFP;
- pB7WG-prom*AtSHMT1*::*AtPGLP1_{S356A}*GFP;
- pB7WG-prom*AtSHMT1*::*AtPGLP1_{S356D}*GFP.

- Gateway® cloning of the *AtPGLP1* ORF without the sequence encoding its chloroplast targeting peptide into pDEST-His₆MBP → pDEST-His₆MBP-*AtPGLP1_{mat}*

The PGLP1 ORF without the sequence encoding its chloroplast targeting peptide was amplified by PCR with the primers 598PRO/599TER and used as a template for the following PCR with GW-FORWARD/GW-REVERSE as primers in order to add *attB* sites for Gateway® cloning. After subcloning into pGEM®-T Easy for sequencing, as previously described, the amplified DNA was introduced into pDONR207 *via* the BP reaction. The plasmid thus generated pDONR207-*AtPGLP1_{mat}* was then used as a template to carry out site directed mutagenesis of T103 and T322 to either alanine or aspartate as described in the paragraph “Site directed mutagenesis”, thus producing:

- pDONR207-*AtPGLP1_{C86A}*;
- pDONR207-*AtPGLP1_{T103A}*;
- pDONR207-*AtPGLP1_{T103D}*;
- pDONR207-*AtPGLP1_{T322A}*;
- pDONR207-*AtPGLP1_{T322D}*;
- pDONR207-*AtPGLP1_{DEL1}*;
- pDONR207-*AtPGLP1_{DEL2}*;

After validation of the mutations, the WT and mutated sequences were introduced into pDEST-His₆MBP *via* LR recombination (see the “pB7WG-prom*AtSHMT1*::*AtPGLP1_{WT}*” paragraph). The following plasmids were used for the production and purification of the corresponding recombinant proteins.

- Cloning *AtiPGAM2* into pET16b → pET16b-*AtiPGAM2*

The ORF of *AtiPGAM2* was previously cloned into pET16b by another team member Samuel MAINGUET using the Gibson strategy. This plasmid was used as a template for site directed mutagenesis of several sites encoding D29, S75, S82, and R290 to N29, T75, A82 or D82 and L290.

The resulting constructs were then used to produce mutated *AtiPGAM2* recombinant proteins thus producing:

- pET16b-*AtiPGAM2*_{D29N};
- pET16b-*AtiPGAM2*_{S75T};
- pET16b-*AtiPGAM2*_{S82A};
- pET16b-*AtiPGAM2*_{S82D};
- pET16b-*AtiPGAM2*_{R290L}.

- Cloning the *AtiPGAM2* gene promoter region into pB7WG → pB7WG-prom*AtiPGAM2*

The cloning of the promoter region of the *AtiPGAM2* gene into pB7WG was performed using genomic DNA extracted from *Arabidopsis thaliana* leaves with specific primers (570TER_prom-iPGAM2-SpeI_R/574PRO_prom-iPGAM2-SacI_F4). The PCR product was first subcloned into pGEM-T Easy® for sequencing then double-digested with *SpeI* and *SacI*, purified and ligated with pB7WG previously digested with the same enzymes to make pB7WG-prom*AtiPGAM2*.

- Cloning of *AtiPGAM2* ORF into pDONR207 → pDONR207-*AtiPGAM2*_{WT}

As described in “RNA extraction and reverse transcription”, *AtiPGAM2* ORF was made from *Arabidopsis thaliana* leaf RNA and then used as a template to amplify the *AtiPGAM2* ORF with specific primers (578PRO/579TER) to add half of the *attB* sites for Gateway® cloning. A second PCR reaction was carried out with GW-FORWARD/GW-REVERSE and the previous PCR product as template to generate the *AtiPGAM2* ORF flanked by full *attB* sites. The amplified sequence was transiently cloned into pGEM®-T Easy for sequencing and after validation it was used in a BP clonase reaction that allowed its transfer by recombination into pDONR207 containing *attP* sites. The BP reaction generated *attL* sites for LR recombination with pB7WG-prom*AtiPGAM2*. The vector pDONR207-*AtiPGAM2*_{WT} was used for site directed mutagenesis of S75 thus producing pDONR207-*AtiPGAM2*_{S75T}. This latter vector was then used for site directed mutagenesis to produce the following double mutated *AtiPGAM2* vectors:

- pDONR207-*AtiPGAM2*_{S75T/D29N};
- pDONR207-*AtiPGAM2*_{S75T/R290L}.

- Gateway® cloning of *AtiPGAM2_{WT}*; *AtiPGAM2_{S75T}*; *AtiPGAM2_{S75T/D29N}*; *AtiPGAM2_{S75TR290L}* into pB7WG-prom*AtiPGAM2* → pB7WG-prom*AtiPGAM2::AtiPGAM2_{WT}*; pB7WG-prom*AtiPGAM2::AtiPGAM2_{S75T}*; pB7WG-prom*AtiPGAM2::AtiPGAM2_{S75T/D29N}*; pB7WG-prom*AtiPGAM2::AtiPGAM2_{S75T/R290L}*

Once validated, the *AtiPGAM2* pDONR207 plasmids described above were used for Gateway® recombination into pB7WG-prom*AtiPGAM2* to make pB7WG-prom*AtiPGAM2::AtiPGAM2_{WT}* and pB7WG-prom*AtiPGAM2::AtiPGAM2_{S75T}* that were used to complement sesquimutant *ipgam1^{+/-}/ipgam2^{-/-}* plants. The other plasmids (*AtiPGAM2_{S75T/D29N}*; *AtiPGAM2_{S75TR290L}*) were used to transform Col-0 plants for phosphoproteomic experiments.

3) Complementation of the *Arabidopsis thaliana* homozygous *pglp1* mutant

- *Agrobacterium*-mediated transformation of *Arabidopsis thaliana*

Agrobacterium-mediated transformation was performed by the floral dip method according to (Clough and Bent, 1998). Electro-competent *Agrobacterium tumefaciens* (GV3101::pMP90) were transformed by electroporation with the plasmid carrying the transgene to be inserted into the plant genome. These bacteria were grown on solid LB medium containing spectinomycin at 50 mg.L⁻¹. A 3 mL pre-culture in liquid LB medium containing spectinomycin at 50 mg.L⁻¹ was started with an isolated colony previously checked by PCR. This preculture was then used to inoculate a 300 mL liquid culture (LB with spectinomycin at 50 mg.L⁻¹) that was grown for 24 h at 30 °C. This culture was centrifuged at 2 800 g for 30 min at room temperature. The supernatant was removed, and the pellet was dissolved in 150 mL of inoculation medium (5 % sucrose (w/v), 0.05 % silwet (v/v)). Flowers of *Arabidopsis thaliana* plants (T₀ plants), cultivated in long days either high CO₂ (1 %) for the *pglp1* mutant or ambient air for *ipgam1^{+/-}/ipgam2^{-/-}* sesquimutants, were immersed in the bacterial solution for 3 min. The plants were then left under a plastic bell, in a wet environment, for 48 h to improve the transformation. Plants were grown in the conditions mentioned earlier until seeds were harvested and kept at 4 °C. Previously sterilized T1 seeds were sown on MS_{1/2} medium containing 15 µg.L⁻¹ glufosinate-ammonium (Pestanal®, 45520, Sigma-Aldrich), to select transformed plants. Resistant plantlets, called T1 plants, were transplanted to soil to first select transformed *ipgam1/ipgam2* double mutants. To do so, a PCR is done with primers specific for the WT genes (SAM001 iPGM1-1 LP/ SAM007 iPGM1start and SAM026 iPGM2-2 LP/ SAM027 iPGM2-2 RP) and another PCR with primers specific for the transgene (596PRO/597TER). Among these resistant plants to the herbicide, homozygous transformed lines with one insertion were selected. For *pglp1* mutants,

first, the selection of the one insertion lines was done on MS_{1/2} medium containing 15 µg.L⁻¹ glufosinate-ammonium (Pestanal®, 45520, Sigma-Aldrich) at and among the descendance of the one insertion plants, the homozygous transformed plants has been selected also on MS_{1/2} medium containing 15 µg.L⁻¹ glufosinate-ammonium.

- Selection of homozygous lines with one insertion

After the *Agrobacterium*-mediated transformation of *Arabidopsis thaliana*, there may be more than one copy of the T-DNA inserted into the plant genome. It is first necessary to select the lines with only one insertion. To do so, progeny of herbicide resistant T1 plants were tested. Therefore, T2 seeds were sown on a solid MS_{1/2} medium with vitamins and 15 µg.L⁻¹ glufosinate-ammonium, the herbicide used for selection. After two weeks, the number of resistant plants was counted; T1 lines containing one T-DNA insertion should give seed that give 75 % of resistant plantlets on selective medium. A selection of resistant plants from identified single insertion lines were transplanted and grown in a growth chamber to obtain seeds (T3 seeds). These seeds were further sown on selective medium to identify homozygous lines where 100 % of the plantlets were herbicide resistant. For each construct, three independent homozygous lines with a single insertion were selected for further characterization.

- Genomic DNA extraction and plant genotyping

One or two *A.thaliana* leaves were collected in a tube containing an iron bead and frozen at -80 °C during at least 2 h. The plant material was then ground twice in -20 °C precooled racks using a ball mill for 30 s at 30 Hz. The ground leaf tissue was quickly spun down and 300 µL of extraction buffer (200 mM Tris-HCl pH 7.5; 25 mM EDTA; 250 mM NaCl and 0.5 % SDS (v/v)) was added and gently mixed by flipping (Edwards et al., 1991). After centrifugation at 1 800 g during 10 min at 20 °C, 300 µL of supernatant were transferred to a clean tube and 300 µL of isopropanol were added, homogenized and left for 5 min at room temperature. After a 20 min centrifugation at 1 800 g and 4 °C, the supernatant was discarded, and the pellet was dried in an overturned tube at 37 °C for at least 2 h. Finally, 100 µL sterilized H₂O was added onto the pellet without shaking and tubes were incubated at 4 °C overnight to allow DNA solubilisation.

This genomic DNA was used as a PCR template to establish the genotype of transgenic lines i.e. the genetic status of T-DNA insertion mutants (homozygous mutant or WT or heterozygous) and the presence of a transgene after various transformations performed in this work. For T-DNA insertion mutants, two PCR reactions are needed to determine their genetic status. Three primers are

designed; two being specific for the gene of interest, flanking the T-DNA insertion site and one specific for the T-DNA of the corresponding collection (SALK). One PCR reaction is performed with the two gene specific primers and reveals the presence/absence of the wild type allele. The other PCR reaction is performed with the T-DNA specific primer and a gene specific primer to reveal the presence of the mutated allele. After agarose gel electrophoresis of the two PCR products and visualization of DNA by UV light, it is easy to determine the genotype of each plant. The three possibilities are:

- A fragment in the PCR for the mutated allele but no fragment in the PCR for the WT allele, the plant is a homozygous mutant.
- A fragment in the PCR for the mutated allele and a fragment in the PCR for the WT allele, the plant is heterozygous for the mutation.
- No fragment in the PCR for the mutated allele and a fragment in the PCR for the WT allele, the plant is a wild-type.

For the presence of the transgene in transformation experiments to complement the *pglp1* homozygous mutant and the *ipgam1^{+/-} /ipgam2^{-/-}* sesquimutants with different forms of the protein, the PCR reaction was performed with specific primers for the inserted *AtPGLP1* or *AtiPGAM* transgenic DNA and if a DNA fragment was observed, the corresponding plant had at least one insertion of the corresponding transgene. Typically, the PCR reaction was performed with 2 μ L of extracted genomic DNA and *Taq* polymerase as described in the “polymerase chain reaction paragraph”. Eventually, to improve the efficiency of the amplification, DMSO was added at a maximal concentration of 5 % (v/v).

4) Biochemistry methods

- Recombinant protein purification

The purification of all recombinant proteins was done with the same following protocol. Only the buffer content was specific for each protein (see Table 4). The affinity chromatography protocol used Ni-NTA-His binding resin (from Sigma-Aldrich **P6611**); a high performance Ni²⁺-charged agarose that allows the purification of recombinant proteins containing His-Tag sequences by metal chelation chromatography. It has a capacity of 5-10 mg His-Tag fusion protein per mL resin.

An over-night 3 mL pre-culture was inoculated with an isolate *E.coli* colony carrying a plasmid allowing the expression of an ORF encoding the protein of interest without any signal peptide. The

Table 4: Description of the different purification buffers, bacteria culture conditions, and antibiotics according to the plasmid and the recombinant proteins.

	AtPGLP1/pDEST-His₆-MBP (His6/AtPGLP1)	AtPGLP1/pET16b (His10/AtPGLP1)	AtGOX/pET28a (His6/AtGOX)	AtiPGAM2/pET16b (His10/AtiPGAM2)
<u>Antibiotic resistance</u>	Ampicillin (50 mg.L ⁻¹)	Ampicillin (50 mg.L ⁻¹)	Kanamycin (50 mg.L ⁻¹)	Ampicillin (50 mg.L ⁻¹)
<u>Culture conditions after IPTG addition</u>	4h at 37 °C	4h at 37 °C	Overnight at 30 °C	Overnight at 19 °C
<u>Lysis buffer</u>	Tris-HCl 50 mM pH7.5; NaCl 150 mM; MgSO ₄ 10 mM; imidazole 5 mM	Tris-HCl 50 mM pH7.5; NaCl 150 mM; MgSO ₄ 10 mM; imidazole 10 mM	Tris-HCl 50 mM pH8; NaCl 1 M; glycerol 10 % (v/v); imidazole 5 mM; FMN 100 µM	Tris-HCl 50 mM pH7.5; NaCl 300 mM; imidazole 5 mM
<u>Washing buffer</u>	Tris-HCl 50 mM pH7.5; NaCl 150 mM; MgSO ₄ 10 mM; imidazole 20 mM	Tris-HCl 50 mM pH7.5; NaCl 150 mM; MgSO ₄ 10 mM; imidazole 75 mM	Tris-HCl 50 mM pH8; NaCl 1 M; glycerol 10 % (v/v); imidazole 5 mM; FMN 100 µM	Tris-HCl 50 mM pH7.5; NaCl 300 mM; imidazole 20 mM
<u>Elution buffer</u>	Tris-HCl 50 mM pH7.5; NaCl 150 mM; MgSO ₄ 10 mM; imidazole 250 mM	Tris-HCl 50 mM pH7.5; NaCl 150 mM; MgSO ₄ 10 mM; imidazole 250 mM	Tris-HCl 50 mM pH8; NaCl 1 M; glycerol 10 % (v/v); imidazole 5 mM; FMN 100 µM	Tris-HCl 50 mM pH7.5; NaCl 300 mM; imidazole 250 mM
<u>Desalting buffer</u>	Tris-HCl 50 mM pH7.5	Tris-HCl 50 mM pH7.5	Tris-HCl 50 mM pH8; glycerol 20 % (v/v); FMN 200 µM	Tris-HCl 50 mM pH7.5

LB medium contained the appropriate antibiotic (see Table 4), and the culture was grown at 37 °C under shaking at 200 rpm. The preculture was then used to inoculate 200 mL of fresh culture (see “Bacterial culture”) in the presence of the same antibiotic. When the culture reached an absorbance of around 0.8 at 600 nm, protein production was induced by 500 μM IPTG addition in the culture conditions indicated in the table below. The bacteria culture was centrifuged at 1 800 g for 30 min and bacteria pellets corresponding to 100 mL of culture were frozen and stored at -20 °C until use (for one month maximum). The bacteria pellet was re-suspended in 3 mL of lysis buffer by pipetting, and cells were broken mechanically with a French press at 3.5 MPa. The bacterial lysate was mixed with five additional mL of lysis buffer and centrifuged at 25 200 g for 30 min. This step separated soluble and insoluble fractions. Meanwhile, 2.5 mL of affinity resin was equilibrated with 30 mL of lysis buffer (3 times with 10 mL) by centrifugation for 5 min at 2 800 g. The soluble fraction (supernatant) was collected and added to the Ni-NTA resin in 15 mL Falcon™ tubes and rotated on a wheel for 2 h at 4 °C to allow the binding of recombinant protein to the Ni²⁺ resin. The tubes were centrifuged for 5 min at 2 800 g and the resin was washed (3 times with 10 mL) with 30 mL of washing buffer containing some imidazole (for the concentrations see the table below) by centrifugation for 5 min at 2 800 g to remove non-specifically bound proteins and those containing consecutive histidine that could loosely bind the resin. Elution was performed with 2.5 mL of a high imidazole concentration elution buffer by centrifugation for 5 min at 2 800 g. The eluent was then desalted by gel filtration chromatography using a PD-10 desalting column (GE Healthcare), previously equilibrated with 5 flows of 3 mL desalting buffer, by centrifugation 2 min at 112 g. The protein concentration was then determined.

- Measurement of protein concentration

Protein concentration was determined using the Pierce™ Coomassie Plus Assay Reagent based on Bradford’s technique (Bradford, 1976). This product is a ready-to-use reagent (B6916, Sigma-Aldrich) that allows a quick measurement of sample protein concentration by spectrophotometry at OD_{595nm}. Assays are carried out with 950 μL of Bradford reagent and 50 μL of sample proteins or standard protein. To calculate the sample’s protein concentration, the OD_{595nm} of the sample was compared to a calibration curve made with different known quantities of serum albumin bovine (SAB).

- Extraction of leaf soluble proteins for AtPGLP activity measurements

Extraction of soluble proteins was performed from approximately 300 mg of *A. thaliana* leaves collected in 2 mL Eppendorf tubes containing two iron beads. Samples were frozen in liquid

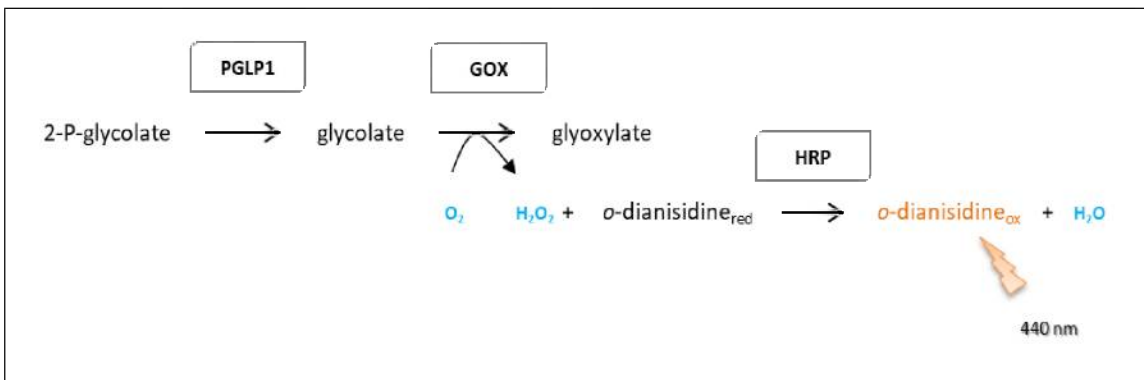


Figure 30: Diagram of the coupled reaction using GOX

2-P-glycolate: 2-phosphoglycolate; PGLP1: phosphoglycolate phosphatase; GOX: glycolate oxidase; $o\text{-dianisidine}_{red/ox}$: $o\text{-dianisidine}$ reduce/oxidized; HRP: horseradish peroxidase

nitrogen and kept at -80 °C until use. Then samples were ground using a ball mill during 60 s at 30 Hz and the resulting powder was re-suspended in 600 µL of extraction buffer (50 mM Tris-HCl pH 8; cOmplete™Mini EDTA-free Protease Inhibitor Cocktail tablets from Roche®; 1 tablet per 50 mL of solution). Samples were centrifuged for 15 min at 22 000 g and only 500 µL of supernatant was collected to avoid the pellet, transferred to a clean tube and centrifuged again as before to clear the lysate from all leaf debris. For activity measurements, protein extracts were desalted on gel filtration chromatography columns (NAP-5, from GE Healthcare) previously equilibrated with 10 mL of extraction buffer. AtPGLP1 activity was then measured using the same protocol as described for the recombinant protein (see below) using 1 mM of 2-PG and 50 µg of soluble protein extract.

- AtPGLP1 activity measurement *via* a coupled reaction

Recombinant AtPGLP1 protein was measured using a coupled reaction (Figure 30) by spectrophotometry at 440 nm with a Cary 50 UV-Vis spectrophotometer and 5 µg of purified recombinant AtPGLP1, 40 µg of purified recombinant AtGOX1, 1U of horseradish peroxidase (HRP, [P8125](#); Sigma-Aldrich), 400 µM *o*-dianisidine dihydrochloride (≥95%, **D3252**; Sigma-Aldrich), 0.01 µM to 5mM and 2-phosphoglycolic acid (lithium salt ≥95.0 %, **72764**; Sigma-Aldrich), in a final volume of 1 mL in the reaction buffer (50 mM Tris-HCl pH 8; 10 mM MgSO₄ and cOmplete™, Mini, EDTA-free Protease Inhibitor Cocktail Tablets provided in EASY packs by Sigma-Aldrich; 1 tablet in 50 mL). The reaction was initiated by addition of AtPGLP1 protein and a direct recording of the activity was measured for several minutes at 30 °C.

- AtPGLP1 activity measurement *via* nuclear magnetic resonance (NMR)

Recombinant AtPGLP1 protein activity was measured by NMR using same buffer, volume and concentrations of 2-PG as described for the coupled reaction technique, however only 2.5 µg of recombinant AtPGLP1 was used. The PGLP1 reaction was performed for 10 s. Before doing the kinetics, several times were tested to find the best time within the initial linear part of the activity to detect glycolate. The reactions were then done at 30 °C and stopped by the addition of 30 µL of 14.3 M hydrochloric acid and the produced glycolate and the remaining 2-PG were measured by NMR. To test the impact of the reduced/oxidized state of the protein on its activity, recombinant protein was incubated for 10 min at 30 °C with two different concentrations of H₂O₂ and DTT (100 mM and 500 mM). In all cases, the reaction was initiated by the addition of recombinant protein.

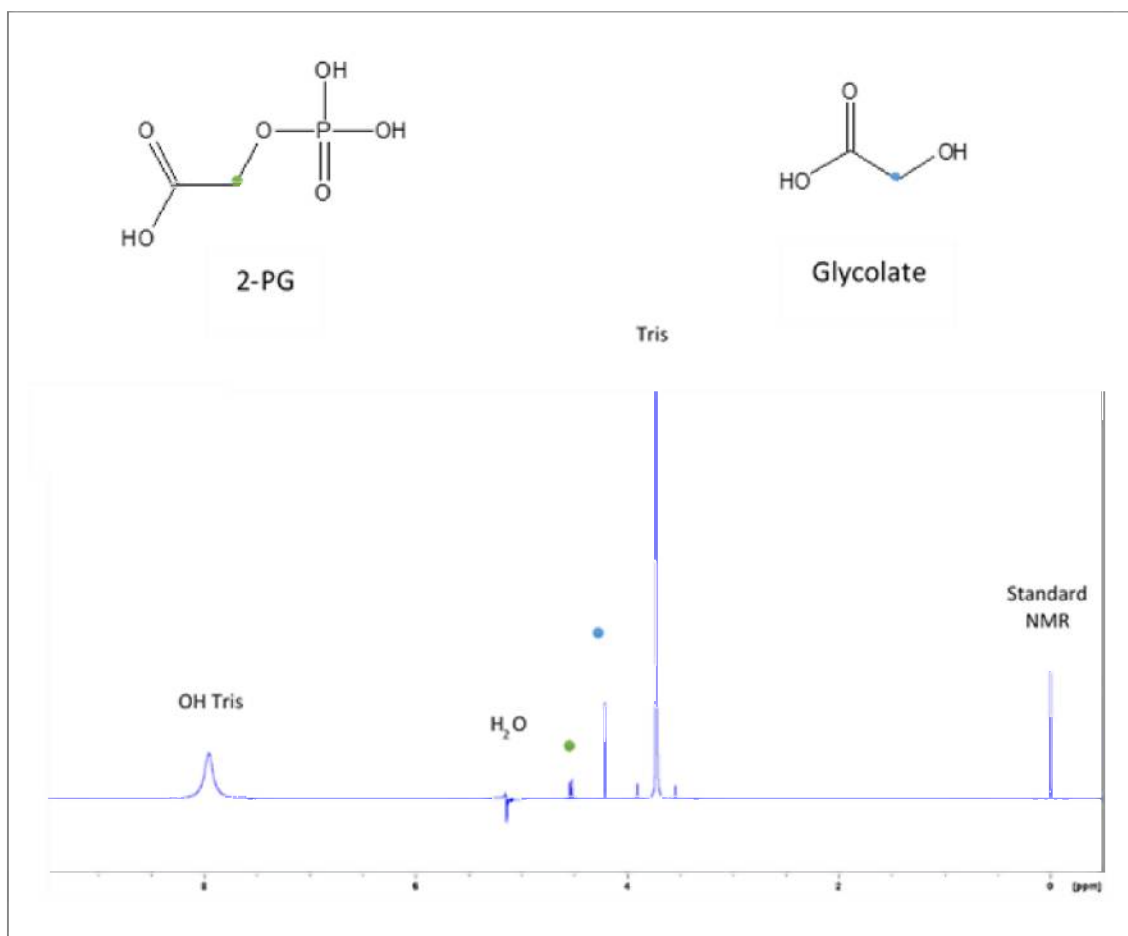


Figure 31: ¹H-NMR spectrum of an AtPGLP1 reaction buffer

Attribution of the ¹H-NMR spectrum of an assay 2 mM 2-PG, 2 mM glycolate, 50 mM Tris, PGLP (0.25 ng/μl), pH 1 with concentrated HCl

The analysis of each sample was immediately performed using the NMR of the SPOmics platform.

The NMR concept: Nuclear magnetic resonance is an analytical chemistry technique that uses the fact that many nuclei have a spin (+1/2 or -1/2), like ^1H , ^{15}N , or ^{13}C , and in absence of an external magnetic field, the nuclear spins are randomly oriented. However, when an external magnetic field is applied (B_0) to these nuclei, two possible orientations are possible, either parallel to the field or antiparallel, but these two positions do not have the same amount of energy. This difference is given by the following equation:

$$\Delta E = h \times \nu \text{ with } \nu = \frac{\gamma B}{2\pi}$$

h : resonance frequency;

γ : gyromagnetic ratio specific to each nucleus;

B : magnetic field;

ν : Planck constant

An oscillating magnetic field is applied (B_1), perpendicular to B_0 to move the spin from a low energy position to a high energy position. At the end of this pulsation, the spins recover their initial orientation with a specific frequency that depends on the initial spin orientation and the energy acquired with the B_1 pulse. This phenomenon is called the relaxation and the specific frequency is known as the Larmor frequency. This motion constitutes a radio-frequency signal, which can be detected. The signal cannot be recording this way because the frequency is too high, so it is mixed to a lower frequency signal to produce an interferogram of low frequency, called the Free Induction Decay (FID) and this frequency is converted into a spectrum (chemical shift in ppm) *via* Fourier transformation. Therefore, the chemical shift relies on the nucleus environment and it is measured with a reference compound. The result is a spectrum with the chemical shift on the X-axis and the signal intensity on the Y-axis.

NMR analysis: ^1H Nuclear Magnetic Resonance experiments were performed using an Ascend 400 MHz NanoBay instrument equipped with an AVANCE III HD console and a Prodigy BBO cryoprobe (^{31}P - ^{15}N) (Bruker). Analyses were performed at 277 K without tube spinning. To obtain a good signal-to-noise ratio 128 scans were done, representing 9.5 min of analysis per sample. The reference used was 3-(trimethylsilyl) propionic-2,2,3,3-d4 acid because it is water soluble. Data were analysed using the TopSpin software (Bruker). Free induction decay signals were processed by performing an exponential line broadening, calculating the Fourier transformation, adjusting the phase and applying a baseline correction. The attribution of each peak of glycolate and 2-PG (Figure 31) was performed

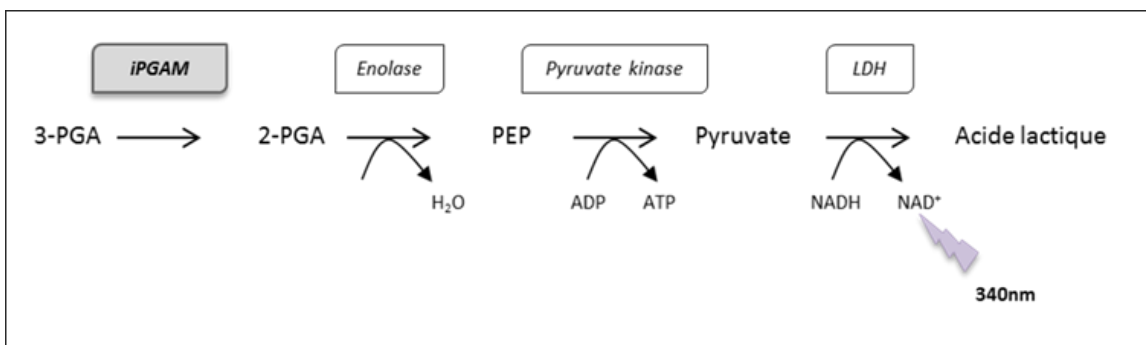


Figure 32: Diagram of the coupled reactions used to measure the activity of *AtiPGAM2*

3-PGA: 3-phosphoglycerate; 2-PGA: 2-phosphoglycerate; PEP: phosphoenolpyruvate; *iPGAM*: phosphoglycerate mutase independent; LDH: lactate dehydrogenase; ADP: adenosine diphosphate; ATP: adenosine triphosphate; NADH: nicotinamide adenine dinucleotide reduced; NAD^+ : nicotinamide adenine dinucleotide

using analytical standards (2-phosphoglycolic acid lithium salt $\geq 95.0\%$, **72764**; Sigma-Aldrich, and glycolic acid *ReagentPlus*[®], 99 %; 124737; Sigma Aldrich).

Calibration curves with known concentrations confirmed that acquisition was quantitative, i.e. that peak areas were proportional to the amount of the molecules present in the sample ($R^2 > 0.98$ for glycolate and $R^2 > 0.96$ for 2-PG). For DTT and H_2O_2 incubation, 2-PG and glycolate signals were not modified.

- *AtPGLP1* activity measurement by Pi sensor

The activity was measured in 384-well black plates (Greiner Bio-One; 781076) in a 20 μ L final volume containing 0.01 μ M to 1 mM 2-PG (2-phosphoglycolic acid lithium salt $\geq 95.0\%$, **72764**; Sigma-Aldrich), 0.25 ng of protein, and 1 mM phosphate sensor final (Invitrogen; PV4406). The reactional buffer is 50 mM Tris pH 7.5; 0.05 % Triton X-100; 10 mM $MgSO_4$ and 20 mM NaCl. The increase of fluorescence of the phosphate sensor was measured during 30 min at 30 °C using a Tecan Infinite M200.

- *AtiPGAM2* activity measurement

The activity of purified recombinant *AtiPGAM2* was measured at 30 °C in the 3-PGA (Sigma P8877) to 2-PGA direction using a coupled reaction (Figure 32) by spectrophotometry with a Varian Cary 50 spectrophotometer to observe NADH disappearance at 340 nm. The reaction buffer was as follows: 30 mM Tris-HCl pH 7.5, 20 mM KCl, 5 mM $MgSO_4$, 1 mM ATP, 0.15 mM NADH and variable concentration of 3-PGA. A large excess (2.5 U) of all enzymes of the coupled reactions, enolase (Sigma E6126; EC 4.2.1.11), pyruvate kinase (Sigma P7768; EC 2.7.1.40) and lactate dehydrogenase (Sigma L2518; EC 1.1.1.27) were used. The reaction was initiated by the addition of 2.5 μ g of recombinant protein.

- Determination of the kinetic parameters of recombinant proteins

To determine the kinetic parameters (K_m and V_{max}) of *AtPGLP1* and *AtiPGAM2*, all enzymes used in the coupled reactions were in excess and the substrates (2-PG and 3-PGA, respectively) were used in a wide range of concentrations. Therefore, since every step is equimolar, it was possible to apply the Michaëlis-Menten equation to calculate K_m and V_{max} (see Figure 33):

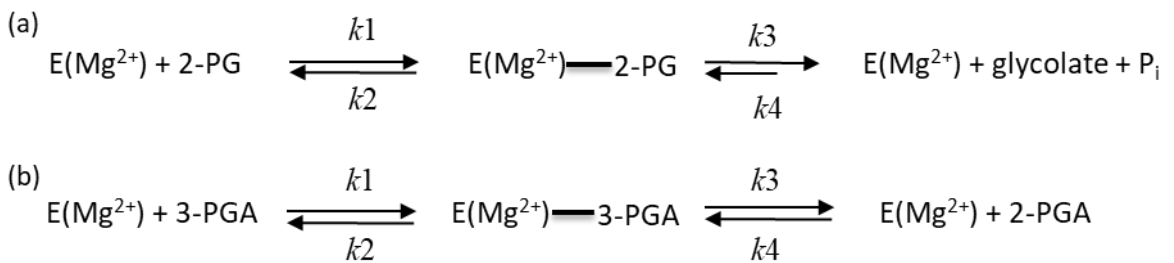


Figure 33: Diagram of the enzymatic reactions

(a) AtPGLP1: phosphoglycolate phosphatase; 2-PG: 2-phosphoglycolate; Pi: inorganic phosphate.

(b) AtiPGAM2: phosphoglycerate mutase independent; 3-PGA: 3-phosphoglycerate; 2-PGA: 2-phosphoglycerate.

$$v = \frac{V_{max} \times [S]}{K_m + [S]} \quad \text{with} \quad K_m = \frac{k_3 + k_2}{k_1} \quad \text{and} \quad V_{max} = k_3 \times [E_0]$$

[S]: Substrate concentration; [E₀]: Enzyme concentration at the beginning of the reaction; K_m is defined as the substrate concentration at which the reaction rate is half of its maximal value.

The determination of these parameters was done with the “Kinetic Enzyme Wizard” of Sigma-Plot (Systat Software Inc.). This software provides several equations to characterize different types of enzymatic reactions. It uses the Marquardt-Levenberg algorithm to resolve nonlinear least squares problems: therefore, this algorithm finds the parameters of the model curve so that the sum of the squares of the deviation is minimized.

- Protein separation by SDS-PAGE

Protein extracts (from either plants or recombinant proteins) can be separated by a 1-dimensional electrophoresis on a polyacrylamide gel according to their molecular mass, when in denaturing conditions (Laemmli, 1970). This gel is composed of two parts: the stacking gel (29:1; 4 % (v/v) acrylamide:bisacrylamide; 125 mM Tris-HCl pH 6.8; 0.1 % (v/v) SDS; 0.1 % (v/v) ammonium persulfate; 0.1 % (v/v) TEMED); that focuses all proteins at the same place on the gel before their separation by the separating gel (29:1; 10 % (v/v) acrylamide:bisacrylamide; 375 mM Tris-HCl pH 8.8; 0.1 % SDS (v/v); 0.1 % ammonium persulfate (v/v); 0.1 % TEMED (v/v)). Protein samples are denatured in a Laemmli buffer (60 mM Tris-HCl; 2 % SDS (v/v); 10 % glycerol (v/v); 2.5 % β-mercaptoethanol (v/v); 0.1 % bromophenol blue (v/v)) for 10 min at 95 °C before loading onto the gel. Protein separation was carried out for 1.5 h in a running buffer (25 mM Tris base, 192 mM glycine, 0.1 % SDS (v/v)) at 110 V. When needed, protein coloration was performed for about 20 min with InstantBlue™ (Euromedex), a ready-to-use solution, very sensitive and without any destaining step. Proteins stained by this technique are compatible with mass spectrometry (MS) analyses.

- Western Blot

After the separation of proteins by SDS-PAGE, the detection of a protein of interest was performed by Western blot using a specific antibody. Proteins were transferred onto a nitrocellulose membrane (Amersham™ Protan™ 0.45 μm, GE Healthcare) for 45 min using a semi-dry trans-blotter (BioRad) at 15 V in transfer buffer (20 mM Tris Base; 192 mM glycine; 0.1 %, SDS (v/v); 20 % ethanol (v/v)). The membrane was then incubated under shaking for 1 h at room temperature in TBST

(20 mM Tris base; 220 mM NaCl; 0.1 % Tween® (v/v)) containing 5 % of SAB (w/v) to coat the membrane with non-specific protein so that the antibodies do not fix to the membrane where there is no protein. Primary antibodies (AC I) were added at an appropriate dilution (1:250 for our anti-*AtPGLP1* serum; 1:500 for anti-GFP, G6539 Sigma) in TBST + SAB and incubated overnight at 4°C under gentle shaking. Membranes were washed 5 times for 10 min with TBST before the addition of secondary antibodies (AC II) directed against the AC I, at an appropriate dilution (1:10 000 for anti-rabbit; 1:2 000 for anti-mouse) and a 1.5 h incubation at room temperature, under shaking. AC II are coupled to HRP protein, therefore, after 5 further washes with TBST, the protein of interest was revealed using an ECL kit («enhanced chemoluminescence»; CPS350, Sigma-Aldrich) and recorded with a ChemiDoc™ imaging system.

- Stomatal aperture

Stomatal aperture assays were carried out on 8 week-old plants, germinated in normal air and cultivated in high CO₂ (1 %) or after their transfer to ambient air for 24 h. Stomatal aperture analyses of complemented *pglp1* mutant (*AtPGLP1*_{WT}-GFP; *AtPGLP1*_{T103D}-GFP; *AtPGLP1*_{T103A}-GFP; *AtPGLP1*_{S356A}-GFP; *AtPGLP1*_{S356D}-GFP), Col-0 and homozygous *pglp1* mutant plants were carried out as described in (Liu et al., 2019) . Measurements were done using the XP-Pen tablet graphic artist 22 EP Pro.

5) Phosphopeptide measurements by PAPPSO

Phosphoproteome analysis of total soluble leaf proteins

- Protein precipitation and in-solution digestion

A 300 µl sample of soluble leaf proteins in extraction buffer (50 mM Tris-HCl pH 8; cOmplete™Mini EDTA-free Protease Inhibitor Cocktail tablets from Roche®; 1 tablet per 50 mL and a Phosphatase Inhibitor Cocktails 1 & 2 (P2850 & P5726, Sigma-Aldrich)) were precipitated overnight in 0.1 M ammonium acetate/cold methanol as in (Hurkman and Tanaka, 1986). Pelleted proteins were solubilized in 200 µL of solubilisation buffer (6 M urea, 2 M thiourea, 10 mM DTT, 30 mM Tris-HCl pH 8.8, and 0.1 % acid-labile surfactant (RapiGest SF, Waters)). Protein amounts were estimated using the PlusOne 2DQuant Kit (GE Healthcare, Little Chalfont, UK) and adjusted to 6 µg µL⁻¹. Then, 1.2 mg of protein were alkylated by the addition of 40 mM iodoacetamide (IAA) and a 1 h incubation in darkness at room temperature, then diluted 8-fold by addition of 50 mM ammonium bicarbonate then trypsin-digested using porcine sequencing grade modified trypsin (Promega) with an enzyme/substrate ratio of 1:60 (w:w). Digestion was stopped by the addition of trifluoroacetic acid

(TFA; pH 2). Peptides were desalted using SepPak C18 cartridges (Vac3cc_500mg_tc18cartridges, WAT036815, Waters). Total proteome analyses were made using a 10 µg aliquot of the protein digest.

- Selective Enrichment of Phosphopeptides

This was performed using a TiO₂ multistep approach as described in (Yue et al., 2015) with some modifications. Peptides were re-suspended in 200 µL of binding solvent (2 M lactic acid/50 % ACN/0,1 % TFA) and incubated with TiO₂ beads slurries at room temperature for 15 min with mixing (end over end rotation) at room temperature. The first round of TiO₂ bead separation (GL Sciences, Tokyo, Japan) was performed with the optimized 1:4 peptide-to-TiO₂ ratio (m/m). A second enrichment was performed with the pass-through from the first TiO₂ enrichment with the same peptide-to-TiO₂ ratio. Then beads were pooled and washed twice with washing solvent (50 % acetonitrile (ACN)/ 0.1 % TFA) and five times with binding solvent, the supernatant was discarded each time. Beads were then incubated 10 min with 200 µL of elution buffer (0.5 % NH₄OH) at room temperature. The eluent was passed over a C8 stage tip filter with adaptor into a clean 2 mL tube by spinning 30 s at 300 g. Finally, 30 % ACN was passed over the C8 stage tip and eluates were completely dried by vacuum centrifugation.

- Nano LC-MS/MS analysis

The enriched phosphopeptide fraction was re-suspended in 30 µL of 2 % CH₃CN; 0.1 % formic acid (FA). HPLC was performed on a Nano-HPLC (Eksigent). Buffers A and B were prepared with 0.1 % FA in water, and with 0.1% FA in ACN, respectively. A 4 µL sample of the peptide solution was loaded at 7.5 µL.min⁻¹ for 1 min on a Biosphere C18 trap-column (particle size: 5 µm, pore size: 12 nm, inner/outer diameters: 360/100 µm, length: 20 mm; NanoSeparations) and desalted with 0.1 % FA, 2 % ACN in water. Then peptides were separated on a thermoregulated biosphere C18 column (particle size: 3 µm, pore size: 12 nm, inner/outer diameters: 360/75 µm, length: 300 mm; NanoSeparations). The peptide separation was achieved at 300 nL.min⁻¹ with the following steps: equilibration in 95 % buffer A for 9 min, separation with a linear gradient from 5 to 30 % of buffer B for 75 min and regeneration with 95 % buffer B for 5 min. Eluted peptides were on-line analyzed with a Q-Exactive PLUS mass spectrometer (ThermoFisher Scientific) using a nano-electrospray interface. Ionization (1.5 kV ionization potential) was performed with a glass needle (non-coated capillary silica tips, 360/20-10, New Objective). Peptide ions were analysed using Xcalibur 4.0.27 with the following data dependent acquisition steps: (1) full MS scan (mass-to-charge ratio (m/z), 350 to 1 400; AGCtarget = 3*10⁶) with a resolution of 70 000 and (2) MS/MS (isolation window = 1,5 m/z,

AGCtarget = 10^5 , max Ion Time = 120 ms, collision energy = 27%; resolution = 17 500). Step 2 was repeated for the eight major ions detected in step 1. Dynamic exclusion was set to 50 s. The doubly, triply and fourthly charged precursor ions were subjected to MS/MS fragmentation. For total proteome analysis, the gradient separation was increased to a 110 min run.

- Protein Identification and Peptide Quantification

Xcalibur raw data were transformed to mzXML open source format and centroided using the MS convert software in the ProteoWizard 3.0.3706 package (Kessner et al., 2008). Protein identification was performed using the X!Tandem Alanine (version 2017.2.1.4; www.thegpm.org) by querying MS/MS data against the TAIR10 protein database and a custom contaminant database. The following parameters were used: one missed trypsin cleavage allowed, alkylation of cysteine was set to static modification, oxidation of methionine and phosphorylation of serine, threonine and tyrosine were set to possible modification. Precursor mass tolerance was set to 10 ppm and fragment ion mass tolerance was 0.02 Da. A refinement search was added with similar parameters except possible N-terminal acetylation, tryptophan oxidation, glutamine and asparagine deamidation and semi-tryptic peptide tolerance. Identified proteins were filtered and grouped using X!TandemPipeline (C++) 0.2.40 (<http://pappso.inra.fr/bioinfo/xtandempipeline/>) (Langella et al., 2017) according to: (1) a minimum of one peptide required with an E-value smaller than 0.005, (2) a protein E-value (calculated as the product of unique peptide E values) smaller than 10^{-3} . Using a reverse version of the TAIR10 database as a decoy, the FDR was estimated by X!Tandem to 0.40 % and 0.96 % for peptide-spectrum match and protein identification, respectively. The same parameters were used for total proteome analysis except the search of phosphoserine phosphothreonine and phosphotyrosine, and semi-tryptic peptides were not tolerated. A minimum of two different peptides was required with an E-value smaller than 0.01, (2) a protein E-value (calculated as the product of unique peptide E-values) smaller than 10^{-3} . The FDR was estimated to 0.06 % and 0.05 % for peptide-spectrum match and protein identification, respectively. For both analyses, relative quantification of peptides was performed on extracted ion currents (XIC) using Masschroq 2.2.17, after LC-MS/MS chromatogram alignment and spike filtering, with quantification of 80 % of the theoretical natural isotopic profile. Only the most intense isotope was considered for peptide quantification.

- Data Analysis

Total proteome data were filtered for shared and unreproducible peptides. Relative protein abundance was thus calculated as the sum of normalized XICs intensities of reproducible and specific

peptides to a protein. Proteome analyses of variance were performed on log₁₀-transformed abundance values. The resulting p-values were adjusted for multiple comparisons (Benjamini and Hochberg, 1995) Proteins with adjusted P-value<0.01 were considered as showing significant abundance variations. To analyse qualitative variations, spectral counts were also used, removing proteins that produced less than five spectra in any sample. To identify proteins showing significant spectral count variations, a general linear model was performed. Proteins with adjusted P-value<0.05 were considered as showing significant abundance variations.

Phosphoproteome analysis of soluble proteins extracted from SDS-PAGE gels

- Recombinant protein preparation for phosphoproteomic

The enzymes (*AtiPGAM2_{WT}*, *AtiPGAM2_{D29N}*, *AtiPGAM2_{R290L}* and the corresponding proteins with the serine 75 mutated in threonine, S75T) were incubated at 30 °C with different 3-PGA (see results “Chapter I”) concentrations during 10 min in a 20 µL reaction buffer 30 mM Tris-HCl pH 7.5, 20 mM KCl, with or without 5 mM MgSO₄ and 2.5 µg of proteins. The reaction was stopped by adding a Laemmli buffer 4X. The protein are then separated in an electrophoresis one-dimensional polyacrylamide gel according to their molecular mass, in denaturing conditions (Laemmli, 1970). The band corresponding to iPGAM2 (61 kDa) was cut according to the molecular weight marker (PageRuler Prestained, Thermo Scientific).

- In gel digestion for recombinant protein analyses

In-gel digestion was performed according to a standard trypsin protocol. Gel pieces were washed three times by successive baths of 10 % acetic acid, 40 % ethanol following by baths of 50/50 50 mM ammonium bicarbonate/ACN. Gel pieces were shrunk with 100 % ACN. Proteins were reduced for 30 min with 10 mM DTT, 50 mM ammonium bicarbonate at 56 °C and alkylated in the dark with 55 mM IAA, 50 mM ammonium bicarbonate for 45 min at room temperature. Gel pieces were washed with 50/50 50 mM ammonium bicarbonate/ACN and then digestion was performed overnight at 37 °C with 100 ng of modified trypsin (Promega) in 50 mM ammonium bicarbonate. Peptides were extracted with 0.5 % TFA and 50 % ACN and then with ACN. Peptide extracts were dried in a vacuum centrifuge.

- Nano LC-MS/MS analysis

The nano LC-MS/MS analysis was done as previously described except that the peptide extracts were re-suspended in 20 μ L of 2 % CH₃CN / 0.1 % FA. HPLC was performed on a Nano-HPLC (Eksigent) and peptide separation was achieved at 300 nL min⁻¹ with a linear gradient from 5 to 30 % of buffer B for 37 min and regeneration with 95 % buffer B for 10 min. Finally, the gradient separation was increased to a 75 min run.

- Protein Identification and Peptide Quantification

This was also done as previously described except for the modification of some parameters. The phosphorylated residues identification was done as previously mentioned for the phosphoproteome of leaf proteins. Identified proteins were filtered and grouped using X!TandemPipeline (C++) 0.2.40 (pappso.inra.fr/bioinfo/xtandempipeline/) (Langella et al., 2017) according to: (1) a minimum of one peptide required with an E-value smaller than 0.001, (2) a protein E-value (calculated as the product of unique peptide E values) smaller than 10⁻⁵. Using a reverse version of the TAIR10 database as a decoy, the FDR was estimated by X!Tandem to 0.14 % and 0.0 % for peptide-spectrum match and protein identification, respectively. For the identification and quantification of the phosphopeptide from the recombinant protein extracted from SDS-PAGE gel the AtiPGAM2 sequence was used.

6) Yeast methods

- Yeast two-hybrid test

AtPGLP1-ORF (WT and mutated versions) devoid of the sequence encoding its chloroplast targeting peptide, sub-cloned into pDONR207 by a BP Gateway reaction, was further cloned into both pDEST-AD and pDEST-BD (generous gift of (Dreze et al., 2010)) by LR Clonase Gateway reactions according to the manufacturer's instructions for DNA amounts and overnight incubation at 25 °C. After proteinase K treatment, constructs were transformed, amplified and validated using *E. coli* DH5 α strain. AD+BD plasmid combinations were further co-transformed into *Saccharomyces cerevisiae* (see "yeast material"). The used transformation protocol was derived and simplified from (Gietz et al., 1992). Basically, the day before transformation, a yeast culture in YPDA medium was started with 3-4 isolated yeast colonies and it was agitated at 200 rpm overnight at 30 °C. Cells were

harvested (7 min at 1 250 g, room temperature), washed with sterile H₂O, then washed and concentrated twice with TE/LiAc buffer (TE: 10 mM Tris-HCl, 1 mM EDTA, pH 7.5 and autoclave; LiAc: 0.1 M lithium acetate pH 7.5 adjusted with 0.5 % (v/v) acetic acid and autoclave). For each tested combination, a 1 mL aliquot of cell suspension was centrifuged in 2 mL safe-lock Eppendorf™ tubes and to the cell pellet was sequentially added: 100 µg of salmon sperm carrier DNA previously denatured 30 min at 95 °C and placed immediately on ice, 1 µg of each type of plasmid DNA (AD and BD) and 220 µL of PEG/TE/LiAc/DMSO buffer (for 10 mL freshly prepared buffer, 5 g polyethylene glycol 3350, 1 mL 10x TE (0.1 M Tris-HCl, 10 mM EDTA, pH 7.5); 1 mL 10x LiAc (1 M lithium acetate pH 7.5 adjusted with 5 % (v/v) acetic acid) , adjust to 10 mL with H₂O; sterilized by filtration and add 10 % DMSO (v/v)) buffer. The mixture was vigorously vortexed, and tubes were placed in an Erlenmeyer and shaken at 200 rpm at 30 °C for 30-40 min. A heat shock was performed at 42 °C in a water bath for 15 min (gently mixed every 5 min) and the tubes were immediately placed into ice for 3 min. 1 mL of cold sterile water was added to each transformation mixture and gently homogenized. Cells were pelleted (3 min at 600 g, room temperature) and re-suspended in TE buffer before plating on SD-Leu-Trp plates. After 3-4 days incubation at 30 °C, a dozen of isolated colonies was picked and mixed in sterile water, the OD_{600 nm} was adjusted to 2 and serial dilutions were performed as indicated on the figures (see results “Chapter II”). 20 µL drops of each dilution were deposited on three different media: SD-Leu-Trp (permissive medium), SD-Leu-Trp-His and SD-Leu-Trp-His+3-AT 1 mM (interaction selective media). To record growth, pictures were taken after 4, 7 and 10 days of incubation at 30 °C.

Annexe: List of primers

LIST OF PRIMERS

PGLP1 primers

What it is for:	name	sequence 5'>3'	Tm °C
PGLP1 ORF mutagenesis			
C86A	665PRO	gaaacttttlatcttccgatGClgatgggtgtgatttggaaag	68.4
	666TER	cttccaaatcacaccatcaGCatcagaagataaaaagtttc	68.4
T103A	541PRO	gatagaggaggattcctgaaGctcttgatatgcttcgtgcc	73.5
	542TER	ggcacgaagcatatcaagagCttcaggaaactccctctatc	73.5
T103D	539PRO	gatagaggaggattcctgaaGAtcttgatatgcttcgtgcc	72.5
	540TER	ggcacgaagcatatcaagaTcttcaggaaactccctctatc	72.5
C232A	667PRO	attcagtatggaaactcGCf atccgtgaaaaccgggg	73.7
	668TER	ccccgggttttccacggatAGCgagtggtccataactgaat	73.7
C239A	669PRO	atccgtgaaaaccggggGctctttccatcgctacaaac	73.7
	670TER	gtttgtagcagatgaaaagaGCccccgggttttccacggat	73.7
C232/239A	671PRO	cagtatggaaactcGCt atccgtgaaaaccggggGctctttccatcgctaca	>75
	672TER	tgtagcagatgaaaagaGCccccgggttttccacggatAGCgagtggtccataactg	>75
C302A	673PRO	atccaaaagtccacagataGCcatgggttggtgatagattg	69.5
	674TER	caatctatcaccaccatgGCtatctgtgacttttggat	69.5
C320A	675PRO/684PRO	ttcgggcagaatggcggGct aagactctactcgtcctc	>75
	676TER/685TER	gaggacgagtagagttcttaGCaccgccattctgcccga	>75
T322A	545PRO	gcagaatggcgggttgaagGctctactcgtcctctcgggtg	>75
	546TER	cacccgagaggacagtagagCcttacaaccgccattctgc	>75
T322D	543PRO	gcagaatggcgggttgaagGAtctactcgtcctctcgggtg	>75
	544TER	cacccgagaggacagtagaTCcttacaaccgccattctgc	>75
T330A	549PRO	ctcgtcctctcgggtgtGcttcaatctctatgttggaaag	73.4
	550TER	ctttccaacatagagatgaaGCaacaccogagaggacgag	73.4
T330D	547PRO	ctcgtcctctcgggtgtGAttcaatctctatgttggaaag	72.4
	548TER	ctttccaacatagagatgaaTCaacaccogagaggacgag	72.4
T322/330A	557PRO	gaatggcgggttgaagGctctactcgtcctctcgggtgtGcttcaatctctatgttg	>75
	558TER	caacatagagattgaaGCaacaccogagaggacgagtagagCcttacaaccgccattc	>75
T322/330D	555PRO	gaatggcgggttgaagGAtctactcgtcctctcgggtgtGAttcaatctctatgttg	>75
	556TER	caacatagagattgaaTCaacaccogagaggacgagtagaTCcttacaaccgccattc	>75
S356A	553PRO	gcaagatctccgattttctgGctccgaaaagccgcaactg	74.7
	554TER	cagttgcggtcttcggagCagaaaaatcggagatcttgc	74.7
S356D	551PRO	gcaagatctccgattttctgGAtccgaaaagccgcaactg	73.7
	552TER	cagttgcggtcttcggatTCcagaaaaatcggagatcttgc	73.7
DEL1	677PRO	gctgttgggttgatttgat -deletion 18nt-aaaattcagtatggaacactc	69.4
	678TER	gagtgttccataactgaatttt -deletion 18nt-atcaaatccaaaccacaacagc	69.4
DEL2	679PRO	ctcaagaatggcaggtgggtggc -deletion 18nt-gttggatccactcaacgtgagcc	>75
	680TER	ggctcacgttgagtggtatccaac -deletion 18nt-gccaccactgccattcttggag	>75
PGLP1 cloning			
PGLP1mat ORF into pET [NdeI-XhoI]	535PRO	gaCATATGacgagttccaatattacaccaagag	65.8
	536TER	gtCTCGAGttatacagttgcggtcttcggag	69.5
PGLP1full ORF -Gateway adaptable	537PRO	TACAAAAAAGCAGGCTTCATgctgagtagatcagttgcttc	70.4
	538TER	CAAGAAAAGCTGGGTCTTatacagttgcggtcttcggag	72.7
mutant pglp1 genotyping (wild type allele)	559PRO	cagtacctgagttctacagagtg	62.7
	560TER	ctgtcactcaactactgatgctc	62.7
GFP fusion with PGLP1mat-ORF [XbaI-ATG_DstopSall] into pBismGFP	580PRO	gaTCTAGAAATGacgagttccaatattacaccaagag	67.2
	581TER	ctGTCGACTacagttgcggtcttcggagac	70.9
PGLP1mat_GFP cassette [XhoI-XhoI] into pET	582PRO	gaCTCGAGATGacgagttccaatattacacc	66.8
	583TER	gtCTCGAGTtatttggatagttccatccatgcccag	67.1
GFP fusion of PGLP1 full ORF [XbaI-ATG_DstopSall] into pBismGFP	584PRO	CTTCTAGAAATGCTGAGTAGATCAGTTGCTTCTGC	68.3
	581TER	ctGTCGACTacagttgcggtcttcggagac	70.9
Cassette PGLP1full_GFP cassette Gateway adaptable	585PRO	TACAAAAAAGCAGGCTTCATGCTGAGTAGATCAGTTGCTTCTGC	72.2
	586TER	CAAGAAAAGCTGGGTCTTATTGTTATAGTTCATCCATGCCATCTG	71.3
PGLP1mat ORF_Gateway adaptable (2016-17)	587PRO	TACAAAAAAGCAGGCTTCACGAGTTCCAATATTACACCAAG	69.4
	538TER	CAAGAAAAGCTGGGTCTTatacagttgcggtcttcggag	72.7
PGLP1mat ORF_Gateway adaptable (2018)	598PRO	TACAAAAAAGCAGGCTTCACGAGTTCCAATATTACACCAAGAG	70.4
	599TER (=538TER)	CAAGAAAAGCTGGGTCTTATACAGTTGCGGCTTTCGGAG	72.7

LIST OF PRIMERS (continued)

PGLP1 plant analysis			
mutant pglp1 genotyping (wild type allele)	559PRO	cagtaccctgagttctacagagtg	62.7
	560TER	ctgtcactcacttactgatgctc	62.7
Transgenic lines genotyping	488PRO (interne prom SHMT1)	GGTTATCGTTGACTGCAC TGACCAG	64.6
	593TER	CCCTTGGCACGAAGCATATCAAGAG	64.6
PCR amplification on transgenic line gDNA for further sequencing of PCR fragment covering the mutation T103A or D and S356A or D	657PRO	CATGCTGAGTAGATCAGTTGCTTC	61
	658PRO	CCTCTTCCAATGACGAGTTC	57.3
	659PRO	GTCACTCACCTTACTGATGC	57.3
	623TER	GGAAGTACTCACACATTATTCTGG	59.3
	624TER	GAACAGGTAGTTTTCCAGTAGTGC	61
	625TER	GGTTTTACGGATACAGAGTGTTC	61
	626TER	CTTGGTGAATATTGGAAGTCTGTC	59.3
	627PRO	GTTTACCCGCAATATATCTCTGTC	61
iPGAM primers			
What it is for:	name	sequence 5'>3'	Tm °C
iPGAM2ORF mutagenesis			
D29N	563PRO	CTATCGGTTTGATTGTTCTCaaATGGATGGGGTGAATCTGATCC	72.3
	564TER	GGATCAGATTACCCCATCCAtT GAGAACAATCAAACCGATAG	72.3
S75T	574PRO	GTACCGCCGTTGGTCTCCCCAct GAAGACGACATGGGAAACAGTG	>75
	575TER	CAGTGTTCCTCATGTCGCTCTTcagTGGGAGACCAACGGCGGTAC	>75
S82D (Gibson strategy)	SAM022 iPGM2S82Dfwd	GGGAAACGATGAAGTTGGCCACAATGCTCTTGG	70.7
	SAM023 iPGM2S82Drev	CAACTTCATCGTTTTCCCATGTCGCTCTTCGCTG	69.5
S82A (Gibson strategy)	SAM019w iPGM2S82Afwd	GGGAAACagTGAAGTTGGCCACAATGCTCTTGG	70.7
	SAM020w iPGM2S82Arev	CAACTTCActTTTTCCCATGTCGCTCTTCGCTG	69.5
R287L	567PRO	CAGTGTGTACATTCaATTTCctTGCTGATCGAATGGTCATGCATG	71.3
	568TER	CATGCATGACCATTTCGATCAGCaAGAAATTGAATGTAACAACATG	71.3
R290L	565PRO	CATTCAATTTCCGTGCTGATCcttATGGTCATGCATGCAAAGGC	72.3
	566TER	GCCTTTGCATGCATGACCATaaGATCAGCACGGAAATTGAATG	72.3
E325A	561PRO	GAATGCTCCAATATGATGGAActCTTAAGCTTCTAGCCGCTATC	74
	562TER	GATAGCGCTAGGAAGCTTAAGagCTCCATCATATTGGAGCATTC	74
Cloning			
Cloning into pET16b (Gibson strategy/sam)	SAM030 pET16b fw	CTCGAGGATCCGGCTGCTAA	61.4
	SAM031 pET16b rev	CTCCATATGACGACCTTCGA	57.3
	SAM036 iPGM2 rev16b	TTAGCAGCCGGATCTTCGAGTCACTTCTCGACGACTTCGATC	76.3
	SAM037 iPGM2 fw16b	TCGAAGGTCGTCATATGGAGGGTAGCTCCGGCGACGTT	75.9
Promoter region cloning	570TER_prom-iPGAM2-Spel_R	caACTAGTaaactgtggattcagatccactcgctcg	69.5
	574PRO_prom-iPGAM2-SacI_F4	gaGAGCTCgagaagaagagtgtgtgctcagtc	71.9
Cloning of iPGAM2-WT-ORF- Gateway adaptable	578PRO	TACAAAAAAGCAGGCTTCATGGGTAGCTCCGGCAGCCTTAAC	74.3
	579TER	CAAGAAAGCTGGGTCTCACTTCTCGACGACTTCGATCAG	73.7
Plant analysis			
iPGAM1 wild-type allele	SAM001 iPGM1-1 LP	ATGTTCTATCAATCTCCGGGG	57.9
	SAM007 iPGM1start	ATGGCTACCTCCTCCGCTTGGA	64
ipgam1 mutant allele (salk_003321)	SAM007 iPGM1start	ATGGCTACCTCCTCCGCTTGGA	64
	LBb1	see table common primers	65.8
iPGAM2 wild-type allele	SAM026 iPGM2-2 LP	ATTGTCTGCAAACCGAGACAC	57.9
	SAM027 iPGM2-2 RP	GGTCCAATTGTTGATGGTGAC	57.9
ipgam2 mutant allele (salk_002280)	SAM027 iPGM2-2 RP	GGTCCAATTGTTGATGGTGAC	57.9
	LBa1	see table common primers	64
Genotyping of transgenic lines	596PRO	CGTTATGCAGGAATGCTCCAATATG	61.3
	597TER	CTTCGATCAGACTTGTCTCATAGTC	61.3
Common primers			
What it is for:	name	sequence 5'>3'	Tm °C
cloning into yeast two hybrid pDEST vectors	AD-FW/pDEST-AD	CGCGTTTGAATCACTACAGGG	62.1
	BD-FW/pDEST-BD	GGCTTCAGTGGAGACTGATATGCCTC	66.4
	B2-STOP/pDEST-Y2H	GGAGACTTGACCAACCTCTGGCG	66.1
cloning into pGEM-T	Direct	acgacgttgtaaaacgacggccag	53.9
	Reverse	caggaaaacagctatgacctgattaccg	53.1
PCR fragment for Gateway BP reaction	GW-FORWARD	GGGGACAAGTTTGTAACAAAAAGCAGGCTTC	66.8
	GW-REVERSE	GGGGACCACTTTGTA CAAGAAAGCTGGGTC	69.5
cloning into pET	PromT7-PRO	TAATACGACTCACTATAGGG	53.2
	TermT7-TER	GCTAGTTATTGCTCAGCGGT	57.3
T-DNA mutant genotyping (Salk collection)	LBa1 (SALK)	tggttcacgtagtggccatcg	64
	LBb1 (SALK)	CGGTGGACCGCTTGTGCAACT	65.8

REFERENCES

A

- Abat JK, Mattoo AK, Deswal R** (2008) S-nitrosylated proteins of a medicinal CAM plant *Kalanchoe pinnata*– ribulose-1,5-bisphosphate carboxylase/oxygenase activity targeted for inhibition. *FEBS J* **275**: 2862–2872
- Ahammed GJ, Li X, Zhang G, Zhang H, Shi J, Pan C, Yu J, Shi K** (2018) Tomato photorespiratory glycolate-oxidase-derived H₂O₂ production contributes to basal defence against *Pseudomonas syringae*. *Plant Cell Environ* **41**: 1126–1138
- Allen KN, Dunaway-Mariano D** (2004) Phosphoryl group transfer: evolution of a catalytic scaffold. *Trends Biochem Sci* **29**: 495–503
- Allen KN, Dunaway-Mariano D** (2016) Catalytic scaffolds for phosphoryl group transfer. *Curr Opin Struct Biol* **41**: 172–179
- Alrefai WA, Gill RK** (2007) Bile Acid Transporters: Structure, Function, Regulation and Pathophysiological Implications. *Pharm Res* **24**: 1803–1823
- Anderson LE** (1971) Chloroplast and cytoplasmic enzymes II. Pea leaf triose phosphate isomerases. *Biochim Biophys Acta - Enzymol* **235**: 237–244
- Andrews M, Condrón LM, Kemp PD, Topping JF, Lindsey K, Hodge S, Raven JA** (2019) Elevated CO₂ effects on nitrogen assimilation and growth of C₃ vascular plants are similar regardless of N-form assimilated. *J Exp Bot* **70**: 683–690
- Andrews M, Raven JA, Lea PJ** (2013) Do plants need nitrate? the mechanisms by which nitrogen form affects plants. *Ann Appl Biol* **163**: 174–199
- Andrews M, Raven JA, Lea PJ, Sprent JI** (2005) A Role for Shoot Protein in Shoot–Root Dry Matter Allocation in Higher Plants. *Ann Bot* **97**: 3–10
- Andriotis VME, Kruger NJ, Pike MJ, Smith AM** (2010) Plastidial glycolysis in developing *Arabidopsis* embryos. *New Phytol* **185**: 649–662
- Aryal UK, Krochko JE, Ross ARS** (2012) Identification of Phosphoproteins in *Arabidopsis thaliana* Leaves Using Polyethylene Glycol Fractionation, Immobilized Metal-ion Affinity Chromatography, Two-Dimensional Gel Electrophoresis and Mass Spectrometry. *J Proteome Res* **11**: 425–437
- Baginsky S, Gruissem W** (2009) The Chloroplast Kinase Network: New Insights from Large-Scale Phosphoproteome Profiling. *Mol Plant* **2**: 1141–1153
- Baldy P, Jacquot JP, Lavergne D, Champigny ML** (1989) Corn phosphoglycolate phosphatase: Modulation of activity by pyridine nucleotides and adenylate energy charge. *Photosynth Res* **22**: 147–155
- Balmer Y, Vensel WH, Tanaka CK, Hurkman WJ, Gelhaye E, Rouhier N, Jacquot J-P, Manieri W, Schürmann P, Droux M, et al** (2004) Thioredoxin links redox to the regulation of fundamental processes of plant mitochondria. *Proc Natl Acad Sci U S A* **101**: 2642–2647
- Bauwe H, Hagemann M, Fernie AR** (2010) Photorespiration: players, partners and origin. *Trends Plant Sci* **15**: 330–336
- Bauwe H, Kolukisaoglu Ü** (2003a) Genetic manipulation of glycine decarboxylation. *J Exp Bot* **54**:

1523–1535

- Bauwe H, Kolukisaoglu Ü** (2003b) Genetic manipulation of glycine decarboxylation. *J Exp Bot* **54**: 1523–1535
- Bayer RG, Stael S, Rocha AG, Mair A, Vothknecht UC, Teige M** (2012) Chloroplast-localized protein kinases: a step forward towards a complete inventory. *J Exp Bot* **63**: 1713–1723
- Becker B** (2013) Snow ball earth and the split of Streptophyta and Chlorophyta. *Trends Plant Sci* **18**: 180–183
- Belanger FC, Ogren WL** (1987) Phosphoglycolate phosphatase: purification and preparation of antibodies. *Photosynth Res* **14**: 3–13
- Benjamini Y, Hochberg Y** (1995) Controlling the False Discovery Rate: A Practical and Powerful Approach to Multiple Testing. *J R Stat Soc Ser B* **57**: 289–300
- Betti M, Bauwe H, Busch FA, Fernie AR, Keech O, Levey M, Ort DR, Parry MAJ, Sage R, Timm S, et al** (2016) Manipulating photorespiration to increase plant productivity: Recent advances and perspectives for crop improvement. *J Exp Bot* **67**: 2977–2988
- Bienert S, Waterhouse A, de Beer TAP, Tauriello G, Studer G, Bordoli L, Schwede T** (2017) The SWISS-MODEL Repository-new features and functionality. *Nucleic Acids Res* **45**: 313–319
- Bienvenut WV, Scarpelli J-P, Dumestier J, Meinnel T, Giglione C** (2017) EnCOUNTER: a parsing tool to uncover the mature N-terminus of organelle-targeted proteins in complex samples. *BMC Bioinformatics* **18**: 182
- Blackburn EA, Fuad FAA, Morgan HP, Nowicki MW, Wear MA, Michels PAM, Fothergill-Gilmore LA, Walkinshaw MD** (2014) Trypanosomatid phosphoglycerate mutases have multiple conformational and oligomeric states. *Biochem Biophys Res Commun* **450**: 936–941
- Blackwell RD, Murray AJS, Lea PJ, Kendall AC, Hall NP, Turner JC, Wallsgrave RM** (1988) The value of mutants unable to carry out photorespiration. *Photosynth Res* **16**: 155–176
- Blank CE, Sánchez-Baracaldo P** (2010) Timing of morphological and ecological innovations in the cyanobacteria – a key to understanding the rise in atmospheric oxygen. *Geobiology* **8**: 1–23
- Bloom AJ** (2015a) Photorespiration and nitrate assimilation: a major intersection between plant carbon and nitrogen. *Photosynth Res* **123**: 117–128
- Bloom AJ** (2015b) The increasing importance of distinguishing among plant nitrogen sources. *Curr Opin Plant Biol* **25**: 10–16
- Bloom AJ** (2015c) Photorespiration and nitrate assimilation: A major intersection between plant carbon and nitrogen. *Photosynth Res* **123**: 117–128
- Bloom AJ, Asensio JSR, Randall L, Rachmilevitch S, Cousins AB, Carlisle EA** (2012) CO₂ enrichment inhibits shoot nitrate assimilation in C₃ but not C₄ plants and slows growth under nitrate in C₃ plants. *Ecology* **93**: 355–367
- Bloom AJ, Lancaster KM** (2018a) Manganese binding to Rubisco could drive a photorespiratory pathway that increases the energy efficiency of photosynthesis. *Nat Plants* **4**: 414–422
- Bloom AJ, Lancaster KM** (2018b) Manganese binding to Rubisco could drive a photorespiratory pathway that increases the energy efficiency of photosynthesis. *Nat Plants* **4**: 414–422

- Bloom AJ, Smart DR, Nguyen DT, Searles PS** (2002a) Nitrogen assimilation and growth of wheat under elevated carbon dioxide. *Proc Natl Acad Sci* **99**: 1730–1735
- Bloom AJ, Smart DR, Nguyen DT, Searles PS** (2002b) Nitrogen assimilation and growth of wheat under elevated carbon dioxide. *Proc Natl Acad Sci U S A* **99**: 1730–1735
- Boex-Fontvieille E, Davanture M, Jossier M, Zivy M, Hodges M, Tcherkez G** (2014) Photosynthetic activity influences cellulose biosynthesis and phosphorylation of proteins involved therein in *Arabidopsis* leaves. *J Exp Bot* **65**: 4997–5010
- Boex-Fontvieille E, Daventure M, Jossier M, Zivy M, Hodges M, Tcherkez G** (2013) Photosynthetic control of *Arabidopsis* leaf cytoplasmic translation initiation by protein phosphorylation. *PLoS One* **8**: 70692–70692
- Boldt R, Edner C, Kolukisaoglu Ü, Hagemann M, Weckwerth W, Wienkoop S, Morgenthal K, Bauwe H** (2005a) GLYCERATE 3-KINASE, the Last Unknown Enzyme in the Photorespiratory Cycle in *Arabidopsis*, Belongs to a Novel Kinase Family. *Plant Cell* **17**: 2413–2420
- Boldt R, Edner C, Kolukisaoglu Ü, Hagemann M, Weckwerth W, Wienkoop S, Morgenthal K, Bauwe H** (2005b) D-GLYCERATE 3-KINASE, the last unknown enzyme in the photorespiratory cycle in *Arabidopsis*, belongs to a novel kinase family. *Plant Cell* **17**: 2413–2420
- Botha C, Dennis T** (1986a) Isozymes of Phosphoglyceromutase from the Developing Endosperm *Ricinus communis* : Isolation and Kinetic Properties ' of The isozymes of phosphoglyceromutase from the developing endosperm of *Ricinus communis* have been partially purified . The purified cyto. **245**: 96–103
- Botha FC, Dennis DT** (1986b) Isozymes of phosphoglyceromutase from the developing endosperm of *Ricinus communis*: Isolation and kinetic properties. *Arch Biochem Biophys* **245**: 96–103
- Bowsher CG, Lacey AE, Hanke GT, Clarkson DT, Saker LR, Stulen I, Emes MJ** (2007a) The effect of Glc6P uptake and its subsequent oxidation within pea root plastids on nitrite reduction and glutamate synthesis. *J Exp Bot* **58**: 1109–1118
- Bowsher CG, Scrase-Field EFAL, Esposito S, Emes MJ, Tetlow IJ** (2007b) Characterization of ADP-glucose transport across the cereal endosperm amyloplast envelope. *J Exp Bot* **58**: 1321–1332
- Bradford MM** (1976) A rapid and sensitive method for the quantitation of microgram quantities of protein utilizing the principle of protein-dye binding. *Anal Biochem* **72**: 248–254
- Brautigam A, Gowik U** (2016) Photorespiration connects C3 and C4 photosynthesis. *J Exp Bot* **67**: 2953–2962
- Breathnach R, Knowles JR** (1977) Phosphoglycerate mutase from wheat germ: studies with 18O-labeled substrate, investigations of the phosphatase and phosphoryl transfer activities, and evidence for a phosphoryl-enzyme intermediate. *Biochemistry* **16**: 3054–3060
- Bryce JH, ap Rees T** (1985) Rapid decarboxylation of the products of dark fixation of CO₂ in roots of *pisum* and *Plantago*. *Phytochemistry* **24**: 1635–1638
- Bult CJ, White O, Olsen GJ, Zhou L, Fleischmann RD, Sutton GG, Blake JA, FitzGerald LM, Clayton RA, Gocayne JD, et al** (1996) Complete genome sequence of the methanogenic archaeon, *Methanococcus jannaschii*. *Science* (80-) **273**: 1058–1073
- Bungard RA, Wingler A, Morton JD, Andrews M, Press MC, Scholes JD** (1999) Ammonium can

- stimulate nitrate and nitrite reductase in the absence of nitrate in *Clematis vitalba*. *Plant Cell Environ* **22**: 859–866
- Burroughs AM, Allen KN, Dunaway-mariano D, Aravind L** (2006a) Evolutionary Genomics of the HAD Superfamily : Understanding the Structural Adaptations and Catalytic Diversity in a Superfamily of Phosphoesterases and Allied Enzymes. **361**: 1003–1034
- Burroughs AM, Allen KN, Dunaway-Mariano D, Aravind L** (2006b) Evolutionary Genomics of the HAD Superfamily: Understanding the Structural Adaptations and Catalytic Diversity in a Superfamily of Phosphoesterases and Allied Enzymes. *J Mol Biol* **361**: 1003–1034
- Busch FA** (2013) Current methods for estimating the rate of photorespiration in leaves. *Plant Biol* **15**: 648–655
- Bustos DM, Iglesias AA** (2002) Non-phosphorylating glyceraldehyde-3-phosphate dehydrogenase is post-translationally phosphorylated in heterotrophic cells of wheat (*Triticum aestivum*). *FEBS Lett* **530**: 169–173
- Bykova N V, Keerberg O, Pärnik T, Bauwe H, Gardeström P** (2005) Interaction between photorespiration and respiration in transgenic potato plants with antisense reduction in glycine decarboxylase. *Planta* **222**: 130–140
- Camejo D, Romero-Puertas MDC, Rodriguez-Serrano M, Sandalio LM, Lazaro JJ, Jimenez A, Sevilla F** (2013) Salinity-induced changes in S-nitrosylation of pea mitochondrial proteins. *J Proteomics* **79**: 87–99
- Campbell JW, Hodgson GI, Watson HC** (1972) Low resolution structure of yeast phosphoglycerate mutase. *Nat New Biol* **240**: 137–139
- Campbell WJ, Ogren WL** (1990) Glyoxylate inhibition of ribulosebiphosphate carboxylase/oxygenase activation in intact, lysed, and reconstituted chloroplasts. *Photosynth Res* **23**: 257–268
- Cao H, Zhou Y, Chang Y, Zhang X, Li C, Ren D** (2019) Comparative phosphoproteomic analysis of developing maize seeds suggests a pivotal role for enolase in promoting starch synthesis. *Plant Sci* **289**: 110243
- Caparrós-Martín JA, McCarthy-Suárez I, Culiáñez-Macià FA** (2013) HAD hydrolase function unveiled by substrate screening: Enzymatic characterization of *Arabidopsis thaliana* subclass I phosphosugar phosphatase AtSgpp. *Planta* **237**: 943–954
- Carnal NW, Black CC** (1979) Pyrophosphate-dependent 6-phosphofructokinase, a new glycolytic enzyme in pineapple leaves. *Biochem Biophys Res Commun* **86**: 20–26
- Corveau D, Kraut A, Stotz HU, Mueller MJ, Couté Y, Rey P** (2016) Characterization of the *Arabidopsis thaliana* 2-Cys peroxiredoxin interactome. *Plant Sci* **252**: 30–41
- Chaouch S, Noctor G** (2010) Myo-inositol abolishes salicylic acid-dependent cell death and pathogen defence responses triggered by peroxisomal hydrogen peroxide. *New Phytol* **188**: 711–718
- Chastain CJ, Ogren WL** (1985) Photorespiration-Induced Reduction of Ribulose Biphosphate Carboxylase Activation Level. *Plant Physiol* **77**: 851–856
- Chern M, Bai W, Chen X, Canlas PE, Ronald PC** (2013) Reduced expression of glycolate oxidase leads to enhanced disease resistance in rice. *PeerJ* **1**: 28
- Chibani K, Couturier J, Selles B, Jacquot J-P, Rouhier N** (2010) The chloroplastic thiol reducing

- systems: dual functions in the regulation of carbohydrate metabolism and regeneration of antioxidant enzymes, emphasis on the poplar redoxin equipment. *Photosynth Res* **104**: 75–99
- Chollet R, Vidal J, O’Leary MH** (1996) PHOSPHOENOLPYRUVATE CARBOXYLASE: A Ubiquitous, Highly Regulated Enzyme in Plants. *Annu Rev Plant Physiol Plant Mol Biol* **47**: 273–298
- Christeller JT, Tolbert NE** (1978a) Phosphoglycolate phosphatase. Effect of cation and pH on activity. *J Biol Chem* **253**: 1786–1790
- Christeller JT, Tolbert NE** (1978b) Phosphoglycolate phosphatase. Purification and properties. *J Biol Chem* **253**: 1780–1785
- Christeller JT, Tolbert NE** (1978c) Mechanism of phosphoglycolate phosphatase. Studies of hydrolysis and transphosphorylation, substrate analogs, and sulfhydryl inhibition. *J Biol Chem* **253**: 1791–1798
- Cleland WW, Andrews TJ, Gutteridge S, Hartman FC, Lorimer GH** (1998) Mechanism of Rubisco: The Carbamate as General Base. *Chem Rev* **98**: 549–562
- Clough SJ, Bent AF** (1998) Floral dip: a simplified method for *Agrobacterium* -mediated transformation of *Arabidopsis thaliana*. *Plant J* **16**: 735–743
- Collakova E, Goyer A, Naponelli V, Krassovskaya I, Gregory 3rd JF, Hanson AD, Shachar-Hill Y** (2008) *Arabidopsis* 10-formyl tetrahydrofolate deformylases are essential for photorespiration. *Plant Cell* **20**: 1818–1832
- Collard F, Baldin F, Gerin I, Bolsée J, Noël G, Graff J, Veiga-da-cunha M, Stroobant V, Vertommen D, Houddane A, et al** (2016a) side products in mammals and yeast. doi: 10.1038/nchembio.2104
- Collard F, Baldin F, Gerin I, Bolsée J, Noël G, Graff J, Veiga-Da-Cunha M, Stroobant V, Vertommen D, Houddane A, et al** (2016b) A conserved phosphatase destroys toxic glycolytic side products in mammals and yeast. *Nat Chem Biol* **12**: 601–607
- Copeland LES, Turner JF** (1987) The Regulation of Glycolysis and the Pentose Phosphate Pathway. *Biochem plants* **11**: 107–128
- Coschigano KT, Melo-Oliveira R, Lim J, Coruzzi GM** (1998) *Arabidopsis* gls Mutants and Distinct Fd-GOGAT Genes: Implications for Photorespiration and Primary Nitrogen Assimilation. *Plant Cell* **10**: 741–752
- Cossins EA, Chen L** (1997) Folates and one-carbon metabolism in plants and fungi. *Phytochemistry* **45**: 437–452
- Cousins AB, Pracharoenwattana I, Zhou W, Smith SM, Badger MR** (2008) Peroxisomal malate dehydrogenase is not essential for photorespiration in *Arabidopsis* but its absence causes an increase in the stoichiometry of photorespiratory CO₂ release. *Plant Physiol* **148**: 786–795
- Crowther GJ, Booker ML, He M, Li T, Raverdy S, Novelli JF, He P, Dale NRG, Fife AM, Barker RH, et al** (2014) Cofactor-Independent Phosphoglycerate Mutase from Nematodes Has Limited Druggability, as Revealed by Two High-Throughput Screens. *PLoS Negl Trop Dis* **8**: 34
- Cui L-L, Lu Y, Li Y, Yang C, Peng X-X** (2016) Overexpression of Glycolate Oxidase Confers Improved Photosynthesis under High Light and High Temperature in Rice . *Front Plant Sci* **7**: 1165
- Dalal J, Lopez H, Vasani NB, Hu Z, Swift JE, Yalamanchili R, Dvora M, Lin X, Xie D, Qu R, et al** (2015) A photorespiratory bypass increases plant growth and seed yield in biofuel crop *Camelina*

- sativa. *Biotechnol Biofuels* **8**: 1–22
- Davis SJ, Vierstra RD** (1998) Soluble, highly fluorescent variants of green fluorescent protein (GFP) for use in higher plants. *Plant Mol Biol* **36**: 521–528
- Delaossa PP, Grana X, Ruizlozano P, Climent F** (1994) Isolation and Characterization of Cofactor-Independent Phosphoglycerate Mutase Gene from Maize. *Biochem Biophys Res Commun* **203**: 1204–1209
- Dellero Y, Jossier M, Glab N, Oury C, Tcherkez G, Hodges M** (2016a) Decreased glycolate oxidase activity leads to altered carbon allocation and leaf senescence after a transfer from high CO₂ to ambient air in *Arabidopsis thaliana*. *J Exp Bot* **67**: 3149–3163
- Dellero Y, Jossier M, Schmitz J, Maurino VG, Hodges M** (2016b) Photorespiratory glycolate-glyoxylate metabolism. *J Exp Bot* **16**: 3041–3042
- Dellero Y, Lamothe-Sibold M, Jossier M, Hodges M** (2015a) *Arabidopsis thaliana* ggt1 photorespiratory mutants maintain leaf carbon/nitrogen balance by reducing RuBisCO content and plant growth. *Plant J* **83**: 1005–1018
- Dellero Y, Lamothe-Sibold M, Jossier M, Hodges M** (2015b) *Arabidopsis thaliana* ggt1 photorespiratory mutants maintain leaf carbon/nitrogen balance by reducing RuBisCO content and plant growth. *Plant J* **83**: 1005–1018
- Dellero Y, Mauve C, Boex-Fontvieille E, Flesch V, Jossier M, Tcherkez G, Hodges M** (2015c) Experimental evidence for a hydride transfer mechanism in plant glycolate oxidase catalysis. *J Biol Chem* **290**: 1689–1698
- Desai UJ, Pfaffle PK** (1995) Single-step purification of a thermostable DNA polymerase expressed in *Escherichia coli*. England
- Douce R, Bourguignon J, Neuburger M, Rébeillé F** (2001) The glycine decarboxylase system: A fascinating complex. *Trends Plant Sci* **6**: 167–176
- Dreze M, Monachello D, Lurin C, Cusick ME, Hill DE, Vidal M, Braun PBT-M in E** (2010) Chapter 12 - High-Quality Binary Interactome Mapping. *Guid. to Yeast Genet. Funct. Genomics, Proteomics, Other Syst. Anal.* Academic Press, pp 281–315
- Duff SMG, Moorhead GBG, Lefebvre DD, Plaxton WC** (1989) Phosphate Starvation Inducible 'Bypasses' of Adenylate and Phosphate Dependent Glycolytic Enzymes in *Brassica nigra* Suspension Cells. *Plant Physiol* **90**: 1275–1278
- Dumont S, Bykova N V, Pelletier G, Dorion S, Rivoal J** (2016) Cytosolic Triosephosphate Isomerase from *Arabidopsis thaliana* Is Reversibly Modified by Glutathione on Cysteines 127 and 218. *Front Plant Sci* **7**: 1942
- Durek P, Schmidt R, Heazlewood JL, Jones A, MacLean D, Nagel A, Kersten B, Schulze WX** (2010) PhosPhAt: the *Arabidopsis thaliana* phosphorylation site database. An update. *Nucleic Acids Res* **38**: 828–834
- Duy D, Soll J, Philippar K** (2007) Solute channels of the outer membrane: From bacteria to chloroplasts. *Biol Chem* **388**: 879–889
- Edwards K, Johnstone C, Thompson C** (1991) A simple and rapid method for the preparation of plant genomic DNA for PCR analysis. *Nucleic Acids Res* **19**: 1349

- Edwards S, Nguyen BT, Do B, Roberts JKM** (1998) Contribution of malic enzyme, pyruvate kinase, phosphoenolpyruvate carboxylase, and the krebs cycle to respiration and biosynthesis and to intracellular pH regulation during hypoxia in maize root tips observed by nuclear magnetic resonance imaging and gas. *Plant Physiol* **116**: 1073–1081
- Eisenhut M, Bräutigam A, Timm S, Florian A, Tohge T, Fernie AR, Bauwe H, Weber APM** (2017) Photorespiration Is Crucial for Dynamic Response of Photosynthetic Metabolism and Stomatal Movement to Altered CO₂ Availability. *Mol Plant* **10**: 47–61
- Eisenhut M, Pick TR, Bordych C, Weber APM** (2013a) Towards closing the remaining gaps in photorespiration - the essential but unexplored role of transport proteins. *Plant Biol* **15**: 676–685
- Eisenhut M, Planchais S, Cabassa C, Guivarc’h A, Justin AM, Taconnat L, Renou JP, Linka M, Gagneul D, Timm S, et al** (2013b) Arabidopsis A BOUT de SOUFFLE is a putative mitochondrial transporter involved in photorespiratory metabolism and is required for meristem growth at ambient CO₂ levels. *Plant J* **73**: 836–849
- Eisenhut M, Ruth W, Haimovich M, Bauwe H, Kaplan A, Hagemann M** (2008) The photorespiratory glycolate metabolism is essential for cyanobacteria and might have been conveyed endosymbiontically to plants. *Proc Natl Acad Sci U S A* **105**: 17199–17204
- Engel N, van den Daele K, Kolukisaoglu Ü, Morgenthal K, Weckwerth W, Pärnik T, Keerberg O, Bauwe H** (2007) Deletion of Glycine Decarboxylase in Arabidopsis Is Lethal under Nonphotorespiratory Conditions. *Plant Physiol* **144**: 1328–1335
- Engel N, Ewald R, Gupta KJ, Zrenner R, Hagemann M, Bauwe H** (2011) The Presequence of Arabidopsis Serine Hydroxymethyltransferase SHM2 Selectively Prevents Import into Mesophyll Mitochondria. *Plant Physiol* **157**: 1711–1720
- Engqvist MKM, Schmitz J, Gertzmann A, Florian A, Jaspert N, Arif M, Balazadeh S, Mueller-Roeber B, Fernie AR, Maurino VG** (2015) GLYCOLATE OXIDASE3, a Glycolate Oxidase Homolog of Yeast L-Lactate Cytochrome c Oxidoreductase, Supports L-Lactate Oxidation in Roots of Arabidopsis. *Plant Physiol* **169**: 1042–1061
- Enzymes C** (u.s.A.). **22**: 237–244
- Esser C, Kuhn A, Groth G, Lercher MJ, Maurino VG** (2014) Plant and Animal Glycolate Oxidases Have a Common Eukaryotic Ancestor and Convergently Duplicated to Evolve Long-Chain 2-Hydroxy Acid Oxidases. *Mol Biol Evol* **31**: 1089–1101
- Evans JR** (2013) Improving Photosynthesis. *Plant Physiol* **162**: 1780–1793
- Facchinelli F, Weber APM** (2011) The metabolite transporters of the plastid envelope: an update. *Front Plant Sci* **2**: 50
- Fahnenstich H, Scarpeci TE, Valle EM, Flügge UI, Maurino VG** (2008) Generation of hydrogen peroxide in chloroplasts of arabidopsis overexpressing glycolate oxidase as an inducible system to study oxidative stress. *Plant Physiol* **148**: 719–729
- Fedosejevs ET, Ying S, Park J, Anderson EM, Mullen RT, She Y-M, Plaxton WC** (2014) Biochemical and molecular characterization of RcSUS1, a cytosolic sucrose synthase phosphorylated in vivo at serine 11 in developing castor oil seeds. *J Biol Chem* **289**: 33412–33424
- Fischer K, Kammerer B, Gutensohn M, Arbinger B, Weber A, Häusler RE, Flügge UI** (1997) A new

- class of plastidic phosphate translocators: a putative link between primary and secondary metabolism by the phosphoenolpyruvate/phosphate antiporter. *Plant Cell* **9**: 453–462
- Flügel F, Timm S, Arrivault S, Florian A, Stitt M, Fernie AR, Bauwe H** (2017) The Photorespiratory Metabolite 2-Phosphoglycolate Regulates Photosynthesis and Starch Accumulation in *Arabidopsis*. *Plant Cell* **29**: 2537–2551
- Flügge UI, Heldt HW** (1984) The phosphate-triose phosphate-phosphoglycerate translocator of the chloroplast. *Trends Biochem Sci* **9**: 530–533
- Fonseca-Pereira P, Souza PVL, Hou L, Schwab S, Geigenberger P, Nunes-Nesi A, Timm S, Fernie AR, Thormählen I, Araújo WL, et al** (2019) Thioredoxin h2 contributes to the redox regulation of mitochondrial photorespiratory metabolism. *Plant Cell Environ* **1–21**
- Fothergill-Gilmore LA, Watson HC** (1989) The phosphoglycerate mutases. *Adv Enzymol Relat Areas Mol Biol* **62**: 227–313
- Foyer CH, Bloom AJ, Queval G, Noctor G** (2009) Photorespiratory Metabolism: Genes, Mutants, Energetics, and Redox Signaling. *Annu Rev Plant Biol* **60**: 455–484
- Fraser HI, Kvaratskhelia M, White MF** (1999) The two analogous phosphoglycerate mutases of *Escherichia coli*. *FEBS Lett* **455**: 344–348
- Frugoli JA, Zhong HH, Nuccio ML, McCourt P, McPeck MA, Thomas TL, McClung CR** (1996) Catalase Is Encoded by a Multigene Family in *Arabidopsis thaliana* (L.) Heynh. *Plant Physiol* **112**: 327–336
- Fuad FAA, Fothergill-Gilmore LA, Nowicki MW, Eades LJ, Morgan HP, McNae IW, Michels PAM, Walkinshaw MD** (2011) Phosphoglycerate mutase from *Trypanosoma brucei* is hyperactivated by cobalt in vitro, but not in vivo. *Metallomics* **3**: 1310–1317
- Funato Y, Hayashi T, Irino Y, Takenawa T, Miki H** (2013) Nucleoredoxin regulates glucose metabolism via phosphofructokinase 1. *Biochem Biophys Res Commun* **440**: 737–742
- Furumoto T, Yamaguchi T, Ohshima-Ichie Y, Nakamura M, Tsuchida-Iwata Y, Shimamura M, Ohnishi J, Hata S, Gowik U, Westhoff P, et al** (2011) A plastidial sodium-dependent pyruvate transporter. *Nature* **476**: 472
- Gao J, Agrawal GK, Thelen JJ, Xu D** (2009) P3DB: a plant protein phosphorylation database. *Nucleic Acids Res* **37**: 960–962
- Garland WJ, Dennis DT** (1980) Plastid and cytosolic phosphofructokinases from the developing endosperm of *ricinus communis*: II. Comparison of the kinetic and regulatory properties of the isoenzymes. *Arch Biochem Biophys* **204**: 310–317
- Geigenberger P, Thormählen I, Daloso DM, Fernie AR** (2017) The Unprecedented Versatility of the Plant Thioredoxin System. *Trends Plant Sci* **22**: 249–262
- Gibson DG, Young L, Chuang R-Y, Venter JC, Hutchison CA 3rd, Smith HO** (2009) Enzymatic assembly of DNA molecules up to several hundred kilobases. *Nat Methods* **6**: 343–345
- Giegé P, Heazlewood JL, Roessner-Tunali U, Harvey Millar A, Fernie AR, Leaver CJ, Sweetlove LJ** (2003) Enzymes of glycolysis are functionally associated with the mitochondrion in *arabidopsis* cells. *Plant Cell* **15**: 2140–2151
- Gietz D, St Jean A, Woods RA, Schiestl RH** (1992) Improved method for high efficiency transformation of intact yeast cells. *Nucleic Acids Res* **20**: 1425

- Gilbert BM, Wolpert TJ** (2013) Characterization of the LOV1-Mediated, Victorin-Induced, Cell-Death Response with Virus-Induced Gene Silencing. *Mol Plant-Microbe Interact* **26**: 903–917
- Givan C V** (1999) Evolving concepts in plant glycolysis: two centuries of progress. *Biol Rev* **74**: 277–309
- Go Y-M, Jones DP** (2009) Thioredoxin Redox Western Analysis. *Curr Protoc Toxicol* **41**: 17–12
- Goetze TA, Philippar K, Ilkavets I, Soll J, Wagner R** (2006) OEP37 Is a New Member of the Chloroplast Outer Membrane Ion Channels. *J Biol Chem* **281**: 17989–17998
- Gohla A** (2019) Do metabolic HAD phosphatases moonlight as protein phosphatases? *Biochim Biophys Acta - Mol Cell Res* **1866**: 153–166
- González M, Delgado-Requerey V, Ferrández J, Serna A, Cejudo FJ** (2019) Insights into the function of NADPH thioredoxin reductase C (NTRC) based on identification of NTRC-interacting proteins in vivo. *J Exp Bot* **70**: 5787–5798
- Govindjee, Shevela D, Bjorn LO** (2017) Evolution of the Z-scheme of photosynthesis: a perspective. *Photosynth Res* **133**: 5–15
- Graña X, de la Ossa PP, Broceño C, Stöcker M, Garriga J, Puigdomènech P, Climent F** (1995) 2,3-Bisphosphoglycerate-independent phosphoglycerate mutase is conserved among different phylogenetic kingdoms. *Comp Biochem Physiol -- Part B Biochem* **112**: 287–293
- Grana X, De Lecea L, El-Maghrabi MR, Urena JM, Caellas C, Carreras J, Puigdomenech P, Pilkis SJ, Climent F** (1992) Cloning and sequencing of a cDNA encoding 2,3-bisphosphoglycerate-independent phosphoglycerate mutase from maize. Possible relationship to the alkaline phosphatase family. *J Biol Chem* **267**: 12797–12803
- Grana X, Urena J, Ludevid D, Carreras J, Climent F** (1989) Purification, characterization and immunological properties of 2,3-bisphosphoglycerate-independent phosphoglycerate mutase from maize (*Zea mays*) seeds. *Eur J Biochem* **186**: 149–153
- Guerra DG, Vertommen D, Fothergill-Gilmore LA, Opperdoes FR, Michels PAM** (2004) Characterization of the cofactor-independent phosphoglycerate mutase from *Leishmania mexicana mexicana*. Histidines that coordinate the two metal ions in the active site show different susceptibilities to irreversible chemical modification. *Eur J Biochem* **271**: 1798–1810
- Hagemann M, Kern R, Maurino VG, Hanson DT, Weber APM, Sage RF, Bauwe H** (2016) Evolution of photorespiration from cyanobacteria to land plants, considering protein phylogenies and acquisition of carbon concentrating mechanisms. *J Exp Bot* **67**: 2963–2976
- Haimovich-Dayana M, Lieman-Hurwitz J, Orf I, Hagemann M, Kaplan A** (2015) Does 2-phosphoglycolate serve as an internal signal molecule of inorganic carbon deprivation in the cyanobacterium *Synechocystis* sp. PCC 6803? *Environ Microbiol* **17**: 1794–1804
- Hajirezaei M, Sonnewald U, Viola R, Carlisle S, Dennis D, Stitt M** (1993) Transgenic potato plants with strongly decreased expression of pyrophosphate:fructose-6-phosphate phosphotransferase show no visible phenotype and only minor changes in metabolic fluxes in their tubers. *Planta* **192**: 16–30
- Hall NP, Kendall AC, Lea PJ, Turner JC, Wallsgrove RM** (1987) Characteristics of a photorespiratory mutant of barley (*Hordeum vulgare* L.) deficient in phosphoglycollate phosphatase. *Photosynth Res* **11**: 89–96

- Hanson AD, Gregory JF** (2011) Folate Biosynthesis, Turnover, and Transport in Plants. *Annu Rev Plant Biol* **62**: 105–125
- Hanson AD, Roje S** (2001) ONE-CARBON METABOLISM IN HIGHER PLANTS. *Annu Rev Plant Physiol Plant Mol Biol* **52**: 119–137
- Hardy P, Baldy P** (1986) Corn phosphoglycolate phosphatase: purification and properties. *Planta* **168**: 245–252
- Hasse D, Hagemann M, Andersson I, Bauwe H** (2010) Crystallization and preliminary X-ray diffraction analyses of the homodimeric glycine decarboxylase (P-protein) from the cyanobacterium *Synechocystis* sp. PCC 6803. *Acta Crystallogr Sect F Struct Biol Cryst Commun* **66**: 187–191
- Haupt-Herting Si, Fock HP** (2002) Oxygen Exchange in Relation to Carbon Assimilation in Water-stressed Leaves During Photosynthesis. *Ann Bot* **89**: 851–859
- Häusler RE, Bailey KJ, Lea PJ, Leegood RC** (1996) Control of photosynthesis in barley mutants with reduced activities of glutamine synthetase and glutamate synthase. *Planta* **200**: 388–396
- Heazlewood JL, Durek P, Hummel J, Selbig J, Weckwerth W, Walther D, Schulze WX** (2008) PhosPhAt: a database of phosphorylation sites in *Arabidopsis thaliana* and a plant-specific phosphorylation site predictor. *Nucleic Acids Res* **36**: 1015–1021
- Heidari B, Matre P, Nemie-Feyissa D, Meyer C, Rognli OA, Møller SG, Lillo C** (2011) Protein Phosphatase 2A B55 and A Regulatory Subunits Interact with Nitrate Reductase and Are Essential for Nitrate Reductase Activation. *Plant Physiol* **156**: 165–172
- Heldt HW, Flügge U-I, Borchert S** (1991) Diversity of Specificity and Function of Phosphate Translocators in Various Plastids. *Plant Physiol* **95**: 341–343
- Herrmann KM, Weaver LM** (1999) The shikimate pathway. *Annu Rev Plant Physiol Plant Mol Biol* **50**: 473–503
- Hess JL, Tolbert NE** (1967) Glycolate pathway in algae. *Plant Physiol* **42**: 371–379
- Hodges M, Dellero Y, Keech O, Betti M, Raghavendra AS, Sage R, Zhu XG, Allen DK, Weber APM** (2016) Perspectives for a better understanding of the metabolic integration of photorespiration within a complex plant primary metabolism network. *J Exp Bot* **67**: 3015–3026
- Hodges M, Jossier M, Boex-Fontvieille E, Tcherkez G** (2013) Protein phosphorylation and photorespiration. *Plant Biol* **15**: 694–706
- Hu J, Huang X, Chen L, Sun X, Lu C, Zhang L, Wang Y, Zuo J** (2015) Site-specific nitrosoproteomic identification of endogenously S-nitrosylated proteins in *Arabidopsis*. *Plant Physiol* **167**: 1731–1746
- Huang H, Pandya C, Liu C, Al-Obaidi NF, Wang M, Zheng L, Toews Keating S, Aono M, Love JD, Evans B, et al** (2015) Panoramic view of a superfamily of phosphatases through substrate profiling. *Proc Natl Acad Sci U S A* **112**: 1974–1983
- Huang S, Jacoby RP, Shingaki-Wells RN, Li L, Millar AH** (2013) Differential induction of mitochondrial machinery by light intensity correlates with changes in respiratory metabolism and photorespiration in rice leaves. *New Phytol* **198**: 103–115
- Huang Y, Blakeley SD, McAleese SM, Fothergill-Gilmore LA, Dennis DT** (1993) Higher-plant cofactor-independent phosphoglyceromutase: purification, molecular characterization and expression.

- Plant Mol Biol **23**: 1039–1053
- Huber SC, Huber JL** (1996) Role and regulation of sucrose-phosphate synthase in higher plants. *Annu Rev Plant Physiol Plant Mol Biol* **47**: 431–444
- Huh DH, Kursell A V, Husic HD** (1989) Kinetic properties of phosphoglycolate phosphatase from *Pisum sativum* and *Phaseolus vulgaris*. *Phytochemistry* **28**: 719–720
- Hummel M, Dobrenel T, Cordewener J (J. HG)., Davanture M, Meyer C, Smeekens S (J. CM)., Bailey-Serres J, America T (A. HP)., Hanson J** (2015) Proteomic LC–MS analysis of *Arabidopsis* cytosolic ribosomes: Identification of ribosomal protein paralogs and re-annotation of the ribosomal protein genes. *J Proteomics* **128**: 436–449
- Hurkman WJ, Tanaka CK** (1986) Solubilization of plant membrane proteins for analysis by two-dimensional gel electrophoresis. *Plant Physiol* **81**: 802–806
- Husic HD, Tolbert NE** (1984) Anion and divalent cation activation of phosphoglycolate phosphatase from leaves. *Arch Biochem Biophys* **229**: 64–72
- Husic HD, Tolbert NE** (1985) Properties of Phosphoglycolate Phosphatase from *Chlamydomonas reinhardtii* and *Anacystis nidulans*. *Plant Physiol* **79**: 394–399
- Igamberdiev AU, Gardeström P** (2003) Regulation of NAD- and NADP-dependent isocitrate dehydrogenases by reduction levels of pyridine nucleotides in mitochondria and cytosol of pea leaves. *Biochim Biophys Acta - Bioenerg* **1606**: 117–125
- Igarashi D, Miwa T, Seki M, Kobayashi M, Kato T, Tabata S, Shinozaki K, Ohsumi C** (2003) Identification of photorespiratory glutamate:glyoxylate aminotransferase (GGAT) gene in *Arabidopsis*. *Plant J* **33**: 975–987
- Iglesias AA, Losada M** (1988) Purification and kinetic and structural properties of spinach leaf NADP-dependent nonphosphorylating glyceraldehyde-3-phosphate dehydrogenase. *Arch Biochem Biophys* **260**: 830–840
- Intergovernmental Panel on Climate Change** (2014) *Climate Change 2014 – Impacts, Adaptation and Vulnerability: Part A: Global and Sectoral Aspects: Working Group II Contribution to the IPCC Fifth Assessment Report: Volume 1: Global and Sectoral Aspects*. doi: DOI: 10.1017/CBO9781107415379
- Iyer LM, Leipe DD, Koonin E V, Aravind L** (2004) Evolutionary history and higher order classification of AAA+ ATPases. *J Struct Biol* **146**: 11–31
- Jackowski G, Kacprzak K, Jansson S** (2001) Identification of Lhcb1/Lhcb2/Lhcb3 heterotrimers of the main light-harvesting chlorophyll a/b–protein complex of Photosystem II (LHC II). *Biochim Biophys Acta - Bioenerg* **1504**: 340–345
- Jamai A, Salomé PA, Schilling SH, Weber APM, McClung CR** (2009) *Arabidopsis* Photorespiratory Serine Hydroxymethyltransferase Activity Requires the Mitochondrial Accumulation of Ferredoxin-Dependent Glutamate Synthase. *Plant Cell* **21**: 595–606
- Jardine KJ, Fernandes de Souza V, Oikawa P, Higuchi N, Bill M, Porras R, Niinemets Ü, Chambers JQ** (2017) Integration of C₁ and C₂ Metabolism in Trees. *Int J Mol Sci* **18**: 2045
- Jedrzejak MJ** (2000) Structure, function, and evolution of phosphoglycerate mutases: Comparison with fructose-2,6-bisphosphatase, acid phosphatase, and alkaline phosphatase. *Prog Biophys*

Mol Biol **73**: 263–287

- Jedrzejas MJ, Chander M, Setlow P, Krishnasamy G** (2000a) Mechanism of catalysis of the cofactor-independent phosphoglycerate mutase from *Bacillus stearothermophilus*: Crystal structure of the complex with 2-phosphoglycerate. *J Biol Chem* **275**: 23146–23153
- Jedrzejas MJ, Chander M, Setlow P, Krishnasamy G** (2000b) Mechanism of Catalysis of the Cofactor-independent Phosphoglycerate Mutase from *Bacillus stearothermophilus* : CRYSTAL STRUCTURE OF THE COMPLEX WITH 2-PHOSPHOGLYCERATE. *J Biol Chem* **275**: 23146–23153
- Ji Y, Li Q, Liu G, Selvaraj G, Zheng Z, Zou J, Wei Y** (2019) Roles of Cytosolic Glutamine Synthetases in Arabidopsis Development and Stress Responses. *Plant Cell Physiol* **60**: 657–671
- Junge W, Nelson N** (2015) ATP Synthase. *Annu Rev Biochem* **84**: 631–657
- Kammerer B, Fischer K, Hilpert B, Schubert S, Gutensohn M, Weber A, Flügge U-I** (1998) Molecular Characterization of a Carbon Transporter in Plastids from Heterotrophic Tissues: The Glucose 6-Phosphate/Phosphate Antiporter. *Plant Cell* **10**: 105–117
- Kebeish R, Niessen M, Thiruveedhi K, Bari R, Hirsch HJ, Rosenkranz R, Stäbler N, Schönfeld B, Kreuzaler F, Peterhänsel C** (2007) Chloroplastic photorespiratory bypass increases photosynthesis and biomass production in *Arabidopsis thaliana*. *Nat Biotechnol* **25**: 593–599
- Keech O, Gardeström P, Kleczkowski LA, Rouhier N** (2017) The redox control of photorespiration: from biochemical and physiological aspects to biotechnological considerations. *Plant Cell Environ* **40**: 553–569
- Kelly GJ, Lutzko E** (1976) Inhibition of spinach-leaf phosphofructokinase by 2-phosphoglycollate. *FEBS Lett* **68**: 55–58
- Kendall AC, Keys AJ, Turner JC, Lea PJ, Mifflin BJ** (1983) The isolation and characterisation of a catalase-deficient mutant of barley (*Hordeum vulgare* L.). *Planta* **159**: 505–511
- Kendall AC, Wallsgrove RM, Hall NP, Turner JC, Lea PJ** (1986) Carbon and nitrogen metabolism in barley (*Hordeum vulgare* L.) mutants lacking ferredoxin-dependent glutamate synthase. *Planta* **168**: 316–323
- Kerchev P, Waszczak C, Lewandowska A, Willems P, Shapiguzov A, Li Z, Alseekh S, Mühlenbock P, Hoerberichts FA, Huang J, et al** (2016) Lack of GLYCOLATE OXIDASE1, but Not GLYCOLATE OXIDASE2, Attenuates the Photorespiratory Phenotype of CATALASE2-Deficient Arabidopsis. *Plant Physiol* **171**: 1704–1719
- Kern R, Bauwe H, Hagemann M** (2011) Evolution of enzymes involved in the photorespiratory 2-phosphoglycolate cycle from cyanobacteria via algae toward plants. *Photosynth Res* **109**: 103–114
- Kern R, Eisenhut M, Bauwe H, Weber APM, Hagemann M** (2013) Does the *Cyanophora paradoxa* genome revise our view on the evolution of photorespiratory enzymes? *Plant Biol* **15**: 759–768
- Keseler IM, Collado-Vides J, Gama-Castro S, Ingraham J, Paley S, Paulsen IT, Peralta-Gil M, Karp PD** (2005) EcoCyc: a comprehensive database resource for *Escherichia coli*. *Nucleic Acids Res* **33**: 334–337
- Kessner D, Chambers M, Burke R, Agus D, Mallick P** (2008) ProteoWizard: open source software for rapid proteomics tools development. *Bioinformatics* **24**: 2534–2536

- Kestler C, Knobloch G, Tessmer I, Jeanclos E, Schindelin H, Gohla A** (2014) Chronophin Dimerization Is Required for Proper Positioning of Its Substrate Specificity Loop. *J Biol Chem* **289**: 3094–3103
- Kim SR, Xu H, Lesmana A, Kuzmanovic U, Au M, Florencia C, Oh EJ, Zhang G, Kim KH, Jin Y-S** (2015) Deletion of PHO13, encoding haloacid dehalogenase type IIA phosphatase, results in upregulation of the pentose phosphate pathway in *Saccharomyces cerevisiae*. *Appl Environ Microbiol* **81**: 1601–1609
- Kim Y, Yakunin AF, Kuznetsova E, Xu X, Pennycooke M, Gu J, Cheung F, Proudfoot M, Arrowsmith CH, Joachimiak A, et al** (2004) Structure- and function-based characterization of a new phosphoglycolate phosphatase from *Thermoplasma acidophilum*. *J Biol Chem* **279**: 517–526
- Kleczkowski LA, Edwards GE, Blackwell RD, Lea PJ, Givan C V** (1990) Enzymology of the reduction of hydroxypyruvate and glyoxylate in a mutant of barley lacking peroxisomal hydroxypyruvate reductase. *Plant Physiol* **94**: 819–825
- Kohzuma K, Froehlich JE, Davis GA, Temple JA, Minhas D, Dhingra A, Cruz JA, Kramer DM** (2017) The Role of Light-Dark Regulation of the Chloroplast ATP Synthase. *Front Plant Sci* **8**: 1248
- Koonin E V, Tatusov RL** (1994) Computer Analysis of Bacterial Haloacid Dehalogenases Defines a Large Superfamily of Hydrolases with Diverse Specificity: Application of an Iterative Approach to Database Search. *J Mol Biol* **244**: 125–132
- Kozaki A, Takeba G** (1996) Photorespiration protects C3 plants from photooxidation. *Nature* **384**: 557–560
- Krapp A, David LC, Chardin C, Girin T, Marmagne A, Leprince A-S, Chaillou S, Ferrario-Méry S, Meyer C, Daniel-Vedele F** (2014) Nitrate transport and signalling in *Arabidopsis*. *J Exp Bot* **65**: 789–798
- Krebbers E, Seurinck J, Herdies L, Cashmore AR, Timko MP** (1988) Four genes in two diverged subfamilies encode the ribulose-1,5-bisphosphate carboxylase small subunit polypeptides of *Arabidopsis thaliana*. *Plant Mol Biol* **11**: 745–759
- Krocová E, Neradová S, Kupcik R, Janovská S, Bílková Z, Heidingsfeld O** (2019) PHO15 genes of *Candida albicans* and *Candida parapsilosis* encode HAD-type phosphatases dephosphorylating 2-phosphoglycolate. *FEMS Yeast Res* **19**: 112
- Kuhn NJ, Setlow B, Setlow P, Cammack R, Williams R** (1995) Cooperative Manganese(II) Activation of 3-Phosphoglycerate Mutase of *Bacillus megaterium*: A Biological pH-Sensing Mechanism in Bacterial Spore Formation and Germination. *Arch Biochem Biophys* **320**: 35–42
- Laemmli UK** (1970) Cleavage of structural proteins during the assembly of the head of bacteriophage T4. *Nature* **227**: 680–685
- Lahiri SD, Zhang G, Dai J, Dunaway-Mariano D, Allen KN** (2004) Analysis of the Substrate Specificity Loop of the HAD Superfamily Cap Domain. *Biochemistry* **43**: 2812–2820
- Lahiri SD, Zhang G, Dunaway-Mariano D, Allen KN** (2002) Caught in the Act: The Structure of Phosphorylated β -Phosphoglucomutase from *Lactococcus lactis*. *Biochemistry* **41**: 8351–8359
- Laisk A, Edwards GE** (2000) A mathematical model of C4 photosynthesis: The mechanism of concentrating CO₂ in NADP-malic enzyme type species. *Photosynth Res* **66**: 199
- Lalonde S V, Konhauser KO** (2015) Benthic perspective on Earth's oldest evidence for oxygenic

- photosynthesis. *Proc Natl Acad Sci U S A* **112**: 995–1000
- Lancien M, Martin M, Hsieh M-H, Leustek T, Goodman H, Coruzzi GM** (2002) Arabidopsis *glt1-T* mutant defines a role for NADH-GOGAT in the non-photorespiratory ammonium assimilatory pathway. *Plant J* **29**: 347–358
- Langella O, Valot B, Balliau T, Blein-Nicolas M, Bonhomme L, Zivy M** (2017) X!TandemPipeline: A Tool to Manage Sequence Redundancy for Protein Inference and Phosphosite Identification. *J Proteome Res* **16**: 494–503
- Lawand S, Dorne A-J, Long D, Coupland G, Mache R, Carol P** (2002) Arabidopsis A BOUT DE SOUFFLE, Which Is Homologous with Mammalian Carnitine Acyl Carrier, Is Required for Postembryonic Growth in the Light. *Plant Cell* **14**: 2161 LP – 2173
- Leadlay PF, Breathnach R, Gatehouse JA, Johnson PE, Knowles JR** (1977) Phosphoglycerate mutase from wheat germ: studies with isotopically labeled 3-phospho-D-glycerates showing that the catalyzed reaction is intramolecular. Appendix: phosphoglycerate mutase from wheat germ: isolation, crystallization, and properties. *Biochemistry* **16**: 3045–3053
- Lee CP, Eubel H, Millar AH** (2010) Diurnal Changes in Mitochondrial Function Reveal Daily Optimization of Light and Dark Respiratory Metabolism in Arabidopsis. *Mol & Cell Proteomics* **9**: 2125–2139
- Lemaire SD, Michelet L, Zaffagnini M, Massot V, Issakidis-Bourguet E** (2007) Thioredoxins in chloroplasts. *Curr Genet* **51**: 343–365
- Levey M, Timm S, Mettler-altmann T, Borghi GL, Koczor M, Arrivault S, Weber APM, Bauwe H, Gowik U, Westhoff P** (2019) Efficient 2-phosphoglycolate degradation is required to maintain carbon assimilation and allocation in the C₄ plant *Flaveria bidentis*. **70**: 575–587
- Li J, Hu J** (2015) Using Co-Expression Analysis and Stress-Based Screens to Uncover Arabidopsis Peroxisomal Proteins Involved in Drought Response. *PLoS One* **10**: 0137762
- Liepman AH, Olsen LJ** (2003) Alanine Aminotransferase Homologs Catalyze the Glutamate:Glyoxylate Aminotransferase Reaction in Peroxisomes of Arabidopsis. *Plant Physiol* **131**: 215 LP – 227
- Liepman AH, Olsen LJ** (2001) Peroxisomal alanine: Glyoxylate aminotransferase (AGT1) is a photorespiratory enzyme with multiple substrates in Arabidopsis thaliana. *Plant J* **25**: 487–498
- Lillo C** (2008) Signalling cascades integrating light-enhanced nitrate metabolism. *Biochem J* **415**: 11–19
- van der Linde K, Gutsche N, Leffers H-M, Lindermayr C, Müller B, Holtgreffe S, Scheibe R** (2011) Regulation of plant cytosolic aldolase functions by redox-modifications. *Plant Physiol Biochem* **49**: 946–957
- Lindermayr C, Saalbach G, Durner J** (2005) Proteomic identification of S-nitrosylated proteins in Arabidopsis. *Plant Physiol* **137**: 921–930
- Linka M, Weber APM** (2005) Shuffling ammonia between mitochondria and plastids during photorespiration. *Trends Plant Sci* **10**: 461–465
- Linka N, Weber APM** (2010) Intracellular metabolite transporters in plants. *Mol Plant* **3**: 21–53
- Liu Y** (2019) Phosphoregulation of photorespiratory enzymes in Arabidopsis thaliana.

- Liu Y, Mauve C, Lamothe-Sibold M, Guérard F, Glab N, Hodges M, Jossier M** (2019) Photorespiratory serine hydroxymethyltransferase 1 activity impacts abiotic stress tolerance and stomatal closure. *Plant Cell Environ* **42**: 2567–2583
- López-Calcagno PE, Fisk S, Brown KL, Bull SE, South PF, Raines CA** (2019) Overexpressing the H₂O₂ protein of the glycine cleavage system increases biomass yield in glasshouse and field-grown transgenic tobacco plants. *Plant Biotechnol J* **17**: 141–151
- Lothier J, Gaufichon L, Sormani R, Lemaître T, Azzopardi M, Morin H, Chardon F, Reisdorf-Cren M, Avice J-C, Masclaux-Daubresse C** (2010) The cytosolic glutamine synthetase GLN1;2 plays a role in the control of plant growth and ammonium homeostasis in *Arabidopsis* rosettes when nitrate supply is not limiting. *J Exp Bot* **62**: 1375–1390
- Lyngstadaas A, Løbner-Olesen A, Grelland E, Boye E** (1999) The gene for 2-phosphoglycolate phosphatase (gph) in *Escherichia coli* is located in the same operon as *dam* and at least five other diverse genes. *Biochim Biophys Acta - Gen Subj* **1472**: 376–384
- Maier A, Fahnenstich H, von Caemmerer S, Engqvist MKM, Weber APM, Flügge UI, Maurino VG** (2012) Transgenic introduction of a glycolate oxidative cycle into *A. Thaliana* chloroplasts leads to growth improvement. *Front Plant Sci* **3**: 1–12
- Mamedov TG, Suzuki K, Miura K, Kucho K, Fukuzawa H** (2001) Characteristics and Sequence of Phosphoglycolate Phosphatase from a Eukaryotic Green Alga *Chlamydomonas reinhardtii*. *J Biol Chem* **276**: 45573–45579
- Marchand C, Le Maréchal P, Meyer Y, Miginiac-Maslow M, Issakidis-Bourguet E, Decottignies P** (2004) New targets of *Arabidopsis* thioredoxins revealed by proteomic analysis. *Proteomics* **4**: 2696–2706
- Matamoros MA, Cutrona MC, Wienkoop S, Begara-Morales JC, Sandal N, Orera I, Barroso JB, Stougaard J, Becana M** (2019) Altered plant and nodule development and protein S-nitrosylation in *Lotus japonicus* mutants deficient in S-nitrosoglutathione reductases. *Plant Cell Physiol* **1**: 1–44
- Maurino VG, Engqvist MKM** (2015) 2-Hydroxy Acids in Plant Metabolism. *Arab B* **13**: 0182
- Mauve C, Giraud N, Boex-Fontvieille ERA, Antheaume I, Tea I, Tcherkez G** (2016) Kinetic commitment in the catalysis of glutamine synthesis by GS1 from *Arabidopsis* using 14N/15N and solvent isotope effects. *Plant Physiol Biochem* **108**: 203–211
- Mazarei M, Lennon KA, Puthoff DP, Rodermeil SR, Baum TJ** (2003) Expression of an *Arabidopsis* phosphoglycerate mutase homologue is localized to apical meristems, regulated by hormones, and induced by sedentary plant-parasitic nematodes. *Plant Mol Biol* **53**: 513–530
- McAleese SM, Jutagir V, Blackburn GM, Fothergill-Gilmore LA** (1987) The bisphosphonate analogue of 2,3-bisphosphoglycerate inhibits yeast but not wheat-germ phosphoglycerate mutase. *Biochem J* **243**: 301–304
- McClung CR** (1997) Regulation of catalases in *Arabidopsis*. *Free Radic Biol Med* **23**: 489–496
- McCurry SD, Pierce J, Tolbert NE, Orme-Johnson WH** (1981) On the mechanism of effector-mediated activation of ribulose biphosphate carboxylase/oxygenase. *J Biol Chem* **256**: 6623–6628
- Mercaldi GF, Pereira HM, Cordeiro AT, Michels PAM, Thiemann OH** (2012) Structural role of the active-site metal in the conformation of *Trypanosoma brucei* phosphoglycerate mutase. *FEBS*

J **279**: 2012–2021

- Messant M, Timm S, Fantuzzi A, Weckwerth W, Bauwe H, Rutherford AW, Krieger-Liszkay A** (2018) Glycolate Induces Redox Tuning Of Photosystem II in Vivo: Study of a Photorespiration Mutant. *Plant Physiol* **177**: 1277–1285
- Meyer Y, Belin C, Delorme-Hinoux V, Reichheld J-P, Riondet C** (2012) Thioredoxin and Glutaredoxin Systems in Plants: Molecular Mechanisms, Crosstalks, and Functional Significance. *Antioxid Redox Signal* **17**: 1124–1160
- Mhamdi A, Noctor G** (2016) High CO₂ Primes Plant Biotic Stress Defences through Redox-Linked Pathways. *Plant Physiol* **172**: 929–942
- Mhamdi A, Queval G, Chaouch S, Vanderauwera S, Van Breusegem F, Noctor G** (2010) Catalase function in plants: A focus on Arabidopsis mutants as stress-mimic models. *J Exp Bot* **61**: 4197–4220
- Miller GAD, Suzuki N, Ciftci-Yilmaz S, Mittler RON** (2010) Reactive oxygen species homeostasis and signalling during drought and salinity stresses. *Plant Cell Environ* **33**: 453–467
- Mishra P, Mishra V, Takabe T, Rai V, Singh NK** (2016) Elucidation of salt-tolerance metabolic pathways in contrasting rice genotypes and their segregating progenies. *Plant Cell Rep* **35**: 1273–1286
- Mittova V, Theodoulou FL, Kiddle G, Gómez L, Volokita M, Tal M, Foyer CH, Guy M** (2003) Coordinate induction of glutathione biosynthesis and glutathione-metabolizing enzymes is correlated with salt tolerance in tomato. *FEBS Lett* **554**: 417–421
- Miziorko HM, Sealy RC** (1980) Characterization of the ribulosebiphosphate carboxylase-carbon dioxide-divalent cation-carboxypentitol biphosphate complex. *Biochemistry* **19**: 1167–1171
- Modde K, Timm S, Florian A, Michl K, Fernie AR, Bauwe H** (2017) High serine:glyoxylate aminotransferase activity lowers leaf daytime serine levels, inducing the phosphoserine pathway in Arabidopsis. *J Exp Bot* **68**: 643–656
- Moison M, Marmagne A, Dinant S, Soulay F, Azzopardi M, Lothier J, Citerne S, Morin H, Legay N, Chardon F, et al** (2018) Three cytosolic glutamine synthetase isoforms localized in different-order veins act together for N remobilization and seed filling in Arabidopsis. *J Exp Bot* **69**: 4379–4393
- Morais MC, Zhang G, Zhang W, Olsen DB, Dunaway-Mariano D, Allen KN** (2004) X-ray Crystallographic and Site-directed Mutagenesis Analysis of the Mechanism of Schiff-base Formation in Phosphonoacetaldehyde Hydrolase Catalysis. *J Biol Chem* **279**: 9353–9361
- Moreno JI, Martín R, Castresana C** (2005) Arabidopsis SHMT1, a serine hydroxymethyltransferase that functions in the photorespiratory pathway influences resistance to biotic and abiotic stress. *Plant J* **41**: 451–463
- Mulo P** (2011) Chloroplast-targeted ferredoxin-NADP(+) oxidoreductase (FNR): structure, function and location. *Biochim Biophys Acta* **1807**: 927–934
- Murashige T, Skoog F** (1962) A Revised Medium for Rapid Growth and Bio Assays with Tobacco Tissue Cultures. *Physiol Plant* **15**: 473–497
- Murray AJ, Blackwell RD, Lea PJ** (1989) Metabolism of Hydroxypyruvate in a Mutant of Barley

- Lacking NADH-Dependent Hydroxypyruvate Reductase, an Important Photorespiratory Enzyme Activity. *Plant Physiol* **91**: 395–400
- Murray AJ, Blackwell RD, Joy KW, Lea PJ** (1987) Photorespiratory N donors, aminotransferase specificity and photosynthesis in a mutant of barley deficient in serine: glyoxylate aminotransferase activity. *Planta* **172**: 106–113
- Nagappa LK, Satha P, Govindaraju T, Balaram H** (2019) Phosphoglycolate phosphatase is a metabolic proofreading enzyme essential for cellular function in *Plasmodium berghei*. *J Biol Chem* **294**: 4997–5007
- Nallamsetty S, Austin BP, Penrose KJ, Waugh DS** (2005) Gateway vectors for the production of combinatorially-tagged His6-MBP fusion proteins in the cytoplasm and periplasm of *Escherichia coli*. *Protein Sci* **14**: 2964–2971
- Neuburger M, Rébeillé F, Jourdain A, Nakamura S, Douce R** (1996) Mitochondria Are a Major Site for Folate and Thymidylate Synthesis in Plants. *J Biol Chem* **271**: 9466–9472
- Niittyla T, Messerli G, Trevisan M, Chen J, Smith AM, Zeeman SC** (2004) A previously unknown maltose transporter essential for starch degradation in leaves. *Science* **303**: 87–89
- Noctor G, Foyer CH** (2000) Homeostasis of adenylate status during photosynthesis in a fluctuating environment. *J Exp Bot* **51**: 347–356
- Noctor G, Mhamdi A** (2017) Climate Change, CO₂, and Defense: The Metabolic, Redox, and Signaling Perspectives. *Trends Plant Sci* **22**: 857–870
- Nölke G, Houdelet M, Kreuzaler F, Peterhänsel C, Schillberg S** (2014) The expression of a recombinant glycolate dehydrogenase polyprotein in potato (*Solanum tuberosum*) plastids strongly enhances photosynthesis and tuber yield. *Plant Biotechnol J* **12**: 734–742
- Norman EG, Colman B** (1991a) Purification and Characterization of Phosphoglycolate Phosphatase from the Cyanobacterium *Coccochloris peniocystis*. *Plant Physiol* **95**: 693–698
- Norman EG, Colman B** (1991b) Purification and characterization of phosphoglycolate phosphatase from the cyanobacterium *Coccochloris peniocystis*. *Plant Physiol* **95**: 693–698
- Nowicki MW, Kuaprasert B, McNae IW, Morgan HP, Harding MM, Michels PAM, Fothergill-Gilmore LA, Walkinshaw MD** (2009) Crystal Structures of *Leishmania mexicana* Phosphoglycerate Mutase Suggest a One-Metal Mechanism and a New Enzyme Subclass. *J Mol Biol* **394**: 535–543
- Nukui M, Mello L V, Littlejohn JE, Setlow B, Setlow P, Kim K, Leighton T, Jedrzejewski MJ** (2007) Structure and molecular mechanism of *Bacillus anthracis* cofactor-independent phosphoglycerate mutase: a crucial enzyme for spores and growing cells of *Bacillus* species. *Biophys J* **92**: 977–988
- Obata T, Witt S, Lisek J, Palacios-Rojas N, Florez-Sarasa I, Yousfi S, Arous JL, Cairns JE, Fernie AR** (2015) Metabolite Profiles of Maize Leaves in Drought, Heat, and Combined Stress Field Trials Reveal the Relationship between Metabolism and Grain Yield. *Plant Physiol* **169**: 2665–2683
- Orea A, Pajuelo P, Pajuelo E, Quidiello C, Romero JM, Márquez AJ** (2002) Isolation of photorespiratory mutants from *Lotus japonicus* deficient in glutamine synthetase. *Physiol Plant* **115**: 352–361
- Ortega-Galisteo AP, Rodríguez-Serrano M, Pazmiño DM, Gupta DK, Sandalio LM, Romero-Puertas**

- MC** (2012) S-Nitrosylated proteins in pea (*Pisum sativum* L.) leaf peroxisomes: changes under abiotic stress. *J Exp Bot* **63**: 2089–2103
- Palmieri MC, Lindermayr C, Bauwe H, Steinhauser C, Durner J** (2010) Regulation of plant glycine decarboxylase by s-nitrosylation and glutathionylation. *Plant Physiol* **152**: 1514–1528
- Pan X, Cao P, Su X, Liu Z, Li M** (2019) Structural analysis and comparison of light-harvesting complexes I and II. *Biochim Biophys Acta - Bioenerg.* doi: <https://doi.org/10.1016/j.bbabi.2019.06.010>
- Parry MAJ, Keys AJ, Madgwick PJ, Carmo-Silva AE, Andralojc PJ** (2008) Rubisco regulation: a role for inhibitors. *J Exp Bot* **59**: 1569–1580
- Parsons JF, Lim K, Tempczyk A, Krajewski W, Eisenstein E, Herzberg O** (2002) From structure to function: YrbI from *Haemophilus influenzae* (HI1679) is a phosphatase. *Proteins Struct Funct Bioinforma* **46**: 393–404
- Pérez-Ruiz JM, Cejudo FJ** (2009) A proposed reaction mechanism for rice NADPH thioredoxin reductase C, an enzyme with protein disulfide reductase activity. *FEBS Lett* **583**: 1399–1402
- Pick TR, Brautigam A, Schulz MA, Obata T, Fernie AR, Weber APM** (2013) PLGG1, a plastidic glycolate glycerate transporter, is required for photorespiration and defines a unique class of metabolite transporters. *Proc Natl Acad Sci* **110**: 3185–3190
- Pierce J, Reddy GS** (1986) The sites for catalysis and activation of ribulosebiphosphate carboxylase share a common domain. *Arch Biochem Biophys* **245**: 483–493
- Plaxton WC** (1996) The organization and regulation of plant glycolysis. *Annu Rev Plant Physiol Plant Mol Biol* **47**: 185–214
- Podestá FE, Plaxton WC** (1994) Regulation of cytosolic carbon metabolism in germinating *Ricinus communis* cotyledons. *Planta* **194**: 381–387
- Portis Jr AR, Li C, Wang D, Salvucci ME** (2007) Regulation of Rubisco activase and its interaction with Rubisco. *J Exp Bot* **59**: 1597–1604
- Portis AR** (1981) Evidence of a Low Stromal Mg²⁺ Concentration in Intact Chloroplasts in the Dark. *Plant Physiol* **67**: 985–989
- Portis AR, Heldt HW** (1976) Light-dependent changes of the Mg²⁺ concentration in the stroma in relation to the Mg²⁺ dependency of CO₂ fixation in intact chloroplasts. *Biochim Biophys Acta - Bioenerg* **449**: 434–446
- Puerto-Galán L, Pérez-Ruiz JM, Ferrández J, Cano B, Naranjo B, Nájera VA, González M, Lindahl AM, Cejudo FJ** (2013) Overoxidation of chloroplast 2-Cys peroxiredoxins: balancing toxic and signaling activities of hydrogen peroxide. *Front Plant Sci* **4**: 310
- Pulido P, Spínola MC, Kirchsteiger K, Guinea M, Pascual MB, Sahrawy M, Sandalio LM, Dietz K-J, González M, Cejudo FJ** (2010) Functional analysis of the pathways for 2-Cys peroxiredoxin reduction in *Arabidopsis thaliana* chloroplasts. *J Exp Bot* **61**: 4043–4054
- Puthiyaveetil S, Kavanagh TA, Cain P, Sullivan JA, Newell CA, Gray JC, Robinson C, van der Giezen M, Rogers MB, Allen JF** (2008) The ancestral symbiont sensor kinase CSK links photosynthesis with gene expression in chloroplasts. *Proc Natl Acad Sci U S A* **105**: 10061–10066
- Queval G, Issakidis-Bourguet E, Hoerberichts FA, Vandorpe M, Gakière B, Vanacker H, Miginiac-**

- Maslow M, Van Breusegem F, Noctor G** (2007) Conditional oxidative stress responses in the Arabidopsis photorespiratory mutant *cat2* demonstrate that redox state is a key modulator of daylength-dependent gene expression, and define photoperiod as a crucial factor in the regulation of H₂O₂-induced cel. *Plant J* **52**: 640–657
- Rachmilevitch S, Cousins AB, Bloom AJ** (2004) Nitrate assimilation in plant shoots depends on photorespiration. *Proc Natl Acad Sci U S A* **101**: 11506–11510
- Rajagopalan A V, Devi MT, Raghavendra AS** (1993) Patterns of phosphoenolpyruvate carboxylase activity and cytosolic pH during light activation and dark deactivation in C3 and C4 plants. *Photosynth Res* **38**: 51–60
- Rao ST, Rossmann MG** (1973) Comparison of super-secondary structures in proteins. *J Mol Biol* **76**: 241–256
- Reiland S, Finazzi G, Endler A, Willig A, Baerenfaller K, Grossmann J, Gerrits B, Rutishauser D, Gruissem W, Rochaix J-D, et al** (2011) Comparative phosphoproteome profiling reveals a function of the STN8 kinase in fine-tuning of cyclic electron flow (CEF). *Proc Natl Acad Sci U S A* **108**: 12955–12960
- Reiland S, Messerli G, Baerenfaller K, Gerrits B, Endler A, Grossmann J, Gruissem W, Baginsky S** (2009) Large-scale Arabidopsis phosphoproteome profiling reveals novel chloroplast kinase substrates and phosphorylation networks. *Plant Physiol* **150**: 889–903
- Reinholdt O, Schwab S, Zhang Y, Reichheld J-P, Fernie AR, Hagemann M, Timm S** (2019) Redox-Regulation of Photorespiration through Mitochondrial Thioredoxin o1. *Plant Physiol* **181**: 442–457
- Renné P, Dreßen U, Hebbeker U, Hille D, Flügge U-I, Westhoff P, Weber APM** (2003) The Arabidopsis mutant *dct* is deficient in the plastidic glutamate/malate translocator DiT2. *Plant J* **35**: 316–331
- Renwick SB** (1998) Purification, crystallization and preliminary X-ray analysis of human recombinant cytosolic serine hydroxymethyltransferase. *Acta Crystallogr Sect D Biol Crystallogr* **54**: 1030–1031
- Reumann S, Babujee L, Ma C, Wienkoop S, Siemsen T, Antonicelli GE, Rasche N, Lüder F, Weckwerth W, Jahn O** (2007) Proteome Analysis of Arabidopsis Leaf Peroxisomes Reveals Novel Targeting Peptides, Metabolic Pathways, and Defense Mechanisms. *Plant Cell* **19**: 3170–3193
- Richardson KE, Tolbert NE** (1961) Phosphoglycolic Acid Phosphatase. *J Biol Chem* **236**: 1285–1290
- Ríos-Soto L, Avitia-Domínguez C, Sierra-Campos E, Valdez-Solana M, Cisneros-Martínez J, Téllez-Valencia* MGP-G and A** (2018) Virtual Screening, Molecular Dynamics and ADME-Tox Tools for Finding Potential Inhibitors of Phosphoglycerate Mutase 1 from Plasmodium falciparum. *Curr Top Med Chem* **18**: 1610–1617
- Rios R, de Buyser J, Henry Y, Ambard-Bretteville F, Rémy R** (1991) Two-dimensional electrophoretic comparison of mitochondrial polypeptides from different wheat (*Triticum aestivum* L.) tissues. *Plant Sci* **76**: 159–166
- van Roermund CWT, Schroers MG, Wiese J, Facchinelli F, Kurz S, Wilkinson S, Charton L, Wanders RJA, Waterham HR, Weber APM, et al** (2016) The Peroxisomal NAD Carrier from Arabidopsis Imports NAD in Exchange with AMP. *Plant Physiol* **171**: 2127–2139

- Rogers WJ, Jordan BR, Rawsthorne S, Tobin AK** (1991) Changes to the stoichiometry of glycine decarboxylase subunits during wheat (*Triticum aestivum* L.) and pea (*Pisum sativum* L.) leaf development. *Plant Physiol* **96**: 952–956
- Rojas CM, Mysore KS** (2012) Glycolate oxidase is an alternative source for H₂O₂ production during plant defense responses and functions independently from NADPH oxidase. *Plant Signal Behav* **7**: 752–755
- Rojas CM, Senthil-Kumar M, Wang K, Ryu C-M, Kaundal A, Mysore KS** (2012) Glycolate Oxidase Modulates Reactive Oxygen Species–Mediated Signal Transduction during Nonhost Resistance in *Nicotiana benthamiana* and *Arabidopsis*. *Plant Cell* **24**: 336–352
- Ros R, Muñoz-Bertomeu J, Krueger S** (2014) Serine in plants: biosynthesis, metabolism, and functions. *Trends Plant Sci* **19**: 564–569
- Rose ZB, Grove DS, Seal SN** (1986) Mechanism of activation by anions of phosphoglycolate phosphatases from spinach and human red blood cells. *J Biol Chem* **261**: 10996–11002
- Rost BBT-M in E** (1996) [31] PHD: Predicting one-dimensional protein structure by profile-based neural networks. *Comput. Methods Macromol. Seq. Anal. Academic Press*, pp 525–539
- Roychowdhury A, Kundu A, Bose M, Gujar A, Mukherjee S, Das AK** (2015) Complete catalytic cycle of cofactor-independent phosphoglycerate mutase involves a spring-loaded mechanism. *FEBS J* **282**: 1097–1110
- Roychowdhury A, Kundu A, Gujar A, Bose M, Das AK** (2014) Expression, purification, crystallization and preliminary X-ray diffraction studies of phosphoglycerate mutase from *Staphylococcus aureus* NCTC8325. *Acta Crystallogr Sect FStructural Biol Commun* **70**: 53–56
- Ruan Y-L** (2014) Sucrose Metabolism: Gateway to Diverse Carbon Use and Sugar Signaling. *Annu Rev Plant Biol* **65**: 33–67
- Rubio-Asensio JS, Bloom AJ** (2016) Inorganic nitrogen form: a major player in wheat and *Arabidopsis* responses to elevated CO₂. *J Exp Bot* **68**: 2611–2625
- Sabularse DC, Anderson RL** (1981) D-Fructose 2,6-bisphosphate: A naturally occurring activator for inorganic pyrophosphate:D-fructose-6-phosphate 1-phosphotransferase in plants. *Biochem Biophys Res Commun* **103**: 848–855
- Sakakibara Y, Kimura H, Iwamura A, Saitoh T, Ikegami T, Kurisu G, Hase T** (2012) A new structural insight into differential interaction of cyanobacterial and plant ferredoxins with nitrite reductase as revealed by NMR and X-ray crystallographic studies. *J Biochem* **151**: 483–492
- Samuilov S, Brilhaus D, Rademacher N, Flachbart S, Arab L, Alfarraj S, Kuhnert F, Kopriva S, Weber APM, Mettler-Altmann T, et al** (2018) The Photorespiratory BOU Gene Mutation Alters Sulfur Assimilation and Its Crosstalk With Carbon and Nitrogen Metabolism in *Arabidopsis thaliana*. *Front Plant Sci* **9**: 1709
- Saroussi S, Schushan M, Ben-Tal N, Junge W, Nelson N** (2012) Structure and flexibility of the C-ring in the electromotor of rotary F₀F₁-ATPase of pea chloroplasts. *PLoS One* **7**: 43045–43045
- Sato S, Nakamura Y, Kaneko T, Asamizu E, Tabata S** (1999) Complete Structure of the Chloroplast Genome of *thaliana* ssc. *DNA Res* **290**: 283–290
- Scagliarini S, Trost P, Valenti V, Pupillo P** (1990) Glyceraldehyde 3-Phosphate:NADP⁺ Reductase of

- Spinach Leaves. *Plant Physiol* **94**: 1337–1344
- Scheibe R, Beck E** (2011) Drought, Desiccation, and Oxidative Stress. *Plant Desiccation Toler* **215**: 209–231
- Schimkat D, Heineke D, Heldt HW** (1990) Regulation of sedoheptulose-1,7-bisphosphatase by sedoheptulose-7-phosphate and glycerate, and of fructose-1,6-bisphosphatase by glycerate in spinach chloroplasts. *Planta* **181**: 97–103
- Schirromeister BE, de Vos JM, Antonelli A, Bagheri HC** (2013) Evolution of multicellularity coincided with increased diversification of cyanobacteria and the Great Oxidation Event. *Proc Natl Acad Sci U S A* **110**: 1791–1796
- Schjoerring JK, MäcK G, Nielsen KH, Husted S, Suzuki A, Driscoll S, Boldt R, Bauwe H** (2006) Antisense reduction of serine hydroxymethyltransferase results in diurnal displacement of NH₄⁺ assimilation in leaves of *Solanum tuberosum*. *Plant J* **45**: 71–82
- Schneider B, Müller R, Frank R, Lingens F** (1991) Complete nucleotide sequences and comparison of the structural genes of two 2-haloalkanoic acid dehalogenases from *Pseudomonas* sp. strain CBS3. *J Bacteriol* **173**: 1530–1535
- Schneider M, Knuesting J, Birkholz O, Heinisch JJ, Scheibe R** (2018) Cytosolic GAPDH as a redox-dependent regulator of energy metabolism. *BMC Plant Biol* **18**: 184
- Schneiderei J, Häusler RE, Fiene G, Kaiser WM, Weber APM** (2006) Antisense repression reveals a crucial role of the plastidic 2-oxoglutarate/malate translocator DiT1 at the interface between carbon and nitrogen metabolism. *Plant J* **45**: 206–224
- Schönberg A, Baginsky S** (2012) Signal integration by chloroplast phosphorylation networks: an update. *Front Plant Sci* **3**: 256
- Schönberg A, Rödiger A, Mehwald W, Galonska J, Christ G, Helm S, Thieme D, Majovsky P, Hoehenwarter W, Baginsky S** (2017) Identification of STN7/STN8 kinase targets reveals connections between electron transport, metabolism and gene expression. *Plant J* **90**: 1176–1186
- Schuller KA, Plaxton WC, Turpin DH** (1990a) Regulation of Phosphoenolpyruvate Carboxylase from the Green Alga *Selenastrum minutum*. *Plant Physiol* **93**: 1303–1311
- Schuller KA, Randall DD** (1989) Regulation of Pea Mitochondrial Pyruvate Dehydrogenase Complex. *Plant Physiol* **89**: 1207 LP – 1212
- Schuller KA, Turpin DH, Plaxton WC** (1990b) Metabolite Regulation of Partially Purified Soybean Nodule Phosphoenolpyruvate Carboxylase. *Plant Physiol* **94**: 1429–1435
- Schulze WX, Yao Q, Xu D** (2015) Databases for Plant Phosphoproteomics. *Plant Phosphoproteomics Methods Protoc* **1306**: 207–216
- Schwarte S, Bauwe H** (2007) Identification of the Photorespiratory 2-Phosphoglycolate Phosphatase, PGLP1, in *Arabidopsis*. *Plant Physiol* **144**: 1580–1586
- Seal SN, Rose ZB** (1987) Characterization of a phosphoenzyme intermediate in the reaction of phosphoglycolate phosphatase. *J Biol Chem* **262**: 13496–13500
- Segerer G, Hadamek K, Zundler M, Fekete A, Seifried A, Mueller MJ, Koentgen F, Gessler M, Jeanclos E, Gohla A** (2016) An essential developmental function for murine phosphoglycolate

- phosphatase in safeguarding cell proliferation. *Sci Rep* **6**: 1–13
- Seifried A, Bergeron A, Boivin B, Gohla A** (2016a) Reversible oxidation controls the activity and oligomeric state of the mammalian phosphoglycolate phosphatase AUM. *Free Radic Biol Med* **97**: 75–84
- Seifried A, Bergeron A, Boivin B, Gohla A** (2016b) Reversible oxidation controls the activity and oligomeric state of the mammalian phosphoglycolate phosphatase AUM. *Free Radic Biol Med* **97**: 75–84
- Seifried A, Schultz J, Gohla A** (2013) Human HAD phosphatases: Structure, mechanism, and roles in health and disease. *FEBS J* **280**: 549–571
- Servaites JC, Ogren WL** (1977) Chemical Inhibition of the Glycolate Pathway in Soybean Leaf Cells. *Plant Physiol* **60**: 461–466
- Sharma OP, Vadlamudi Y, Liao Q, Strodel B, Suresh Kumar M** (2013) Molecular modeling, dynamics, and an insight into the structural inhibition of cofactor independent phosphoglycerate mutase isoform 1 from *Wuchereria bancrofti* using cheminformatics and mutational studies. *J Biomol Struct Dyn* **31**: 765–778
- Shen BR, Wang LM, Lin XL, Yao Z, Xu HW, Zhu CH, Teng HY, Cui LL, Liu EE, Zhang JJ, et al** (2019) Engineering a New Chloroplastic Photorespiratory Bypass to Increase Photosynthetic Efficiency and Productivity in Rice. *Mol Plant* **12**: 199–214
- Shigekawa K, Dower WJ** (1989) Electroporation: a general approach to the introduction of macromolecules into prokaryotic and eukaryotic cells. *Aust J Biotechnol* **3**: 56–62
- da Silva TC, Polli JE, Swaan PW** (2013) The solute carrier family 10 (SLC10): Beyond bile acid transport. *Mol Aspects Med* **34**: 252–269
- Simic P, Willuhn J, Sahm H, Eggeling L** (2002) Identification of glyA (encoding serine hydroxymethyltransferase) and its use together with the exporter ThrE to increase L-threonine accumulation by *Corynebacterium glutamicum*. *Appl Environ Microbiol* **68**: 3321–3327
- Simkin AJ, Lopez-Calcagno PE, Davey PA, Headland LR, Lawson T, Timm S, Bauwe H, Raines CA** (2017) Simultaneous stimulation of sedoheptulose 1,7-bisphosphatase, fructose 1,6-bisphosphate aldolase and the photorespiratory glycine decarboxylase-H protein increases CO₂ assimilation, vegetative biomass and seed yield in *Arabidopsis*. *Plant Biotechnol J* **15**: 805–816
- Singh P, Kumar PA, Abrol YP, Naik MS** (1986) Photorespiratory nitrogen cycle – A critical evaluation. *Physiol Plant* **66**: 169–176
- Singh PK, Kushwaha S, Mohd S, Pathak M, Misra-Bhattacharya S** (2013) In vitro gene silencing of independent phosphoglycerate mutase (iPGM) in the filarial parasite *Brugia malayi*. *Infect Dis Poverty* **2**: 5
- Skryhan K, Gurrieri L, Sparla F, Trost P, Blennow A** (2018) Redox Regulation of Starch Metabolism. *Front Plant Sci* **9**: 1344
- Smeeckens S, Ma J, Hanson J, Rolland F** (2010) Sugar signals and molecular networks controlling plant growth. *Curr Opin Plant Biol* **13**: 273–278
- Somerville CR** (2001) An Early *Arabidopsis* Demonstration. Resolving a Few Issues Concerning Photorespiration. *Plant Physiol* **125**: 20–24

- Somerville CR, Ogren WL** (1979) A phosphoglycolate phosphatase-deficient mutant of *Arabidopsis*. *Nature* **280**: 833–836
- Somerville CR, Ogren WL** (1980a) Photorespiration mutants of *Arabidopsis thaliana* deficient in serine-glyoxylate aminotransferase activity. *Proc Natl Acad Sci* **77**: 2684–2687
- Somerville CR, Ogren WL** (1980b) Photorespiration mutants of *Arabidopsis thaliana* deficient in serine-glyoxylate aminotransferase activity. *Proc Natl Acad Sci* **77**: 2684–2687
- Somerville CR, Ogren WL** (1981) Photorespiration-deficient Mutants of *Arabidopsis thaliana* Lacking Mitochondrial Serine Transhydroxymethylase Activity . *Plant Physiol* **67**: 666–671
- Somerville CR, Ogren WL** (1980c) Inhibition of photosynthesis in *Arabidopsis* mutants lacking leaf glutamate synthase activity. *Nature* **286**: 257–259
- Somerville CR, Ogren WL** (1982) Mutants of the cruciferous plant *Arabidopsis thaliana* lacking glycine decarboxylase activity . *Biochem J* **202**: 373–380
- Somerville CR, Portis AR, Ogren WL** (1982) A Mutant of *Arabidopsis thaliana* Which Lacks Activation of RuBP Carboxylase In Vivo. *Plant Physiol* **70**: 381–387
- Somerville SC, Ogren WL** (1983) An *Arabidopsis thaliana* mutant defective in chloroplast dicarboxylate transport. *Proc Natl Acad Sci* **80**: 1290–1294
- Song Z-B, Xiao S-Q, You LAN, Wang S-S, Tan HAO, Li K-Z, Chen L-M** (2013) C1 metabolism and the Calvin cycle function simultaneously and independently during HCHO metabolism and detoxification in *Arabidopsis thaliana* treated with HCHO solutions. *Plant Cell Environ* **36**: 1490–1506
- South PF, Cavanagh AP, Liu HW, Ort DR** (2019) Synthetic glycolate metabolism pathways stimulate crop growth and productivity in the field. *Science* (80-) **363**: 9077
- South PF, Walker BJ, Cavanagh AP, Rolland V, Badger M, Ort DR** (2017) Bile Acid Sodium Symporter BASS6 Can Transport Glycolate and Is Involved in Photorespiratory Metabolism in *Arabidopsis thaliana* . *Plant Cell* **29**: 808–823
- Spreitzer RJ, Salvucci ME** (2002) RUBISCO: Structure, Regulatory Interactions, and Possibilities for a Better Enzyme. *Annu Rev Plant Biol* **53**: 449–475
- Stein M, Gabdouliline RR, Wade RC** (2010) Cross-species analysis of the glycolytic pathway by comparison of molecular interaction fields. *Mol Biosyst* **6**: 152–164
- Stumpf PK** (1948) Carbohydrate metabolism in higher plants; pea aldolase. *J Biol Chem* **176**: 233–241
- Sun SN, Wang Q, Sun CC, Liu FJ, Bi HG, Ai XZ** (2017) Response and adaptation of of cucumber seedlings to high temperature stressphotosynthesis. *Chinese J Appl Ecol* **28**: 1603–1610
- Tabita FR, Hanson TE, Li H, Satagopan S, Singh J, Chan S** (2007) Function, Structure, and Evolution of the RubisCO-Like Proteins and Their RubisCO Homologs. *Microbiol Mol Biol Rev* **71**: 576–599
- Tabita FR, Satagopan S, Hanson TE, Kreel NE, Scott SS** (2008) Distinct form I, II, III, and IV Rubisco proteins from the three kingdoms of life provide clues about Rubisco evolution and structure/function relationships. *J Exp Bot* **59**: 1515–1524
- Taira M, Valtersson U, Burkhardt B, Ludwig RA** (2004) *Arabidopsis thaliana* GLN2-Encoded Glutamine Synthetase Is Dual Targeted to Leaf Mitochondria and Chloroplasts. *Plant Cell* **16**:

2048–2058

- Takahashi S, Bauwe H, Badger M** (2007) Impairment of the Photorespiratory Pathway Accelerates Photoinhibition of Photosystem II by Suppression of Repair But Not Acceleration of Damage Processes in Arabidopsis. *Plant Physiol* **144**: 487–494
- Takahashi S, Murata N** (2005) Interruption of the Calvin cycle inhibits the repair of Photosystem II from photodamage. *Biochim Biophys Acta - Bioenerg* **1708**: 352–361
- Tang G-Q, Hardin SC, Dewey R, Huber SC** (2003) A novel C-terminal proteolytic processing of cytosolic pyruvate kinase, its phosphorylation and degradation by the proteasome in developing soybean seeds. *Plant J* **34**: 77–93
- Taniguchi M, Taniguchi Y, Kawasaki M, Takeda S, Kato T, Sato S, Tabata S, Miyake H, Sugiyama T** (2002) Identifying and characterizing plastidic 2-oxoglutarate/malate and dicarboxylate transporters in Arabidopsis thaliana. *Plant Cell Physiol* **43**: 706–717
- Tatusov RL, Altschul SF, Koonin E V** (1994) Detection of conserved segments in proteins: iterative scanning of sequence databases with alignment blocks. *Proc Natl Acad Sci* **91**: 12091 LP – 12095
- Tcherkez G, Bligny R, Gout E, Mahé A, Hodges M, Cornic G** (2008) Respiratory metabolism of illuminated leaves depends on CO₂ and O₂ conditions. *Proc Natl Acad Sci* **105**: 797–802
- Tcherkez GGB, Farquhar GD, Andrews TJ** (2006) Despite slow catalysis and confused substrate specificity, all ribulose biphosphate carboxylases may be nearly perfectly optimized. *Proc Natl Acad Sci* **103**: 7246–7251
- Teresa Pellicer M, Felisa Nuñez M, Aguilar J, Badia J, Baldoma L** (2003) Role of 2-phosphoglycolate phosphatase of Escherichia coli in metabolism of the 2-phosphoglycolate formed in DNA repair. *J Bacteriol* **185**: 5815–5821
- Tetlow IJ, Bowsher CG, Emes MJ** (1996) Reconstitution of the hexose phosphate translocator from the envelope membranes of wheat endosperm amyloplasts. *Biochem J* **319**: 717 LP – 723
- Thaller MC, Schippa S, Rossolini GM** (1998) Conserved sequence motifs among bacterial, eukaryotic, and archaeal phosphatases that define a new phosphohydrolase superfamily. *Protein Sci* **7**: 1647–1652
- The UniProt Consortium** (2016) UniProt: the universal protein knowledgebase. *Nucleic Acids Res* **45**: 158–169
- Thelen JJ, Miernyk JA, Randall DD** (2000) Pyruvate dehydrogenase kinase from Arabidopsis thaliana: a protein histidine kinase that phosphorylates serine residues. *Biochem J* **349**: 195–201
- Thelen JJ, Miernyk JA, Randall DD** (1998) Partial purification and characterization of the maize mitochondrial pyruvate dehydrogenase complex. *Plant Physiol* **116**: 1443–1450
- Tikhonov AN, Subczynski WK** (2019) Oxygenic photosynthesis: EPR study of photosynthetic electron transport and oxygen-exchange, an overview. *Cell Biochem Biophys* **77**: 47–59
- Timm S, Bauwe H** (2013a) The variety of photorespiratory phenotypes - employing the current status for future research directions on photorespiration. *Plant Biol* **15**: 737–747
- Timm S, Bauwe H** (2013b) The variety of photorespiratory phenotypes - employing the current status for future research directions on photorespiration. *Plant Biol* **15**: 737–747

- Timm S, Florian A, Arrivault S, Stitt M, Fernie AR, Bauwe H** (2012a) Glycine decarboxylase controls photosynthesis and plant growth. *FEBS Lett* **586**: 3692–3697
- Timm S, Florian A, Fernie AR, Bauwe H** (2016) The regulatory interplay between photorespiration and photosynthesis. *J Exp Bot* **67**: 2923–2929
- Timm S, Florian A, Jahnke K, Nunes-Nesi A, Fernie AR, Bauwe H** (2011a) The Hydroxypyruvate-Reducing System in Arabidopsis: Multiple Enzymes for the Same End. *Plant Physiol* **155**: 694–705
- Timm S, Florian A, Jahnke K, Nunes-Nesi A, Fernie AR, Bauwe H** (2011b) The hydroxypyruvate-reducing system in arabidopsis: Multiple enzymes for the same end. *Plant Physiol* **155**: 694–705
- Timm S, Florian A, Wittmiß M, Jahnke K, Hagemann M, Fernie AR, Bauwe H** (2013) Serine Acts as a Metabolic Signal for the Transcriptional Control of Photorespiration-Related Genes in Arabidopsis. *Plant Physiol* **162**: 379–389
- Timm S, Giese J, Engel N, Wittmiß M, Florian A, Fernie AR, Bauwe H** (2018) T-protein is present in large excess over the other proteins of the glycine cleavage system in leaves of Arabidopsis. *Planta* **247**: 41–51
- Timm S, Mielewicz M, Florian A, Frankenbach S, Dreissen A, Hocken N, Fernie AR, Walter A, Bauwe H** (2012b) High-to-Low CO₂ Acclimation Reveals Plasticity of the Photorespiratory Pathway and Indicates Regulatory Links to Cellular Metabolism of Arabidopsis. *PLoS One* **7**: 42809
- Timm S, Nunes-Nesi A, Pärnik T, Morgenthal K, Wienkoop S, Keerberg O, Weckwerth W, Kleczkowski LA, Fernie AR, Bauwe H** (2008) A Cytosolic Pathway for the Conversion of Hydroxypyruvate to Glycerate during Photorespiration in *Arabidopsis*. *Plant Cell* **20**: 2848–2859
- Timm S, Wittmiß M, Gamlien S, Ewald R, Florian A, Frank M, Wirtz M, Hell R, Fernie AR, Bauwe H** (2015a) Mitochondrial dihydrolipoyl dehydrogenase activity shapes photosynthesis and photorespiration of Arabidopsis Thaliana. *Plant Cell* **27**: 1968–1984
- Timm S, Wittmiß M, Gamlien S, Ewald R, Florian A, Frank M, Wirtz M, Hell R, Fernie AR, Bauwe H** (2015b) Mitochondrial dihydrolipoyl dehydrogenase activity shapes photosynthesis and photorespiration of Arabidopsis Thaliana. *Plant Cell* **27**: 1968–1984
- Timson DJ** (2016) Metabolic Enzymes of Helminth Parasites: Potential as Drug Targets. *Curr Protein Pept Sci* **17**: 280–295
- Toivola J, Nikkanen L, Dahlström KM, Salminen TA, Lepistö A, Vignols HF, Rintamäki E** (2013) Overexpression of chloroplast NADPH-dependent thioredoxin reductase in Arabidopsis enhances leaf growth and elucidates in vivo function of reductase and thioredoxin domains. *Front Plant Sci* **4**: 389
- Traut TW** (1994) Dissociation of Enzyme Oligomers: A Mechanism for Allosteric Regulation. *Crit Rev Biochem Mol Biol* **29**: 125–163
- Umezawa T, Sugiyama N, Takahashi F, Anderson JC, Ishihama Y, Peck SC, Shinozaki K** (2013) Genetics and Phosphoproteomics Reveal a Protein Phosphorylation Network in the Abscisic Acid Signaling Pathway in Arabidopsis thaliana. *Sci Signal* **6**: 6–8
- Ushijima T, Hanada K, Gotoh E, Yamori W, Kodama Y, Tanaka H, Kusano M, Fukushima A, Tokizawa**

- M, Yamamoto YY, et al** (2017) Light Controls Protein Localization through Phytochrome-Mediated Alternative Promoter Selection. *Cell* **171**: 1316–1325
- Vandenabeele S, Vanderauwera S, Vuylsteke M, Rombauts S, Langebartels C, Seidlitz HK, Zabeau M, Van Montagu M, Inzé D, Van Breusegem F** (2004) Catalase deficiency drastically affects gene expression induced by high light in *Arabidopsis thaliana*. *Plant J* **39**: 45–58
- Vaughn KC, Campbell WH** (1988) Immunogold Localization of Nitrate Reductase in Maize Leaves. *Plant Physiol* **88**: 1354–1357
- Verschueren KHG, Seljée F, Rozeboom HJ, Kalk KH, Dijkstra BW** (1993) Crystallographic analysis of the catalytic mechanism of haloalkane dehalogenase. *Nature* **363**: 693–698
- Vescovi M, Zaffagnini M, Festa M, Trost P, Lo Schiavo F, Costa A** (2013) Nuclear accumulation of cytosolic glyceraldehyde-3-phosphate dehydrogenase in cadmium-stressed *Arabidopsis* roots. *Plant Physiol* **162**: 333–346
- Vitlin Gruber A, Feiz L** (2018) Rubisco Assembly in the Chloroplast. *Front Mol Biosci* **5**: 24
- Vlastaridis P, Kyriakidou P, Chaliotis A, Van de Peer Y, Oliver SG, Amoutzias GD** (2017) Estimating the total number of phosphoproteins and phosphorylation sites in eukaryotic proteomes. *Gigascience* **6**: 1–11
- Voll LM, Jamai A, Renné P, Voll H, McClung CR, Weber APM** (2006) The Photorespiratory *Arabidopsis* *shm1* Mutant Is Deficient in SHM1. *Plant Physiol* **140**: 59–66
- Voss I, Sunil B, Scheibe R, Raghavendra AS** (2013) Emerging concept for the role of photorespiration as an important part of abiotic stress response. *Plant Biol* **15**: 713–722
- Walker BJ, South PF, Ort DR** (2016) Physiological evidence for plasticity in glycolate/glycerate transport during photorespiration. *Photosynth Res* **129**: 93–103
- Walker RP, Leegood RC** (1995) Purification, and phosphorylation in vivo and in vitro, of phosphoenolpyruvate carboxykinase from cucumber cotyledons. *FEBS Lett* **362**: 70–74
- Wallsgrave RM, Kendall AC, Hall NP, Turner JC, Lea PJ** (1986) Carbon and nitrogen metabolism in a barley (*Hordeum vulgare* L.) mutant with impaired chloroplast dicarboxylate transport. *Planta* **168**: 324–329
- Wallsgrave RM, Turner JC, Hall NP, Kendall AC, Bright SWJ** (1987) Barley Mutants Lacking Chloroplast Glutamine Synthetase—Biochemical and Genetic Analysis. *Plant Physiol* **83**: 155–158
- Weber A, Servaites JC, Geiger DR, Kofler H, Hille D, Gröner F, Hebbeker U, Flügge UI** (2000) Identification, purification, and molecular cloning of a putative plastidic glucose translocator. *Plant Cell* **12**: 787–802
- Weber APM, Linka N** (2011) Connecting the Plastid: Transporters of the Plastid Envelope and Their Role in Linking Plastidial with Cytosolic Metabolism. *Annu Rev Plant Biol* **62**: 53–77
- Westram A, Lloyd JR, Roessner U, Riesmeier JW, Kossmann J** (2002) Increases of 3-phosphoglyceric acid in potato plants through antisense reduction of cytoplasmic phosphoglycerate mutase impairs photosynthesis and growth, but does not increase starch contents. *Plant Cell Environ* **25**: 1133–1143
- van Wijk KJ, Friso G, Walther D, Schulze WX** (2014) Meta-Analysis of *Arabidopsis thaliana* Phospho-

- Proteomics Data Reveals Compartmentalization of Phosphorylation Motifs. *Plant Cell* **26**: 2367–2389
- Williams A, Petriacq P, Schwarzenbacher RE, Beerling DJ, Ton J** (2018) Mechanisms of glacial-to-future atmospheric CO₂ effects on plant immunity. *New Phytol* **218**: 752–761
- Wingler A, Lea PJ, Quick WP, Leegood RC** (2000) Photorespiration: metabolic pathways and their role in stress protection. *Philos Trans R Soc Lond B Biol Sci* **355**: 1517–1529
- Wingler A, Quick WP, Bungard RA, Bailey KJ, Lea PJ, Leegood RC** (1999) The role of photorespiration during drought stress: an analysis utilizing barley mutants with reduced activities of photorespiratory enzymes. *Plant Cell Environ* **22**: 361–373
- Wu J, Zhang Z, Zhang Q, Han X, Gu X, Lu T** (2015) The molecular cloning and clarification of a photorespiratory mutant, *oscdm1*, using enhancer trapping. *Front Genet* **6**: 1–17
- Wu M-X, Smyth DA, Black CC** (1983) Fructose 2,6-Bisphosphate and the Regulation of Pyrophosphate-Dependent Phosphofructokinase Activity in Germinating Pea Seeds. *Plant Physiol* **73**: 188–191
- Xu G, Fan X, Miller AJ** (2012) Plant Nitrogen Assimilation and Use Efficiency. *Annu Rev Plant Biol* **63**: 153–182
- Xu H, Kim S, Sorek H, Lee Y, Jeong D, Kim J, Oh EJ, Yun EJ, Wemmer DE, Kim KH, et al** (2016) PHO13 deletion-induced transcriptional activation prevents sedoheptulose accumulation during xylose metabolism in engineered *Saccharomyces cerevisiae*. *Metab Eng* **34**: 88–96
- Xu H, Zhang J, Zeng J, Jiang L, Liu E, Peng C, He Z, Peng X** (2009) Inducible antisense suppression of glycolate oxidase reveals its strong regulation over photosynthesis in rice. *J Exp Bot* **60**: 1799–1809
- Yamada K, Lim J, Dale JM, Chen H, Shinn P, Palm CJ, Southwick AM, Wu HC, Kim C, Nguyen M, et al** (2003) Empirical Analysis of Transcriptional Activity in the *Arabidopsis* Genome. *Science* (80-) **302**: 842–846
- Ye N, Yang G, Chen Y, Zhang C, Zhang J, Peng X** (2014) Two Hydroxypyruvate Reductases Encoded by *OshPR1* and *OshPR2* are Involved in Photorespiratory Metabolism in Rice. *J Integr Plant Biol* **56**: 170–180
- Ytterberg AJ, Peltier J-B, van Wijk KJ** (2006) Protein profiling of plastoglobules in chloroplasts and chromoplasts. A surprising site for differential accumulation of metabolic enzymes. *Plant Physiol* **140**: 984–997
- Yu H, Dranchak P, Li Z, MacArthur R, Munson MS, Mehzabeen N, Baird NJ, Battalie KP, Ross D, Lovell S, et al** (2017) Macrocyclic peptides delineate locked-open inhibition mechanism for microorganism phosphoglycerate mutases. *Nat Commun* **8**: 14932
- Yue X, Schunter A, Hummon AB** (2015) Comparing multistep immobilized metal affinity chromatography and multistep TiO₂ methods for phosphopeptide enrichment. *Anal Chem* **87**: 8837–8844
- Zaffagnini M, Fermani S, Costa A, Lemaire SD, Trost P** (2013a) Plant cytoplasmic GAPDH: redox post-translational modifications and moonlighting properties. *Front Plant Sci* **4**: 450
- Zaffagnini M, Morisse S, Bedhomme M, Marchand CH, Festa M, Rouhier N, Lemaire SD, Trost P**

- (2013b) Mechanisms of nitrosylation and denitrosylation of cytoplasmic glyceraldehyde-3-phosphate dehydrogenase from *Arabidopsis thaliana*. *J Biol Chem* **288**: 22777–22789
- Zandalinas SI, Mittler R, Balfagón D, Arbona V, Gómez-Cadenas A** (2018) Plant adaptations to the combination of drought and high temperatures. *Physiol Plant* **162**: 2–12
- Zecher R, Wolf HU** (1980) Partial purification and characterization of human erythrocyte phosphoglycollate phosphatase. *Biochem J* **191**: 117–124
- Zelitch I, Schultes NP, Peterson RB, Brown P, Brutnell TP** (2009) High Glycolate Oxidase Activity Is Required for Survival of Maize in Normal Air. *Plant Physiol* **149**: 195–204
- Zhang B, Liu J-Y** (2017) Serine phosphorylation of the cotton cytosolic pyruvate kinase GhPK6 decreases its stability and activity. *FEBS Open Bio* **7**: 358–366
- Zhang Q, Lee J, Pandurangan S, Clarke M, Pajak A, Marsolais F** (2013) Characterization of *Arabidopsis* serine:glyoxylate aminotransferase, AGT1, as an asparagine aminotransferase. *Phytochemistry* **85**: 30–35
- Zhang Y, Foster JM, Kumar S, Fougere M, Carlow CKS** (2004) Cofactor-independent Phosphoglycerate Mutase Has an Essential Role in *Caenorhabditis elegans* and Is Conserved in Parasitic Nematodes. *J Biol Chem* **279**: 37185–37190
- Zhao Z, Assmann SM** (2011) The glycolytic enzyme, phosphoglycerate mutase, has critical roles in stomatal movement, vegetative growth, and pollen production in *Arabidopsis thaliana*. *J Exp Bot* **62**: 5179–5189
- Zhou H, Zhao J, Yang Y, Chen C, Liu Y, Jin X, Chen L, Li X, Deng XW, Schumaker KS, et al** (2012) UBIQUITIN-SPECIFIC PROTEASE16 Modulates Salt Tolerance in *Arabidopsis* by Regulating Na⁺/H⁺ Antiport Activity and Serine Hydroxymethyltransferase Stability. *Plant Cell* **24**: 5106–5122
- Zimmermann P, Hirsch-Hoffmann M, Hennig L, Gruissem W** (2004) GENEVESTIGATOR. *Arabidopsis* microarray database and analysis toolbox. *Plant Physiol* **136**: 2621–2632
- (1976) Inhibition of spinach-leaf phosphofructokinase by 2-phosphoglycollate. *FEBS Lett* **68**: 55–58
- (1987) Photorespiratory N donors, aminotransferase specificity and photosynthesis in a mutant of barley deficient in serine: glyoxylate aminotransferase activity. *Planta* **172**: 106–113

Titre : Caractérisation de deux enzymes du métabolisme primaire chez *Arabidopsis thaliana* : la phosphoglycérate mutase et la phosphoglycolate phosphatase.

Mots clés: *Arabidopsis thaliana*, Photorespiration, Glycolyse, PGLP1, iPGAM, Métabolisme

Les plantes sont des organismes sessiles. Elles doivent réagir rapidement et efficacement aux stress biotiques et abiotiques qu'elles subissent. Pour cela, elles utilisent plusieurs niveaux de régulation. L'un d'eux, rapide et réversible, consiste à ajouter des modifications post-traductionnelles (PTMs) sur ses enzymes. La PTM la plus répandue est la phosphorylation protéique, qui intervient dans diverses voies du métabolisme primaire. La glycolyse permet la production d'énergie (ATP) et de pouvoir réducteur à partir de glucose. La régulation de la phosphoglycérate mutase d'*Arabidopsis thaliana* (AtiPGAM) a été étudiée grâce à une analyse d'un site de phosphorylation dans le but d'élucider le mécanisme réactionnel. La photorespiration est un processus essentiel pour les organismes photosynthétiques.

Ce cycle, initié par l'activité oxygénase de la ribulose-1,5-biphosphate carboxylase / oxygénase (RuBisCO), produit notamment une molécule de 2-phosphoglycolate (2-PG), toxique pour la plante. Le recyclage, coûteux, du 2-PG par le cycle photorespiratoire se déroule dans quatre compartiments (chloroplaste, peroxyosome, mitochondrie et cytosol). Sept des huit enzymes du cycle photorespiratoire sont phosphorylables. La phosphoglycolate phosphatase (AtPGLP1), première enzyme du cycle, est associée à quatre phosphosites. Des approches *in vitro* et *in planta* développées chez *A. thaliana* ont permis d'acquérir de nouvelles données sur la régulation post-traductionnelle de cette protéine, à la fois par phosphorylation et par oxydo-réduction.

Title : Characterization of two primary metabolism enzymes in *Arabidopsis thaliana*: phosphoglycerate mutase and phosphoglycolate phosphatase

Keywords *Arabidopsis thaliana*, Photorespiration, Glycolysis, PGLP1, iPGAM, Metabolism

As sessile organisms, plants need to rapidly and effectively react to environmental abiotic and biotic stresses. To do so, various regulatory mechanisms exist that include post-translational modifications (PTMs) of proteins. One of the most prevalent PTM is protein phosphorylation that has been shown to occur in many metabolic pathways. Glycolysis allows the production of energy (as ATP) and reducing power from glucose. In this context, the regulation of *Arabidopsis thaliana* phosphoglycerate mutase (AtiPGAM) was studied by analysing a phosphorylation site potentially involved in the reaction mechanism of this glycolytic enzyme. The photorespiratory cycle is a major metabolic pathway occurring in all photosynthetic organisms. It is initiated by the oxygenase

activity of the ribulose-1,5-bisphosphate carboxylase/oxygenase (RuBisCO) and leads to the production of toxic 2-phosphoglycolate (2-PG) molecules. The costly recycling of 2-PG by the photorespiratory cycle takes place in four different compartments (chloroplast, peroxisome, mitochondrion and cytosol). Seven of the eight core photorespiratory enzymes appear to be phosphorylated. Phosphoglycolate phosphatase (AtPGLP1), the first enzyme of the cycle that metabolizes 2-PG to glycolate, is associated with four phosphosites. *In vivo* and *in vitro* approaches using *Arabidopsis thaliana* have allowed us to obtain further insights into the post-translational regulation of this protein by protein phosphorylation and by oxidation-reduction.

